Aus der Klinik und Poliklinik für Neurologie
Sektion für Translationale Neurodegeneration "Albrecht Kossel"

Untersuchungen zu pathophysiologischen Merkmalen des Morbus Niemann-Pick Typ C1

Habilitationsschrift

zur

Erlangung des akademischen Grades

Doctor philosophiae naturalis habilitatus (Dr. phil. nat. habil.)

der Universitätsmedizin Rostock

vorgelegt von Dr. phil. nat. Moritz Johannes Frech

geb. am 7. März 1969 in Mannheim
wohnhaft in Neu Broderstorf

Rostock, den 14.8.2019

Gutachter:
Prof. Dr. Dr. A. Hermann, Universitätsmedizin Rostock
Prof. Dr. med. H. Lerche, Universitätsklinikum Tübingen
Prof. Dr. med. S. Petri, Medizinische Hochschule Hannover

Jahr der Verteidigung: 2020

https://doi.org/10.18453/rosdok_id00002734

Inhalt

1. Einleitung

1.1. Morbus Niemann-Pick Typ C

Morbus Niemann-Pick Typ C ist eine seltene autosomal rezessive, lysosomale Lipidose, mit einer Inzidenz von 1:120000[1]. Mutationen im *NPC1*- oder *NPC2*-Gen ziehen die Expression von nicht funktionalen oder in der Funktion reduzierten Protein nach sich. In 95% der Fälle liegt eine Mutation im *NPC1*-Gen vor (Morbus Niemann-Pick Typ C1 oder NPC1), in lediglich 5% eine Mutationen im *NPC2*-Gen. Das NPC1-Protein transportiert Cholesterol in Lysosomen und späten Endosomen aus dem Lumen in den zytoplasmatischen Raum. Hierbei scheint es sich um eine kooperativen Mechanismus zu handeln, bei dem das NPC2-Protein Cholesterol bindet und dieses dann an das NPC1-Protein weiterreicht. Jüngste Arbeiten zur Aufklärung der 3D-Struktur des NPC1-Proteins weisen darauf hin, dass das Protein eine transmembranäre Pore besitzt, durch die wahrscheinlich Cholesterol ausgeschleust wird[2,3]. Die Dysfunktion von NPC1- oder NPC2-Protein führt zu einer Akkumulation von unverestertem Cholesterol in den Lysosomen. Diese Akkumulationen werden mit Hilfe des Filipin-Tests nachgewiesen, der in der klinischen Diagnostik zur Anwendung kommt[4].

NPC1 ist als neuroviszerale Erkrankung definiert, wobei viszerale und neurologische Symptome zu unterschiedlichen Zeitpunkten und in verschieden starker Ausprägung auftreten[1]. Viszeral sind Funktionsstörungen in Leber, Milz und Lunge zu beobachten. Zu den neurologischen Symptomen zählen unter anderem motorische Dysfunktionen wie Dystonie und zerebelläre Ataxie. Die Ataxie beruht auf der Degeneration von Purkinjezellen, wobei die zu Grunde liegenden pathophysiologischen Vorgänge schlecht verstanden und bisher kaum untersucht sind. Auf funktioneller neuronaler Ebene sind Veränderungen in der synaptischen Transmission zu beobachten. Hippokampale CA1-Pyramidenzellen eines murinen NPC1-Modells zeigen eine Erhöhung der Frequenz von spontanen exzitatorischen postsynaptischen Strömen auf[5], sowie Veränderungen in der Regulation von AMPA-Rezeptoren[6]. In Neuronen des Neokortex sind Störungen in der Langzeitpotenzierung (long term potentiation, LTP)[7] und in der Langzeitdepression (long term depression, LDP) von Purkinjezellen eines NPC1-defizienten Mausmodells beschrieben[8]. Die veränderte LDP könnte auf der verringerten Anzahl von inhibitorischen Synapsen beruhen, die in der zerebellären Molekularschicht von NPC1-defizienten Mäusen festgestellt wurden[9]. Untersuchungen, die sich mit den pathophysiologischen Mechanismen und Symptomen von NPC1 befassen wurden überwiegend an murinen NPC1-Modellsystemen durchgeführt. Studien an humanen Geweben beschränken sich auf postmortem Biopsien und schließen somit funktionelle Studien aus. Hier stellen humane induzierte pluripotente Stammzellen eine sehr gute Möglichkeit dar, die Palette von *in vitro* Krankheitsmodellen zu erweitern.

1.2. Verwendung induzierter pluripotenter Stammzellen als Krankheitsmodelle

Die Verwendung von induzierten pluripotenten Stammzellen (IPS-Zellen) bietet einen sehr guten Ansatz für die Entwicklung von neuronalen zellulären Modellsystemen, die als Grundlage für sowohl mechanistische Fragestellungen, als auch die Entwicklung neuer Therapieoptionen dienen können. Die Erstbeschreibung von murinen induzierten pluripotenten Stammzellen durch Takahashi und Kollegen im Jahr 2006[10] und kurz darauf von humanen induzierten pluripotenten Stammzellen[11,12], stellt einen der größten Fortschritte in der Stammzellforschung dar. Für die Gewinnung von IPS-Zellen können verschiedene somatische Zellen genutzt werden. Das ursprüngliche Protokoll beruht auf der Verwendung von Fibroblasten, welche mittels Retroviren mit den Transkriptionsfaktoren Sox2, Klf4, Oct4 und c-Myc transfiziert wurden. Die so gewonnenen IPS-Zellen weisen typische Merkmale embryonaler Stammzellen auf[11,13] und können in gewebespezifische Zellen differenziert werden. Dies bietet den einzigartigen Zugang für Untersuchung an Zellen, die nur eingeschränkt zur Verfügung stehen, wie z.B. Zellen des zentralen Nervensystems. Darüber hinaus besteht aber auch die Möglichkeit, IPS-Zellen von Patienten zu gewinnen die unter einer seltenen Erbkrankheit leiden, für die meistens keine *in vitro* Krankheitsmodelle oder Tiermodelle zur Verfügung stehen. Solche patientenspezifischen IPS-Zellen ermöglichen es, pathogene Mechanismen von Erkrankungen zu studieren und stellen für die Grundlagenforschung ein wertvolles Werkzeug dar. Andererseits könnten Mutationen in patientenspezifischen IPS-Zellen korrigiert und diese im Rahmen einer Zellersatztherapie für die Behandlung von hereditären Erkrankungen eingesetzt werden. Denkbar ist ein solches Vorgehen für neurodegenerative Erkrankungen, wie Morbus Parkinson. Hierbei können aus patientenspezifischen IPS-Zellen autologe Zellen für Zellersatztherapien gewonnen werden, die keine Abstoßungsreaktion des Körpers hervorrufen[14].

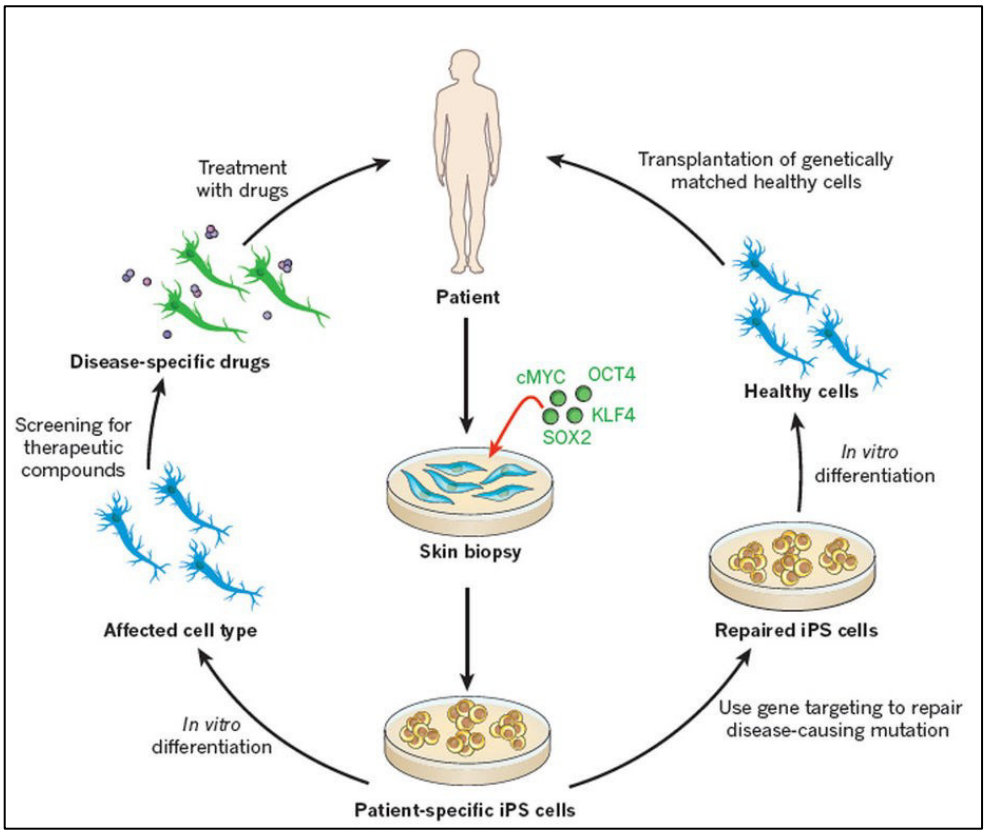

Abbildung 1 Schematische Übersicht über die Verwendung von patientenspezifischen IPS-Zellen nach Robinton und Daley (2012). Ausgehend von z.B. Fibroblasten können über eine Reprogrammierung dieser Zellen patientenspezifische IPS-Zellen gewonenn werden. Diese lassen sich in verschiedenste Zelltypen differenzieren, die dann ihrerseits für die Untersuchung pathogener Mechanismen und für die Wirkstofffindung verwendet werden können. Im Rahmen von Zellersatztherapien ist es denkbar Mutationen der patientenspezifischen IPS-Zellen zu korrigieren und diese dann für Transplantationen zu verwenden.

In Bezug auf die Verwendung von patientenspezifischen IPS-Zellen als *in vitro* Krankheitsmodell für neurodegenerativen Erkrankungen müssen IPS-Zellen nicht nur in gewebespezifische Zelltypen, wie Neurone und Gliazellen, differenziert werden, sondern sie müssen auch die pathophysiologischen Merkmale der entsprechenden Erkrankung aufweisen. Für NPC1 zählen hierzu untere anderem die Anreicherung von Cholesterol und Gangliosiden, Astrogliose, Hypo- und Hyperphosphorylierung von Intermediärfilamenten, verringerte Aktivität der Proteinkinase C (PKC), Veränderungen der Autophagie, oxidativer Stress, Veränderungen der synaptischen Transmission und Funktion von Ionenkanälen, morphologische Veränderungen von Neuronen, progressive Neurodegeneration bzw. Absterben von Neuronen sowie die Demyelinisierung auf Grund von Funktions- oder Entwicklungsstörung von Oligodendrozyten.

2. Zielstellung

Induzierte pluripotente Stammzellen haben sich seit ihrer Erstbeschreibung zu einem unverzichtbaren Ansatz in der Erforschung von neurodegenerativen Erkrankungen erwiesen. Dies ist auch durch den rasanten Anstieg an Publikationen belegt, die die Entwicklung von humanen IPS-Zell-basierten Krankheitsmodellen beinhalten.
Zu Beginn der Arbeiten stand ein solches Modellsystem für NPC1 nicht zur Verfügung.

Hieraus ergaben sich folgende Zielstellungen:

- Reprogrammierung von NPC1 patientenspezifischen Fibroblasten in patientenspezifische IPS-Zellen
- Differenzierung der patientenspezifischen IPS-Zellen in Neurone und Gliazellen
- Untersuchungen der neuronal differenzierten Zellen hinsichtlich der Ausprägung von pathophysiologischen Merkmalen, als Beleg für die Verwendbarkeit der Zellen als NPC1 *in vitro* Modellsystem
- Funktionelle Beschreibungen der neuronal differenzierten Zellen als Grundlage für den Vergleich mit einem murinen NPC1 Modell
- Funktionelle Untersuchungen an zerebellären Purkinjezellen eines NPC1-Mausmodells

Mit diesem dualen Ansatz, unter Verwendung eines humanen neuronalen Zellmodells und eines murinen Tiermodells, wurden vergleichende bzw. sich ergänzende Untersuchungen durchgeführt, die zu einem weitergehenden Verständnis der pathophysiologischen Mechanismen des Morbus Niemann-Pick Typ C1 beitragen und als Grundlage für die Entwicklung und Erprobung neuer Behandlungsstrategien dienen.

3. Übersicht über die kumulierten Originalarbeiten

3.1. Entwicklung von NPC1 patientenspezifischen IPS-Zellen

Trilck M; Hübner R; Seibler P; Klein C; Rolfs A; ***Frech MJ*** *(2013): Niemann-Pick type C1 patient-specific induced pluripotent stem cells display disease specific hallmarks. Orphanet J Rare Dis; 8:144. doi: 10.1186/1750-1172-8-144. IF 3,45*

Hintergrund

Die Beschreibung einer erfolgreichen Reprogrammierung von humanen Fibroblasten erfolgte 2007 durch Takahashi und Kollegen[11]. Eine erste Verwendung von humanen IPS-Zellen als Modellsystem wurde 2009 für die familiäre Dysautonomie publiziert[15]. Dieser Arbeit folgten schnell, insbesondere für neurodegenerative Erkrankungen wie Morbus Parkinson oder Morbus Alzheimer, weitere Beschreibungen von patientenspezifischen IPS-Zellen. Zu Beginn unserer Arbeiten über pathophysiologische Prozesse von NPC1 stand kein solches Modellsystem zur Verfügung. Der Großteil der bis dahin publizierten Daten beruhte auf Untersuchungen an NPC1 patientenspezifischen Fibroblasten oder Tiermodellen[1]. Daher war es zunächst unser Ziel NPC1 patientenspezifische IPS-Zellen herzustellen und zu untersuchen ob diese und deren differenzierten Derivate pathophysiologische Merkmale, wie z.B. die Akkumulation von Cholesterol, aufweisen.

Ergebnis

Mit Hilfe der von Takahashi et al. beschriebenen Methodik zur Reprogrammierung von humanen Fibroblasten[11] ist es gelungen, patientenspezifische IPS-Zellen aus Fibroblasten eines NPC1-Patienten und eines gesunden Probanden zu generieren (Abb. 2). Die Fibroblasten wurden mittels retroviraler Transfektion von Sox2, Klf4, Oct4 und c-Myc in IPS-Zellen überführt. Anschließend wurden die reprogrammierten Zellen auf verschiedene Pluripotenzmarker hin untersucht. Die IPS-Zellen erscheinen in einem Nachweis der alkalischen Phosphatase bläulich (Abb. 2, links). Mittels immunzytochemischer Färbungen wurden die Pluripotenzmarker Nanog, Oct4, SSEA3, SSEA4, Tra-1-60 und Tra-1-81 nachgewiesen (Abb. 2, links). Weiterhein besitzen die IPS-Zellen die Fähigkeit in Zellen der drei Keimblätter zu differenzieren und Teratome zu bilden (Abb. 2, rechts).

Bezüglich der Ausprägung von pathophysiologischen Merkmalen, konnte sowohl in den IPS-Zellen, als auch in den daraus abgeleiteten differenzierten Derivaten Cholesterolakkumulationen nachgewiesen werden (s.a. Trilck et al. 2013**,** Figure 5). NPC1-defiziente Fibroblasten zeigten hierbei, im Gegensatz zu gesunden Fibroblasten, typische perinukleäre Akkumulationen von Cholesterol. Diese, wenn auch diffuser, konnten ebenso in NPC1-defizienten neuralen Derivaten der IPS-Zellen nachgewiesen werden.

Weiterhin wurde durch elektrophysiologische Untersuchungen mit Hilfe von Patch-Clamp-Messungen die Reifung in funktionelle Neurone belegt (s.a. Trilck et al. 2013, Figure 4.). Die Zellen wiesen spannungs-aktivierte Ionenkanäle, wie Na^+- und K^+- Kanäle auf und generierten spontane Aktionspotentiale. Zudem bildeten sie chemische Synapsen aus, was durch die Messung von postsynaptischen Strömen demonstriert wurde (s.a. Trilck et al. 2013). Eine eingehendere funktionelle Untersuchung der verschiedenen Linien ist in 3.3 beschrieben.

Schlussfolgerung

Es wurden Fibroblasten eines NPC1-Patienten in patientenspezifische IPS-Zellen überführt, welche in neurale Progenitorzellen und abschließend in funktionelle Neuronen und Gliazellen differenziert wurden. Diese und weitere NPC1- und NPC2-defizienten patientenspezifische IPS-Zelllinien bilden die Grundlage für die weiteren Untersuchungen (s. 3.2, 3.3 und 3.4) zu den pathophysiologischen Mechanismen von NPC1.

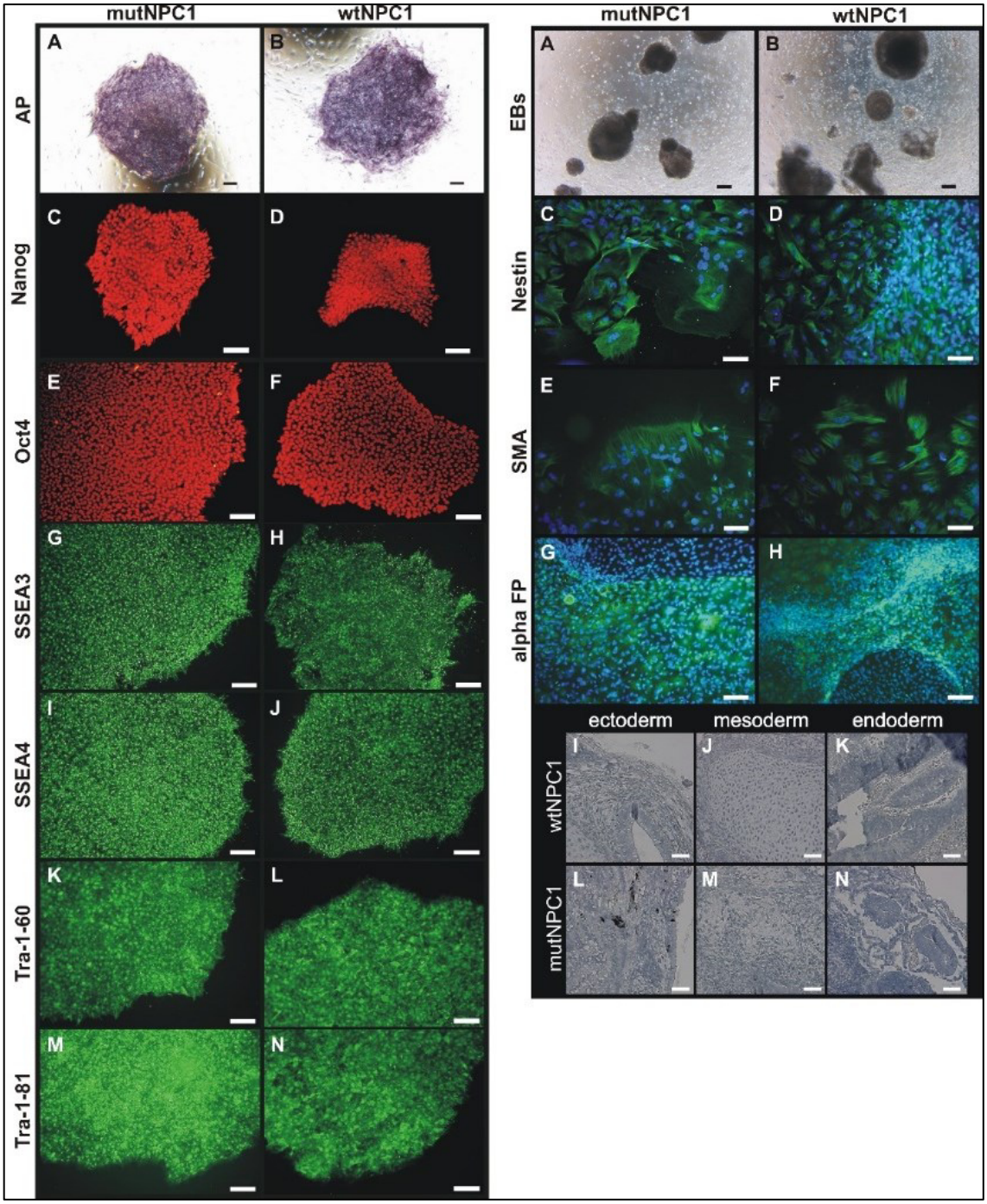

Abbildung 2 Links: Figure 2 aus Trilck et al., 2013. (A, B) Nachweis der alkalischen Phosphatase. (C-N) Immunzytochemische Färbungen für die Pluripotenzmarker Nanog, Oct4, SSEA3, SSEA4, Tra-1-60 und Tra-1-81. Maßstab: 100 µm. **Rechts**: Figure 3 aus Trilck et al., 2013. Unter speziellen Kulturbedingungen bilden IPS-Zellkolonien sogenannte *Embryoid Bodies* aus (A, B), die Zelltypen der verschiedenen Keimblätter enthalten. (C, D) Nestin: Ektoderm; (E, F) smooth muscle actin: Mesoderm; (G, H) alpha fetoprotein: Endoderm. (I-N). Als weiterer Pluripotenznachweis wurden immundefizienten Mäusen IPS-Zellen subkutan injiziert. Diese Zellen bilden Teratome aus, welche Gewebestrukturen beinhalten, die für die entsprechenden Keimblätter typisch sind. Maßstab: 50 µm.

3.2. Akkumulation von Cholesterol und Sphingolipiden

Trilck M; Peter F; Zheng C; Frank M; Dobrenis K; Mascher H, Rolfs A; ***Frech MJ*** *(2017): Diversity of glycosphingolipid GM2 and cholesterol accumulation in NPC1 patient-specific iPSC-derived neurons. Brain Res; 1657:52-61. doi: 10.1016/j.brainres.2016.11.031. IF 2,75*

s.a. Peter F; Trilck M; Rabenstein M; Rolfs A; ***Frech MJ*** *(2017): Dataset in support of the generation of Niemann-Pick disease type C1 patient-specific iPS cell lines carrying the novel NPC1 mutation c.1180T>C or the prevalent c.3182T>C mutation – analysis of pluripotency and neuronal differentiation. Data Brief; 12:123-131. doi: 10.1016/j.dib.2017.03.042. z.Z. ohne IF*

Hintergrund

Untersuchungen zur Aufklärung pathogener Mechanismen von NPC zeigen in murinen NPC1-Modellen eine Reihe von NPC1-typischen Merkmalen auf. Auf zellulärer Ebene können die Akkumulationen von Cholesterol, den Gangliosiden GM2 und GM3, morphologische Veränderungen der Neurone, Astrogliose, aber auch funktionelle Veränderungen, z.B. in der synaptischen Transmission, beobachtet werden.

Ergebnis

Bezüglich der Ausprägung von NPC1-spezifischen pathophysiologischen Merkmalen, spiegeln die generierten IPS-Zellen und deren zellulären Derivate, im Folgenden als NPC1-defiziente Zellen bezeichnet, verschiedene relevante Ausprägungen wider. Hierzu gehört zu allererst die typische Akkumulation von Cholesterol, die mittels Filipinfärbung, in Neurone und Gliazellen nachgewiesen wurde (Abb. 3, s.a. Trilck et al. 2017**,** Figure 3). Im Gegensatz zu Untersuchungen an NPC1-defizienten Mäusen[16], weisen die Neurone allerdings auch Akkumulationen in den Ausläufern und nicht nur in den Zellkörpern auf (Abb. 3, B-D, s.a. Trilck et al. 2017. Figure 1). Als weiterer Unterschied zu Beschreibungen im NPC1-Mausmodell konnten keine auffälligen morphologischen Veränderungen, wie Meganeurite an Neuronen, beobachtet werden[17]. In Übereinstimmung mit murinen Modellen zeigte sich aber eine Anreicherung von GM2, jedoch nur in Neuronen und nicht in Gliazellen (s.a. Trilck et al. 2017, Figure 3). Die Akkumulation der Ganglioside GM2 und GM3 ist ebenso wie die Cholesterolakkumulation als humanes pathologisches Merkmal beschrieben[1], wobei keine Anreicherung von GM3 festgestellt werden konnte. Jedoch zeigten die differenzierten IPS-Zellen eine verringerte Aktivität des katabolen Enzyms Hexoaminodase A (HexA), aber nicht des Enzyms B4GALNT1 (beta-1,4 n-acetylgalactosaminyltransferase 1) auf (s.a. Trilck et al. 2017). Molekulare Docking-Simulationen ergaben, dass Cholesterol in der Lage ist an Hex A zu binden, was als Hinweis darauf gedeutet werden kann, dass Cholesterol den GM2-Abbauweg beeinflusst und anschließend zur Akkumulation von GM2 führt. Diese Vermutung wird durch Arbeiten von Anheuser und Kollegen[18] unterstützt, in denen gezeigt

wurde, dass die Aktivität von HexA durch den Cholesterolgehalt von Zellmembranen beeinflusst werden kann.

Schlussfolgerung

Dies ist die erste Studie die eine Anreicherung von GM2 in neuronalen Derivaten patientenspezifischer IPS-Zellen belegt. Damit wurde für die NPC1-defizienten Zellen ein weiteres humanes pathophysiologisches Merkmal nachgewiesen, welches aufzeigt, dass die patientenspezifischen IPS-Zellen bzw. deren differenzierten Derivate, zur Verwendung als Krankheitsmodell geeignet sind.

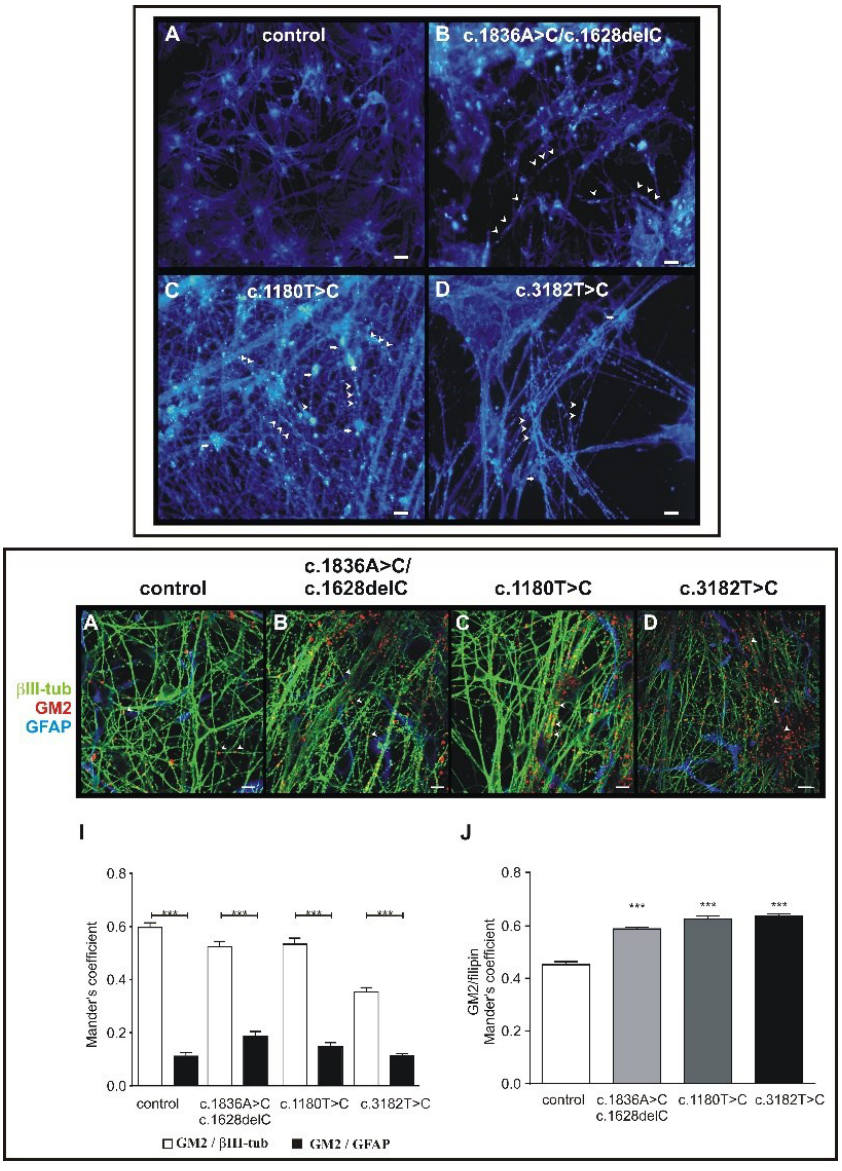

Abbildung 3 Oben: Figure 1 Trilck et al., 2017. Neuronal differenzierte NPC1-defiziente Zellen (B-D) weisen im Gegensatz zu Kontrollzellen (A) verstärkt Chlosterolakkumulationen auf (blau = Filipin). Maßstab: 20 µm **Unten**: Immunzytochmische Färbungen für βIII-Tubulin (grün, A-D), GM2 (rot, A-D) und GFAP (blau, A-D). Kolokalisationsanalysen zeigten, dass GM2 in Neuronen aber nicht in Gliazellen zu finden war (I) und dass GM2 stark mit Filipin kolokalisiert (J). Maßstab: 10 µm.

3.3. Astrogliose in NPC1-defizienten Zellen

*Peter F; Rost S; Rolfs A; **Frech MJ** (2017): Activation of PKC triggers rescue of NPC1 patient specific iPSC derived glial cells from gliosis. Orphanet J Rare Dis; 12(1):145. doi: 10.1186/s13023-017-0697-y. IF 3,45*

Hintergrund

Im zentralen Nervensystem ist die Rolle von Astrogliose nach Schädigungen des Gehirns oder im Zuge von neurodegenerativen Erkrankungen, wie Morbus Alzheimer oder Morbus Parkinson, noch nicht völlig aufgeklärt[19,20]. In Bezug auf NPC1 finden sich in postmortalen Biopsien von NPC1-Patienten ebenso Zeichen von Astrogliose[21–23], wie in murinen NPC1-Zellmodellen[24,25]. Besonders im Kleinhirn ist Astrogliose zu beobachten, wobei deren Beitrag zu den neurodegenerativen Prozessen noch kontrovers diskutiert wird. Es ist nicht abschließend geklärt, ob Astrogliose als Reaktion auf den Verlust der Purkinjezellen auftritt oder zu diesem beiträgt[26–28]. Inwieweit Astrozytenkulturen, die aus NPC1-defizienten IPS-Zellen gewonnen wurden, Astrogliose aufweisen war zum Zeitpunkt der Aufnahme der Untersuchungen nicht bekannt. Ebenso war ungeklärt, ob NPC1-defiziente Astrozyten ähnliche strukturelle Veränderung und Änderungen der Phosphorylierung von Vimentin aufweisen wie patientenspezifische Fibroblasten und ob diese durch die Aktivierung der Proteinkinase C (PKC) rückgängig gemacht werden können.

Ergebnis

Astrogliose ist durch verstärkte Proliferation der Astrozyten gekennzeichnet, die über Proliferationsmarker, wie BrdU oder Ki67 nachgewiesen werden kann. Zudem weisen diese reaktiven Astrozyten einen erhöhten Anteil an den Intermediärfilamenten GFAP und Vimentin auf[29]. In Bezug auf die hier verwendeten NPC1-defizienten Zellen zeigten kombinierte immunzytochemische Färbungen von GFAP, Vimentin und/oder Ki67 einen signifikant erhöhten Anteil an GFAP/Vimentin positiven Zellen ($GFAP^+$-/$Vimentin^+$), sowie von $GFAP^+$-/$Ki67^+$-Zellen (Abb. 4). Zudem war der Gehalt an GFAP und Vimentin in den Zellen erhöht (Abb. 4). Dies belegt, dass die Zellkulturen der NPC1-defizienten Zellen reaktive Astrozyten beinhalten und somit Astrogliose vorlag. Es sei hier vermerkt, dass dies eine intrinsische Eigenschaft der Zellkulturen widerspiegelt und Astrogliose nicht von außen induziert wurde.

Weitere Untersuchungen beschäftigten sich mit der Organisation und dem Phosphorylierungsstatus der Intermediärfilamente GFAP und Vimentin. Diese Studien beruhten auf der Beobachtung, dass Vimentin in NPC1-patientenspezifischen Fibroblasten eine veränderte Organisation und eine Hypophosphorylierung aufzeigten[30,31]. Die Autoren folgerten, dass diese Veränderungen auf einer verminderten Aktivität der Proteinkinase C

(PKC) beruht, die ihrerseits durch die NPC1-typischen Cholesterolakkumulationen bedingt wird[30–32]. Alle NPC1-defizienten Zelllinien zeigten eine veränderte Organisation von GFAP und Vimentin, die in einer ungeordneten Aggregation der Filamente zum Ausdruck kam. Dies ist besonders anschaulich in den Vimentin-Färbungen zu sehen (s.a. Peter et al., 2017, Figure 2). Die Bestimmung der Anteile an phosphoryliertem Vimentin und GFAP mittels Western Blot zeigte signifikant reduzierte Proteinmengen in allen NPC1-defizienten Zelllinien und weist somit auf eine Hypophosphorylierung der Intermediärfilamente hin (Abb. 4). Für NPC1-defiziente Fibroblasten konnte bereits gezeigt werden, dass eine Behandlung mit dem PKC-Aktivator PMA (Phorbol-12-myristat-13-acetat) zu einer erhöhten Phosphorylierung von Vimentin und in der Folge zu einer Normalisierung der Vimentinassemblierung führt[30,31]. In den hier verwendeten NPC1-defizienten Zelllinien wurden vergleichbare Ergebnisse erzielt (Abb. 4). Eine Behandlung der Zellen mit PMA über 24 Stunden resultierte in einer signifikanten Erhöhung der Anteile an phosphoryliertem Vimentin und GFAP (s.a. Peter et al., 2017, Figure 5). Darüber hinaus führte die Behandlung der Zellen mit PMA zu einer signifikanten Reduktion von $GFAP^+$-/$Vimentin^+$-Zellen und $GFAP^+$-/$Ki67^+$-Zellen, d.h. zu einer signifikanten Abschwächung der Astrogliose (s.a. Peter et al., 2017, Figure 4). Ebenso waren die Cholesterolakkumulationen signifikant reduziert (s.a. Peter et al., 2017, Figure 6).

Schlussfolgerung

Die NPC1-defizienten Zelllinien wiesen verschiedene zelluläre Merkmale von Astrogliose auf. Darüber hinaus bewirkt eine Aktivierung der Proteinkinase C, durch PMA, nicht nur eine signifikante Reduktion der Astrogliose sondern auch der Cholesterol- und GM2-Akkumulationen[33]. Zum einen zeigt diese und die unter 3.1 und 3.2 beschriebenen Arbeiten, dass die patientenspezifischen IPS-Zellen verschiedene pathophysiologische Merkmale aufweisen und somit ein zelluläres NPC1-Modellsystem darstellen (*Disease Modelling*). Die Abschwächung dieser Merkmale durch die Anwendung des PKC-Aktivators PMA belegt zudem die Verwendbarkeit im Rahmen der Entwicklung bzw. Erprobung von neuen Wirkstoffen (*Drug Discovery*). Zudem unterstützen diese Untersuchungen die Hypothese einer Beteiligung der Proteinkinase C an den pathophysiologischen Mechanismen von NPC1. Hieraus könnten Entwicklungsmöglichkeiten für zukünftige Therapeutika abgeleitet werden, die auf der Inhibition von Proteinkinasen beruhen.

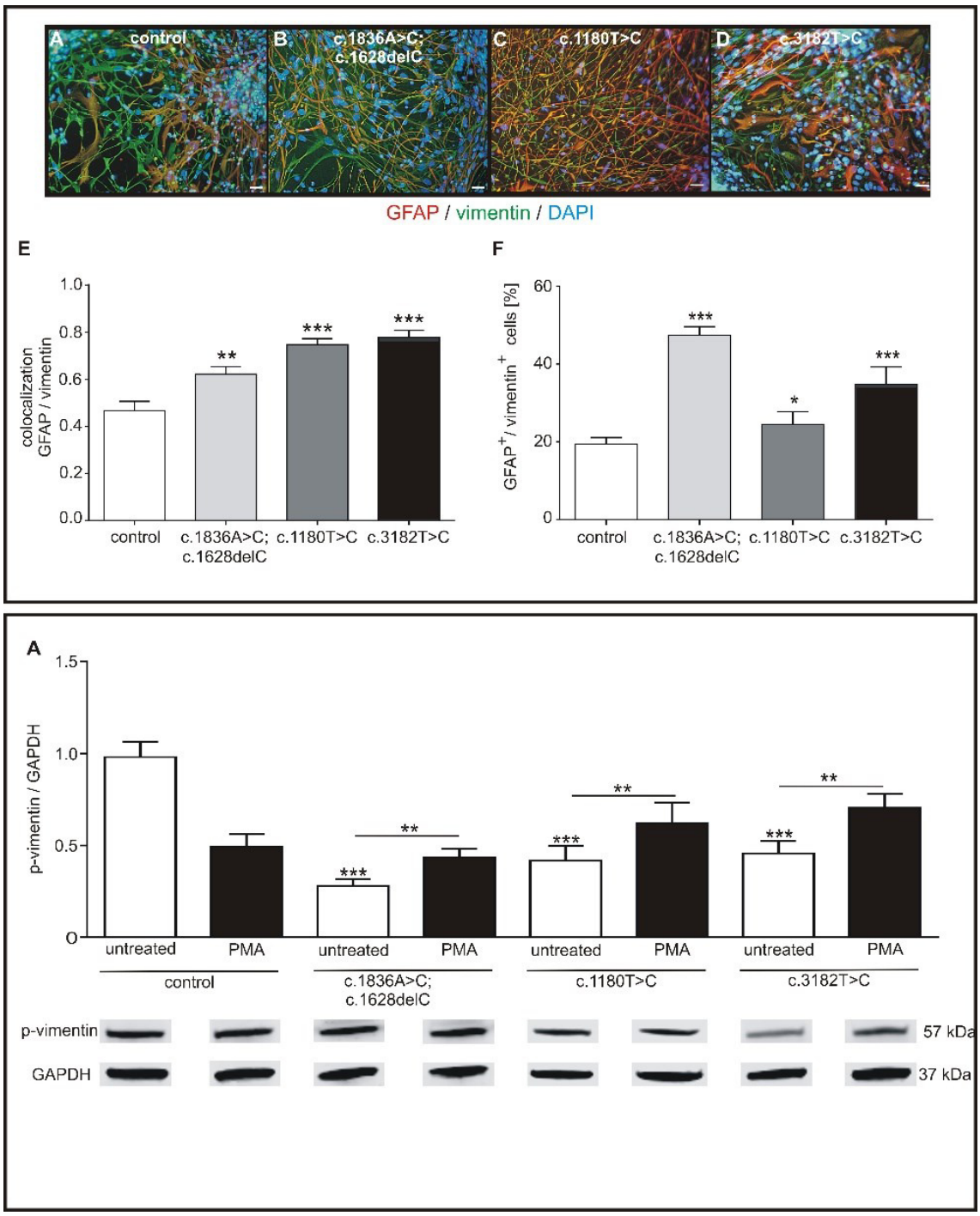

Abbildung 4 **Oben**: Figure 1 verändert aus Peter et al., 2017. Immunzytochemischer Nachweis der Intermediärfilamente GFAP (rot), Vimentin (grün) und Kernfärbung mit DAPI (blau, A-D). Alle NPC1-defizienten Zelllinien zeigten in der Kolokalisationsanalyse (E) und FACS-Analyse einen signifikant erhöhten Anteil an $GFAP^+$-/$Vimentin^+$ -Zellen. Maßstab: 100 µm. **Unten**: Figure 5 verändert aus Peter et al., 2017. Western Blot zur Bestimmung des Anteils an phosphoryliertem Vimentin (p-vimentin). Im Vergleich zur Kontrolllinie war der Gehalt an phosphoryliertem Vimentin in allen NPC1-defizienten Linien signifikant erniedrigt (weiße Balken). Die Behandlung der Zellen mit PMA (schwarze Balken) resultierte in einer Erhöhung von phosphoryliertem Vimentin.

3.4. Funktioneller Phänotyp von NPC1-defizienten Neuronen

Rabenstein M; Peter F; Joost S; Trilck M; Rolfs A; ***Frech MJ*** *(2017): Decreased calcium flux in Niemann-Pick type C1 patient-specific iPSC-derived neurons due to higher amount of calcium-impermeable AMPA receptors. Mol Cell Neurosci; 83:27-36. doi: 10.1016/j.mcn.2017.06.007. IF 3,08*

Hintergrund

Cholesterol ist ein wichtiger Bestandteil der Lipidmembran. In Bezug auf Neurone werden cholesterolreiche Mikrodomänen, sogenannte *Lipid Rafts*, als Bereiche diskutiert in denen unter anderem Ionenkanälen lokalisiert sind[34]. Entzieht man den Zellmembranen Cholesterol, z.B. durch das Lösungsmittel Triton, so führt dies zu Veränderungen in der Aggregation von Glutamat-Rezeptoren und $GABA_A$-Rezeptoren[35]. Daher kann man vermuten, dass eine Störung in der neuronalen Cholesterol-Homöostase, wie sie in NPC1 vorliegt, auch Störungen in der Funktion von Neuronen, beispielsweise in der synaptischen Transmission, nach sich zieht. Veränderungen auf funktioneller Ebene sind in einer Reihe von Arbeiten an murinen NPC1-Modellen beschrieben. Funktionelle Daten über humane NPC1-defiziente Neuronen lagen jedoch nicht vor. Folglich war eine funktionelle Charakterisierung der NPC1-defizienten Neurone Gegenstand weiterer Untersuchungen. Diese umfassten elektrophysiologische Messungen mit Hilfe der Patch-Clamp Technik und mikrofluorimetrische Messungen der intrazellulären Kalziumkonzentration.

Ergebnis

Mit Hilfe von Patch-Clamp-Messungen wurden für Neurone typische spannungsaktivierte und ligandenaktivierte Ionenkanäle untersucht. Die Messungen zeigten in Neuronen aller Zelllinien Ströme auf, die durch spannungsaktivierte Na^+-, K^+- und teils Ca^{2+}-Kanäle vermittelt waren (Abb. 5). Die Stromdichten dieser Ströme waren, im Vergleich der Zelllinien untereinander, ebenso wenig verschieden wie die Membrankapazitäten der Neurone (s.a. Rabenstein et al., 2017, Figure 1). Die Etablierung von chemischen Synapsen konnte durch Messung von postsynaptischen Strömen nachgewiesen werden (Abb. 5). Diese Ergebnisse belegen, dass die Zellen neuronale Netzwerke ausbilden. Ein Vergleich der Netzwerkeigenschaften von NPC1-defizienten Neuronen und Neuronen der Kontrolllinien war jedoch nicht möglich, da die Anzahl der gemessenen postsynaptischen Ströme zu gering war. Unterschiede fanden sich jedoch in den Stromantworten der Neurone auf die Applikation verschiedener Agonisten von Liganden-aktivierten Kanälen[36]. Besonders auffällig war hier eine Reduktion von AMPA-Rezeptor (AMPA-R) vermittelten Strömen. Sowohl die Stromantworten als auch die durch AMPA induzierten Erhöhungen der intrazellulären Ca^{2+}-Konzentration ($Ca^{2+}_{[i]}$), fielen in NPC1-defizienten Zellen geringer aus

(s.a. Rabenstein et al., 2017, Figure 2). Die Ca^{2+}-Permeabilität von AMPA-R wird maßgeblich durch die Stöchiometrie der Untereinheitenzusammensetzung bestimmt, wobei Ca^{2+}-impermeable Rezeptoren die GluA2-Untereinheit beinhalten[37]. Es war daher zu vermuten, dass die reduzierten Ca^{2+}-Ströme auf einen erhöhten Anteil von Ca^{2+}-impermeablen AMPA-R beruhen. Diese Vermutung konnte über die Analyse der GluA2-Proteinmenge bestätigt werden. Wir konnten zeigen, dass NPC1-defiziente Zellen einen erhöhten Anteil an membranständigen GluA2-Untereinheiten besitzen (Abb. 5) und diese somit für die verminderten Ca^{2+}-Einströme verantwortlich waren.

Schlussfolgerung

Patientenspezifische IPS-Zellen können in funktionelle Neurone differenziert werden, was durch die Expression von spannungsaktivierten und ligandenaktivierten Ionenkanäle gezeigt wurde. Des Weiteren sind die Zellen in der Lage, neuronale Netzwerke auszubilden. Ein erhöhter Anteil an Glutamat-Rezeptoren, die die GluA2-Untereinheit beinhalten, resultiert in einem reduzierten Kalziumeinstrom durch AMPA-R. Vergleichbare Ergebnisse die an kortikalen Neuronen eines murinen NPC1-Modells beschrieben wurden, können als Hinweis darauf gewertet werden, dass NPC1-defiziente Neurone Dysfunktionen in der synaptischen Transmission aufweisen und diese zu den pathophysiologischen Mechanismen von NPC1 beitragen.

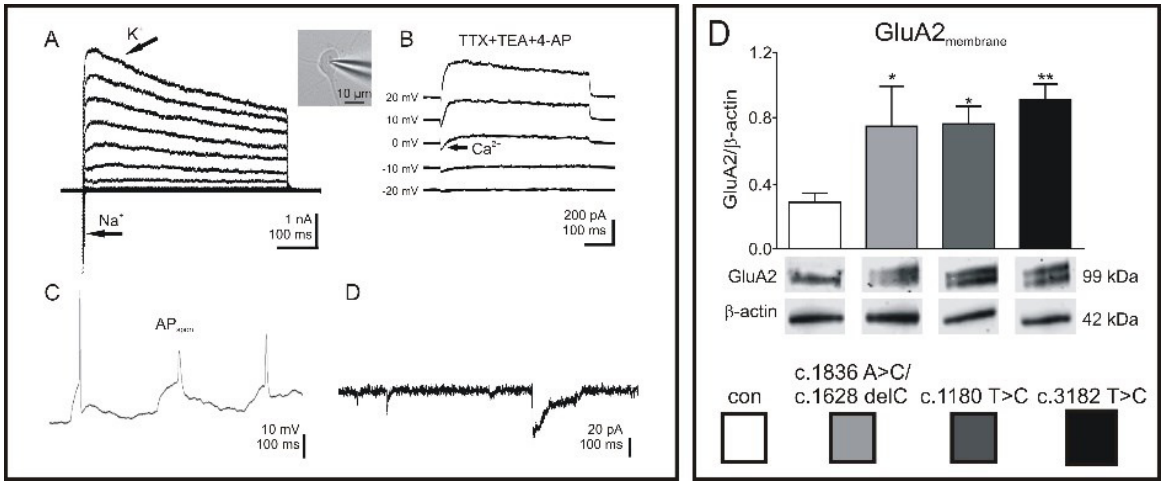

Abbildung 5 Links: Figure 1 verändert aus Rabenstein et al., 2017. Eine eingehende elektrophysiologische Charakterisierung der neuronal differenzierten Zellen zeigte, dass diese typische elektrophysiologische neuronale Merkmale aufweisen. Hierzu gehören durch spannungsaktvierte Na^+- und K^+-Kanäle (A) und Ca^{2+}-Kanäle (B) vermittelte Ströme (A, B), spontane Aktionspotentiale (C) und postsynaptische Ströme (D). **Rechts**: Figure 4 verändert aus Rabenstein et al., 2017. Western Blot Analysen der Expression von GluA2. NPC1-defiziente Zellen zeigten im Gegensatz zur Kontrolllinie signifikant erhöhte Proteinmengen von GluA2 in isolierten Zellmembranen.

3.5. Funktionelle Analyse von Purkinjezellen des NPC1-Mausmodells

*Rabenstein M; Peter F; Rolfs A; **Frech MJ** (2018): Impact of reduced cerebellar EAAT expression on purkinje cell firing pattern of NPC1-deficient Mice. Sci Rep; 8(1):3318. doi: 10.1186/s13023-017-0697-y. IF 4,26*

Hintergrund

Die Untersuchungen zur Aufklärung und Behandlung pathogener Mechanismen von NPC1 greifen auf ein breites Spektrum von Modellsystemen zurück. Bezüglich muriner Modelle ist der Mausstamm $Npc1^{nih}$ (BALB/cNctr-$NPC1^{m1N}$/J) am weitesten verbreitet. Neben einer reduzierten Lebensspanne sind diese Mäuse hauptsächlich durch eine stark ausgeprägte Ataxie gekennzeichnet[38,39], welche auf einem selektiven Absterben von Purkinjezellen des Kleinhirns beruht[40] (s.a. Rabenstein et al., 2018, Figure 1). Die pathogenen Mechanismen die zu diesem Untergang beitragen sind ebenso wenig geklärt wie die Frage, ob Purkinjezellen in NPC1-defizienten Mäusen auf funktioneller Ebene pathophysiologische Veränderungen aufweisen.

GABAerge Purkinjezellen stellen im Kleinhirn die einzigen efferenten Zellen zu nachgeschalteten Regionen des Gehirns, wie den Thalamus, dar. Hierbei zeichnen sich Purkinjezellen durch die Fähigkeit aus, intrinsisch Aktionspotentiale zu generieren. Die Entstehung dieser Feuermuster ist unabhängig von synaptischen Eingängen, wird jedoch durch diese moduliert. Veränderungen in den Feuermustern sind unter anderem für spinozerebelläre Ataxien (spinocerebellar ataxias, SCAs) beschrieben und tragen wahrscheinlich zum Untergang der Purkinjezellen bei. Die bei den SCAs beobachteten Veränderungen beruhen teils auf einer verminderten Expression von βIII-Spektrin. Dieses dient als Ankerprotein für Ionenkanäle und membranständige Transporter der EAAT-Familie (Excitatory Amino Acid Transporter). Somit können Mutationen im βIII-Spektrin bzw. eine verringerte Expression, eine Reduktion von EAAT nach sich ziehen und dies kann zu Veränderungen der intrinsischen Feuermuster der Purkinjezellen führen. Inwieweit Änderungen in der Expression von βIII-Spektrin und/oder EAAT in NPC1-defizienten Purkinjezellen vorliegen und diese zu Veränderungen der intrinsisch generierten Feuermuster führen, war Gegenstand der im Folgenden beschriebenen Untersuchungen.

Ergebnis

Expressionsanalysen mittels Western Blot zeigten veränderte Proteinmengen von βIII-Spektrin und EAAT in Lysaten des Kleinhirns von NPC1-defizienten Mäusen. Es wurden signifikant reduzierte Proteinmenge von βIII-Spektrin und EAAT1, 2 und 4 festgestellt (Abb. 6., s.a. Rabenstein et al., 2018, Figure 2). Inwieweit sich die verringerte Expression

auf die Feuermuster auswirkt, wurde mit elektrophysiologischen Messungen mittels der Patch-Clamp-Technik untersucht. Die Messungen erbrachten verschiedene Feuermuster, nach denen die untersuchten Purkinjezellen in folgende Gruppen eingeteilt wurden. a) tonisch-feuernde Zellen, b) Zellen, die Gruppen von Aktionspotentialen generierten, sogenannte burst oder c) inaktive Zellen, die keine Aktionspotentiale generierten (s.a. Rabenstein et al., 2018, Figure 3). Zunächst konnte in der Verteilung der Feuermuster zwischen Wildtypmäusen ($NPC1^{+/+}$) und NPC1-defizienten Mäusen ($NPC1^{-/-}$) keine Unterschiede festgestellt werden. Da die Aktivität der Purkinjezellen durch EAAT moduliert werden kann und dieser nicht nur als Glutamat-Transporter fungiert, sondern auch eine für Chlorid permeable Ionenpore besitzt, wurde eine erhöhte intrazelluläre Chloridkonzentration ($Cl^-_{[i]}$) verwendet. Dies hat eine Verschiebung des Chloridumkehrpotentials zu einem weniger negativen Wert zur Folge und erhöht somit die Erregbarkeit der Zellen. Unter diesen experimentellen Bedingungen beobachteten wird eine differenzielle Veränderung in der Verteilung der Feuermuster der Purkinjezellen von $NPC1^{+/+}$- und $NPC1^{-/-}$-Mäusen (s.a. Rabenstein et al., 2018, Figure 3), was auf eine Beteiligung von EAAT4 hinweist. Weiterhin beobachteten wir Änderungen in der Verteilung der Feuermuster nach der Applikation von TBOA (threo-β-benzyloxyaspartic acid), einem Antagonisten von EAAT (Abb. 6, s.a. Rabenstein et al., 2018, Figure 4). Die Applikation von TBOA beeinflusste das Feuermuster individueller Purkinjezellen dahingehend, dass z.B. tonisch feuernde Zellen keine Aktionspotentiale mehr generierten oder das Feuermuster änderten und Aktionspotentiale in bursts generierten. Ebenso bewirkte TBOA Änderungen in der Frequenz oder der Länge der bursts. Diese Ergebnisse unterstützen die Annahme, dass EAAT4 zu den beobachteten Effekten beiträgt.

Schlussfolgerung

Ein Vergleich der Feuermuster der Aktionspotentiale von NPC1$^{+/+}$- und NPC1$^{-/-}$-Mäusen zeigte keine Unterschiede auf, wobei jedoch eine Veränderung der intrazellulären Chloridhomöostase in einer veränderten Verteilung der Feuermuster resultierte. Diese Änderungen beruhen wahrscheinlich auf einer verminderten Expression des exzitatorischen Aminosäuretransporter EAAT4, sowie des Ankerproteins βIII-Spektrin. Es bleibt zu klären inwieweit Bergmann-Gliazellen zu dem beobachteten Effekt beitragen, da diese im Kleinhirn exklusiv EAAT1 exprimieren und die Expression von EAAT1 ebenfalls erniedrigt war. Solche Untersuchungen könnten Aufschluss darüber bringen, ob eine Degeneration der Bergmann Gliazellen dem Untergang der Purkinjezellen vorrausgeht oder Folge dessen ist.

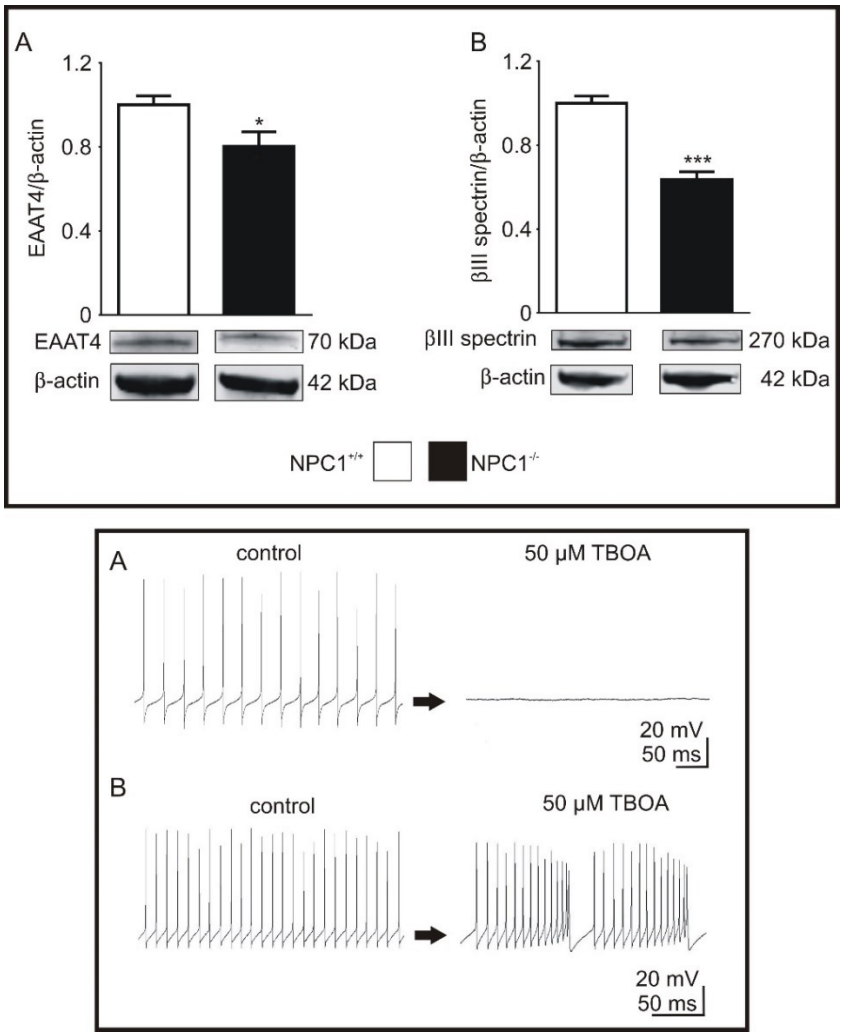

Abbildung 6 Oben: Figure 2 verändert aus Rabenstein et al., 2018. Der Nachweis von EAAT4 und βIII-Spektrin mittels Western Blot zeigte für beide Proteine eine signifikant geringere Menge in Kleinhirnlysaten von NPC1-defizienten Mäusen. **Unten**: Figure 4 verändert nach Rabenstein et al., 2018. Die Applikatoin von TBAO veränderte das Feuermuster individueller Purkinjezellen. Tonisch feuernde Zellen generierten z.B. keine Aktionspotentiale mehr (A) oder wechselten in ein Feuermuster mit bursts (B).

3.6. Zusammenfassung der Ergebnisse der kumulierten Arbeiten

1. Fibroblasten von NCP1-Patienten und gesunden Probanden wurden mittels retroviraler Transfektion von Sox2, Klf4, Oct4 und c-Myc in patientenspezifische IPS-Zellen reprogrammiert.
2. Diese patientenspezifischen IPS-Zellen wurden weiterhin zu neuronalen Progenitorzellen und abschließend in Neurone und Gliazellen differenziert.
3. Die NPC1-defizienten Zellen zeigten NPC1-typische zelluläre Merkmale, wie Akkumulationen von Cholesterol und dem Gangliosid GM2 und Astrogliose. Im Zuge dieser Untersuchungen wurden Veränderungen in der Struktur der Intermediärfilamente Vimentin und GFAP gefunden. Zudem konnten für beide Intermediärfilamente eine Hypophosphorylierung aufgezeigt werden. Diese beruht wahrscheinlich auf einer verminderten Aktivität der PKC. Hierfür spricht der Befund, dass die Hypophosphorylierung durch die Applikation des PKC-Aktivators PMA aufgehoben werden konnte. Ebenso waren eine Abschwächung der Astrogliose und eine Reduktion der Akkumulation von Cholesterol und GM2 zu beobachten.
4. Funktionelle Untersuchungen der neuronal differenzierten Zellen wiesen Veränderungen der synaptischen Transmission bzw. der daran beteiligten Ionenkanäle auf. NPC1-defiziente Neurone des IPS-Zell-basierten Modellsystems zeigten einen verringerten Stromfluss bzw. einen verringerten Anstieg der intrazellulären Ca^{2+}-Konzentration nach Aktivierung von ionotropen Glutamat-Rezeptoren. Diesem Befund liegt eine Anreicherung von Glutamat- Rezeptoren zu Grunde, welche die GluA2-Rezeptoruntereinheit beinhalten und somit nicht permeabel für Ca^{2+} sind.
5. Vergleichende Arbeiten zur synaptischen Transmission in neuronal differenzierten IPS-Zellen und NPC1-defizienten Mäusen befassten sich zunächst mit zerebellären Purkinjezellen, da diese mit fortschreitender Erkrankung zu Grunde gehen. Hier standen zunächst Untersuchungen über die intrinsische Generierung von Aktionspotentialen in Purkinjezellen im Vordergrund. Ein Vergleich der Feuermuster der Aktionspotentiale von $NPC1^{+/+}$- und $NPC1^{-/-}$-Mäusen zeigte keinen Unterschied auf. Eine Veränderung der intrazellulären Chloridhomöostase resultierte jedoch in einer veränderten Verteilung der Feuermuster. Diese Änderungen beruhen wahrscheinlich auf einer verminderten Expression von EAAT1,2 und 4 und/oder βIII-Spektrin.

4. Einordnung der Ergebnisse in den Kontext aktueller Forschung

4.1. Verwendung von IPS-Zellen als NPC1- Krankheitsmodell

Induzierte pluripotente Stammzellen haben sich seit ihrer Erstbeschreibung zu einem unverzichtbaren Ansatz in der Erforschung verschiedenster Erkrankungen und für die Suche nach neuen Wirkstoffen für deren Behandlung erwiesen. Besonders für neurodegenerative Erkrankungen stellen sie einen einzigartigen Zugang zu gewebespezifischen Zellen dar, die sonst nur schwer oder gar nicht verfügbar sind. Die Bedeutung dieser Technologie lässt sich ebenso daran ablesen, dass John Gurdon und Shinya Yamanaka 2012 der Nobelpreis für Medizin verliehen wurde, wie an der stetig wachsenden Anzahl von Publikationen, die auf IPS-Zellen basierende Modellsysteme zum Inhalt haben[13,41]. Dies trifft auch für die Familie lysosomaler Speichererkrankungen, die rund 50 Erbkrankheiten umfasst, zu, für die auf IPS-Zellen basierende Modellsysteme beschrieben sind. Hierzu gehören unter anderem Morbus Fabry, Morbus Gaucher, Morbus Pompe und andere [42]. Bezüglich NPC1 haben wir 2013 ein erstes *in vitro* Modellsystem beschrieben, dem Modellsysteme anderer Arbeitsgruppen folgten[43].

Die erfolgreiche Reprogrammierung von drei patientenspezifischen Fibroblastenlinien in IPS-Zellen zeigt, dass es grundlegend möglich ist, Fibroblasten, die eine Mutation im *NPC1* Gen tragen, zu reprogrammieren. Die so gewonnenen IPS-Zellen weisen typische Pluripotenzmarker auf und können über den Embryoid Body Assay oder den Teratom-Assay in Zellen bzw. Gewebe der drei Keimblätter differenziert werden, was deren pluripotenten Status belegt. Die von neu etablierten NPC1-defizienten Zelllinien weisen als IPS-Zellen, als neurale Progenitorzellen und neuronal differenzierte Zellen die für NPC1 typischen Cholesterolakkumulationen auf. Dies ist ein grundlegendes pathophysiologisches Merkmal von NPC1, das auch für, auf IPS-Zellen basierenden NPC1-Modellsystemen andere Arbeitsgruppen, beschrieben ist[43]. Ein weiterer Vergleich ist hingegen schwierig, da in den Arbeiten anderer Arbeitsgruppen keine eingehendere Beschreibung der Zellen und hier insbesondere eine funktionelle Charakterisierung durchgeführt wurden. Die generierten IPS-Zelllinien weisen pathophysiologische Merkmale auf, die sie mit humanen NPC1-defizienten Fibroblasten oder Zellen aus NPC1-defizienten Mäusen gemeinsam haben. Hierzu gehört neben der Akkumulation von Cholesterol die Akkumulation von GM2[17], Veränderungen in der Struktur des Intermediärfilaments Vimentin, bzw. Veränderungen im Phosphorylierungsstatus von Vimentin[30,31], Gliose[44], Störungen der Autophagie, die in einer erhöhten Expression von autophagosomalen Markerproteinen wie LC3B zum Ausdruck kommen[45,46] sowie Anzeichen oxidativen Stresses[47].

Neben einem Vergleich der phänotypischen Ausprägung der, auf IPS-Zellen basierenden Zelllinien untereinander, mit murinen Modellsystemen oder humanen postmortem Biopsien, ist die Anwendbarkeit [47–49] der Zelllinien im Rahmen der Suche und Erprobung von neuen Wirkstoffen von besonderem Interesse. Für NPC1 stehen hier derzeit verschiedene Behandlungsstrategien im Fokus. Hierzu gehört die Anwendung von Miglustat, einem Inhibitor der Glukosylzeramidsynthase, der für die Behandlung des Morbus Gaucher eingesetzt wird[48,50]. Des Weiteren wird die Anwendung von 2-Hydroxypropyl-β-Cyclodextrin in klinischen Studien erprobt[49]. Weitere, noch experimentelle Ansätze beinhalten die Anwendung von pharmakologischen Chaperonen, die eine Degradation von fehlgefalteten Proteinen im endoplasmatischen Retikulum unterbinden und somit die Menge an funktionalem Protein erhöhen. Erfolgsversprechend haben sich hier Oxysterol-Derivate gezeigt. So konnte mit 25-Hydroxycholesterol eine Reduktion des Cholesterolgehalts und eine Verbesserung des NPC1-Phänotyps in Fibroblasten erzielt werden[51,52]. Vergleichbare Ergebnisse konnten wir an NPC1-defizienten Neuronen erzielen. Die Behandlung der Zellen mit 25-Hydroxycholesterol resultiert in einer Erhöhung des NPC1-Proteingehalts und führt in der Folge zu einer Abschwächung der Cholesterolakkumulationen[53]. Diese Ergebnisse belegen, dass NPC1-defiziente Neurone auf eine Behandlung mit Chaperonen reagieren und eröffnen somit den Zugang für die Suche und Prüfung neuer Wirksubstanzen an einem humanen neuronalen Zellmodell. Vergleichbare Untersuchungen, an solchen Zellmodellen, sind derzeit in der Fachliteratur nicht beschrieben.

Ebenso wird über die Anwendung von Aktivatoren von Proteinkinasen diskutiert, da diese einen positiven Einfluss auf die phänotypische Ausprägung von NPC1 in Zellmodellen haben[54]. Wie unter 3.1 beschrieben, mildert die Behandlung mit dem PKC-Aktivator PMA verschiedene phänotypische Ausprägungen ab. Auch hier beschränken sich Studien in der Fachliteratur auf Untersuchungen an humanen Fibroblasten. Somit stellen die von uns generierten NPC1-defizienten neuronalen Zelllinien und die damit erzielten Ergebnisse eine sehr gute Grundlage für die Aufklärung der pathogenen Mechanismen in betroffenen Zelltypen dar.

4.2. Funktionelle Charakterisierung neuronal differenzierten IPS-Zellen

Eine detaillierte funktionelle Analyse von neuronal differenzierten NPC1 patientenspezifischer IPS-Zellen ist in der Literatur nicht beschriebenen, was einen Vergleich der von uns erzielten Ergebnisse nicht möglich macht. Es ergeben sich jedoch Übereinstimmungen mit Ergebnissen, die an NPC1-defizienten Mäusen erzielt wurden. Hierzu zählen unter anderem Veränderungen der neuronalen Netzwerkaktivität[55] bzw. der synaptischen Transmission[56] und ein erhöhter Anteil an AMPA-Rezeptoren, die die GluA2-Untereinheit enthalten[57]. Dieser, in kortikalen Neuronen beschriebene erhöhte Anteil an membranständigen GluA2-Untereinheiten, beruht wahrscheinlich auf einer gestörten Internalisierung der Rezeptoren[57]. Die Regulation der in der Synapse vorhandenen AMPA-Rezeptoren erfolgt über laterale Diffusion oder Internalisierung der Rezeptoren[37]. Hierbei werden Untereinheiten phosphoryliert. Die Phosphorylierung wird ihrerseits durch Proteinkinasen, wie PKC, reguliert[59]. Es kann daher vermutet werden, dass der gestörten Internalisierung der AMPA-Rezeptoren eine verminderte Funktion von PKC zugrunde liegt. Eine weitere Ursache für die mangelnde Internalisierung könnten Störungen im vesikulären Transport der Rezeptoren in die bzw. aus der Synapse sein, der an Zytoskelettproteine gekoppelt ist. Hier zeigen erste Untersuchungen durch unsere Arbeitsgruppe, dass NPC1-defiziente Zellen des IPS-Zell-basierten Modellsystems, ein verändertes Expressionsprofil der drei Neurofilament-Untereinheiten, NF-L, NF-M und NF-H, aufweisen. Neurofilamente gehören ebenso wie Vimentin und GFAP zur Familie der Intermediärfilamente des Typs III. Dies stellt eine interessante Verbindung zu den Ergebnissen bzgl. der Untersuchungen zur Gliose dar (s. 3.1) in denen wir Änderungen des Phosphorylierungsstatus und der Zusammensetzung der Intermediärfilamente GFAP und Vimentin beschrieben haben. Es ist denkbar, dass Neurofilamente in NPC1-defizienten Neuronen ähnlichen strukturellen Veränderungen unterliegen. Hinzukommt, dass NPC1-defiziente Neurone, des IPS-Zell-basierten Modellsystems, Vimentin exprimieren[33]. Vimentin wird während der Reifung von Neuronen exprimiert, ist an der Stabilisierung von dendritischen Strukturen beteiligt und über die Entwicklung der Neurone hinweg durch Neurofilamente ersetzt[60]. Interessanterweise kann Vimentin aber auch in geschädigten Neuronen gefunden werden. Dies wird in Zusammenhang mit Morbus Alzheimer als *damage-response*- Mechanismus diskutiert, durch den betroffene Neurone versuchen, geschädigte dendritischen Strukturen wieder in Funktion zu setzen[61]. Es ist durchaus denkbar, dass dies auch für NPC1-defiziente Neurone zutrifft.

4.3. Funktionelle Analyse von Purkinjezellen des NPC1-Mausmodells

Purkinje-Zellen stellen den einzigen neuronalen Ausgang aus der Kleinhirnrinde dar. Der Verlust dieser Zellen oder eine Störung ihrer Aktivität führen zu Ataxie, einem wesentlichen klinischen Merkmal von NPC1[1], das auch die Familie der erblichen spinozerebellären Ataxien (spinocerebellar ataxias ‚SCAs) auszeichnet[62,63]. Für die Pathogenese der verschiedenen SCAs wird βIII-Spektrin als gemeinsame Schlüsselkomponente diskutiert[63]. βIII-Spektrin ist in der Aufrechterhaltung von dendritischen Strukturen von Purkinjezellen beteiligt und fungiert als Ankerprotein für Ionenkanäle und EAAT, die wiederum die intrinsische Aktivität der Purkinjezellen modulieren[64]. Es ist daher denkbar, dass die veränderten Feuermuster, die an Purkinjezellen von NPC1-defizienten Mäusen gemessen wurden, auf der verringerten Expression von βIII-Spektrin beruhen, die ihrerseits die verringerte Expression von EAAT1,2 und 4 zur Folge haben könnte. Ein solcher pathogener Mechanismus wird für SCA5 diskutiert, in dem eine verringerte Expression von βIII-Spektrin zum Verlust von EAAT4 führt. Ebenso wurde für SCA5 gezeigt, dass Bergmann-Glia Zellen die Expression von EAAT1 verringern, obwohl sie keinen Verlust von βIII-Spektrin erleiden. Es wird vermutet, dass dies auf einer veränderten Interaktion von Bergmann-Gliazellen und Purkinjezellen beruht. In Bezug auf unsere Ergebnisse aus NPC1-defizienten Mäusen ist dies von Interesse, da wir sowohl eine Reduktion von EAAT1, welches von Bergmann-Gliazellen exprimiert werden, als auch von EAAT4, welches nur von Purkinjezellen exprimiert wird, beschrieben haben. Dies legt den Schluss nah, das sowohl Störungen in der Funktion von Bergmann-Gliazellen als auch von Purkinjezellen an den pathogenen Mechanismen beteiligt sind, die zur Degeneration der Purkinjezellen führen. Die beobachteten Veränderungen der Feuermuster der intrinsisch generierten Aktionspotentiale, könnten auf der verringerten Expression von βIII-Spektrin und einer daraus resultierenden Reduktion der EAAT4-Expressoin beruhen. EAAT4 wird im Kleinhirn nur von Purkinjezellen exprimiert und fungiert nicht nur als Glutamat-Transporter, sondern beinhaltet auch eine Chlorid-permeable Ionenpore. Dies kann den Effekt der erhöhten intrazellulären Chlorid-Konzentration auf die Feuermuster erklären. Durch eine Erhöhung der intrazellulären Chlorid-Konzentration verschiebt das Chlorid-Gleichgewichtspotential. Hierdurch wird der hyperpolarisierende Einfluss von Chlorid auf das Membranpotential verringert und die Erregbarkeit der Zellen erhöht. Dies könnte Exzitotoxizität nach sich ziehen, die auf einem erhöhten Kalziumeinstrom durch spannungsaktivierte Kalziumkanälen oder exzitatorischen Glutamat-Rezeptoren beruht. In diesem Zusammenhang kann auch die beobachtete Reduktion von EAAT1 und 2 gesehen werden. EAAT entfernen Glutamat aus der sub-synaptischen Region und modulieren somit

die synaptische Übertragung. Eine verringerte Expression könnte eine verlängerte Verweildauer von Glutamat in der Synapse zur Folge haben und so zu Änderungen der synaptischen Transmission führen. Hierzu zeigen laufende Untersuchungen zur GABAergen Transmission, dass Purkinjezellen von NPC1-defizienten Mäusen eine erhöhte Frequenz von GABAergen postsynaptischen Strömen aufweisen. Diese GABAergen Eingänge auf die Purkinjezellen werden ihrerseits durch glutamaterge Synapsen moduliert. Eine Aktivierung dieser glutamatergen Synapsen hat in $NPC1^{+/+}$-Mäusen eine Frequenzsteigerung der GABAergen postsynaptischen Ströme zur Folge, in $NPC1^{-/-}$-Mäusen jedoch nicht[65]. Diese ersten Ergebnisse zeigen, dass die synaptische Transmission im Kleinhirn von $NPC1^{-/-}$-Mäusen gestört ist. Wir vermuten, dass diese Störungen auf einer Dysfunktion/Dyslokalisation von Glutamat-Rezeptoren beruhen. Hierfür spricht auch, dass wir in Kleinhirnlysaten eine Hypophosphorylierung von AMPA-Rezeptoren nachweisen konnten, die auf einer Dysfunktion von PKC beruhen könnte. Wir vermuten auf Grunde dieser Ergebnisse und der an den neuronal differenzierten IPS-Zellen erzielten Ergebnisse, dass eine Dysfunktion von Proteinkinasen ein grundlegenden pathophysiologischen Mechanismus von NPC1 darstellt und zu verschiedenen weiteren pathophysiologischen Merkmalen beiträgt.

4.4. Schlussfolgerung

Die Arbeiten an den NPC1-defizienten Mäusen und neuronal differenzierten IPS-Zellen zeigen, wie wertvoll eine Kombination aus *in vitro* und *in vivo* Modellsystemen ist, da eine gemeinsame Betrachtung der jeweiligen Erkenntnisse neue Einblicke in pathophysiologischen Vorgänge ermöglichen. Die an differenzierten IPS-Zellen und an NPC1-defiziente Mäusen erzielten Ergebnisse legen nahe, dass die Phosphorylierung verschiedenster Zielproteine, wie Intermediärfilamente und Ionenkanälen, eine zentrale Rolle in den pathophysiologischen Prozessen einnimmt. So unterliegt z.B. die Stöchiometrie von AMPA-Rezeptoren einer starken, auch aktivitätsabhängigen Regulation[37] und wird über den Austausch der Untereinheiten bestimmt. Hierbei werden Untereinheiten phosphoryliert und anschließend internalisiert. Die Phosphorylierung wird ihrerseits durch Proteinkinasen, wie PKC, reguliert[59]. Es ist daher zu vermuten, dass dem erhöhten Anteil von GluA2-Untereinheiten eine verminderte Funktion von PKC zugrunde liegt. Ebenso könnte die Hypophosphorylierung von Zytoskelettproteinen und die daraus resultierenden Strukturänderungen Einfluss auf die Lokalisation und/oder den Transport von Ionenkanälen nehmen. Zieht man die reduzierten AMPA-Rezeptor vermittelten Ca^{2+}-Ströme in Betracht, so könnte dies wiederum ein negativen Einfluss auf die Aktivität der PKC haben, da diese

durch Ca^{2+} reguliert. Hieraus kann man einen sich selbstverstärkenden Kreislauf ableiten, der zu neurodegenerativen Prozessen beitragen könnte (Abb. 7). Eine solche Rückkopplung könnte sich besonders negativ auf neuronale Strukturen auswirken, die eine hohe Dichte an AMPA-Rezeptoren aufweisen, wie z.B. Dendriten. Morphologische Veränderungen von dendritischen Strukturen sind für neurodegenerative und neuropsychiatrische Erkrankungen beschrieben[66,67]. Weiterhin beschreibt López-Doménech und Kollegen, dass dem Absterben von Neuronen morphologische Veränderungen von Dendriten vorausgehen[68]. Hierbei beruhte die Degeneration der Dendriten auf einem gestörten Transport von Mitochondrien. Dies hat eine mangelnde energetische Versorgung der Dendriten zur Folge und führt zu deren Degeneration, die letztendlich in einem Absterben des gesamten Neurons mündet. Interessanterweise sind für NPC1 morphologische und funktionelle Veränderungen für Mitochondrien beschrieben[69,70]. Man kann hier nur spekulieren ob diese, zusammen mit einem gestörten Transport von Mitochondrien, zu den neurodegenerativen Prozessen in NPC1 beitragen. Vorstellbar wäre ein gestörter Transport, der auf Veränderungen von Filamenten des Zytoskeletts beruht, wie wir sie für Vimentin und GFAP beschrieben haben. Beide Intermediärfilamente sind am vesikulären Transport und dessen Regulation beteiligt[71]. Als weiteren Hinweis auf einen gestörten vesikulären Transport kann die Akkumulation von Autophagosomen herangezogen werden, die in einem murinen NPC1-Modell beobachtet wurde[45,46,72]. Die Autoren dieser Studie vermuten als Ursache einen gestörten Abtransport der Autophagosomen. Eine vergleichbare Erhöhung des Autophagosomen-Markers LC3BII wurde in dem hier beschriebenen IPS-Zell-basierten Zellmodellen beobachtet [73]. Inwieweit an dieser Anhäufung von Autophagosomen eine Störung im Transport dieser beteiligt ist, ist ebenso Gegenstand aktueller Untersuchungen wie die Frage ob auch der Transport anderer Organellen wie Mitochondrien betroffen sein könnte. Erste Ergebnisse zeigen Veränderungen in der Geschwindigkeit und der zurückgelegten Strecke von Mitochondrien auf[74].

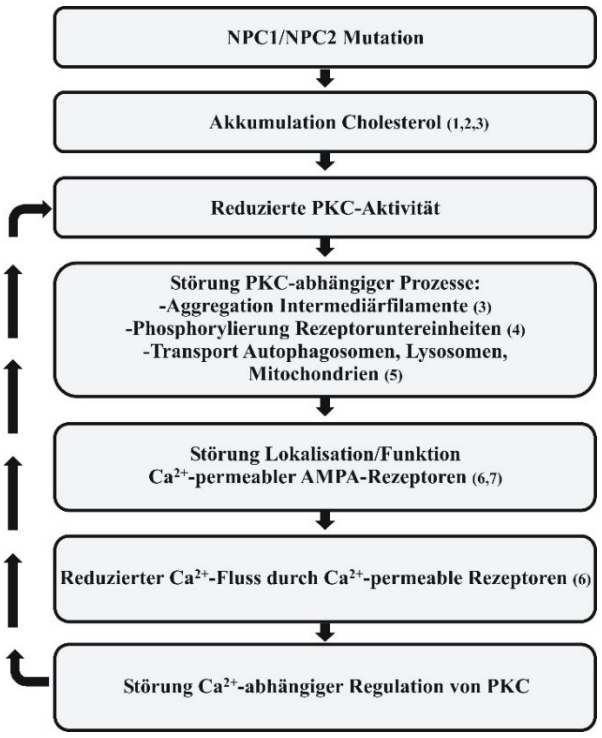

Abbildung 7 Hypothetischer Kreislauf der zu den pathogenen Mechanismen in NPC1 beitragen könnte. Ausgehend von einer reduzierten PKC-Aktivität ergeben sich verschiedene Konsequenzen für PKC-abhängige Prozesse. Unter anderem kann sich eine verminderte Phosphorylierung in Störungen der Funktion und/oder Lokalisation von Ca^{2+}-permeablen Ionenkanälen niederschlagen. Dies kann wiederum die Ca^{2+}-abhängige Regulation von Proteinkinasen beeinträchtigen und somit die Dysfunktion dieser verstärken. Ebenso könnte sich eine Hypophosphorylierung von Zytoskelettproteinen negativ auswirken, da diese an intrazellulären Transportprozessen beteiligt sind. (1) Trilck et al., 2013; (2) Trilck et al. 2017; (3) Peter et al., 2017; (4) Rabenstein et al., 2019; (5) Liedtke et al., 2019; (6) Rabenstein et al., 2017; (7) Feng et al., 2019

Die oben aufgeführten Arbeiten belegen die Etablierung eines humanen zellulären Modellsystems für NPC1, welches Untersuchungen an NPC1-defizienten Neuronen und Gliazellen ermöglicht. Die Ausprägung pathophysiologischer Merkmale *in vitro* gewährleistet weiterführende Untersuchungen auf zellulärer Ebene, die zum besseren Verständnis der pathogenen Mechanismen von NPC1 beitragen werden. Hieraus können Ansätze für die Entwicklung und Überprüfung neuer Interventionsstrategien erarbeitet werden wie z.B. die Anwendung von PKC-Aktivatoren oder die Anwendung pharmakologischer Chaperone. Die funktionellen Untersuchungen im murinen NPC1-Modell legen hierbei die Grundlage für eine *in vivo* Erprobung von Wirkstoffen, z.B. auf zellulärer Ebene, an Purkinjezellen. Die Verwendung von humanen patientenspezifischen IPS-Zellen und NPC1-defizienten Mäusen bietet den Vorteil, die Stärken der jeweiligen Modellsysteme zu kombinieren. Hieraus ergeben sich neue Erkenntnisse über die pathogenen Mechanismen des Morbus Niemann Pick Typ C1, die als Grundlage für einen translationalen Ansatzes zur Behandlung von Patienten dienen können.

5. Literaturverzeichnis

1. Vanier, M. T. Niemann-Pick disease type C. *Orphanet J Rare Dis* **5,** 16; 10.1186/1750-1172-5-16 (2010).
2. Li, X., Saha, P., Li, J., Blobel, G., Pfeffer, S. R. Clues to the mechanism of cholesterol transfer from the structure of NPC1 middle lumenal domain bound to NPC2. *Proc Natl Acad Sci U S A* **113,** 10079–10084; 10.1073/pnas.1611956113 (2016).
3. Li, X., Lu, F., Trinh, M. N., Schmiege, P., Seemann, J., Wang, J., Blobel, G. 3.3 Å structure of Niemann-Pick C1 protein reveals insights into the function of the C-terminal luminal domain in cholesterol transport. *Proc Natl Acad Sci U S A* **114,** 9116–9121; 10.1073/pnas.1711716114 (2017).
4. McKay Bounford, K., Gissen, P. Genetic and laboratory diagnostic approach in Niemann Pick disease type C. *J Neurol* **261,** 569–575; 10.1007/s00415-014-7386-8 (2014).
5. Wasser, C. R., Ertunc, M., Liu, X., Kavalali, E. T. Cholesterol-dependent balance between evoked and spontaneous synaptic vesicle recycling. *J Physiol* **579,** 413–429 (2007).
6. D'Arcangelo, G.,Grossi, D.,,De Chiara, G., de Stefano, M.C.,.Cortese, G.,Citro, G., Rufini, S., Tancredi, V., Merlo, D., Frank, C., D'Arcangelo, G. Glutamatergic neurotransmission in a mouse model of Niemann-Pick type C disease. *Brain Res* **1396,** 11–19 (2011).
7. Avchalumov, Y., Kirschstein, T., Lukas, J., Luo, J., Wree, A., Rolfs, A., Köhling, R. Increased excitability and compromised long-term potentiation in the neocortex of NPC1(-/-) mice. *Brain Res* **1444,** 20–26 (2012).
8. Sun, C. L., Su, L. D., Li, Q., Wang, X. X., Shen, Y. Cerebellar long-term depression is deficient in Niemann-Pick type C disease mice. *Cerebellum* **10,** 88–95; 10.1007/s12311-010-0233-2 (2011).
9. Caporali, P., Bruno, F., Palladino, G., Dragotto, J., Petrosini, L., Mangia, F., Erickson, R. P., Canterini, S., Fiorenza, M. T. Developmental delay in motor skill acquisition in Niemann-Pick C1 mice reveals abnormal cerebellar morphogenesis. *Acta neuropathol commun* **4,** 94; 10.1186/s40478-016-0370-z (2016).
10. Takahashi, K., Yamanaka, S. Induction of pluripotent stem cells from mouse embryonic and adult fibroblast cultures by defined factors. *Cell* **126,** 663–676 (2006).
11. Takahashi, K., Tanabe, K., Ohnuki, M., Narita, M., Ichisaka, T., Tomoda, K., Yamanaka, S. Induction of pluripotent stem cells from adult human fibroblasts by defined factors. *Cell* **131,** 861–872 (2007).
12. Park, I. H., Zhao, R., West, J. A., Yabuuchi, A., Huo, H., Ince, T. A., Lerou, P. H., Lensch, M. W., Daley, G. Q. Reprogramming of human somatic cells to pluripotency with defined factors. *Nature* **451,** 141–146 (2008).
13. Robinton, D. A., Daley, G. Q. The promise of induced pluripotent stem cells in research and therapy. *Nature* **481,** 295–305; 10.1038/nature10761 (2012).
14. Garreta, E., Sanchez, S., Lajara, J., Montserrat, N., Belmonte, J. C. I. Roadblocks in the Path of iPSC to the Clinic. *Curr transplant rep* **5,** 14–18; 10.1007/s40472-018-0177-x (2018).
15. Lee, G., Papapetrou, E. P.,Kim, H., Chambers, S. M., Tomishima, M. J., Fasano, C. A., Ganat, Y. M., Menon, J., Shimizu, F., Viale, A., Tabar, V., Sadelain, M., Studer, L.

Modelling pathogenesis and treatment of familial dysautonomia using patient-specific iPSCs. *Nature* **461,** 402–406 (2009).

16. Karten, B., Vance, D. E., Campenot, R. B., Vance, J. E. Cholesterol accumulates in cell bodies, but is decreased in distal axons, of Niemann-Pick C1-deficient neurons. *J Neurochem* **83,** 1154–1163 (2002).
17. Zervas, M., Dobrenis, K., Walkley, S. U. Neurons in Niemann-Pick disease type C accumulate gangliosides as well as unesterified cholesterol and undergo dendritic and axonal alterations. *J Neuropathol Exp Neurol* **60,** 49–64 (2001).
18. Anheuser, S., Breiden, B., Schwarzmann, G., Sandhoff, K. Membrane lipids regulate ganglioside GM2 catabolism and GM2 activator protein activity. *J Lipid Res* **56,** 1747–1761; 10.1194/jlr.M061036 (2015).
19. Pekny, M., Pekna, M. Reactive gliosis in the pathogenesis of CNS diseases. *Biochim Biophys Acta* **1862,** 483–491; 10.1016/j.bbadis.2015.11.014 (2016).
20. Osborn, L. M., Kamphuis, W., Wadman, W. J., Hol, E. M. Astrogliosis: An integral player in the pathogenesis of Alzheimer's disease. *Prog Neurobiol* **144,** 121–141; 10.1016/j.pneurobio.2016.01.001 (2016).
21. Chiba, Y., Komori, H., Takei, S., Hasegawa-Ishii, S., Kawamura, N., Adachi, K., Nanba, E., Hosokawa, M., Enokido, Y., Kouchi, Z., Yoshida, F., Shimada, A. Niemann-Pick disease type C1 predominantly involving the frontotemporal region, with cortical and brainstem Lewy bodies: an autopsy case. *Neuropathology* **34,** 49–57; 10.1111/neup.12047 (2014).
22. Cologna, S. M., Cluzeau, C. V., Yanjanin, N. M., Blank, P. S., Dail, M. K., Siebel, S., Toth, C. L., Wassif, C. A., Lieberman, A. P., Porter, F. D. Human and mouse neuroinflammation markers in Niemann-Pick disease, type C1. *J Inherit Metab Dis* **37,** 83–92; 10.1007/s10545-013-9610-6 (2014).
23. Yamashita, S. A case of a girl with poor school achievement, ataxia and neurological deterioration. *Neuropathology* **32,** 105–109; 10.1111/j.1440-1789.2011.01230.x (2012).
24. Baudry, M., Yao, Y., Simmons, D., Liu, J., Bi, X. Postnatal development of inflammation in a murine model of Niemann-Pick type C disease: immunohistochemical observations of microglia and astroglia. *Exp Neurol* **184,** 887–903 (2003).
25. Pressey, S. N. R., Smith, D. A., Wong, A. M. S., Platt, F. M., Cooper, J. D. Early glial activation, synaptic changes and axonal pathology in the thalamocortical system of Niemann-Pick type C1 mice. *Neurobiol Dis* **45,** 1086–1100; 10.1016/j.nbd.2011.12.027 (2012).
26. Lopez, M. E., Scott, M. P. Genetic dissection of a cell-autonomous neurodegenerative disorder: lessons learned from mouse models of Niemann-Pick disease type C. *Dis Model Mech* **6,** 1089–1100 (2013).
27. Lopez, M. E., Klein, A. D., Dimbil, U. J., Scott, M. P. Anatomically Defined Neuron-Based Rescue of Neurodegenerative Niemann-Pick Type C Disorder. *J Neurosci* **31,** 4367–4378; 10.1523/JNEUROSCI.5981-10.2011 (2011).
28. Erickson, R. P. Current controversies in Niemann-Pick C1 disease: steroids or gangliosides; neurons or neurons and glia. *J Appl Genet* **54,** 215–224; 10.1007/s13353-012-0130-0 (2013).

29. Hol, E. M., Pekny, M. Glial fibrillary acidic protein (GFAP) and the astrocyte intermediate filament system in diseases of the central nervous system. *Current Opin Cell Biol* **32,** 121–130; 10.1016/j.ceb.2015.02.004 (2015).
30. Walter, M., Chen, F. W., Tamari, F., Wang, R., Ioannou, Y. A. Endosomal lipid accumulation in NPC1 leads to inhibition of PKC, hypophosphorylation of vimentin and Rab9 entrapment. *Biol Cell* **101,** 141–152 (2009).
31. Tamari, F., Chen, F. W., Li, C., Chaudhari, J., Ioannou, Y. A. PKC activation in Niemann pick C1 cells restores subcellular cholesterol transport. *PLoS One* **8,** e74169 (2013).
32. Levin, E. C., Acharya, N. K., Sedeyn, J.C., Venkataraman, V., D'Andrea, M. R., Wang, H. Y., Nagele, R. G. Neuronal expression of vimentin in the Alzheimer's disease brain may be part of a generalized dendritic damage-response mechanism. *Brain Res* **1298,** 194–207 (2009).
33. Peter, F. Untersuchung zur Gliose im Morbus Niemann-Pick Typ C unter Verwendung von induzierten pluripotenten Stammzellen. Inauguraldissertation zur Erlangung des akademischen Grades Doktor der Medizinwissenschaften (Dr. rer. hum) der Universitätsmedizin Rostock (2018).
34. Lingwood, D., Simons, K. Lipid rafts as a membrane-organizing principle. *Science* **327,** 46–50 (2010).
35. Hering, H., Lin, C. C., Sheng, M. Lipid rafts in the maintenance of synapses, dendritic spines, and surface AMPA receptor stability. *J Neurosci* **23,** 3262–3271 (2003).
36. Joost, S. Funktionelle Untersuchungen eines humanen neuronalen in vitro Modells des Morbus Niemann-Pick Typ C1 basierend auf differenzierten patientenspezifischen induzierten pluripotenten Stammzellen. Masterarbeit zur Erlangung des akademischen Grades Master of Science an der Universitätsmedizin Rostock (2014).
37. Henley, J. M., Wilkinson, K. A. Synaptic AMPA receptor composition in development, plasticity and disease. *Nat Rev Neurosci* **17,** 337–350; 10.1038/nrn.2016.37 (2016).
38. Pentchev, P. G., Comly, M. E., Kruth, H.S., Patel, S., Proestel, M., Weintroub, H. The cholesterol storage disorder of the mutant BALB/c mouse. A primary genetic lesion closely linked to defective esterification of exogenously derived cholesterol and its relationship to human type C Niemann-Pick disease. *J Biol Chem* **261,** 2772–2777 (1986).
39. Davidson, C. D., Ali, N. F., Micsenyi, M. C., Stephney, G., Renault, S., Dobrenis, K., Ory, D. S., Vanier, M. T., Walkley, S.U. Chronic cyclodextrin treatment of murine Niemann-Pick C disease ameliorates neuronal cholesterol and glycosphingolipid storage and disease progression. *PLoS One* **4,** e6951 (2009).
40. Lopez, M. E., Klein, A. D., Scott, M. P. Complement is dispensable for neurodegeneration in Niemann-Pick disease type C. *J Neuroinflammation* **9,** 216; 10.1186/1742-2094-9-216 (2012).
41. Shi, Y., Inoue, H., Wu, J. C., Yamanaka, S. Induced pluripotent stem cell technology: a decade of progress. *Nat Rev Drug Discov* **16,** 115–130; 10.1038/nrd.2016.245 (2017).
42. Xu, M., Motabar, O., Ferrer, M., Marugan, J. J., Zheng, W., Ottinger, E. A. Disease models for the development of therapies for lysosomal storage diseases. *Ann N Y Acad Sci* **1371,** 15–29; 10.1111/nyas.13052 (2016).
43. Ordonez, M. P., Steele, J. W. Modeling Niemann Pick type C1 using human embryonic and induced pluripotent stem cells. *Brain Res*; 10.1016/j.brainres.2016.03.007 (2016).

44. German, D. C., Liang, C. L., Song, T., Yazdani, U., Xie,C., Dietschy, J. M. Neurodegeneration in the Niemann-Pick C mouse: glial involvement. *Neurosci* **109,** 437–450; 10.1016/s0306-4522(01)00517-6 (2002).
45. Maetzel, D., Sarkar, S., Wang, H., Abi-Mosleh, L., Xu, P., Cheng, A. W., Gao, Q., Mitalipova, M., Jaenisch, R. Genetic and Chemical Correction of Cholesterol Accumulation and Impaired Autophagy in Hepatic and Neural Cells Derived from Niemann-Pick Type C Patient-Specific iPS Cells. *Stem Cell Reports* **2,** 866–880 (2014).
46. Meske, V., Erz, J., Priesnitz, T., Ohm, T.-G. The autophagic defect in Niemann-Pick disease type C neurons differs from somatic cells and reduces neuronal viability. *Neurobiol Dis* **64,** 88–97; 10.1016/j.nbd.2013.12.018 (2014).
47. Vázquez, M. C., Balboa, E., Alvarez, A. R, Zanlungo, S. Oxidative stress. A pathogenic mechanism for Niemann-Pick type C disease. *Oxid Med Cell Longev* 2012**,** 205713; 10.1155/2012/205713 (2012).
48. Cuisset, J. M., Sukno, S., Trauffler, A., Latour, P., Dobbelaere, D., Michaud, L., Vallée, L. Impact of miglustat on evolution of atypical presentation of late-infantile-onset Niemann-Pick disease type C with early cognitive impairment, behavioral dysfunction, epilepsy, ophthalmoplegia, and cerebellar involvement: a case report. *J Med Case Rep* **10,** 241; 10.1186/s13256-016-1038-9 (2016).
49. Yergey, A. L., Blank, P. S., Cologna, S. M., Backlund, P. S., Porter, F.D., Darling, A.J. Characterization of hydroxypropyl-beta-cyclodextrins used in the treatment of Niemann-Pick Disease type C1. *PLoS One* **12,** e0175478; 10.1371/journal.pone.0175478 (2017).
50. Héron, B., Valayannopoulos, V., Baruteau, J., Chabrol, B., Ogier, H., Latour, P., Dobbelaere, D., Eyer, D., Labarthe, F., Maurey, H., Cuisset, J. M., de Villemeur, T. B., Sedel, F., Vanier, M. T. Miglustat therapy in the French cohort of paediatric patients with Niemann-Pick disease type C. *Orphanet J Rare Dis* **7,** 36; 10.1186/1750-1172-7-36 (2012).
51. Ohgane, K., Karaki, F., Dodo, K., Hashimoto, Y. Discovery of oxysterol-derived pharmacological chaperones for NPC1: implication for the existence of second sterol-binding site. *Chem Biol* **20,** 391–402 (2013).
52. Ohgane, K., Karaki, F., Noguchi-Yachide, T., Dodo, K., Hashimoto, Y. Structure-activity relationships of oxysterol-derived pharmacological chaperones for Niemann-Pick type C1 protein. *Bioorg Med Chem Lett* **24,** 3480–3485 (2014).
53. Völkner, C., Peter F., Liedtke, M., Rabenstein, M., Frech, M. J. Evaluation of potential pharmacological chaperones in a neuronal cell model derived from Niemann-Pick type C1 patient specific induced pluripotent stem cells. *13th Göttingen Meeting of the German Neuroscience Society* (2019).
54. Alkon, D. L. Compositions and methods to treat niemann-pick disease. Available at *https://encrypted.google.com/patents/WO2015148975A1?cl=en* (Google Patents, 2015).
55. Feng, X., Bader, B. M., Yang, F., Segura, M., Schultz, L., Schröder, O. H.,Rolfs, A., Luo, J. Improvement of impaired electrical activity in NPC1 mutant cortical neurons upon DHPG stimulation detected by micro-electrode array. *Brain Res* 10.1016/j.brainres.2018.05.009 (2018).
56. Rabenstein, M., Peter, F., Joost, S., Trilck, M., Rolfs, A., Frech, M. J. Decreased calcium flux in Niemann-Pick type C1 patient-specific iPSC-derived neurons due to higher

amount of calcium-impermeable AMPA receptors. *Mol Cell Neurosci* 10.1016/j.mcn.2017.06.007 (2017).

57. Feng, X., Yang, F., Rabenstein, M., Wang, Z., Frech, M. J., Wree, A., Bräuer, A. U., Witt, M., Gläser, A., Hermann, A., Rolfs, A., Luo, J. Stimulation of mGluR1/5 improves defective internalization of AMPA receptors in NPC1 mutant mouse. *Cereb Cortex*, in Druck (2019).
58. Feng, X., Yang, F., Rabenstein, M., Wang, Z., Frech, M. J., Wree, A., Bräuer, A. U., Witt, M., Gläser, A., Hermann, A., Rolfs, A., Luo, J. Stimulation of mGluR1/5 improves defective internalization of AMPA receptors in NPC1 mutant mouse. *Cereb Cortex*, in Druck (2019).
59. Lee, H. K., Takamiya, K., Han, J. S., Man, H., Kim, C. H., Rumbaugh, G., Yu, S., Ding, L., He, C., Petralia, R. S., Wenthold, R. J., Gallagher, M., Huganir, R. L. Phosphorylation of the AMPA Receptor GluR1 Subunit Is Required for Synaptic Plasticity and Retention of Spatial Memory. *Cell* **112,** 631–643; 10.1016/S0092-8674(03)00122-3 (2003).
60. Kirkcaldie, M. T. K., Dwyer, S. T. The third wave: Intermediate filaments in the maturing nervous system. *Mol Cell Neurosci* **84,** 68–76; 10.1016/j.mcn.2017.05.010 (2017).
61. Levin, E. C., Acharya, N. K., Sedeyn, J. C., Venkataraman, V., D'Andrea, M. R., Wang, H. Y., Nagele, R. G. Neuronal expression of vimentin in the Alzheimer's disease brain may be part of a generalized dendritic damage-response mechanism. *Brain Res* **1298,** 194–207; 10.1016/j.brainres.2009.08.072 (2009).
62. Bird, T. D. *GeneReviews®. Hereditary Ataxia Overview* (Seattle (WA), 1993).
63. Perkins, E., Suminaite, D., Jackson, M. Cerebellar ataxias. B-III spectrin's interactions suggest common pathogenic pathways. *J Physiol* **594,** 4661–4676; 10.1113/JP271195 (2016).
64. Engbers, J. D. T., Fernandez, F. R., Turner, R. W. Bistability in Purkinje neurons: ups and downs in cerebellar research. *Neural Netw* **47,** 18–31; 10.1016/j.neunet.2012.09.006 (2013).
65. Rabenstein, M., Völkner, C., Liedtke, M., Rolfs, A., Frech, M. J. GABAergic Synaptic Input to Cerebellar Purkinje Cells is Affected in a Niemann-Pick Type C1 Mouse Model. *13th Göttingen Meeting of the German Neuroscience Society* (2019).
66. Kulkarni, V. A., Firestein, B. L. The dendritic tree and brain disorders. *Mol Cell Neurosci* **50,** 10–20; 10.1016/j.mcn.2012.03.005 (2012).
67. Fiala, J. C., Spacek, J., Harris, K. M. Dendritic spine pathology: cause or consequence of neurological disorders? *Brain Res Brain Res Rev* **39,** 29–54 (2002).
68. López-Doménech, G., Higgs, N. F., Vaccaro, V., Roš, H., Arancibia-Cárcamo, I. L., MacAskill, A. F., Kittler, J. T. Loss of Dendritic Complexity Precedes Neurodegeneration in a Mouse Model with Disrupted Mitochondrial Distribution in Mature Dendrites. *Cell Rep* **17,** 317–327; 10.1016/j.celrep.2016.09.004 (2016).
69. Yu, W., Gong, J. S., Ko, M., Garver, W. S., Yanagisawa, K., Michikawa, M. Altered cholesterol metabolism in Niemann-Pick type C1 mouse brains affects mitochondrial function. *J Biol Chem.* **280,** 11731–11739 (2005).
70. Woś, M., Szczepanowska, J., Pikuła, S., Tylki-Szymańska, A., Zabłocki, K., Bandorowicz-Pikuła, J. Mitochondrial dysfunction in fibroblasts derived from patients

with Niemann-Pick type C disease. *Arch Biomed Biophys* **593,** 50–59; 10.1016/j.abb.2016.02.012 (2016).

71. Margiotta, A., Bucci, C. Role of Intermediate Filaments in Vesicular Traffic. *Cells* **5**; 10.3390/cells5020020 (2016).
72. Sarkar, S., Carroll, B., Buganim, Y., Maetzel, D., Ng, A. H., Cassady, J. P., Cohen, M. A., Chakraborty, S., Wang, H., Spooner, E., Ploegh, H., Gsponer, J., Korolchuk, V. I., Jaenisch, R. Impaired autophagy in the lipid-storage disorder Niemann-Pick type C1 disease. *Cell Rep* **5,** 1302–1315; 10.1016/j.celrep.2013.10.042 (2013).
73. Liedtke, M. Untersuchungen zur Autophagie in neuronalen Abkömmlingen von NPC1/2 Patienten-spezifischen induzierten pluripotenten Stammzellen. Masterarbeit an der Universitätsmedizin Rostock 2017 (2017).
74. Liedtke, M., Völkner, C., Rabenstein, M., Peter, F., Frech, M. J. Impaired organell transport in a neuronal cell model derived from Niemann-Pick type C1 patient specific induced pluripotent stem cells. *13th Göttingen Meeting of the German Neuroscience Society* 2019 (2019).

6. Publikationsliste

Die in der Habilitationsschrift kumulierten Arbeiten sind *kursiv* aufgeführt.

6.1. Fachartikel mit Impact Factor

1. **Frech MJ**; Deitmer JW; Backus KH (1999): Intracellular chloride and calcium transients evoked by gamma-aminobutyric acid and glycine in neurons of the rat inferior colliculus. J Neurobiol. 40(3):386-396. doi: 10.1002/(SICI)1097-4695(19990905)40:3<386::AID-NEU10>3.0.CO;2-D. IF 2,97
2. Hack I; **Frech MJ**; Dick O; Peichl L; Brandstätter JH (2001): Heterogeneous distribution of AMPA glutamate receptor subunits at the photoreceptor synapses of rodent retina. Eur J Neurosci. 13(1):15-24. doi: 10.1111/j.1460-9568.2001.01357.x. IF 2,94
3. **Frech MJ**; Perez-Leon J; Wässle H; Backus KH (2001): Characterization of the spontaneous synaptic activity of amacrine cells in the mouse retina. J Neurophysiol. 86(4):1632-1643. doi: 10.1152/jn.2001.86.4.1632. IF 2,40
4. Perez-Leon J; **Frech MJ**; Schröder JE; Fischer F; Kneussel M; Wässle H; Backus KH (2003): Spontaneous Synaptic Activity in an Organotypic Culture of the Mouse Retina. Invest Ophthalmol Vis Sci. 44(3):1376-1387. doi: 10.1167/iovs.02-0702. IF 2,22
5. **Frech MJ**; Backus KH (2004): Characterization of inhibitory postsynaptic currents in rod bipolar cells of the mouse retina. Vis Neurosci. 21(4):645-652. doi: 10.1017/S0952523804214134 . IF 1,87
6. Christoph T; Bahrenberg G; de Vry J; Englberger W; Erdmann VA; **Frech MJ**, Kögel B; Rohl T; Schiene K; Schröder W; Seibler J; Kurreck J (2007): Investigation of TRPV1 loss-of-function phenotypes in transgenic shRNA expressing and knockout mice. Mol Cell Neurosci. 37(3):579-589. doi: 10.1016/j.mcn.2007.12.006. IF 3,08
7. Morgan PJ; Ortinau S; Frahm J; Krüger N; Rolfs A, **Frech MJ** (2009): Protection of neurons derived from human neural progenitor cells by veratridine. Neuroreport. 20(13):1225-1229. doi: 10.1097/WNR.0b013e32832fbf49. IF 0,68
8. Schmöle AC; Brennführer A; Karapetyan G; Jaster R; Pews-Davtyan A.; Hübner R, Ortinau S; Beller M; Rolfs A; **Frech MJ**. (2010): Novel indolylmaleimide acts as GSK-3beta inhibitor in human neural progenitor cells. Bioorg Med Chem. 18(18):6785-6795. doi: 10.1016/j.bmc.2010.07.045. IF 2,29
9. Ortinau S; Schmich J; Block S; Liedmann A; Jonas L; Weiss DG, Helm CA; Rolfs A; **Frech MJ** (2010): Effect of 3D-scaffold formation on differentiation and survival in human neural progenitor cells. Biomed Eng Online. 9(1):70. doi: 10.1186/1475-925X-9-70. IF 2,03
10. Giese AK; Frahm J; Hübner R; Luo J; Wree A; **Frech MJ**, Rolfs A; Ortinau S (2010): Erythropoietin and the effect of oxygen during proliferation and differentiation of human neural progenitor cells. BMC Cell Biol. 11(1):94. doi: 10.1186/1471-2121-11-94. IF 2,96
11. Pews-Davtyan A; Tillack A; Schmöle AC.; Ortinau S; **Frech MJ**; Rolfs A; Beller M (2010): A new facile synthesis of 3-amidoindole derivatives and their evaluation as

potential GSK-3beta inhibitors. Org Biomol Chem. 8(5):1149–1153. doi: 10.1039/b920861e. IF 3,23

12. Hübner R; Schmöle AC; Liedmann A; **Frech MJ**; Rolfs, A.; Luo, J. (2010): Differentiation of human neural progenitor cells regulated by Wnt-3a. Biochem Biophys Res Commun. 400(3):358-362. doi: 10.1016/j.bbrc.2010.08.066. IF 1,99
13. Lange C; Mix E.; Frahm J; Glass A; Müller J.; Schmitt O, Schmöle AC; Klemm K; Ortinau S; Hübner R; **Frech MJ**; Wree A; Rolfs A (2011): Small molecule GSK-3 inhibitors increase neurogenesis of human neural progenitor cells. Neurosci Lett. 488 (1):36-40. doi: 10.1016/j.neulet.2010.10.076. IF 2,49
14. Mazemondet O; Hübner R; Frahm J; Koczan D; Bader BM; Weiss DG, Uhrmacher AM; **Frech MJ**; Rolfs A; Luo J (2011): Quantitative and kinetic profile of Wnt/beta-catenin signaling components during human neural progenitor cell differentiation. Cell Mol Biol Lett. 16(4):515-538. doi: 10.2478/s11658-011-0021-0. IF 2,05
15. Yan X; Lukas J.; Witt M; Wree A; Hübner R; **Frech MJ**, Köhling R; Rolfs A; Luo J. (2011): Decreased expression of myelin gene regulatory factor in Niemann-Pick type C 1 mouse. Metab Brain Dis. 26(4):299-306. doi: 10.1007/s11011-011-9263-9. IF 1,83
16. Hovakimyan M; Stachs O; Reichard M; Mascher H; Lukas J; **Frech MJ**; Guthoff R; Witt M; Rolfs A; Wree A (2011): Morphological alterations of the cornea in the mouse model of niemann-pick disease type c1. Cornea. 30(7):796-803. doi: 0.1097/ICO.0b013e3182012a33. IF 1,18
17. Morgan PJ; Liedmann A; Hübner R; Hovakimyan M; Rolfs A; **Frech MJ** (2012): Human Neural Progenitor Cells Show Functional Neuronal Differentiation and Regional Preference After Engraftment onto Hippocampal Slice Cultures. Stem Cells Dev. 21(9):1501-1512. Doi: 10.1089/scd.2011.0335. IF 2,23
18. Morgan PJ; Hübner R; Rolfs A; **Frech MJ** (2013): Spontaneous calcium transients in human neural progenitor cells mediated by transient receptor potential channels. Stem Cells Dev. 22(18):2477-2486. doi: 10.1089/scd.2013.0061. IF 2,23
19. Eisenlöffel C; Schmöle AC; Pews-Davtyan A; Brennführer A; Kuznetsov SA; Hübner R, Frech S; Schult C; Junghanss C; Beller M; Rolfs A; **Frech MJ** (2013): Interference of a novel indolylmaleimide with microtubules induces mitotic arrest and apoptosis in human progenitor and cancer cells. Biochem Pharmacol. 85(6):763-771. doi: 10.1016/j.bcp.2012.12.013. IF 3.19
20. Hovakimyan M; Maass F; Petersen J.; Holzmann C; Witt M; Lukas J, **Frech MJ**; Hübner, R.; Rolfs, A.; Wree, A. (2013): Combined therapy with cyclodextrin/allopregnanolone and miglustat improves motor but not cognitive functions in Niemann-Pick Type C1 mice. Neuroscience. 252:201-211. doi: 10.1016/j.neuroscience.2013.08.001 . IF 3,23
21. *Trilck M; Hübner R; Seibler P; Klein C; Rolfs A; Frech MJ (2013): Niemann-Pick type C1 patient-specific induced pluripotent stem cells display disease specific hallmarks. Orphanet J Rare Dis; 8:144. doi: 10.1186/1750-1172-8-144. IF 3,45*
22. *Trilck M; Peter F; Zheng C; Frank M; Dobrenis K; Mascher H, Rolfs A; **Frech MJ** (2017): Diversity of glycosphingolipid GM2 and cholesterol accumulation in NPC1 patient-specific iPSC-derived neurons. Brain Res; 1657:52-61. doi: 10.1016/j.brainres.2016.11.031. IF 2,75*
23. *Peter F; Trilck M; Rabenstein M; Rolfs A; **Frech MJ** (2017): Dataset in support of the generation of Niemann-Pick disease type C1 patient-specific iPS cell lines carrying*

the novel NPC1 mutation c.1180T>C or the prevalent c.3182T>C mutation – analysis of pluripotency and neuronal differentiation. Data Brief; 12:123-131. doi: 10.1016/j.dib.2017.03.042. z.Z. ohne IF

24. Mußmann C; Hübner R; Trilck M; Rolfs A; **Frech MJ** (2014): HES5 is a key mediator of Wnt-3a-induced neuronal differentiation. Stem Cells Dev. 23(12):1328-1339. doi: 10.1089/scd.2013.0557. IF 2,23
25. Kretzschmar C; Roolf C; Langhammer TS.; Sekora A; Pews-Davtyan A; Beller M; **Frech MJ**; Eisenlöffel C; Rolfs A; Junghanss C (2014): The novel arylindolylmaleimide PDA-66 displays pronounced antiproliferative effects in acute lymphoblastic leukemia cells. BMC Cancer. 14:71. doi: 10.1186/1471-2407-14-71. IF 3,77
26. Narendra Talabattula VA; Morgan PJ; **Frech MJ**; Uhrmacher AM; Herchenröder O; Pützer BM, Rolfs A; Luo J (2017): Non-canonical pathway induced by Wnt3a regulates β-catenin via Pyk2 in differentiating human neural progenitor cells. Biochem Biophys Res Commun. 491(1):40-46. doi: 10.1016/j.bbrc.2017.07.030. IF 2,47
27. *Peter F; Rost S; Rolfs A; **Frech MJ** (2017): Activation of PKC triggers rescue of NPC1 patient specific iPSC derived glial cells from gliosis. Orphanet J Rare Dis; 12(1):145. doi: 10.1186/s13023-017-0697-y. IF 3,45*
28. *Rabenstein M; Peter F; Joost S; Trilck M; Rolfs A; **Frech MJ** (2017): Decreased calcium flux in Niemann-Pick type C1 patient-specific iPSC-derived neurons due to higher amount of calcium-impermeable AMPA receptors. Mol Cell Neurosci; 83:27-36. doi: 10.1016/j.mcn.2017.06.007. IF 3,08*
29. *Rabenstein M; Peter F; Rolfs A; **Frech MJ** (2018): Impact of reduced cerebellar EAAT expression on purkinje cell firing pattern of NPC1-deficient Mice. Sci Rep; 8(1):3318. doi: 10.1186/s13023-017-0697-y. IF 4,26*
30. Feng X, Yang F, Rabenstein M, Wang Z, **Frech MJ**, Wree A, Bräuer AU, Witt M, Gläser A, Hermann A, Rolfs A, Luo J (2019): Stimulation of mGluR1/5 improves defective internalization of AMPA receptors in NPC1, Cereb Cortex, in Druck, IF 5,44
31. Peter F, Völkner F, Liedtke M, Krohn S, Lindner I, Murua Escobar H, Hermann A, **Frech MJ** (2019): Generation of a Niemann-Pick Type C2 patient-derived iPSC line. Stem Cell Res; in Revision, IF 3,93

6.2. Fachartikel z.Z. ohne Impact Factor

1. Liedmann A; Frech S; Morgan PJ; Rolfs A; **Frech MJ** (2012): Differentiation of human neural progenitor cells in functionalized hydrogel matrices. Biores Open Access. 1(1):16–24. doi: 10.1089/biores.2012.0209. z.Z. ohne IF
2. Liedmann A; Rolfs A; **Frech MJ** (2012): Cultivation of human neural progenitor cells in a 3-dimensional self-assembling peptide hydrogel. J Vis Exp. (59):e3830. doi: 10.3791/3830. z.Z ohne IF
3. **Frech MJ**; Rabenstein M; Bovensiepen K; Rost S; Rolfs A (2015): Cyclodextrin Alters GABAergic Input to CA1 Pyramidal Cells in Wild-Type But Not in NPC1-Deficient Mice. Biores Open Access. 4(1):358-362. doi: 10.1089/biores.2015.0023. z.Z. ohne IF

6.3. Übersichtsartikel

1. Schmöle AC; Hübner R; Beller M; Rolfs A; **Frech MJ** (2013): Small Molecules in Stem Cell Research. Curr Pharm Biotechnol. 14(1):36–45. doi: 10.2174/1389201011314010007. IF 2,46
2. Lukas J, Pospech J, Oppermann C, Hund C, Iwanova K, Pantoom S, Petters J, **Frech MJ**, et al., (2019): Role of endoplasmic reticulum stress and protein misfolding in disorders of the liver and pancreas, Adv Med Sci; 64, 315–323; 10.1016/j.advms.2019.03.004, IF 2,08

6.4. Buchkapitel

1. Trilck M; Hübner R; **Frech MJ** (2016): Generation and neuronal differentiation of patient-specific induced pluripotent stem cells derived from Niemann-Pick type C1 fibroblasts. Methods Mol Biol; 1353:233–259. doi: 10.1007/7651_2014_166.

6.5. Patentschriften

1. Beller M; Lukas J; **Frech MJ**; Junghanss C; Rolfs A; Pews-Davtyan A; Eisenlöffel C (2017): Use of maleimide derivatives for preventing and treating leukemia: US9724331.

6.6. Konferenzbeiträge

1. **Frech MJ**, Deitmer JW, Backus KH (1998) GABA and Glycine evoked Ca^{2+} influx into neurons of the rat inferior colliculus; Proceedings of the 26th Göttingen Neurobiology Conference, Göttingen, Germany
2. **Frech MJ**, Pérez-Leon J, Wässle H, Backus KH (1999) Characterization of synaptic currents in mammalian retinal bipolar cells; Proceedings of the 27th Göttingen Neurobiology Conference, Göttingen, Germany
3. Backus KH, **Frech MJ**, Pérez-Leon J (1999) Functionally different inhibitory receptors in retinal bipolar and amacrine cells, Society for Neuroscience 29th Annual Meeting in Miami, USA
4. Backus KH, **Frech MJ**, Kraushaar U (2000) Functionally different inhibitory receptors control signal processing in sensory systems, Jahrestagung der Deutschen Zoologischen Gesellschaft, Bonn, Germany
5. **Frech MJ**, Backus KH (2000) Characterization of inhibitory postsynaptic currents in amacrine cells of the mouse retina, Society for Neuroscience 30th Annual Meeting in New Orleans, USA
6. **Frech MJ**, Schröder J, Kröger S, Backus KH (2002) Altered calcium currents in retinal ganglion cells from agrin-/- mice. 81. Tagung der Deutschen Physiologischen Gesellschaft, Tübingen, Germany
7. Korte SM, **Frech MJ**, Backus KH (2002) Activation of nicotinic acetylcholine receptors enhances GABAergic transmission in the inferior colliculus of the rat, 3rd Forum of European Neuroscience, Paris, France
8. **Frech MJ**, Kögel B, Schiene K, Christoph T (2006) Characterization of a TRPV1 shRNA transgenic mouse model, 5th FENS Forum of European Neuroscience, Vienna, Austria
9. **Frech MJ**, (2006) Automated patch clamping in cardiac safety pharmacology, 4th International Forum Life Science Automation, Rostock/ Warnemünde, oral presentation
10. **Frech MJ**, Ortinau S, Rolfs A (2008) Protection of neurons derived from human fetal mesencephalic progenitor cells by the action of veratridine, 6th Forum of European Neuroscience, Geneva, Switzerland
11. **Frech MJ** (2008) What goes on during neural differentiation – experimental in vitro approaches, 5th Stem Cell School in Regenerative Medicine, Berlin, Germany, oral presentation
12. Morgan P, Frahm J, Ortinau S, Rolfs A, **Frech MJ** (2008) Neuroprotective effect of veratridine on cultured human fetal mesencephalic neural progenitor cells, 6th Stem Cell School in Regenerative Medicine, Berlin, Germany
13. Morgan P, Ortinau S, Rolfs, **Frech MJ** (2009) Neuronal differentiation in a human neural progenitor cell line co-cultured with rat hippocampal brain slices, 7th Stem Cell School in Regenerative Medicine, Odense, Denmark
14. Liedmann A, Jonas L, **Frech MJ**, Rolfs A, Ortinau S (2009) Differentiation and Survival of Human Neural Progenitor Cells in Functionalized 3D Scaffolds, 7th Stem Cell School in Regenerative Medicine, Odense, Denmark
15. Schmöle AC, Brennführer A, Pews-Dayvtan A, Tillack A, **Frech MJ**, Beller M, Rolfs A, Ortinau S (2009) Inhibition of Glycogen Synthase Kinase-3β by novel small

molecules activates Wnt signaling in Human Neural Progenitor Cells, 7th Stem Cell School for Regenerative Medicine, Odense, Denmark

16. Schmöle AC, Brennführer A, Pews-Dayvtan A, Tillack A, **Frech MJ**, Beller M, Rolfs A, Ortinau S (2009) New designed small molecules act as GSK-3 inhibitors in human neural progenitor cells, Wnt Signalling in Development and Disease, Arolla, Switzerland
17. Schmöle AC, Brennführer A, Pews-Dayvtan A, Tillack A, **Frech MJ**, Beller M, Rolfs A, Ortinau S (2009) New designed small molecules canonical as Wnt modulators in human neural progenitor cells, 8th Stem Cell School in Regenerative Medicine, Prague, Czech Republic
18. Karapetyan G, Schmöle AC, Brennführer A, Jaster R, Pews-Davytan A, Hübner R, Ortinau S, Rolfs A, **Frech MJ**, Beller M (2010) The synthesis of novel indolylmaleimides and the biological activity as GSK-3β inhibitors in human neural progenitor cells, Gordon Research Conference - High Throughput Chemistry & Chemical Biology, Les Diablerets, Switzerland
19. Schmöle AC, Maciolek L, Brennführer A, Jaster R, Pews-Davtyan A, Beller M, Rolfs A, **Frech MJ** (2010) Novel indolylmaleimide acts as GSK-3β inhibitor in human neural progenitor cells, 9th Stem Cell School in Regenerative Medicine, Stockholm, Sweden
20. Hübner R, Schmöle AC, Liedmann A, **Frech MJ**, Rolfs A, Luo J (2010) Differentiation of human neural progenitor cells regulated by Wnt-3a, 9th Stem Cell School in Regenerative Medicine, Stockholm, Sweden
21. Liedmann A, Jonas L, Rolfs A, **Frech MJ** (2010) Differentiation and survival of human neural progenitor cells in functionalized 3D scaffolds, 9th Stem Cell School in Regenerative Medicine, Stockholm, Sweden
22. Morgan J, Ortinau S, Rolfs A, **Frech MJ** (2010) Co-culture of human neural progenitor cells with rat hippocampal brain slices: influence of neural environment on differentiation, 9th Stem Cell School in Regenerative Medicine, Stockholm, Sweden
23. Morgan PJ, Rolfs A, **Frech MJ** (2010) Co-culture of human neural progenitors with rat hippocampal brain slices: influence of neural environment on differentiation, 7th FENS Forum of European Neuroscience, Amsterdam, Netherlands
24. Morgan PJ, Ortinau S, Rolfs A **Frech MJ** (2011) Co-culture of human neural progenitor cells with rat hippocampal brain slices: influence of neural environment on differentiation, 9th Göttingen Meeting of the German Neuroscience Society, Göttingen, Germany
25. Liedmann A, Morgan PJ, Rolfs A, **Frech MJ** (2011) Differentiation and Survival of Human Neural Progenitor Cells in self-assembling peptide hydrogel 3D Scaffolds, 9th Göttingen Meeting of the German Neuroscience Society, Göttingen, Germany
26. Trilck M, Hübner R, Seibler P, Klein C, Rolfs A, **Frech MJ** (2013) Generation of Niemann Pick Type C1 patient specific induced pluripotent stem cells, 10th Göttingen Meeting of the German Neuroscience Society, Göttingen, Germany
27. Trilck M, Hübner R, Seibler P, Klein C, Rolfs A. **Frech MJ** (2013), Modeling of Niemann-Pick type C1 disease using patient-specific induced pluripotent stem cells. Michael, Marcia, and Christa Parseghian Scientific Conference for Niemann-Pick Type C Research, South Bend, USA

28. Trilck M, Joost SME, Runge F, Rolfs A, **Frech MJ** (2014), Niemann-Pick Type C1 Patient-Specific Neuronal Cells, Fraunhofer Life Science Symposium Leipzig, Medicinal Stem Cell Products, Leipzig, Germany
29. Runge F, Trilck M, Rolfs A, **Frech MJ** (2015) Regulation of the Cytoskeleton Protein Vimentin Is Altered in Niemann-Pick Type C1 Patient-Specific iPSC Derived Cells, 11th Göttingen Meeting of the German Neuroscience Society, Göttingen, Germany
30. Trilck M, Joost SME, Runge F, Rolfs A **Frech MJ** (2015) Neuronal Differentiation of Niemann-Pick Type C1 patient-specific induced pluripotent stem cells, 11th Göttingen Meeting of the German Neuroscience Society, Göttingen, Germany
31. Rabenstein M, Bovensiepen K, Rolfs A, **Frech MJ** (2015) Cyclodextrin mimics alteration of inhibitory synaptic transmission observed in CA1 pyramidal cells of NPC1 deficient mice, 11th Göttingen Meeting of the German Neuroscience Society, Göttingen, Germany
32. Eisenlöffel C, **Frech MJ**, Rolfs A, Pews-Davtyan A, Beller M, Youssef F, Trantakis C, Nestler U, Merz F, Müller W (2015) PDA66 – a small molecule with broad pre-clinical activity against Glioblastoma, 60th Annual Meeting of the German Society for Neuropathology and Neuroanatomy (DGNN), Berlin Germany
33. Runge F, Trilck M, Rolfs A, **Frech MJ** (2015) Indications for gliosis in Niemann-Pick Type C1 patient-specific iPSC derived glia cells, XII European Meeting on Glial Cells in Health and Disease, Bilbao, Spain
34. Peter F, Rabenstein M, Rolfs A, **Frech MJ** (2016) Gliosis in Niemann-Pick Type C1 Patient-Specific iPSC derived glia cells, 10th FENS Forum of European Neuroscience, Copenhagen, Denmark
35. Rabenstein M, Peter F, Rolfs A, **Frech MJ** (2016) Disturbed intrinsic spontaneous activity of cerebellar purkinje cells in a Niemann-Pick Type C1 mouse model, 10th FENS Forum of European Neuroscience, Copenhagen, Denmark
36. Peter F, Rabenstein F, Rolfs A, **Frech MJ** (2017) Rescue of gliosis in Niemann-Pick Type C1 patient-specific iPSC derived glia cells, 11th Göttingen Meeting of the German Neuroscience Society, Göttingen, Germany
37. Rabenstein M, Peter F, Rolfs A, **Frech MJ** (2017) iPSC derived neurons as a human model to study altered AMPA receptor function in Niemann-Pick Type C1, 11th Göttingen Meeting of the German Neuroscience Society, Göttingen, Germany
38. Rabenstein M, Rolfs A, **Frech MJ** (2017) Impact of altered expression of excitatory amino acid transporter on intrinsic spontaneous activity of cerebellar purkinje cells – possible contribution to the pathophysiology of Niemann-Pick disease Type C1?, Society for Neuroscience Meeting, Washington DC, USA
39. Rabenstein M, Rolfs A, **Frech MJ** (2018) GABAergic Synaptic input to cerebellar purkinje cells is affected in a Niemann-Pick Type C1 mouse model, 11th FENS Forum of European Neuroscience, Berlin, Germany

40. Völkner C, Peter F, Liedtke M, Rabenstein M, **Frech MJ** (2019), Evaluation of potential pharmacological chaperones in a neuronal cell model derived from Niemann-Pick type C1 patient specific induced pluripotent stem cells, 13th Göttingen Meeting of the German Neuroscience Society; Göttingen, Germany
41. Liedtke M, Völkner C, Rabenstein M, Peter F, **Frech MJ** (2019), Impaired organell transport in a neuronal cell model derived from Niemann-Pick type C1 patient specific induced pluripotent stem cells, 13th Göttingen Meeting of the German Neuroscience Society; Göttingen, Germany
42. Rabenstein M, Völkner C, Liedtke M, Rolfs A, **Frech MJ** (2019), GABAergic Synaptic Input to Cerebellar Purkinje Cells is Affected in a Niemann-Pick Type C1 Mouse Model, 13th Göttingen Meeting of the German Neuroscience Society; Göttingen, Germany

7. Erklärungen

Hiermit erkläre ich, Dr. phil. nat. Moritz Johannes Frech, dass die vorliegende Arbeit von mir selbstständig und ohne fremde Hilfe sowie nur unter Benutzung der angegebenen Quellen und Hilfsmittel erstellt worden ist. Die den benutzten Werken wörtlich oder inhaltlich entnommenen Stellen sind als solche kenntlich gemacht.

Ich versichere weiterhin, dass diese Arbeit nicht vorher und auch nicht gleichzeitig bei einer anderen als der genannten Fakultät zur Eröffnung des Habilitationsverfahrens eingereicht worden ist.

Weiterhin erkläre ich, dass ich die deutsche Staatsbürgerschaft besitze und mir die Bestimmungen der Habilitationsordnung bekannt sind und von mir anerkannt werden.

Rostock den, 14 August 2019 Dr. Moritz Johannes Frech

8. Sonderdrucke der zitierten Originalarbeiten

ORPHANET JOURNAL OF RARE DISEASES

RESEARCH Open Access

Niemann-Pick type C1 patient-specific induced pluripotent stem cells display disease specific hallmarks

Michaela Trilck[1†], Rayk Hübner[1†], Philip Seibler[2], Christine Klein[2], Arndt Rolfs[1] and Moritz J Frech[1*]

Abstract

Background: Niemann-Pick type C1 disease (NPC1) is a rare progressive neurodegenerative disorder caused by mutations in the NPC1 gene. In this lysosomal storage disorder the intracellular transport and sequestration of several lipids like cholesterol is severely impaired, resulting in an accumulation of lipids in late endosomes and lysosomes. The neurological manifestation of the disease is caused by dysfunction and cell death in the central nervous system. Several animal models were used to analyze the impaired pathways. However, the underlying pathogenic mechanisms are still not completely understood and the genetic variability in humans cannot be reflected in these models. Therefore, a human model using patient-specific induced pluripotent stem cells provides a promising approach.

Methods: We reprogrammed human fibroblasts from a NPC1 patient and a healthy control by retroviral transduction with Oct4, Klf4, Sox2 and c-Myc. The obtained human induced pluripotent stem cells (hiPSCs) were characterized by immunocytochemical analyses. Neural progenitor cells were generated and patch clamp recordings were performed for a functional analysis of derived neuronal cells. Filipin stainings and the Amplex Red assay were used to demonstrate and quantify cholesterol accumulation.

Results: The hiPSCs expressed different stem cell markers, e.g. Nanog, Tra-1-81 and SSEA4. Using the embryoid body assay, the cells were differentiated in cells of all three germ layers and induced teratoma in immunodeficient mice, demonstrating their pluripotency. In addition, neural progenitor cells were derived and differentiated into functional neuronal cells. Patch clamp recordings revealed voltage dependent channels, spontaneous action potentials and postsynaptic currents. The accumulation of cholesterol in different tissues is the main hallmark of NPC1. In this study we found an accumulation of cholesterol in fibroblasts of a NPC1 patient, derived hiPSCs, and neural progenitor cells, but not in cells derived from fibroblasts of a healthy individual. These findings were quantified by the Amplex Red assay, demonstrating a significantly elevated cholesterol level in cells derived from fibroblasts of a NPC1 patient.

Conclusions: We generated a neuronal model based on induced pluripotent stem cells derived from patient fibroblasts, providing a human *in vitro* model to study the pathogenic mechanisms of NPC1 disease.

Keywords: Niemann-Pick Type C1, Induced pluripotent stem cells, Lysosomal storage disorder, Neural progenitor cells, Neural differentiation

* Correspondence: moritz.frech@med.uni-rostock.de
†Equal contributors
[1]Albrecht-Kossel-Institute for Neuroregeneration (AKos), University of Rostock, Gehlsheimer Strasse 20, D-18147 Rostock, Germany
Full list of author information is available at the end of the article

Background

Human induced pluripotent stem cells (hiPSCs) feature three major advantages in the field of stem cell research. First, cells can be obtained by reprogramming different somatic cells [1-4] without raising ethical concerns, as it is the case with embryonic stem cells. Second, the pluripotent potential of the cells offers the opportunity to differentiate them into each cell of the body, e.g. motor neurons [5], cardiomyocytes [6], pancreatic insulin-producing cells [7], or male germ cells [8]. Third, iPS cells and subsequently differentiated cells have the same genetic information as the donor cells. Different diseases have already been modeled by using human iPS cells, e.g. Parkinson disease [9], metabolic liver disorders [10], retinal degeneration [11], Huntington disease [12], and mucopolysaccharidosis type IIIB, a fatal lysosomal storage disorder [13], and have been successfully utilized e.g. in drug screening [14].

Taken together, these characteristics of the cells are excellent prerequisites to model diseases *in vitro*. However, no *in vitro* model for Niemann-Pick disease Type C1 (NPC1) based on hiPS cells is currently available. NPC1 is a rare progressive neurodegenerative disease caused by mutations in the NPC1 gene located on chromosome 18q11 encoding for a 1278-amino acid intracellular membrane glycoprotein [15-17]. It is inherited in an autosomal recessive manner and shows a prevalence of 1:120.000 live births [18]. A mutation in the NPC1 gene leads to an impaired lipid transport and sequestration resulting in e.g. a cholesterol accumulation in the late endosome and lysosome [19]. The clinical manifestation varies from neonatal icterus and hepatosplenomegaly in early childhood, cerebellar ataxia, seizures, gelastic cataplexy, and vertical supranuclear palsy in adolescence, to progressive neurological degradation, psychoses, and dementia in adulthood [18]. The symptoms are diverse and show intrafamilial variability [18,20].

The pathogenic mechanisms ultimately leading to a massive degeneration and loss of neurons in the CNS, especially Purkinje cells in the cerebellum, are not exactly understood. Most of our knowledge regarding NPC1 is based on cell models like human fibroblasts [21-23] and animal models like mouse [24], cat [25], and fruit fly [26]. Studies using these models have neither revealed the mechanisms leading to the selective massive degeneration of neurons nor found drugs, which can efficiently halt disease progression. Although the function of NPC1 in lipid trafficking is evolutionary highly conserved [27], the widely used murine BALB/c NPC1 model [28] cannot exactly reproduce human pathology. For example, neurofibrillary tangles composed of tau protein, which are seen in human NPC1 neurons, are absent in this model reflecting obvious biochemical and physiological differences [29]. Thus, studies utilizing disease-specific human neurons hold great promise to significantly increase our knowledge in understanding the pathological mechanism leading to massive neuronal degeneration. Recently, a human neuronal NPC1 model was reported based on multipotent adult stem cells [30].

In our study, we generated patient-specific induced pluripotent stem cells from a NPC1 patient and a healthy individual. The hiPS cell lines were differentiated into neural progenitor cells and subsequently differentiated into functional neurons to gain a human neuronal model of NPC1 disease.

Methods

Cell culture

Human dermal fibroblast cell lines GM18436 and GM05659 (Coriell Institute for Medical Research, Camden, USA) were obtained by skin biopsies from one-year old male Caucasian donors. GM18436 exhibits compound heterozygous mutations in the NPC1 gene (c.1628delC and GLU612ASP), representing a frameshift mutation and a missense mutation, respectively. The mutations lead to a non-functional protein as demonstrated by cholesterol esterification assay [31]. Fibroblast cell line GM05659 is obtained from a healthy donor. In the following cells of the cell line GM18436 will be referred to as mutNPC1 and cells of the cell line GM05659 will be referred to as wtNPC1. Cells were cultivated in fibroblast medium containing DMEM high glucose, 10% FBS and 1% Penicillin/ Streptomycin. Mitotically inactivated mouse embryonic fibroblasts (GlobalStem, Rockville, USA) were used as the feeder cell layer for hiPSCs. Cells were plated in fibroblast medium at a density of 33.000 cells/ cm^2 onto 0.1% gelatine coated wells in fibroblast medium 24 h before hiPS cell split. HiPS cells were cultured on a feeder cell layer in iPS medium containing DMEM/ F12, 20% knockout serum replacement, 1% Penicillin/ Streptomycin, 1% GlutaMAX, 1% MEM non essential amino acids, 0.2% 2-mercaptoethanol, and 10 to 15 ng/ ml hFGF-2 (Globalstem, Rockeville, USA). hiPS cells on matrigel (BD Biosciences, Heidelberg, Germany) were cultured in mTESR1 medium (Stemcell Technologies, Grenoble, France). Medium was changed daily and cells were passaged weekly using 10 μM ROCK inhibitor Y-27632 (Stemgent, Cambridge, USA) for increased plating efficiency. HiPS cells growing on a feeder cell layer were split mechanically weekly using pulled glass hooks by performing the cut and paste technique. Cells growing on matrigel were harvested enzymatically using 1 mg/ ml dispase (Stemcell Technologies, Grenoble, France) for 7 min and large bore tips to break down large clumps according to manufacturer's recommendations. HEK293FT cells (Invitrogen, Darmstadt, Gemany) used to obtain the viral vectors were cultivated in fibroblast

medium without Penicillin/ Streptomycin. All cells were cultivated at 37°C in a saturated humidity atmosphere containing 5% CO_2.

Generation of retroviruses

Retroviral pMIG vectors containing the cDNA of the human genes Oct4, Sox2, Klf4, and c-Myc were used as described recently [32]. Briefly, 3×10^6 HEK293FT cells per 10 cm-dish were seeded onto ten dishes and incubated overnight. A solution containing 2.5 μg retroviral vector encoding for GFP and one of the transcription factors (Sox2, Klf4, Oct4, or c-Myc) was incubated with 0.25 μg VSV-G and 2.25 μg Gag-Pol in X-tremeGENE9 (Roche, Mannheim, Germany)/ DMEM High Glucose mixture (1:4) which was added to each of the dishes. Medium was renewed after 18 h and cells were incubated further for 48 h. Subsequently, the virus-containing medium was collected and passed through a 0.45 μm filter. To concentrate the virus, the medium was centrifuged at 70.000 × g at 4°C for 90 min, resuspended in 0.1 to 1 ml DMEM medium, and stored at −80°C. All four vectors contained a GFP sequence thus enabling titering by determining the percentage of GFP positive HEK293FT cells using FACS. Therefore, 1×10^5 HEK293FT cells were seeded per 12-well in Penicillin/ Streptomycin free fibroblast medium containing 5 μg/ ml protamine sulfate and concentrated virus in the following volumes: 6.25 μl, 12.5 μl, 25 μl, and 50 μl. After 48 h cells were washed with PBS containing Ca^{2+}/ Mg^{2+}, trypsinized and centrifuged for 5 min at 500 × g. Pellet was resuspended in 100 μl PBS without Ca^{2+}/ Mg^{2+} and fixed by adding 100 μl of 4% paraformaldehyde for 15 min. Afterwards, the percentage of GFP positive cells was determined via FACS analysis.

Transduction of human fibroblasts

For transduction, 1×10^5 fibroblasts were seeded per cavity of a 6-well plate and cultured for 18 h in fibroblast medium without Penicillin/ Streptomycin. Afterwards, fibroblast medium without Penicillin/ Streptomycin was supplemented with a volume of retrovirus of Sox2, Oct4, Klf4 (corresponding to 70 – 80% infection efficiency), and c-Myc (corresponding to 40–50% infection efficiency) in the presence of 5 μg/ ml protamine sulfate. Cells were incubated for 48 h. Subsequently, medium was aspirated and cells were washed twice with PBS containing Ca^{2+}/ Mg^{2+}. Transduced cells were trypsinized and reseeded onto a gelatin coated 6 cm-dish. The next day, medium was replaced with iPS medium supplemented with 0.5 mM valproic acid to further increase the efficiency of reprogramming. Medium was changed daily and valproic acid was omitted after seven days.

Generation of hiPS cell lines

Initial hiPS colonies were routinely observed after three to four weeks. For further cultivation, they were picked using a 100 μl pipette tip and a pulled glass hook. Single colonies were transferred to the cavities of a 24-well plate, coated with 0.1% gelatin and 45.000 feeder cells/ cm^2. After 4 to 7 days of proliferation hiPS colonies were mechanically divided into two to four pieces and further expanded. Within six weeks each single hiPS colony was expanded to obtain different clones.

Karyotyping

Karyotyping was performed by Giemsa Trypsin banding. In short, colonies were incubated with a colcemid solution (10 μg/ ml in HBSS) for three hours to arrest cells in metaphase. Cells were treated with trypsin (0.25%) and the enzymatic reaction was stopped with Amniomax solution (Invitrogen, Darmstadt, Germany). Cells were centrifuged at 300 × g for 10 min and the pellet was resuspended in 4 ml hypotonic potassium chloride solution (5.62%). Cells were incubated for 5 min at 37°C and centrifuged at 300 × g for 10 min. The cells were resuspended and fixed in 5 ml glacial acetic acid and methanol (1:3) and subsequently centrifuged for 7 min at 350 × g. This step was repeated once. Finally, most of the supernatant was removed and cells were resuspended. Cell suspension was dropped onto cold slides and dried at 100°C for 1 h. Giemsa solution (5%) was added and incubated for 5 min. Slides were washed in distilled water two times, dried at room temperature and sealed with cover slips.

Sequencing

Genomic DNA of fibroblasts, iPS cells grown on matrigel or neural progenitor cells were isolated using AllPrep Kit (Qiagen, Hilden, Germany) according to the manufacturer's recommendations. Exon regions were amplified using HotStart Taq (Qiagen, Hilden, Germany) as follows: 95°C for 15 min followed by 13 cycles of 94°C for 30 s, 66°C for 30 s with 1.5°C decrease/ cycle and 72°C for 20 s; followed by 8 cycles of 94°C for 30 s, 46.5°C for 30 s with 1°C increase/ cycle and 72°C for 20 s; followed by 13 cycles of 94°C for 30 s, 66°C for 30 s with 1.5°C decrease/ cycle and 72°C for 20 s; followed by 11 cycles of 94°C for 30 s, 54.5°C for 30 s with 1°C increase/ cycle and 72°C for 20 s. Products were purified using ExoSAP Kit (USB Europe GmbH, Staufen, Germany) according to manufacturer's recommendations. Sequence analysis was performed on a 3130XL Genetic Analyzer (Applied Biosystems, Carlsbad, USA).

Alkaline phosphatase staining

HiPSCs were cultivated on a feeder cell layer for five days. Medium was removed, cells were washed with PBS

and fixed with ice-cold methanol (100%) for 10 min at −20°C. Methanol was removed and cells were washed with PBS. Subsequently, cells were incubated at room temperature for 15 min with the staining solution: 75% distilled water, 10% sodium chloride solution (1 M), 10% Tris solution (1 M, pH 9.8), 5% magnesium chloride solution (1 M), and NBT/ BCIP solution (1:50, Roche, Mannheim, Germany). Staining solution was removed and cells were washed with distilled water. Microphotographs were taken using a Nikon Eclipse TS100 (Nikon, Düsseldorf, Germany).

Immunocytochemistry

Cells were fixed at room temperature for 15 minutes in 4% paraformaldehyde, washed with PBS and stored in 0.02% NaN_3 at 4°C. Immunocytochemistry was performed for Nanog (1:100, rabbit IgG polyclonal), Oct4 (1:100, rabbit IgG polyclonal), SSEA3 (1:100, rat IgM), SSEA4 (1:100, mouse IgG_3), Tra-1-60 (1:100, mouse IgM), Tra-1-81 (1:100, mouse IgM, all Stemgent, Cambridge, USA), Smooth muscle actin (SMA, 1:50, mouse monoclonal, Dako, Glostrup, Denmark), alpha fetoprotein (alpha FP, 1:500, mouse monoclonal IgG, Sigma-Aldrich, Hamburg, Germany), Nestin (1:100, mouse monoclonal, R&D, Wiesbaden, Germany), MAP2ab (1:100, mouse monoclonal, Chemicon, Schwalbach, Gemany), Tuj1 (1:100, mouse monoclonal Tu-20, Santa Cruz biotechnology, Heidelberg, Germany) and Sox-2 (1:200, rabbit monoclonal, Abcam, Cambridge, UK). Blocking and permeabilization was carried out using 0.3% Triton X-100 and 5% normal goat serum (Dako, Glostrup, Denmark) for 30 min at room temperature. Cells were incubated with primary antibodies for 3 hours at room temperature in 1% normal goat serum, followed by three washing steps with PBS. Alexa Fluor 568 (1:1000, goat anti-mouse IgG or goat anti-rabbit IgG, Invitrogen, Darmstadt, Germany), Alexa Fluor 488 (1:1000, goat anti-mouse IgG or goat anti-rabbit IgG, Invitrogen, Darmstadt, Germany), or Alexa Fluor 488 (1:1000, goat anti-mouse IgM or goat anti-rat IgM, Invitrogen, Darmstadt, Germany) were used as secondary antibodies, incubated 1 h at room temperature with 1% normal goat serum in PBS. After washing with PBS, cells were stained with DAPI (5 minutes, 250 ng/ ml), washed three times and mounted with Mowiol-DABCO mounting medium. Pictures were taken with a Biozero 8000 microscope system (Keyence, Hamburg, Germany).

Generation of embryoid bodies

To generate embryoid bodies (EBs), whole hiPS colonies were mechanically lifted off the feeder cell layer and transferred into a 15 ml conical tube. Once the colonies settled at the bottom of the conical tube, the medium was removed and 5 ml of differentiation medium, containing knockout DMEM, 20% FBS, 1% MEM non-essential amino acids, 2 mM GlutaMAX, and 0.1 mM beta-mercaptoethanol, was added. Afterwards, colonies were transferred into the cavity of a low attachment 6-well plate and incubated at 37°C/ 5% CO_2. Medium was changed every second day until EBs were formed. After five to seven days EBs were transferred onto gelatin coated glass cover slips and supplied with differentiation medium. Once EBs were attached, medium was changed every second or third day. After 10 days of random differentiation, spread cells were washed with PBS and fixed with 4% PFA for 15 min. Fixed cells were washed with PBS and immunocytochemical stainings for nestin (ectoderm), smooth muscle actin (mesoderm), and alpha-fetoprotein (endoderm) were performed.

Teratoma formation assay

Immunodeficient (SCID) hairless mice (Charles River Laboratories, Sulzfeld, Germany) were used for the teratoma formation assay. HiPSCs for injection were cultured on feeder cells in 6-well culture plates. For each injection the amount of 3 cavities of a 6-well culture plate were collected mechanically and centrifuged for 2 min at 200 × g. The pellet was resuspended in 1 ml of 0.25% trypsin/ EDTA. After 1 min, the reaction was stopped by adding 2 ml of fibroblast medium and centrifuged again for 2 min at 200 × g. Cells were resuspended in 140 μl of cold DMEM/ F12 and stored on ice. Directly before injection, cell suspension was mixed with 60 μl matrigel. Cells were injected subcutaneously into the flank of the hind limb. After 8–12 weeks, when tumors were clearly visible, the animals were sacrificed and tumors were removed. Tumor tissue was fixed in 4% formalin for 12 to 18 hours and embedded in paraffin for subsequent staining.

H&E staining of tumor sections

4 μm thick tumor tissue sections were deparaffinized in xylol for 10 min and a descending ethanol concentration for 5 min each. Afterwards, the sections were washed in distilled water and stained with Mayers hematoxylin (Merck, Darmstadt, Germany) for 1 min. Next, the tissue was washed two times in distilled water and stained with eosin Y (Sigma-Aldrich, Hamburg, Germany) for 2 min. The slides were washed again twice and then dehydrated using an ascending ethanol concentrattion and xylol. Slides were mounted in Mowiol-DABCO. Microphotographs were taken with a Biozero 8000 microscope system (Keyence, Hamburg, Germany).

Neural differentiation

To differentiate hiPS colonies into neural direction, the colonies were cut, transferred to Poly-L-ornithine

(15 μg/ ml)/ laminin (10 μg/ ml) coated dishes, and cultivated for 10 days in medium consisting of Neurobasal, DMEM/ F12, 1xN2 supplement, 1xB27 supplement, GlutaMAX (2 mM) complemented with mouse recombinant noggin F_c-chimera (500 ng/ ml, R&D, Wiesbaden, Germany), SB431542 (20 μM, Sigma-Aldrich, Hamburg, Germany) and hFGF-2 (5 ng/ ml, GlobalStem, Rockeville, USA). Neural rosettes were manually isolated using pulled glass hooks, gently trypsinized, and seeded as single cells on Poly-L-ornithine/ laminin coated dishes in medium consisting of Neurobasal, DMEM/ F12, 1×N2, 1×B27, and GlutaMAX (2 mM) supplemented with hFGF-2 (10 ng/ ml) and hEGF (10 ng/ ml, Peprotech, Hamburg, Germany). Neural progenitor cells were seeded at high densities (100–150.000 cells/ cm^2) and passaged one day after reaching confluence using Trypsin/ Benzonase. Differentiation was induced by seeding the cells at a density of 50.000 cells/ cm^2 and withdrawal of growth factors in the presence of BDNF (20 ng/ ml, Peprotech, Hamburg, Germany).

Patch clamp recordings

Patch clamp recordings were performed using an EPC-10 amplifier (Heka, Lambrecht, Germany). Patch pipettes were pulled from borosilicate glass tubing (Harvard Apparatus, Holliston, USA). The internal solution contained (mM): KCl 130, NaCl 10, HEPES 10, EGTA 11, $MgCl_2 \times 6H_2O$ 1, $CaCl_2 \times H_2O$ 2, Mg-ATP 2. pH was adjusted to 7.2. When filled, electrodes had a resistance of 6–8 MΩ. Cell cultures were continuously superfused with an extracellular solution, consisting of (mM): NaCl 125, KCl 2.5, $CaCl_2 \times H_2O$ 2, $MgCl_2 \times 6H_2O$ 1, $NaHCO_3$ 26, $NaH_2PO_4 \times H_2O$ 1.25, glucose$\times H_2O$ 25. Solution was continuously bubbled with carbogen to maintain a pH of 7.4. Recordings were made in the whole cell configuration with holding potentials (VH) of −60 or −80 mV. Current voltage responses were evoked by applying 100 ms voltage steps from −60 mV to +50 mV in 10 mV increments. Data were filtered at 3 kHz, digitized and stored on-line using Pulse (Heka, Lambrecht, Germany). Na^+ and K^+ currents were identified via their I-V relationship. Na^+ currents were antagonized in some experiments by TTX (1 μM). Current clamp mode was used to apply current steps to induce action potentials or to measure spontaneous action potentials. Postsynaptic currents were measured in the voltage clamp mode at a VH of −60 mV. Mini Analysis 6 (Synaptosoft, USA) was used to analyse recordings of post-synaptic currents. Data are given as mean ± SEM.

Filipin staining

Filipin is a polyene antibiotic which binds to free cholesterol and is widely used to analyze the sequestration of unesterified cholesterol in NPC1-deficient cells. Therefore, cells were fixed with 4% paraformaldehyde (in PBS) for 15 min, washed with PBS and incubated at room temperature for 45 min in the dark with a staining solution containing 100 μg/ ml Filipin (Polysciences, Eppelheim, Germany) in PBS. Cells were washed twice with PBS for 5 min. Slides were mounted using Mowiol-DABCO and sealed with cover slips. After 12 h of drying in the dark at room temperature, fluorescence pictures were taken with a Biozero 8000 microscope (Keyence, Hamburg, Germany).

Amplex red assay

To quantify the amount of cholesterol we used the Amplex Red cholesterol assay [33]. Fibroblasts, iPS cells grown on matrigel and neural progenitor cells were harvested in PBS/ SDS (0.1%) at room temperature, sheared through a 27 G needle and cholesterol levels were determined using the Amplex Red cholesterol assay kit (Molecular Probes, Darmstadt, Gemany) according to the manufacturer's instructions. Protein concentrations in lysates were measured using the bicinchoninic acid assay (BCA, Pierce, USA).

Statistical analysis

Analysis of the data was carried out with GraphPad Prism 5 (GraphPad Software Inc., USA). Data are given as mean ± SEM. Unless otherwise stated, unpaired t-tests were used to test for significance, with * = $p<0.05$ and ** = $p<0.01$, *** = $p<0.001$.

Results

Reprogramming of mutNPC1 and wtNPC1 fibroblasts

We reprogrammed fibroblasts originating from a male patient with an early-infantile form of NPC1 characterized by massive accumulation of unesterified cholesterol in lysosomal and late endosomal structures. Cells derived from this donor will be referred to as mutNPC1 and cells derived from age- and sex-matched fibroblasts of a healthy individual will be referred to as wtNPC1.

After three to four weeks of cultivation, the first hiPSC colonies appeared characterized by their embryonic stem (ES) cell-like morphology, e.g. round to oval shape with a sharp border and a high nuclear to cytoplasm ratio (Figure 1A-D). Mechanically isolated colonies were expanded to hiPSC lines on irradiated mouse embryonic fibroblasts and later also on matrigel (Figure 1C,D). The morphology of mutNPC1 and wtNPC1 hiPSCs was similar in both culture systems. The karyotype of the cells was analyzed to rule out any chromosomal abnormalities, which may have arisen during reprogramming, where our hiPSCs displayed a normal karyotype (Figure 1E,F). Sequencing of the hiPSCs revealed that the mutations in the NPC1 gene were maintained (data not shown).

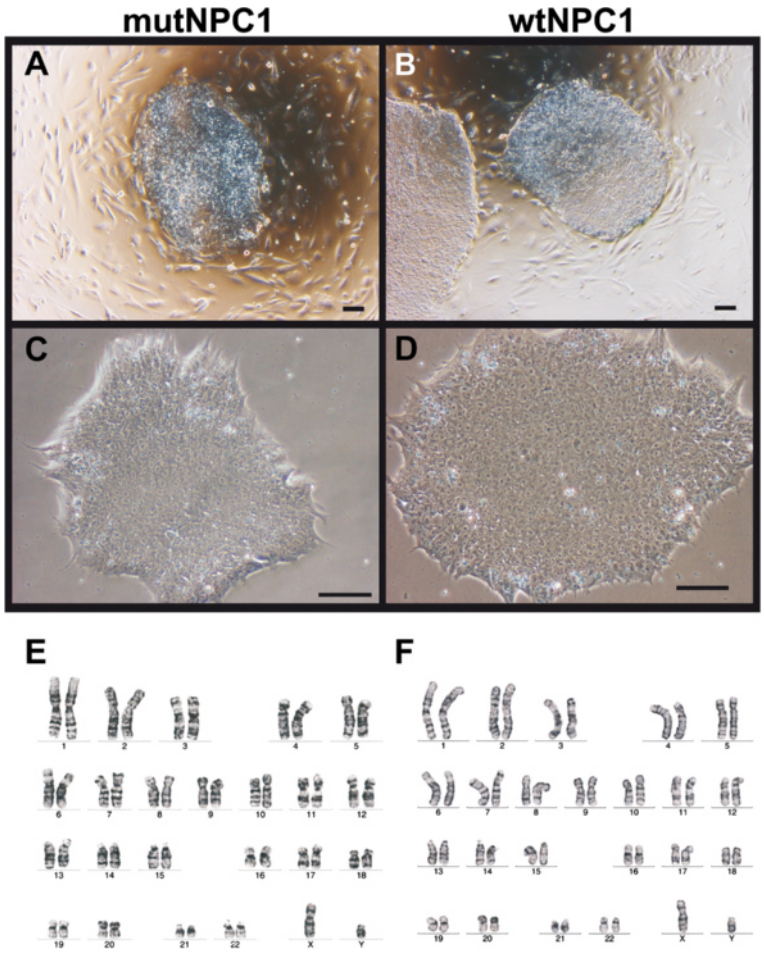

Figure 1 Colonies of fibroblast-derived human iPSCs. Images of hiPSC colonies cultured on mouse feeder cells **(A,B)** or matrigel **(C,D)**. The colonies could be easily distinguished by their morphology, showing a high nuclear to cytoplasm ratio and sharp borders, resembling the morphology of human embryonic stem cells (scale bars = 100 μm). The hiPSCs-derived from fibroblasts of a NPC1-patient **(E)** and unaffected individual **(F)** displayed a normal karyotype. Karyotyping was performed by Giemsa Trypsin banding.

Pluripotency of mutNPC1 and wtNPC1 hiPSCs

HiPSCs derived from of mutNPC1 and wtNPC1 human fibroblasts were characterized regarding their pluripotency. First, we analyzed the alkaline phosphatase (AP) expression. All hiPSCs colonies demonstrated strong AP expression (Figure 2A,B). The expression of several transcription factors and surface markers was determined by immunocytochemistry. HiPSCs displayed a high expression of the transcription factors Nanog (Figure 2C,D) and Oct4 (Figure 2E,F). The glycosphingolipids SSEA3 and SSEA4 (Figure 2G-J), were strongly expressed as well as the keratan sulfate antigens Tra-1-60 and Tra-1-81 (Figure 2K-N). No obvious differences between mutNPC1 and wtNPC1 cells in marker expression could be observed. The spontaneous differentiation by embryoid body (EB) formation into cells of all three germ layers was also used to verify the pluripotency (Figure 3A-H). Herein, cells from all three germ layers were identified, thus proving the pluripotency of the hiPSCs *in vitro*. The induction of teratoma was used as an *in vivo* pluripotency assay. The hiPSCs induced teratomas in immunodeficent mice, and the analysis of the tumors revealed tissues of all three germ layers (Figure 3I-N).

Neuronal differentiation of mutNPC1 and wtNPC1 hiPS cells

In a last step, we generated neural progenitor cells, which were positive for Nestin and Sox2 (Figure 4A,B,E,F). Differentiated neural progenitor cells expressed neuronal markers like MAP2 (Figure 4C,G), and Tuj1 (Figure 4D,H) demonstrating the neuronal phenotype of the cells. Furthermore, we proved the differentiation into functional neuronal cells by means of patch clamp recordings. In these experiments we observed voltage dependent Na^+ and K^+ channels (Na_Vs and K_Vs) (Figure 4I) after three to four weeks of differentiation, where inward currents could be blocked by TTX (Figure 4K). Although the cells exhibited Na_Vs, they did not demonstrate any

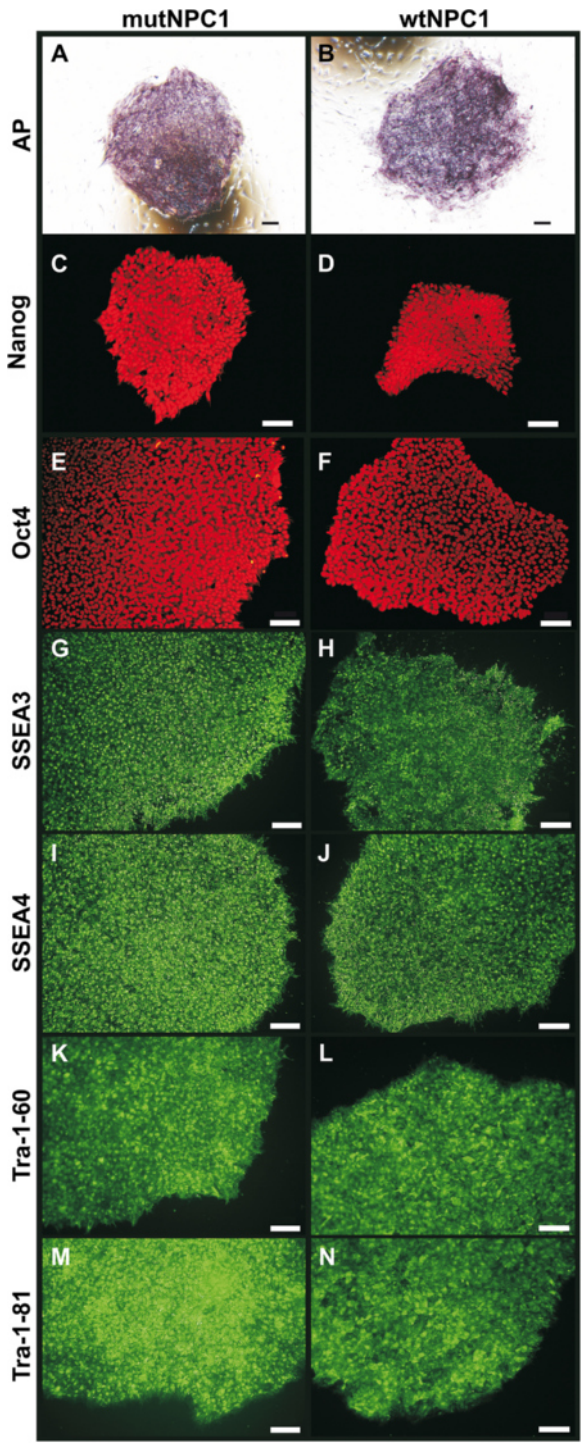

Figure 2 Detection of pluripotency markers in hiPSCs. hiPSCs-derived from fibroblasts of NPC1 patient (mutNPC1) and unaffected control (wtNPC1) showed a strong alkaline phosphatase (AP) staining **(A,B)** and expressed a set of pluripotency markers **(C-N)** demonstrating the pluripotent state of the cells (scale bars = 100 μm).

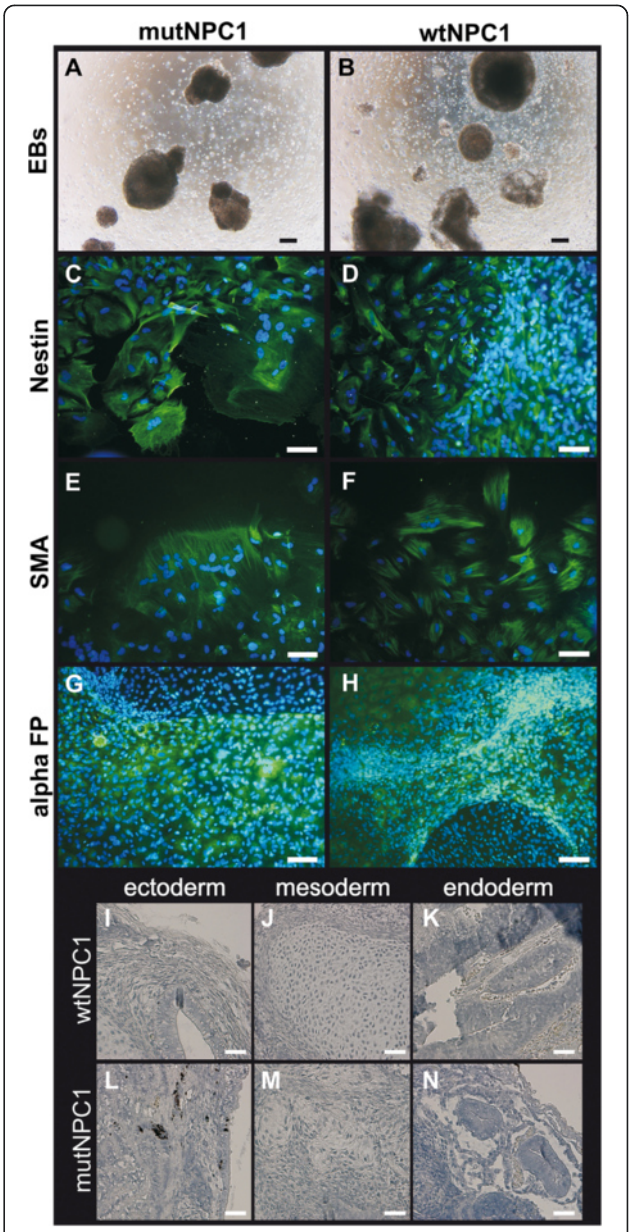

Figure 3 Embryoid body formation and teratoma induction. Free floating embryoid bodies (EBs) of mutNPC1 and wtNPC1 hiPSCs were generated **(A,B)**, which subsequently spontaneously differentiated **(C-H)**. EBs of both cell lines were positive for markers of the three germ layers, namely Nestin **(C,D)** for ectoderm, smooth muscle actin (SMA) for mesoderm **(E,F)**, and alpha fetoprotein (alpha FP) for endoderm **(G,H)**. Nuclei were stained by DAPI, shown in blue, staining of Nestin, SMA and alpha FP is shown in green (scale bars **A-H** = 100 μm). HiPSCs of the mutNPC1 and wtNPC1 cell lines were injected in immunodeficient mice and tumors were extracted after 8–12 weeks. MutNPC1 and wtNPC1 hiPSCs induced teratomas contained structures typical for the ectoderm **(I,J)**, mesoderm **(K,L)**, and endoderm (**M,N**, scale bars I-N = 50 μm).

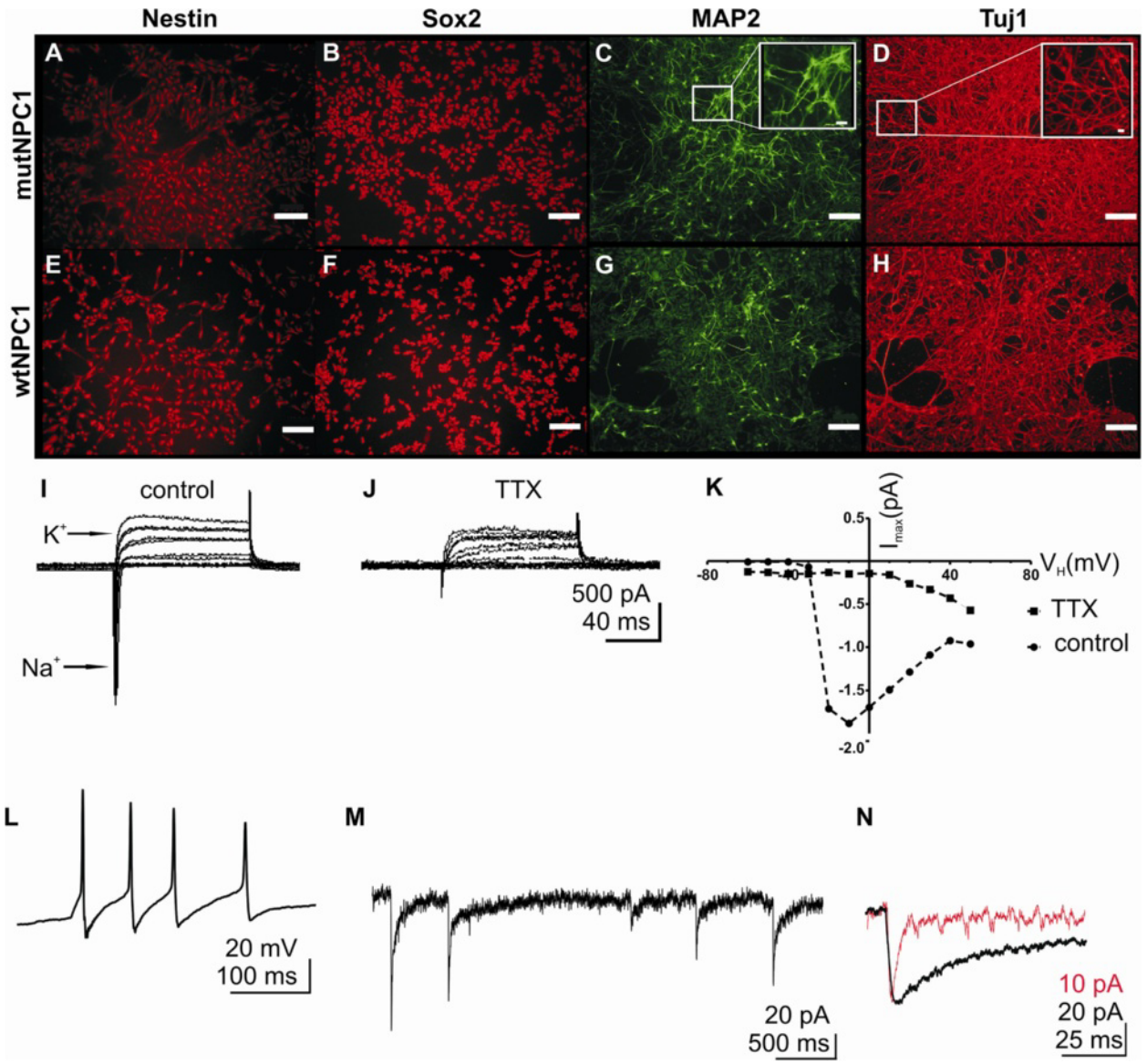

Figure 4 Differentiation of neural progenitor cells. HiPSC cell lines were directed to neural progenitor cells **(A,B,E,F)** and subsequently differentiated into neuronal cells. Neural progenitor cells expressed typical markers like Nestin (**A,E,** shown in red) or Sox2 (**B,F** shown in red). Differentiation of neural progenitor cells was induced by withdrawal of growth factors and resulted in cells demonstrating a neuronal morphology, expressing neuronal markers like MAP2 (**C,G** shown in green) and Tuj1 (**D,H** shown in red). Inset in **C** and **D** shows an example of a higher magnification to demonstrate the dense network of processes built up by the cells during differentiation. Patch clamp experiments were performed to analyze the maturation of the cells into functional neuronal cells. Voltage steps elicited inward and outward directed Na^+ and K^+ currents **(I)**, where Na^+ currents could be blocked by TTX **(J)** and possessed I/ V relationship typical for voltage gated Na^+ channels **(K)**. The example shows recordings of a mutNPC1 cell, differentiated for four weeks. After 7–9 weeks of differentiation, we observed spontaneous action potentials **(L)** as well as spontaneous postsynaptic currents **(M)**. **(N)** shows a superimposed average of spontaneous postsynaptic currents with fast decay kinetics (red trace) and slow decay kinetics (black trace), indicating input of different synaptic sites. The example shows recordings of a mutNPC1 cell, differentiated for 7 weeks.

spontaneous action potentials in the current clamp mode. But, we observed spontaneous action potentials after 7–8 weeks of differentiation (Figure 4L). In addition, we recorded spontaneous postsynaptic currents. An example of a mutNPC1 cell is shown in Figure 4M. The analysis of the decay kinetics (Figure 4N) revealed a rise time of 2.1 ± 1.1 ms. Analysing the decay kinetics we found a group of post synaptic currents best fitted by a mono-exponential function (τ: 3.5 ± 0.4 ms, Figure 4N, black trace) with a mean amplitude of 29.5 ± 1.1 pA, and a group best fitted

by a bi-exponential function (τ1: 9.9 ± 1.9 ms, τ2: 124.7 ± 23.8 ms, Figure 4N, red trace) with a mean amplitude of 68.1 ± 7.1 pA.

mutNPC1 cells accumulated cholesterol

The hallmark of NPC1 is abnormal cholesterol trafficking resulting in an accumulation of cholesterol. Free cholesterol can be visualized by Filipin. An analysis of the cholesterol distribution in mutNPC1 fibroblasts, iPSCs, and derived neural progenitor cells (Figure 5A,C,E) revealed an accumulation of cholesterol. In contrast, an accumulation was not detectable in the fibroblasts, iPSCs, or neural progenitor cells of the wtNPC1 counterpart (Figure 5B,D,F). As a next step, we used the Amplex Red assay [33] to confirm and quantify the observed cholesterol accumulations. The experiments revealed a significantly increased cholesterol content in mutNPC1 cells in comparison to wtNPC1 cells (Figure 5G) (fibroblasts: mutNPC1: 13.7 ± 0.5 μg vs. wtNPC1: 7.3 ± 0.3 μg; iPSCs: mutNPC1: 11.6 ± 0.6 μg vs. wtNPC1: 8.9 ± 0.7 μg; neural progenitor cells: mutNPC1: 23.6 ± 0.9 μg vs. wtNPC1: 14.2 ± 1.6 μg).

Discussion

In this study we aimed to reprogram fibroblasts originating from a NPC1 patient with an early-infantile form of

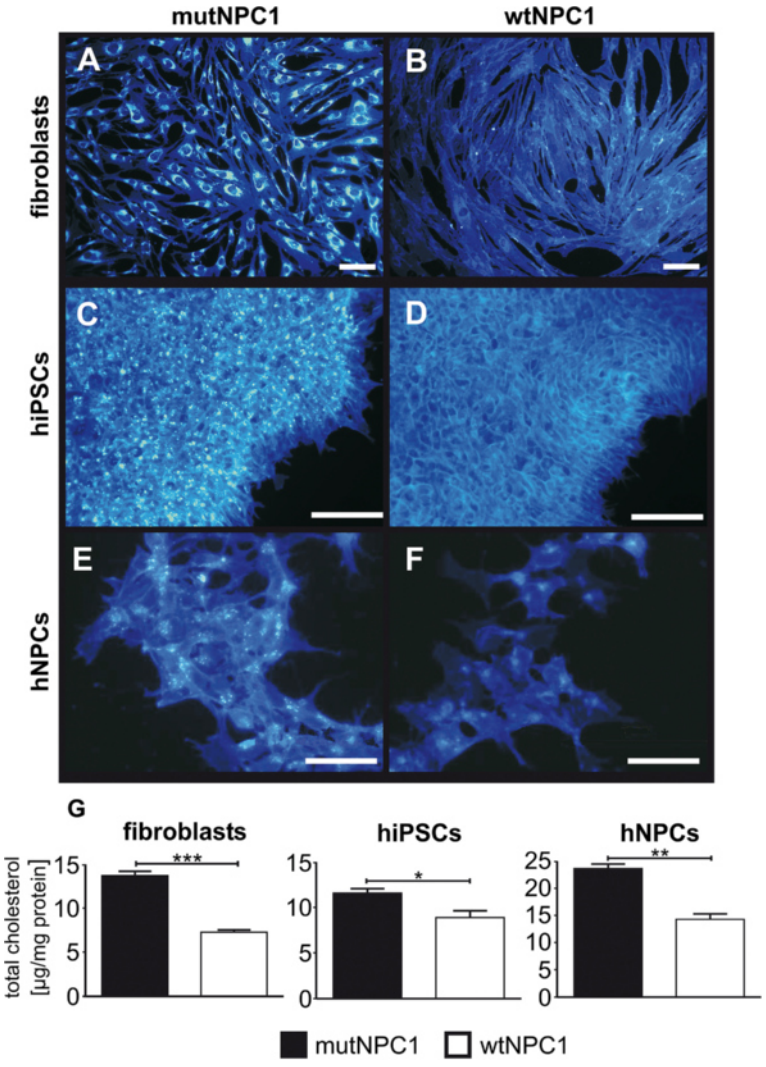

Figure 5 Cholesterol accumulation in fibroblasts, hiPSCs, and neural progenitor cells. Cholesterol accumulation is one of the hallmarks of NPC1 disease. Filipin stainings of fibroblast (**A,B**, shown in blue) are used for diagnostics, where fibroblasts of NPC1 patients with a "classic" biochemical phenotype demonstrate a clear perinuclear accumulation **(A)** in contrast to fibroblasts of an unaffected individual **(B)**. These differences were found in hiPSCs **(C,D)** and neural progenitor cells (hNPCs, **E,F**) derived from mutNPC1 and wtNPC1 fibroblasts. (scale bar = 100 μm). A quantification of the amount of cholesterol **(G)** in fibroblasts, iPSCs, and hNPCs revealed elevated cholesterol levels in mutNPC1 cell lines (black bars) in contrast to wtNPC1 cell lines (white bars). The total amount differed slightly between the cell lines but the relative proportion was comparable.

the disease. Therefore, we used retroviruses expressing Oct4, Klf4, Sox2, and c-Myc in combination with GFP. These factors have been described previously to be efficient in generating hiPSCs [34]. The retroviral particles used in this study were successfully used to reprogram skin fibroblasts of Parkinsons disease into hiPSCs [32]. HiPS colonies were chosen based on an absent GFP-signal indicating a silenced expression of transcription factors [35] and were subcultured to stable hiPSC lines. The obtained mutNPC1 and wtNPC1 hiPSC lines were characterized by their ES-cell like morphology, the expression of alkaline phosphatase, and the pluripotency markers Nanog, Oct4, SSEA3, SSEA4, Tra-1-60, Tra-1-81. A comparable expression of Tra-1-81 was reported for NPC1 knock-down and control ES cells [36]. However, comparative analyses of additional pluripotency markers were not performed in this study. We found no obvious differences between mutNPC1 and wtNPC1 cells in pluripotency marker expression. These results are in accordance with other studies dealing with patient-specific induced pluripotent stem cells in a variety of other diseases [9]. However, to our knowledge this is the first study describing the expression of pluripotency markers SSEA3, SSEA4, and Tra-1-60 in pluripotent cells harboring disease-causing mutations in the NPC1 gene. In addition, the widely known risk of chromosomal abnormalities, potentially occurring during iPS generation and expansion [37], did not arise in our cell lines as proved by karyotyping. The spontaneous differentiation by embryoid body (EB) formation [38] into cells of all three germ layers and the induction of teratomas in immunodeficient mice [39] further demonstrated the pluripotent state of the mutNPC1 and wtNPC1 hiPSCs.

We further differentiated the hiPSCs into neural progenitor cells to generate a suitable *in vitro* disease model. So far, two human cellular neural models based on NPC1-knockdown have been reported. These include SH-SY5Y neuroblastoma cells [40] and human embryonic stem cells [36], which resemble the phenotype only in some aspects of the NPC1 disease. Therefore, they are not an appropriate model to analyze the influence of specific mutations in a patient-specific (epi)genetic background. Here, we generated homogenous neural progenitor cells based on mutNPC1 and wtNPC1 hiPSCs, which were positive for neural markers Nestin and Sox2 [41]. In contrast, Ordonez et al. [36] obtained a homogenous population of neural stem cells from control hESCs but not from NPC1 knock-down hESCs. The authors speculate that these findings might be based on the genetic background of the cells [36].

Our differentiated neural progenitor cells expressed the neuronal markers MAP2 and Tuj1. We did not observe obvious morphological differences between mutNPC1 and wtNPC1 neuronal cells. In contrast, distortion of neuronal shape and extensive growth of ectopic neurites have been reported for multipotent adult stem cells (MASCs) derived cells [30]. However, a further detailed analysis of our neural progenitor cells and derived neuronal cells will be performed to analyze changed morphology of neuronal cells and perturbances of proliferation, described for murine neural stem cells [42]. In a first set of experiments, we demonstrated the differentiation of neural progenitor cells into functional neuronal cells by means of patch clamp recordings. We observed voltage dependent Na^+ and K^+ channels, where inward currents were blocked by TTX. Spontaneous action potentials and postsynaptic currents could only be observed in cells differentiated for 7–8 weeks, indicating the maturation time of human neural progenitor cells to functional neurons, as described for interneurons derived from hiPSCs [43,44]. The here recorded spontaneous postsynaptic currents displayed different amplitudes and the time constants of the current decay could be fitted with mono-exponential or bi-exponential functions. The differences between the time constants may indicate different types of synaptic input, where currents with small amplitudes and fast mono-exponential decay suggest excitatory and events with larger amplitudes and slow bi-exponential decay suggest inhibitory input [45,46]. These preliminary results indicate that the differentiated cells are able to build up chemical synapses. This is of special interest as recent studies described disturbed transmitter release in NPC1 deficient mice, where a higher rate of glutamate release was observed leading to higher frequency of excitatory postsynaptic currents [47]. Thus, our cells provide a platform to study such alterations in synaptic transmission in human neuronal cells gained from different individuals. Ultimately, these results demonstrate a maturation into functional neuronal cells, where future studies will focus on the nature of the expressed voltage and ligand gated ion channels in mutNPC1 and wtNPC1 neuronal cells.

Our neural progenitor cells were analyzed regarding their impaired cholesterol trafficking by Filipin. It visualizes free cholesterol and is routinely used for human dermal fibroblasts in the diagnostics of the NPC1 disease [20]. We found clear cholesterol accumulation in mutNPC1 fibroblasts, hiPSCs, and derived neural progenitor cells. In contrast, such an accumulation was not observed in the fibroblasts, hiPSCs, or neural progenitor cells of the wtNPC1 counterpart. The accumulation pattern of cholesterol in the herein described cells was comparable to accumulations described in a NPC1 knock-down mouse model [48], and SH-SY5Y neuroblastoma cells [40]. Recently, a neural model based on multipotent adult stem cells was described [30]. The neural differentiated progeny of these cells, demonstrated a comparable accumulation of cholesterol, where

this derivation method is only applicable to early passages (<3 passages) of fibroblasts, potentially limiting its use with characterized cell lines from cell repositories.

Finally, we used the Amplex Red assay to confirm and quantify the observed cholesterol accumulations in our cells. These experiments revealed significantly increased cholesterol content in mutNPC1 cells in comparison to wtNPC1 cells, which was conserved in fibroblasts, hiPSCs, and derived neural progenitor cells. To our knowledge this is the first analysis of cholesterol distribution using Filipin staining and cholesterol quantification in hiPSCs and neural progenitor cells derived from human NPC1 deficient fibroblasts.

Conclusion

In this study we generated, for the first time, induced pluripotent stem cells derived from fibroblasts of a NPC1 patient. The cells demonstrated an accumulation of cholesterol, resembling the phenotype of NPC1 deficient cells, and can provide an *in vitro* model of NPC1. We are convinced that the here reported hiPSCs and the derived neural progenitor cells are an excellent model to study the influence of the specific mutation on the phenotype, e.g. consequences of a misfolded NPC1 protein. Moreover, the cells provide the opportunity to analyze the consequences of a NPC1 mutation on the patient-specific (epi)genetic background, and will thus serve to elucidate further the pathogenic mechanisms of this fatal lysosomal storage disorder.

Competing interests

The authors declare that they have no competing interests.

Authors' contributions

MT: conception and design, collection and/ or assembly of data, data analysis and interpretation, manuscript writing. RH: conception and design, collection and/ or assembly of data, data analysis and interpretation, manuscript writing. PS: collection and/ or assembly of data, manuscript writing. CK: collection and/ or assembly of data, manuscript writing. AR: conception and design, manuscript writing, final approval of manuscript. MJF: conception and design, collection and/ or assembly of data, data analysis and interpretation, manuscript writing, final approval of manuscript. All authors read and approved the final manuscript.

Acknowledgements

The authors thank Sebastian Rost for his excellent technical support.

Author details

[1]Albrecht-Kossel-Institute for Neuroregeneration (AKos), University of Rostock, Gehlsheimer Strasse 20, D-18147 Rostock, Germany. [2]Institute of Neurogenetics, University of Lübeck, Maria-Goeppert-Strasse 1, 23562 Lübeck, Germany.

Received: 3 July 2013 Accepted: 15 September 2013
Published: 18 September 2013

References

1. Takahashi K, Tanabe K, Ohnuki M, Narita M, Ichisaka T, Tomoda K, Yamanaka S: **Induction of pluripotent stem cells from adult human fibroblasts by defined factors.** *Cell* 2007, **131:**861–872.
2. Park IH, Zhao R, West JA, Yabuuchi A, Huo H, Ince TA, Lerou PH, Lensch MW, Daley GQ: **Reprogramming of human somatic cells to pluripotency with defined factors.** *Nature* 2008, **451:**141–146.
3. Ye Z, Zhan H, Mali P, Dowey S, Williams DM, Jang YY, Dang CV, Spivak JL, Moliterno AR, Cheng L: **Human-induced pluripotent stem cells from blood cells of healthy donors and patients with acquired blood disorders.** *Blood* 2009, **114:**5473–5480.
4. Liu H, Ye Z, Kim Y, Sharkis S, Jang YY: **Generation of endoderm-derived human induced pluripotent stem cells from primary hepatocytes.** *Hepatology* 2010, **51:**1810–1819.
5. Karumbayaram S, Novitch BG, Patterson M, Umbach JA, Richter L, Lindgren A, Conway AE, Clark AT, Goldman SA, Plath K, *et al*: **Directed differentiation of human-induced pluripotent stem cells generates active motor neurons.** *Stem Cells* 2009, **27:**806–811.
6. Zhang J, Wilson GF, Soerens AG, Koonce CH, Yu J, Palecek SP, Thomson JA, Kamp TJ: **Functional cardiomyocytes derived from human induced pluripotent stem cells.** *Circ Res* 2009, **104:**e30–e41.
7. Zhang D, Jiang W, Liu M, Sui X, Yin X, Chen S, Shi Y, Deng H: **Highly efficient differentiation of human ES cells and iPS cells into mature pancreatic insulin-producing cells.** *Cell Res* 2009, **19:**429–438.
8. Yang S, Bo J, Hu H, Guo X, Tian R, Sun C, Zhu Y, Li P, Liu P, Zou S, *et al*: **Derivation of male germ cells from induced pluripotent stem cells in vitro and in reconstituted seminiferous tubules.** *Cell Prolif* 2012, **45:**91–100.
9. Park IH, Arora N, Huo H, Maherali N, Ahfeldt T, Shimamura A, Lensch MW, Cowan C, Hochedlinger K, Daley GQ: **Disease-specific induced pluripotent stem cells.** *Cell* 2008, **134:**877–886.
10. Rashid ST, Corbineau S, Hannan N, Marciniak SJ, Miranda E, Alexander G, Huang-Doran I, Griffin J, Ahrlund-Richter L, Skepper J, *et al*: **Modeling inherited metabolic disorders of the liver using human induced pluripotent stem cells.** *J Clin Invest* 2010, **120:**3127–3136.
11. Jin ZB, Okamoto S, Osakada F, Homma K, Assawachananont J, Hirami Y, Iwata T, Takahashi M: **Modeling retinal degeneration using patient-specific induced pluripotent stem cells.** *PLoS ONE* 2011, **6:**e17084.
12. Zhang N, An MC, Montoro D, Ellerby LM: **Characterization of human Huntington's disease cell model from induced pluripotent stem cells.** *PLoS Curr* 2010, **2**, RRN1193.
13. Lemonnier T, Blanchard S, Toli D, Roy E, Bigou S, Froissart R, Rouvet I, Vitry S, Heard JM, Bohl D: **Modeling neuronal defects associated with a lysosomal disorder using patient-derived induced pluripotent stem cells.** *Hum Mol Genet* 2011, **20:**3653–3666.
14. Yokoo N, Baba S, Kaichi S, Niwa A, Mima T, Doi H, Yamanaka S, Nakahata T, Heike T: **The effects of cardioactive drugs on cardiomyocytes derived from human induced pluripotent stem cells.** *Biochem Biophys Res Commun* 2009, **387:**482–488.
15. Morris JA, Zhang D, Coleman KG, Nagle J, Pentchev PG, Carstea ED: **The genomic organization and polymorphism analysis of the human Niemann-Pick C1 gene.** *Biochem Biophys Res Commun* 1999, **261:**493–498.
16. Carstea ED, Morris JA, Coleman KG, Loftus SK, Zhang D, Cummings C, Gu J, Rosenfeld MA, Pavan WJ, Krizman DB, *et al*: **Niemann-Pick C1 disease gene: homology to mediators of cholesterol homeostasis.** *Science* 1997, **277:**228–231.
17. Davies JP, Ioannou YA: **Topological analysis of Niemann-Pick C1 protein reveals that the membrane orientation of the putative sterol-sensing domain is identical to those of 3-hydroxy-3-methylglutaryl-CoA reductase and sterol regulatory element binding protein cleavage-activating protein.** *J Biol Chem* 2000, **275:**24367–24374.
18. Vanier MT: **Niemann-Pick disease type C.** *Orphanet J Rare Dis* 2010, **5:**16.
19. Sokol J, Blanchette-Mackie J, Kruth HS, Dwyer NK, Amende LM, Butler JD, Robinson E, Patel S, Brady RO, Comly ME, *et al*: **Type C Niemann-Pick disease: lysosomal accumulation and defective intracellular mobilization of low density lipoprotein cholesterol.** *J Biol Chem* 1988, **263:**3411–3417.
20. Wraith JE, Baumgartner MR, Bembi B, Covanis A, Levade T, Mengel E, Pineda M, Sedel F, Topcu M, Vanier MT, *et al*: **Recommendations on the diagnosis and management of Niemann-Pick disease type C.** *Mol Genet Metab* 2009, **98:**152–165.
21. Liscum L, Ruggiero RM, Faust JR: **The intracellular transport of low density lipoprotein-derived cholesterol is defective in Niemann-Pick type C fibroblasts.** *J Cell Biol* 1989, **108:**1625–1636.
22. Zampieri S, Mellon SH, Butters TD, Nevyjel M, Covey DF, Bembi B, Dardis A: **Oxidative stress in NPC1 deficient cells: protective effect of allopregnanolone.** *J Cell Mol Med* 2009, **13:**3786–3796.

23. Kwon HJ, Abi-Mosleh L, Wang ML, Deisenhofer J, Goldstein JL, Brown MS, Infante RE: **Structure of N-terminal domain of NPC1 reveals distinct subdomains for binding and transfer of cholesterol.** *Cell* 2009, **137:**1213–1224.
24. Loftus SK, Morris JA, Carstea ED, Gu JZ, Cummings C, Brown A, Ellison J, Ohno K, Rosenfeld MA, Tagle DA, *et al*: **Murine model of Niemann-Pick C disease: mutation in a cholesterol homeostasis gene.** *Science* 1997, **277:**232–235.
25. Vite CH, Ding W, Bryan C, O'Donnell P, Cullen K, Aleman D, Haskins ME, Van Winkle T: **Clinical, electrophysiological, and serum biochemical measures of progressive neurological and hepatic dysfunction in feline Niemann-Pick type C disease.** *Pediatr Res* 2008, **64:**544–549.
26. Huang X, Suyama K, Buchanan J, Zhu AJ, Scott MP: **A drosophila model of the Niemann-Pick type C lysosome storage disease: dnpc1a is required for molting and sterol homeostasis.** *Development* 2005, **132:**5115–5124.
27. Karten B, Peake KB, Vance JE: **Mechanisms and consequences of impaired lipid trafficking in Niemann-Pick type C1-deficient mammalian cells.** *Biochim Biophys Acta* 2009, **1791:**659–670.
28. Pentchev PG, Gal AE, Booth AD, Omodeo-Sale F, Fouks J, Neumeyer BA, Quirk JM, Dawson G, Brady RO: **A lysosomal storage disorder in mice characterized by a dual deficiency of sphingomyelinase and glucocerebrosidase.** *Biochim Biophys Acta* 1980, **619:**669–679.
29. Walkley SU, Suzuki K: **Consequences of NPC1 and NPC2 loss of function in mammalian neurons.** *Biochim Biophys Acta* 2004, **1685:**48–62.
30. Bergamin N, Dardis A, Beltrami A, Cesselli D, Rigo S, Zampieri S, Domenis R, Bembi B, Beltrami CA: **A human neuronal model of Niemann Pick C disease developed from stem cells isolated from patient's skin.** *Orphanet J Rare Dis* 2013, **8:**34.
31. Sun X, Marks DL, Park WD, Wheatley CL, Puri V, O'Brien JF, Kraft DL, Lundquist PA, Patterson MC, Pagano RE, *et al*: **Niemann-Pick C variant detection by altered sphingolipid trafficking and correlation with mutations within a specific domain of NPC1.** *Am J Hum Genet* 2001, **68:**1361–1372.
32. Seibler P, Graziotto J, Jeong H, Simunovic F, Klein C, Krainc D: **Mitochondrial parkin recruitment is impaired in neurons derived from mutant PINK1 induced pluripotent stem cells.** *J Neurosci* 2011, **31:**5970–5976.
33. Tängemo C, Weber D, Theiss S, Mengel E, Runz H: **Niemann-Pick type C disease: characterizing lipid levels in patients with variant lysosomal cholesterol storage.** *J Lipid Res* 2011, **52:**813–825.
34. Huangfu D, Maehr R, Guo W, Eijkelenboom A, Snitow M, Chen AE, Melton DA: **Induction of pluripotent stem cells by defined factors is greatly improved by small-molecule compounds.** *Nat Biotechnol* 2008, **26:**795–797.
35. Yao S, Sukonnik T, Kean T, Bharadwaj RR, Pasceri P, Ellis J: **Retrovirus silencing, variegation, extinction, and memory are controlled by a dynamic interplay of multiple epigenetic modifications.** *Mol Ther* 2004, **10:**27–36.
36. Ordonez MP, Roberts EA, Kidwell CU, Yuan SH, Plaisted WC, Goldstein LS: **Disruption and therapeutic rescue of autophagy in a human neuronal model of Niemann Pick type C1.** *Hum Mol Genet* 2012, **21:**2651–2662.
37. Mayshar Y, Ben David U, Lavon N, Biancotti JC, Yakir B, Clark AT, Plath K, Lowry WE, Benvenisty N: **Identification and classification of chromosomal aberrations in human induced pluripotent stem cells.** *Cell Stem Cell* 2010, **7:**521–531.
38. Sheridan SD, Surampudi V, Rao RR: **Analysis of embryoid bodies derived from human induced pluripotent stem cells as a means to assess pluripotency.** *Stem Cells Int* 2012, **2012:**738910.
39. Lensch MW, Schlaeger TM, Zon LI, Daley GQ: **Teratoma formation assays with human embryonic stem cells: a rationale for one type of human-animal chimera.** *Cell Stem Cell* 2007, **1:**253–258.
40. Rodriguez-Pascau L, Coll MJ, Casas J, Vilageliu L, Grinberg D: **Generation of a human neuronal stable cell model for Niemann-Pick C disease by RNA interference.** *JIMD Rep* 2012, **4:**29–37.
41. Elkabetz Y, Panagiotakos G, Al Shamy G, Socci ND, Tabar V, Studer L: **Human ES cell-derived neural rosettes reveal a functionally distinct early neural stem cell stage.** *Genes Dev* 2008, **22:**152–165.
42. Yang SR, Kim SJ, Byun KH, Hutchinson B, Lee BH, Michikawa M, Lee YS, Kang KS: **NPC1 gene deficiency leads to lack of neural stem cell self-renewal and abnormal differentiation through activation of p38 mitogen-activated protein kinase signaling.** *Stem Cells* 2006, **24:**292–298.
43. Nicholas CR, Chen J, Tang Y, Southwell DG, Chalmers N, Vogt D, Arnold CM, Chen YJ, Stanley EG, Elefanty AG, *et al*: **Functional maturation of hPSC-derived forebrain interneurons requires an extended timeline and mimics human neural development.** *Cell Stem Cell* 2013, **12:**573–586.
44. Marin O: **Human cortical interneurons take their time.** *Cell Stem Cell* 2013, **12:**497–499.
45. Protti DA, Gerschenfeld HM, Llano I: **GABAergic and glycinergic IPSCs in ganglion cells of rat retinal slices.** *J Neurosci* 1997, **17:**6075–6085.
46. Frech MJ, Perez-Leon J, Wassle H, Backus KH: **Characterization of the spontaneous synaptic activity of amacrine cells in the mouse retina.** *J Neurophysiol* 2001, **86:**1632–1643.
47. Wasser CR, Ertunc M, Liu X, Kavalali ET: **Cholesterol-dependent balance between evoked and spontaneous synaptic vesicle recycling.** *J Physiol* 2007, **579:**413–429.
48. Klein A, Maldonado C, Vargas LM, Gonzalez M, Robledo F, Perez de Arce K, Munoz FJ, Hetz C, Alvarez AR, Zanlungo S: **Oxidative stress activates the c-Abl/p73 proapoptotic pathway in Niemann-Pick type C neurons.** *Neurobiol Dis* 2011, **41:**209–218.

doi:10.1186/1750-1172-8-144
Cite this article as: Trilck *et al.*: Niemann-Pick type C1 patient-specific induced pluripotent stem cells display disease specific hallmarks. *Orphanet Journal of Rare Diseases* 2013 **8**:144.

Brain Research 1657 (2017) 52–61

Contents lists available at ScienceDirect

Brain Research

journal homepage: www.elsevier.com/locate/bres

Research report

Diversity of glycosphingolipid GM2 and cholesterol accumulation in NPC1 patient-specific iPSC-derived neurons

Michaela Trilck [a,f,1], Franziska Peter [a,1], Chaonan Zheng [a,e], Marcus Frank [b], Kostantin Dobrenis [c], Hermann Mascher [d], Arndt Rolfs [a], Moritz J. Frech [a,*]

[a] Albrecht-Kossel-Institute for Neuroregeneration (AKos), University Medicine Rostock, Gehlsheimer Straße 20, 18147 Rostock, Germany
[b] Medical Biology and Electron Microscopy Center, University Medicine Rostock, Strempelstraße 14, 18057 Rostock, Germany
[c] Dominick P. Purpura Department of Neuroscience, Albert Einstein College of Medicine, Rose F. Kennedy Center for Research on Intellectual and Developmental Disabilities, 1410 Pelham Parkway South, Bronx, NY 10461, USA
[d] pharm-analyt Labor GmbH, Ferdinand-Pichler-Gasse 2, 2500 Baden, Austria
[e] Leibniz Institute for Catalysis, University of Rostock, Rostock, Germany
[f] Institute of Neurogenetics, University of Luebeck, Maria-Goeppert-Str. 1, 23562 Luebeck, Germany

ARTICLE INFO

Article history:
Received 22 July 2016
Received in revised form 22 November 2016
Accepted 27 November 2016
Available online 5 December 2016

Keywords:
iPSCs
iPSC-derived neurons
Niemann-Pick disease Type C1
Cholesterol
Glycosphingolipids
GM2
Molecular docking

ABSTRACT

Niemann-Pick disease Type C1 (NPC1) is a rare progressive neurodegenerative disorder caused by mutations in the *NPC1* gene. On the cellular level *NPC1* mutations lead to an accumulation of cholesterol and gangliosides. As a thorough analysis of the severely affected neuronal cells is unfeasible in NPC1 patients, we recently described the cellular phenotype of neuronal cells derived from NPC1 patient iPSCs carrying the compound heterozygous mutation c.1836A>C/c.1628delC. Here we expanded the analysis to cell lines carrying the prevalent mutation c.3182T>C and the novel mutation c.1180T>C, as well as to the determination of GM2 and GM3 gangliosides in NPC1 patient-specific iPSC-derived neurons and glia cells. Immunocytochemical detection of GM2 revealed punctated staining pattern predominantly localized in neurons. Detection of cholesterol by filipin staining showed a comparable staining pattern, colocalized with GM2, indicating a deposit of GM2 and cholesterol in the same cellular compartments. Accumulations were not only restricted to cell bodies, but were also found in the neuronal extensions. A quantification of the GM2 amount by HPLC-MS/MS confirmed significantly higher amounts in neurons carrying a mutation. Additionally, these cells displayed a lowered activity of the catabolic enzyme Hex A, but not B4GALNT1. Molecular docking simulations indicated binding of cholesterol to Hex A, suggesting cholesterol influences the GM2 degradation pathway and, subsequently, leading to the accumulation of GM2. Taken together, this is the first study showing an accumulation of GM2 in neuronal derivatives of patient-specific iPSCs and thus proving further disease-specific hallmarks in this human *in vitro* model of NPC1.

1. Introduction

Niemann-Pick disease Type C1 (NPC1) is classified as a lysosomal storage disorder as well as a rare neurodegenerative disease. It is inherited in an autosomal recessive manner with a prevalence of 1:120,000 live births (Patterson et al., 2012). The disease is caused by mutations in the *NPC1* gene. NPC1 is characterized by severe varying neurological symptoms as delayed motor milestones, clumsiness, speech delay, cataplexy, vertical supranuclear gaze palsy, ataxia, learning disabilities, and psychiatric problems and is accompanied by a progressive neurodegeneration (Vanier, 2010). Recently, we described the complete genomic sequence of 57,052 kb corresponding to the transcribed region of human NPC1 including several exonic and intronic single nucleotide polymorphisms (Bauer et al., 2002). Since that, we aimed to improve diagnostic tools by e.g. the description of new a biomarker for NPC1 (Giese et al., 2015) and, furthermore, to improve our understanding of the pathogenic mechanism by using e.g., the commonly used BALB/c-*npc1*^{nih} NPC1 mouse model (Pentchev et al., 1986). The pathogenic mechanisms of the neurodegenerative processes

* Corresponding author.
E-mail addresses: michaela.trilck@neuro.uni-luebeck.de (M. Trilck), franziska.peter2@uni-rostock.de (F. Peter), cnzheng2009@163.com (C. Zheng), marcus.frank@med.uni-rostock.de (M. Frank), kostantin.dobrenis@einstein.yu.edu (K. Dobrenis), hermann.mascher@pharm-analyt.com (H. Mascher), arndt.rolfs@med.uni-rostock.de (A. Rolfs), moritz.frech@med.uni-rostock.de (M.J. Frech).
[1] These authors contributed equally.

http://dx.doi.org/10.1016/j.brainres.2016.11.031
0006-8993/

of NPC1 are not well understood, although the cellular phenotype is well described. However, a thorough analysis of the severely affected neuronal cells in regards to cholesterol and glycosphingolipid accumulation is unfeasible in NPC1 patients. Therefore, we recently generated a human neuronal cell model for NPC1, based on induced pluripotent stem cells (iPSCs) (Trilck et al., 2013, 2016). Since then, several other iPSC model systems have followed demonstrating the applicability of such model systems to study NPC1 (Bergamin et al., 2013; Maetzel et al., 2014; Yu et al., 2014). The generated cell models greatly facilitate the analysis of cellular phenotypes and the pathogenic mechanism of NPC1. However, even though NPC1 is a rare hereditary disease, there are more than three hundred mutations described (Stenson et al., 2003) and no clear genotype-clinical phenotype correlation has been established based on the type of mutation (e.g. homozygous vs. compound heterozygous, or position of mutation). It is just known that stop codons and missense mutations in the sterol-sensing domain lead commonly to an infantile form of NPC1, whereas missense mutations in the cysteine-rich loop result in diverse disease manifestation (Millat et al., 2001). Here, we investigated the cellular phenotype of different *NPC1* mutations using iPSC-derived neuronal cells. Our recent description of NPC1 patient-specific iPSC was based on cells carrying the compound heterozygous mutation c.1836A>C/c.1628delC. This mutation is located in the sterol sensing domain generally leading to an early infantile systemic onset of the disease (Park et al., 2003; Sun et al., 2001). Here, we expanded our analysis to a novel homozygous mutation c.1180T>C. The localization of the mutations might lead to an alteration of the sterol sensing domain or a premature termination, commonly accompanied by a severe phenotype due to the lack of functional NPC1 protein. Second, we used cells carrying the prevalent homozygous c.3182T>C mutation, located in the Cysteine-rich luminal loop (Millat et al., 2001), commonly accompanied by an early systemic onset and a juvenile or adolescent onset of neurological symptoms (Imrie et al., 2015). Skin fibroblasts of NPC1 patients display typically abnormal filipin pattern demonstrating pathological accumulations of cholesterol (Ory, 2000). Accordingly, we found cholesterol accumulations in our recently described NPC1 patient-specific iPS cells and their neuronal derivatives (Trilck et al., 2013). Besides the accumulation of cholesterol, an accumulation of the ganglioside GM2 and GM3 is found in patients' brain (Vanier, 1999). Because less is known about such accumulations and distribution of GM2 and GM3 in human cellular *in vitro* model systems, we extended our analysis to GM2 and GM3 in this study, which is, to our knowledge, not undertaken until now.

2. Results

In this study we analyzed the NPC1 phenotypes of patient-specific iPSC-derived neuronal cells carrying different mutations of the *NPC1* gene. By detection and quantification of cholesterol, GM2 and GM3, we compared the cellular phenotype of two homozygous *NPC1* mutations, namely the homozygous c.1180T>C and the prevalent homozygous c.3182T>C mutation and the compound heterozygous mutation c.1836A>C/c.1628delC.

2.1. Cholesterol accumulation

To analyze and compare the NPC1 phenotype, filipin staining was performed to monitor cholesterol accumulation. After six weeks of differentiation, cell lines with *NPC1* mutation showed cholesterol accumulations appearing in a fluorescent punctated staining pattern (Fig. 1A–D). Filipin-positive cholesterol accumulation was not only present in cell bodies but also in the cellular extensions of the NPC1-deficient cells (Fig. 1A–D, marked by arrowheads). The quantification of the filipin fluorescence demonstrated a significantly increased signal in all cell lines carrying a *NPC1* mutation in comparison to the control cell line (Fig. 1E). The quantification of the total amount of cholesterol by using the Amplex Red assay (Fig. 1F), revealed a significantly higher amount of cholesterol in cells carrying the c.3182T>C mutation and the c.1836A>C/c.1628delC mutation, but not in cells with the homozygous mutation c.1180T>C (Fig. 1F). This leads to the speculation that in the cells carrying the c.1180T>C mutation, the distribution but not the total amount of cholesterol is altered.

2.2. Accumulation of GM2 and GM3

We were further interested in the amount of the glycosphingolipids GM2 and GM3, as less is known about accumulations of these glycosphingolipids in human cellular model systems. The analysis of GM2 by immunostainings revealed a dotted staining pattern in all cell lines (Fig. 2A–D). By visual observation GM2 appeared predominantly colocalized with neuronal structures. Therefore, we performed triple immunostaining of neuronal differentiated cells for βIII-tub, GFAP and GM2 (Fig. 3A–D). Subsequently, we performed colocalization analysis of GM2 vs. βIII-tub and GM2 vs. GFAP to reveal the distribution of GM2 among neuronal and glial cells. By using the Mander's coefficients, the analysis revealed a clear colocalization of GM2 with βIII-tub (Fig. 3I, white bars), indicated by a coefficient larger than 0.5. Regarding GFAP (Fig. 3I, black bars), the Mander's coefficients indicates a colocalization, but a coefficient below 0.2 presents more likely coincidental colocalization based on background. Taken together, Mander's coefficients and Costes automatic threshold determination (data not shown) demonstrated predominant colocalization of GM2 with the neuronal marker βIII-tub but not with the glial marker GFAP suggesting the GM2 accumulation as a neuron-specific phenotype of the disease. This finding is in accordance with results obtained from a NPC1 mouse model describing a lack of GM2 staining in astrocytes (Taniguchi et al., 2001). Regarding the punctated staining pattern of GM2 and cholesterol we wondered if the deposits were located in the same cellular compartments and thus performed a combined staining of GM2 and filipin (Fig. 3E-H). We found a strong colocalization in all three mutant cells lines and in a lesser extend in the control cell line (Fig. 3J) indicating a deposit of cholesterol and GM2 in the same cellular compartments. In addition, we performed transmission electron microscopy (TEM) to elucidate the subcellular location (Fig. 4). TEM revealed electron-dense globular material (indicated by arrows) close to the plasma membrane and in cytoplasmic vesicular structures in neurites of cultures from every cell line. The accumulations of such osmiophilic material appeared to be larger in mutant cell lines c.1180T>C and c.1836A>C/c.1628delC (Fig. 4B,D) in comparison to the control cell line and the cell line c.3182T>C (Fig. 4A,C). The distribution of these electron-dense deposits in the cytoplasm and near the outer membrane (arrows) of neuronal extensions is strongly reminiscent of the distribution of GM2 deduced by our immunocytochemical staining and suggests that GM2 is part of these typical electron-dense deposits in our cell culture model of NPC1. Next, we quantified the accumulation of GM2, observed in the immunocytochemical stainings. Thus, we performed HPLC-MS/MS for GM2 (Fig. 5A) and GM3 (Fig. 5B). In accordance with the immunocytochemical stainings, we found in the control cell line and in the cells with the c.3182T>C mutation comparable amounts of GM2. In contrast, we measured a fourfold, significantly higher amount of GM2 in the cell lines with the c.1180T>C homozygous mutation and the c.1836A>C/c.1628delC heterozygous mutation, the potentially more severe *NPC1* mutations. Besides GM2 we analyzed the amount of GM3 ganglioside, which also accumulates in NPC1 (Fig. 5B). Unexpectedly, we could not confirm an increased amount of GM3, but a decreased GM3

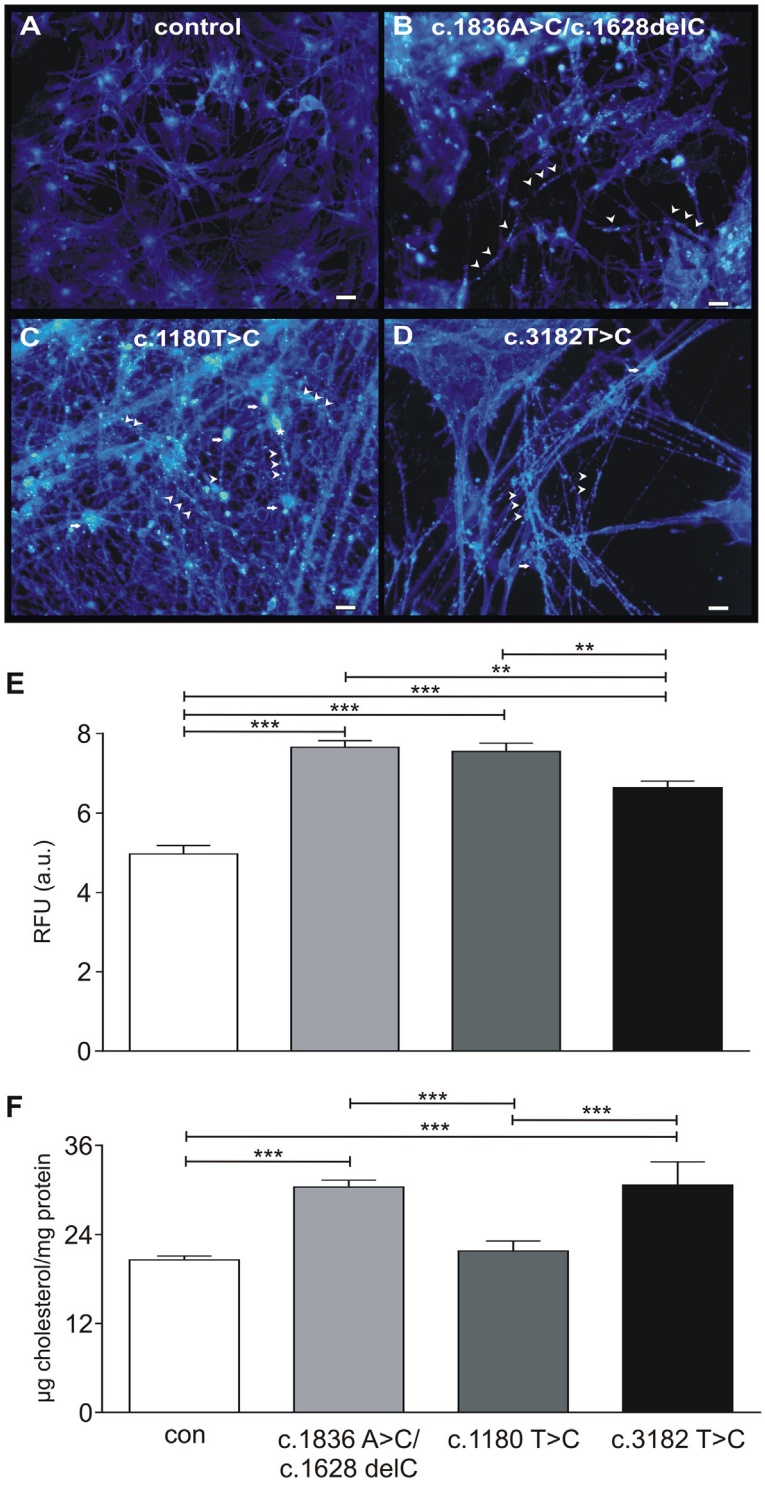

Fig. 1. Accumulation of cholesterol. Visualization of cholesterol was performed by filipin staining (blue) in control cells (A) and cells carrying a mutation (B–D). Cells were differentiated for 6 weeks. Cells carrying a *NPC1* mutation showed cholesterol accumulation not only in the cell bodies but also in cellular processes (B–D, arrowheads). Scale 20 µm. (E) Analysis of the filipin fluorescence intensity demonstrated a significantly increased signal in all cell lines carrying a *NPC1* mutation in comparison to the control cell line. (F) Quantification of the total cholesterol by Amplex Red assay revealed higher amounts of cholesterol in two NPC1 mutant cell lines. The amount of cholesterol did not differ between control cells and cells with the c.1180T > C homozygous mutation, although these cells displayed clear accumulations in the filipin staining. ** = $p < 0.01$; *** = $p < 0.001$. Data for quantification were obtained at least from three independent experiments.

content in all cells carrying a *NPC1* mutation. However, cells carrying the c.1180T>C mutation displayed an amount comparable to the amount of control cells. To further understand the reason for the changes in GM2 and GM3, we investigated the possibility of altered expression levels of the enzymes synthesizing GM2 from GM3 (B4GALNT1) and degrading GM2 to GM3 (Hex A). Determined by RT-qPCR, the transcription level of Hex A was significantly increased in cells with the c.3182T>C homozygous mutation, but not in the two other mutant cell lines (Fig. 6A). The level of Hex A protein, evaluated by western blot analysis, differed significantly

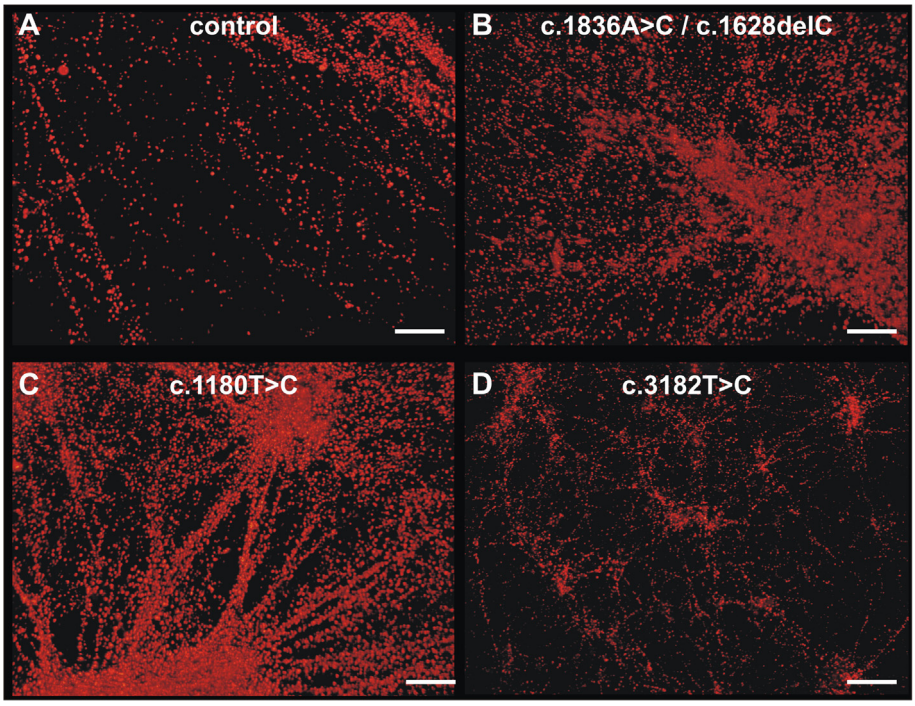

Fig. 2. Immunocytochemical detection of GM2. Immunocytochemical stainings of GM2 (A–D, red) revealed a punctated staining pattern in all cell lines. Scale 100 µm.

among all cell lines. Control cell line, cells with the c.1180T>C homozygous mutation and cells with the c.3182T>C mutation showed comparable protein level. Cells with the compound heterozygous mutation c.1836A>C/c.1628delC had the highest protein level of all cell lines. In regards to B4GALNT1 the transcription level was comparable among all cell lines (Fig. 6B). Regarding the B4GALNT1 protein level, western blot analysis revealed comparable protein level, in which the highest protein amount was detected in cells with the compound heterozygous *NPC1* mutation c.1836A>C/c.1628delC (Fig. 6D). However, taken together, we assumed that the observed GM2 accumulation was not based on an altered B4GALNT1 level, but on a hampered expression or function of Hex A. Thus, we next assayed Hex A enzyme activity (Fig. 6E). Cells with the homozygous mutation c.1180T>C had the lowest enzyme activity, while the expression and amount was undistinguishable from the control cells. In contrast, cells with the heterozygous mutation c.1836A>C/c.1628delC possessed the highest amount of Hex A and demonstrated an enzyme activity comparable to the activity of control cells. These findings suggest a compensatory mechanism in the cell lines with the heterozygous mutation c.1836A>C/c.1628delC and to some extent to the cells with the homozygous mutation c.3182T>C. However, cells with the c.1180T>C homozygous mutation had the lowest Hex A activity, but was indistinguishable from control cells in the Hex A protein level, thus suggesting another reason for the GM2 accumulation. As in NPC1 fibroblasts a reduced activity for glycosylceramidase is reported (Salvioli et al., 2004), which can be re-established by cholesterol depletion, we wondered, whether a similar interaction of cholesterol with the GM2 degradation enzyme Hex A might take place. To answer this question, we used molecular docking as an *in silico*-method to estimate the binding affinities of cholesterol and GM2 to Hex A. Cholesterol and GM2 were successfully docked into the active site of Hex A and the calculated binding energy revealed that cholesterol might have a higher affinity (binding energy: −8.3 kcal/mol) than GM2 (binding energy: −7.1 kcal/mol) to the enzyme. These results hint to a cholesterol-based competitive block of the enzyme activity resulting in the accumulation of GM2 and merit further investigation with human *in vitro* cell models to elucidate an inhibitory action of cholesterol on degradation pathways leading to an accumulation of gangliosides.

3. Discussion

The cellular phenotypic hallmark of NPC1 disease is the accumulation of cholesterol within the late endosomes and lysosomes. We found that neuronal cells with mutated *NPC1* genotype showed massive cholesterol accumulation in the cell bodies comparable to other human neuronal *in vitro* disease models for NPC1 (Bergamin et al., 2013; Ordonez, 2012; Ordonez and Steele, 2016). Additionally, we detected cholesterol accumulations partially in the neuronal extensions of these cells. This is controversial to the findings in the cell models described by Ordonez (Ordonez, 2012) and Bergamin (Bergamin et al., 2013) and to data obtained from a NPC1 mouse model (Karten et al., 2002). Karten and colleagues stated that cholesterol accumulates in the perikarya of neurons whereas the distal axons and dendrites are depleted of cholesterol (Karten et al., 2003). We want to highlight our finding as a species-specific discovery suggesting abnormal transport processes, which may contribute to neuronal dysfunction and death. The accumulation of cholesterol in the axons and dendrites might lead to hampered motility of anterograde and retrograde vesicle transport. This is supported by the finding of Walter and co-workers (Walter et al., 2009), who showed that stimulated organelle motility by Rab9 overexpression leads to an amelioration of cholesterol accumulation. Furthermore, Rab9 interacts with the intermediate filament vimentin, which allows or blocks the transport mechanism within the cells based on the assembly of vimentin (Walter et al., 2009). Preliminary data using our cell model demonstrate an altered state of phosphorylation of vimentin resulting in a changed assembly of vimentin filaments, which might play a role in the cholesterol entrapment in neuronal NPC1-deficient cells (Franziska Peter, personal communication).

In addition to an accumulation of cholesterol a massive accumulation of the glycosphingolipids GM2 and GM3 have been described for NPC1 (Pentchev et al., 1994; Sun et al., 2001). We

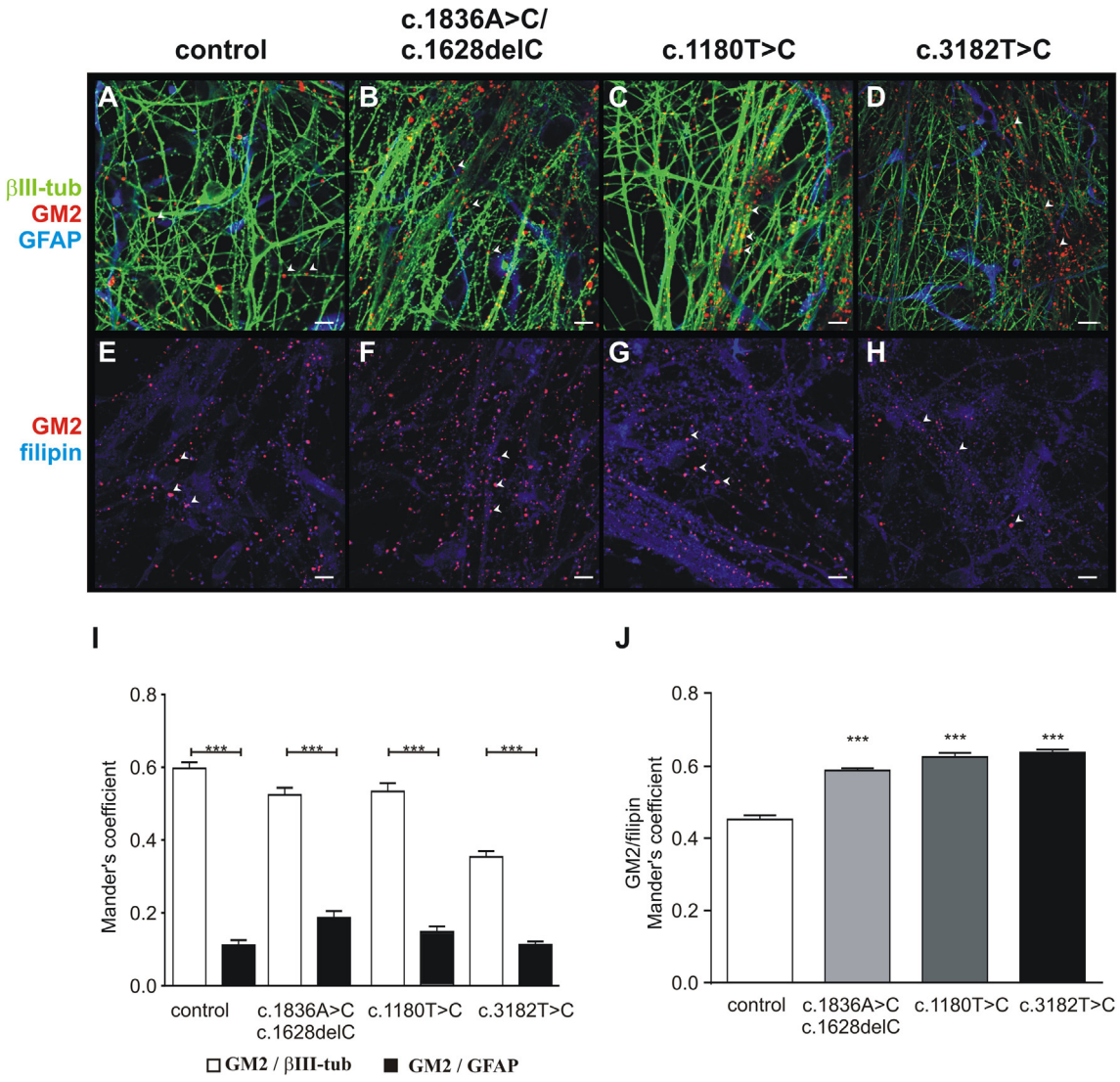

Fig. 3. Colocalization of GM2, βIII-tub, GFAP and filipin. Simultaneously immunocytochemical stainings of GM2 (red), βIII-tub (green), and GFAP (blue) were used to study the localization of GM2. Confocal pictures demonstrated that GM2 is predominantly located with βIII-tub-positive neuronal structures indicated by arrowheads (A–D, scale 10 μm). (I) This observation is affirmed by the analysis of the colocalization using Mander's coefficients, indicating a strong localization of GM2 with βIII-tub (white bars), but not with GFAP (black bars). Simultaneously immunocytochemical staining of GM2 (red) and filipin (blue, E–H) were used to analyze colocalization of GM2 and filipin (J). Mander's coefficients indicate a strong colocalization of GM2 and cholesterol, indicating an accumulation in the same cellular compartments. ** = $p < 0.01$; *** = $p < 0.001$. Data for colocalization were obtained at least from three independent experiments. For each experiment a total of 12 randomly selected visual fields were analyzed.

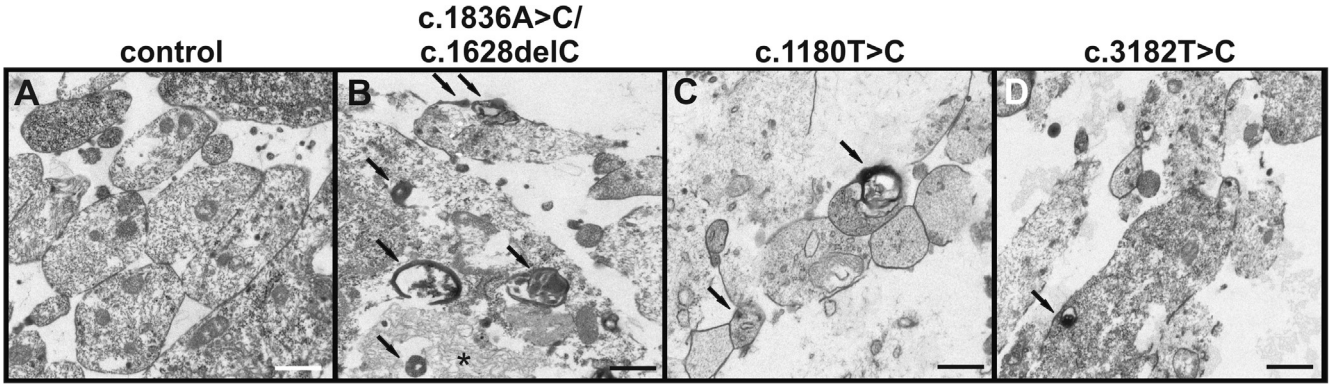

Fig. 4. Transmission electron microscopy. TEM analysis demonstrated electron-dense globular material (black) close to the plasma membrane and in cytoplasmic vesicular structures (arrows). Such deposits were observed more frequently in the cell lines carrying a NPC1 mutation. Scale show 500 nm.

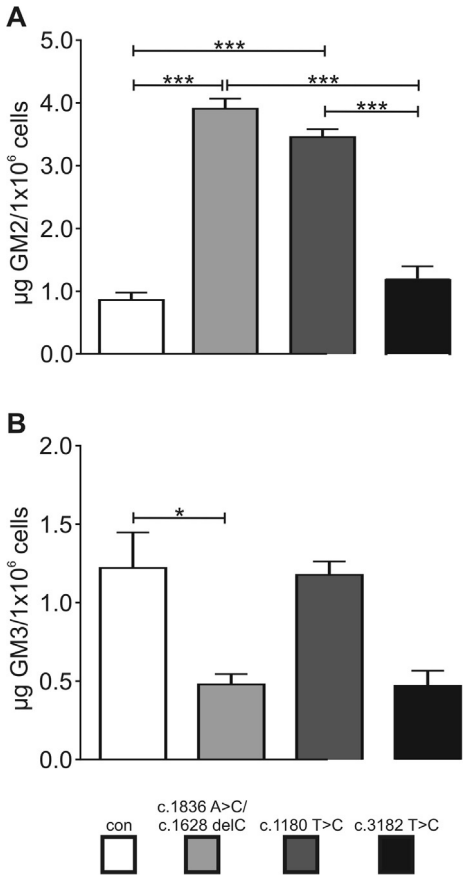

Fig. 5. Quantification of GM2 and GM3 levels with HPLC-MS/MS. Amounts of GM2 (A) and GM3 (B) were analyzed in cells after 6 weeks of differentiation. The amount of GM2 increased in two cell lines carrying a *NPC1* mutation but GM3 was unexpectedly not increased in any cell line. * = $p < 0.05$. Data for quantification were obtained at least from three independent experiments.

observed slight expression of GM2 in neural progenitor cells (data not shown), while neuronal differentiated cells displayed pronounced expression of GM2. Similar results were shown by Bergamin and colleagues (Bergamin et al., 2013), demonstrating a GM2 accumulation in NPC1 patient-derived hSKIN-MAS cells. Only neuronal differentiated cells showed these GM2 accumulations but not fibroblasts or undifferentiated hSKIN-MAS cells. This neuron-specific accumulation of the GM2 ganglioside (Walkley et al., 2000) is comparable to our model system. Interestingly, the control hSKIN-MAS cells showed no GM2-positive staining, while we have shown that all four cell lines express GM2 independent of their genotype. This is not unexpected, as neuronal cells synthesize GM2 physiologically as e.g., a component of glycosphingolipid-enriched microdomains in neuronal cell membranes (Walkley et al., 2000). An additional divergence between our study and the one of Bergamin (Bergamin et al., 2013) is the staining pattern of GM2, as we observed a GM2-positive punctated staining along the axons and dendrites of the neuronal cells while the GM2 staining was restricted to the cell body of differentiated hSKIN-MAS cells. In post-mortem brain slices of human infantile NPC1 patients, GM2-immunoreactivity was granular in appearance (Zervas et al., 2001). This punctated staining pattern is consistent with our findings and highlights the comparability of our human neuronal *in vitro* system with the human *in vivo* state. Further analysis of the GM2 accumulation revealed a colocalization of GM2 and filipin indicating a deposit of GM2 and cholesterol in the same cellular compartments. The localization of the electron-dense material, demonstrated by TEM, was consistent with the immunocytochemical staining of GM2. The mutant cell lines with prominent GM2 staining showed such inclusions in their cell bodies as well as near membranes of neurites more frequently than the other cell lines, although a quantitative analysis was not done, similar membranous cytoplasmic bodies were described for the GM2 gangliosidosis Tay-Sachs disease (Terry and Weiss, 1963) and Sandhoff disease (Suzuki et al., 1971). The punctated staining pattern of GM2 might be based on a disturbed metabolism of GM2 within the cell, since glycosphingolipids are in part synthesized in the Golgi and related structures and digested in late endosomes and lysosomes (Gallala and Sandhoff, 2011; Möbius et al., 1999). A recent study reported GM2 accumulation in mitochondrial- and lysosomal-enriched fractions of ethanol-induced apoptotic murine neurons (Saito et al., 2012), hinting to an intrinsic process in degenerating neurons. A possible explanation for our described distribution pattern could be that the NPC1-diseased neurons try to transport this debilitating material to their outer membranes to release it into the extracellular space. Concurrent, vesicular transport defects were, besides cholesterol, also described for GM2, including the role of Rab proteins (Choudhury et al., 2002), which leads to the assumption that trafficking defects lead to cholesterol and GM2 accumulation in NPC1-diseased neurons. The quantification of the GM2 level revealed a significantly higher amount in two of the NPC1 patient cell lines in comparison to the control cell line. In regards to GM3, we found an increase of the GM3 amount in the control cells and in the cells with the c.1180T>C mutation. This is, at least partly, consistent with the additional accumulation of GM3 described by Zervas and colleagues (Zervas et al., 2001).

As the amount of glycosphingolipids can be modulated by the relevant metabolic enzymes, we checked the mRNA and protein levels of the GM2 synthesis protein B4GALNT1 and the GM2 degradation enzyme Hex A. Regarding Hex A, we observed an increase of protein amount in cells with the compound heterozygous mutation, accompanied by a slightly increase of the B4GALNT1 level, and moreover, a Hex A activity indistinguishable from control. In contrast, cells with the c.1180T>C homozygous mutation demonstrated a protein level comparable to the control cells, but the lowest Hex A activity of all cell lines. The increased amount of Hex A protein could reflect a feedback loop, ending up in a normalized activity level of Hex A. Taken together with the fact that cells with the c.1180T>C homozygous mutation displayed a comparable level of Hex A to the control cells, but a decreased Hex A activity, one can speculate that the Hex A enzyme is antagonized by cholesterol. It has been previously reported that accumulated cholesterol may directly cause reduction in stability and activity of glycosylceramidase in NPC1 fibroblasts (Salvioli et al., 2004). We have now shown by molecular docking that cholesterol has a higher binding affinity to Hex A than its substrate GM2. Consequently, it might be possible that the high cholesterol content in NPC1 lysosomes could lead to an accumulation of GM2 into storage bodies, as a consequence of inhibitory interactions. Indeed, a study investigating basic GM2 catabolism provided evidence that membrane cholesterol content affects natural GM2 hydrolysis in the presence of the GM2 activator protein (Anheuser et al., 2015). The here observed colocalization of cholesterol and GM2 and the results of the docking simulation fit into the line of evidence, suggesting the accumulation of GM2 due to a reduced metabolic turn over based on a disturbed Hex A and/or GM2 activator protein activity. Thus, an elevated cholesterol level in late endosomes/lysosomes, might be an explanation of the here observed punctated GM2 staining pattern. The observation that cells with the homozygous mutation c.1180T>C demonstrated a cholesterol content indistinguishable from control cells, but in parallel showed the punctated staining pattern of cholesterol and GM2 accumulations can be explained by the assumed effect of cholesterol on Hex A activity.

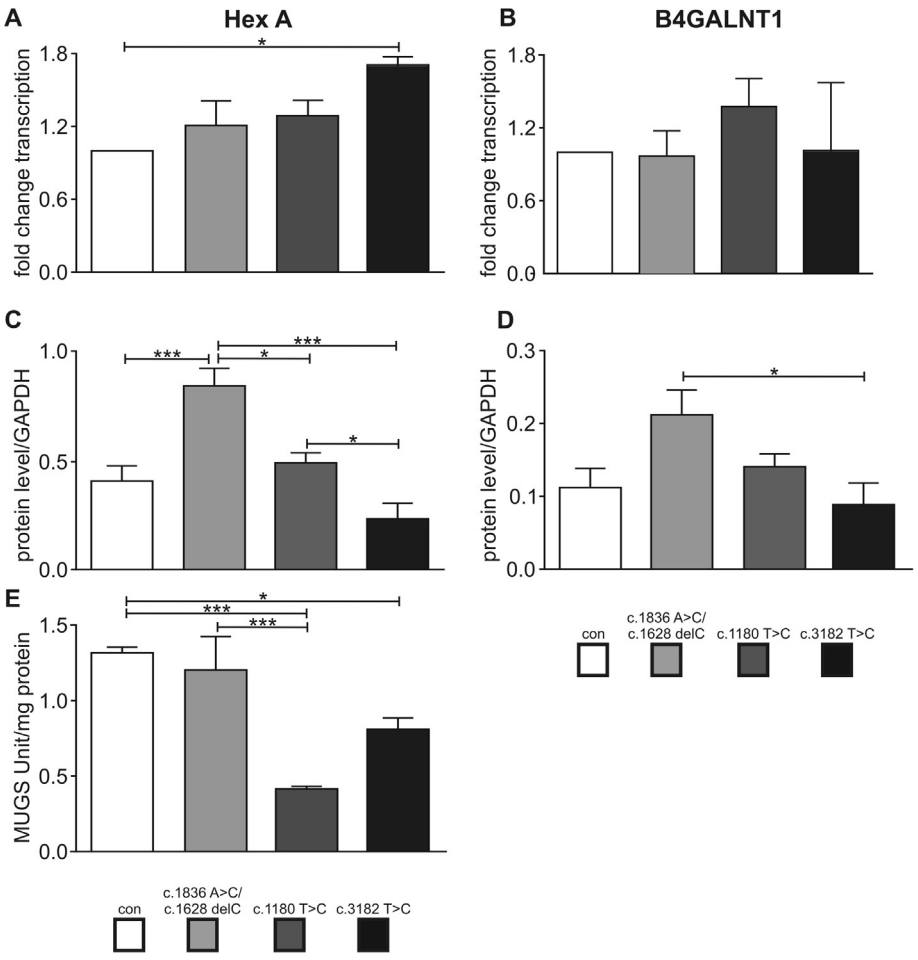

Fig. 6. RT-qPCR, western blot analysis and Hex A activity analysis. RT-qPCR analysis of GM2 degradation enzyme Hex A (A) and GM2 biosynthesis enzyme B4GALNT1 (B). Western blot analysis of the protein level of Hex A (C) revealed the highest amount of protein in the cell line with the compound heterozygous mutation c.1836A > C/c.1628delC. The protein level of B4GALNT1 (D) was only different between the cells carrying the homozygous mutation c.3182T > C and the compound heterozygous mutation c.1836A > C/c.1628delC. Regarding the Hex A enzyme activity (E), we found a significant reduction in the homozygous mutated c.1180T > C line and the cell line with the homozygous mutation c.3182T > C in comparison to the control cell line. * = $p < 0.05$, *** = $p < 0.001$. Data for quantification were obtained at least from three independent experiments.

Alternatively, the GM2 accumulation in our NPC1 model system might be a secondary effect of the cholesterol accumulation not related to GM2 ganglioside anabolic and catabolic enzymes. Gondré-Lewis and colleagues described a double knockout mouse with deficiency in NPC1 and GM2/GD2 synthase (Gondre-Lewis et al., 2003) in which the block of GM2 synthase led to reduction or absence of cholesterol accumulation normally seen in cortical neurons with NPC1 deficiency. This led them to suggest that cholesterol accumulation in NPC1 may be secondary to ganglioside accumulation. These views are not strictly self-exclusive as it is also possible that accumulation of either GM2 or cholesterol contributes to changes that aggravate increases in the other. In addition, it has been suggested that NPC1 may play a role in the trafficking of both unesterified cholesterol, and GM2 and GM3 gangliosides, thus its deficiency maybe initiate accumulation for both compound classes (Zervas et al., 2001).

In summary, we have described neuronal cells derived from three NPC1 patient-specific iPS cell lines. Cell lines carrying *NPC1* mutations differed in regards to accumulation of cholesterol, GM2 and GM3 gangliosides, as well as in activity of the GM2 degradation enzyme Hex A. Whether this hints towards a genotype-dependent lipid accumulation is enigmatic. To assume a simple genotype-clinical phenotype correlation is complicated, as also evidenced by a recently published case report on the heterogeneous clinical manifestations of monozygotic twins suffering from NPC1 (Benussi et al., 2014). Further comparative studies are required to gain a better understanding of the pathogenic mechanism and the correlation between mutation, heterogeneity and epigenetic aspects. However, iPSC-based models provide a powerful tool to elucidate such aspects as well as aspects of the catabolism of membrane components and their contribution to pathogenic mechanism of lysosomal storage disorders.

4. Experimental procedure

4.1. Cell culture

Neural progenitor cells (NPCs) were used to obtain neuronal derivatives of all used cells lines. For terminal neuronal differentiation NPCs were plated at a density of 45,000 cells/cm^2 in differentiation medium composed of DMEM, 40% DMEM/F-12, 1X B27, 0.5% penicillin/streptomycin, which was changed every 4 days over a period of 6 weeks. Generation of iPSCs and subsequently of neural progenitor cells (NPCs) were done as recently described (Trilck et al., 2013, 2016). Supplementary information are given in Peter et al. (Peter et al., 2016).

4.2. Immunocytochemistry

For immunocytochemistry, NPCs were plated on glass cover slips and differentiated as described above. Cells were fixed at room temperature for 15 min in 4% PFA, washed with PBS and stored in 0.02% NaN_3 at 4 °C. Immunocytochemistry was performed for beta III-tubulin (1:100, mouse IgG Tu-20, Santa Cruz biotechnology, Germany or rabbit IgG, Abcam, United Kingdom), GFAP (1:500, rabbit IgG, Dako, Denmark), and GM2 (1:10, mouse IgM, Dr. Dobrenis, New York, USA). Blocking and permeabilization was carried out using 0.3% Triton X-100 and 5% normal goat serum (Dako, Denmark; in PBS) for 30 min at room temperature. Cells were incubated with primary antibodies for 2 h at room temperature in 1% normal goat serum, followed by three washing steps with PBS. Alexa Fluor 568 (1:500, goat anti-mouse IgG or goat anti-rabbit IgG or goat anti-mouse IgM, Invitrogen, Germany) and Alexa Fluor 488 (1:500, goat anti-mouse IgG or goat anti-rabbit IgG or goat anti-mouse IgM or goat anti-rat IgM, Invitrogen, Germany) were used as secondary antibodies, incubated 1 h at room temperature. After washing with PBS, cells were stained with DAPI (5 min, 250 ng/ml), washed three times and mounted with Mowiol-DABCO mounting medium. Pictures were taken with a Biozero 8000 microscope system (Keyence, Germany).

4.3. Colocalization analysis

Colocalization analysis was performed in three independent experiments with digital confocal microscopy images (LSM780, Carl Zeiss; Germany, 63x oil immersion lens) taken of randomly chosen fields from each group (N = 3, n = 12). Mander's coefficient (Manders et al., 1993) and Costes automatic threshold (Costes et al., 2004) were used to determine colocalization of GM2 and beta III-tubulin (βIII-tub), GM2 and GFAP, and of GM2 and filipin. Mander's coefficient represents the proportion of overlapping pixels in two channels and it ranges from 0 for no colocalization to 1 for absolute colocalization. The Mander's coefficient is not dependent on signal intensities of both channels so it can be used even if the intensities differ strongly (Manders et al., 1993). Costes automatic threshold quantifies amount of colocalization automatically based on spatial statistics. Therefore, correlation in different regions of the two-dimensional histogram of a two-color image is used to automatically estimate the threshold by identifying the pixel values with a positive Pearson's correlation coefficient (Costes et al., 2004). NIH Image J software (Schneider et al., 2012) plugin JaCoP (Bolte and Cordelieres, 2006) was used for analysis and determination of colocalization.

4.4. Filipin staining

Filipin was used to analyze the sequestration of unesterified cholesterol (Norman et al., 1972). Cells were fixed with 4% PFA (in PBS) for 15 min, washed with PBS and incubated at room temperature for 45 min in the dark with a staining solution containing 100 μg/ml filipin (Polysciences, Germany) in PBS. Cells were washed twice with PBS for 5 min. Slides were mounted using Mowiol-DABCO and sealed with cover slips. After 12 h of drying in the dark at room temperature, fluorescence pictures were taken with a Biozero 8000 microscope system (Keyence, Germany). The fluorescence intensity of filipin was analyzed using NIH Image J software (Schneider et al., 2012). Data is given as relative fluorescent units (RFU) in arbitrary units (a.u.).

4.5. Quantification of cholesterol amount

The amount of total cholesterol was quantified as recently described (Trilck et al., 2013). Briefly, neuronal differentiated cells were washed with HBSS and harvested with Accutase® (STEMCELL Technologies, Germany). Enzymatic reaction was stopped with medium, and cells were centrifuged at 500*g* for 5 min. Cell pellets were resuspended in 0.1% SDS solution (in PBS) and lysis of the cells was performed by 5 freeze and thaw cycles using liquid nitrogen and tap water, respectively. Levels of total cholesterol were determined using the Amplex Red Cholesterol Assay Kit (Molecular Probes, Germany). Protein concentrations in lysates were measured using the bicinchoninic acid assay (BCA, Thermo Fisher Scientific, USA).

4.6. HPLC-MS/MS

For lipid analysis, cells were washed with HBSS and harvested with Accutase® (STEMCELL Technologies, Germany). Enzymatic reaction was stopped with medium, cells were counted and afterwards centrifuged at 500*g* for 5 min. Cell pellets were immediately stored at −80 °C until further analysis. Total lipid extractions were obtained by using ultrasonic tissue disintegration for 2 min. Total lipids were extracted into an ethanolic solution of internal standard (deuterated). Thereafter, High Performance Liquid Chromatography-Mass Spectroscopy (HPLC-MS/MS) was carried out on a C8 column (ACE 3C8, 5062.1 mm) for determination of GM2 (isoform C18-0) and GM3 (isoform C24-1). The values were expressed as μg per sample and normalized to μg per 10^6 cells.

4.7. Transmission electron microscopy

Differentiated neuronal cells were washed with PBS, pre-fixed with 4% PFA for 15 min at room temperature and covered with PBS containing 0.02% sodium azide for storage at +4 °C. For Transmission Electron Microscopy (TEM), cells were postfixed for at least one hour with a solution of 2% glutaraldehyde and 1% paraformaldehyde in 0.1 M sodium-phosphate buffer (PB). Following two washes in PBS, the cells were covered with a layer of 2% low-melt agarose. After hardening of the agarose the embedded cell blocks were gently detached from the coverslips and slices with embedded cells were transferred to glass vials for postfixation with an aqueous solution of 1% osmiumtetroxide for 1 h, followed by two rinses with distilled water. Further processing of the specimens included dehydration through an ascending acetone series to 100% acetone, followed by infiltration with epoxy resin (Epon 812, Serva, Germany). The agarose blocks with cell layers were transferred to rubber molds and cured at 60 °C. Resin blocks were trimmed using the Leica EM Trim 2 (Leica Microsystems, Germany). Semithin sections (approx. 0.5 μm) and thin sections (approx. 50–70 nm) were cut on an ultramicrotome (Ultracut S, Reichert, Austria) with a diamond knife (Diatome, Switzerland). Thin sections were transferred to copper grids, stained with uranyl acetate and lead citrate and examined on a Zeiss EM902 electron microscope operated at 80 kV (Carl Zeiss, Germany). Digital images were acquired with a side-mounted 1x2 k FT-CCD Camera (Proscan, Germany), using iTEM camera control and imaging software (Olympus Soft Imaging Solutions, Germany).

4.8. Reverse transcription quantitative real-time polymerase chain reaction

For reverse transcription quantitative real-time polymerase chain reaction (RT-qPCR) neuronal differentiated control cells as well as differentiated NPC1 mutant cell lines were cultivated in 24-well plates (Sarstedt, Germany) for 6 weeks. Cells were harvested, cDNA was synthesized using FastLane cDNA Kit (Qiagen, Germany) and PCR was performed using FastStart DNA SYBRGreen Plus Kit (Roche, Germany). QuantitTect Primer Assays (Qiagen, Germany) were used for lysosomal β-hexosaminidase A (Hex A,

NM_000520) and B4GALNT1 (NM_001276469). A LightCycler Nano (Roche, Germany) in combination with the LightCycler Nano 1.1 software was used to quantify mRNA transcription in neuronal differentiated cells. The following cycling parameters were used: initial denaturation at 95 °C for 600 s; 40 cycles of 20 s at 95 °C for denaturation, 20 s at 55 °C for annealing and 23 s at 72 °C for extension. Final melting was carried out at 65 °C for 60 s and 20 s at 95 °C. PCR products were verified by size in agarose-gel electrophoresis and melting point analysis. Tested gene mRNA amount was normalized to the reference gene glucose-6-phosphate-dehydrogenase (G6PD). All samples were run in duplicate. Relative changes in mRNA amount were calculated using the Pfaffl method (Pfaffl, 2001) or ΔCt values.

4.9. Western blot

Western blot analysis was performed as described earlier (Giese et al., 2010) with minor modifications. Neuronal differentiated cells were lysed in ice cold RIPA buffer. Protein concentrations in lysates were measured using the bicinchoninic acid assay (BCA, Thermo Fisher Scientific, USA). Samples were boiled for 5 min at 95 °C in 5× sample buffer and separated by SDS-PAGE with precast gels (4–15%, Bio-Rad Laboratories GmbH, Germany). Proteins were transferred to nitrocellulose membrane with a *trans*-blot turbo transfer system (all Bio-Rad Laboratories GmbH, Germany). Membrane was washed with TBS, then blocked with TBST containing 0.1% Tween 20 and 5% skim milk powder (pH 7.6) for 1 h at room temperature and incubated with primary antibodies (rabbit polyclonal anti-B4GALNT1, 1:250, Aviva Systems Biology, USA; rabbit polyclonal anti-Hex A, 1 μg/μl stock solution, 1:250, GeneTex, USA; mouse monoclonal anti-GAPDH, 1:10,000, Abcam, United Kingdom) at least 1 h in TBST containing 3% skim milk powder. Between the usages of several antibodies, blots were rinsed 3 times with TBST and incubated with fluorescent dye-conjugated secondary antibodies (Alexa Fluor 680 LT goat anti-rabbit IgG, 1:20,000; Alexa Fluor 800 goat anti-mouse IgG; all Molecular Probes, Germany). As a molecular weight marker, the Precision Plus Protein Dual Xtra Standards (Bio-Rad Laboratories GmbH, Germany) was used. Visualization and quantification (semi-quantitative method) were performed with the Odyssey Infrared Imaging System (LI-COR Biosciences GmbH, Germany). Expression of glyceraldehyde 3-phosphate dehydrogenase (GAPDH) was used for normalization.

4.10. Molecular docking

Molecular docking simulation was used to predict the binding modes and estimate the binding affinities of cholesterol and GM2 to Hex A. The structures of cholesterol and Hex A were built using chembio3D, where energy minimization was also performed. Three-dimensional coordinates of the X-ray crystal structure of the human Hex A were obtained from the Protein Data Bank (PDB, code 2GK1; Lemieux et al., 2006). Molecular docking was performed with the AutoDock Vina 1.1.2 (Trott and Olson, 2010). The search space was 30 Å × 30 Å × 30 Å, which encompassed the whole active site.

4.11. Determination of lysosomal β-hexosaminidase a specific activity

This was carried out based on that previously described (Dobrenis, 1998). Following 3 washes with Dulbecco's phosphate buffered saline, cultures in 6-well plates were individually harvested mechanically using a cell scraper and cold homogenizing buffer [0.1% Triton X-100 in 0.1 M sodium citrate/citric acid, pH 5.5, with 0.05% bovine serum albumin (BSA)]. After freeze-thawing, samples were sonicated, microcentrifuged (20 min. with 10,000 rpm), and each supernatant assayed in triplicate. Enzyme activity was determined using standard fluorogenic artificial substrate 4-methylumbelliferyl-2-acetamido-2-deoxy-6-sulfate-β-D-glucopyranoside (MUGS) (Research Products International, USA; cat# 64150) effectively cleaved by the Hex A isozyme (EC 3.2.1.52). The assay was performed at 37 °C in citric acid/sodium phosphate buffer at pH 4.5 for 0.5 h. Protein was determined colorimetrically using the bicinchoninic acid assay (BCA, USA) with BSA as the standard. Data are expressed as specific activity, i.e. Units (U) of activity/mg of protein where 1U equals 1 nmol substrate cleaved per hour at 37 °C. For these determinations, 3 independent subcultures were prepared, in duplicate, for each cell line.

4.12. Statistical analysis

Data represent at least three independent experiments, done at least in duplicates. Analysis of the data was carried out with GraphPad Prism 6 (GraphPad Software Inc., USA). Data are given as mean ± sem. Unless otherwise stated, one-way ANOVA or student's *t*-test were used to test for significance, with * = $p < 0.05$; ** = $p < 0.01$, *** = $p < 0.001$. $p < 0.05$ was assigned to indicate statistically significant differences.

Funding

This research did not receive any specific grant from funding agencies in the public, commercial, or not-for-profit sectors.

Authors' contributions

M. Trilck, F. Peter, K. Dobrenis, M. Frank, H. Mascher: conception and design of study, acquisition, analysis, and interpretation of data, drafting and revising manuscript. A. Rolfs, M.J. Frech: conception and design of study, analysis and interpretation of data, drafting and revising manuscript

Conflict of interest

The authors declare no competing financial interests.

Acknowledgements

We thank Centogene AG, Rostock, Germany, for providing human fibroblasts, Sarah M. E. Joost and Michael Rabenstein for providing electrophysiological data, Sebastian Rost for his excellent technical support, Ute Schulz for technical assistance with electron microscopy, and Pancrazio Papapietro for technical assistance with enzyme assays.

References

Anheuser, S., Breiden, B., Schwarzmann, G., Sandhoff, K., 2015. Membrane lipids regulate ganglioside GM2 catabolism and GM2 activator protein activity. J. Lipid Res. 56 (9), 1747–1761. http://dx.doi.org/10.1194/jlr.M061036.

Bauer, P., Knoblich, R., Bauer, C., Finckh, U., Hufen, A., Kropp, J., Braun, S., Kustermann-Kuhn, B., Schmidt, D., Harzer, K., Rolfs, A., 2002. NPC1: complete genomic sequence, mutation analysis, and characterization of haplotypes. Hum. Mutat. 19 (1), 30–38.

Benussi, A., Alberici, A., Premi, E., Bertasi, V., Cotelli, M.S., Turla, M., Dardis, A., Zampieri, S., Marchina, E., Paghera, B., Gallivanone, F., Castiglioni, I., Padovani, A., Borroni, B., 2014. Phenotypic heterogeneity of Niemann-Pick disease type C in monozygotic twins. J. Neurol. (0340–5354 (Linking))

Bergamin, N., Dardis, A., Beltrami, A., Cesselli, D., Rigo, S., Zampieri, S., Domenis, R., Bembi, B., Beltrami, C.A., 2013. A human neuronal model of Niemann Pick C disease developed from stem cells isolated from patient's skin. Orphanet J. Rare Dis. 8 (34). http://dx.doi.org/10.1186/1750-1172-8-34.

Bolte, S., Cordelieres, F.P., 2006. A guided tour into subcellular colocalization analysis in light microscopy. J. Microsc. 224 (Pt 3), 213–232.

Choudhury, A., Dominguez, M., Puri, V., Sharma, D.K., Narita, K., Wheatley, C.L., Marks, D.L., Pagano, R.E., 2002. Rab proteins mediate Golgi transport of caveola-

internalized glycosphingolipids and correct lipid trafficking in Niemann-Pick C cells. J. Clin. Invest. 109 (12), 1541–1550. http://dx.doi.org/10.1172/JCI15420.
Costes, S.V., Daelemans, D., Cho, E.H., Dobbin, Z., Pavlakis, G., Lockett, S., 2004. Automatic and quantitative measurement of protein-protein colocalization in live cells. Biophys. J. 86 (6), 3993–4003. http://dx.doi.org/10.1529/biophysj.103.038422.
Dobrenis, K., 1998. Microglia in cell culture and in transplantation therapy for central nervous system disease. Methods (San Diego, Calif.) 16 (3), 320–344. http://dx.doi.org/10.1006/meth.1998.0688.
Gallala, H.D., Sandhoff, K., 2011. Biological function of the cellular lipid BMP-BMP as a key activator for cholesterol sorting and membrane digestion. Neurochem. Res. 36 (9), 1594–1600. http://dx.doi.org/10.1007/s11064-010-0337-6.
Giese, A.K., Frahm, J., Hübner, R., Luo, J., Wree, A., Frech, M.J., Rolfs, A., Ortinau, S., 2010. Erythropoietin and the effect of oxygen during proliferation and differentiation of human neural progenitor cells. BMC Cell Biol. 11 (1), 94.
Giese, A.-K., Mascher, H., Grittner, U., Eichler, S., Kramp, G., Lukas, J., te Vruchte, D., Al Eisa, N., Cortina-Borja, M., Porter, F.D., Platt, F.M., Rolfs, A., 2015. A novel, highly sensitive and specific biomarker for Niemann-Pick type C1 disease. Orphanet J. Rare Dis. 10 (1), 2006. http://dx.doi.org/10.1186/s13023-015-0274-1.
Gondre-Lewis, M.C., McGlynn, R., Walkley, S.U., 2003. Cholesterol accumulation in NPC1-deficient neurons is ganglioside dependent. Curr. Biol. 13 (15), 1324–1329.
Imrie, J., Heptinstall, L., Knight, S., Strong, K., 2015. Observational cohort study of the natural history of Niemann-Pick disease type C in the UK: a 5-year update from the UK clinical database. BMC Neurol. 15, 257. http://dx.doi.org/10.1186/s12883-015-0511-1.
Karten, B., Vance, D.E., Campenot, R.B., Vance, J.E., 2002. Cholesterol accumulates in cell bodies, but is decreased in distal axons, of Niemann-Pick C1-deficient neurons. J. Neurochem. 83 (5), 1154–1163.
Karten, B., Vance, D.E., Campenot, R.B., Vance, J.E., 2003. Trafficking of cholesterol from cell bodies to distal axons in Niemann Pick C1-deficient neurons. J. Biol. Chem. 278 (6), 4168–4175.
Lemieux, M.J., Mark, B.L., Cherney, M.M., Withers, S.G., Mahuran, D.J., James, M.N.G., 2006. Crystallographic structure of human beta-hexosaminidase A: interpretation of Tay-Sachs mutations and loss of G_{M2} ganglioside hydrolysis. J. Mol. Biol. 359 (4), 913–929. http://dx.doi.org/10.1016/j.jmb.2006.04.004.
Maetzel, D., Sarkar, S., Wang, H., Abi-Mosleh, L., Xu, P., Cheng, A.W., Gao, Q., Mitalipova, M., Jaenisch, R., 2014. Genetic and chemical correction of cholesterol accumulation and impaired autophagy in hepatic and neural cells derived from Niemann-Pick Type C patient-specific iPS cells. Stem Cell Rep. 2 (6), 866–880.
Manders, E.M.M., Verbeek, F.J., Aten, J.A., 1993. Measurement of co-localization of objects in dual-colour confocal images. J. Microsc. 169 (3), 375–382. http://dx.doi.org/10.1111/j.1365-2818.1993.tb03313.x.
Millat, G., Marçais, C., Tomasetto, C., Chikh, K., Fensom, A.H., Harzer, K., Wenger, D. A., Ohno, K., Vanier, M.T., 2001. Niemann-Pick C1 disease: correlations between NPC1 mutations, levels of NPC1 protein, and phenotypes emphasize the functional significance of the putative sterol-sensing domain and of the cysteine-rich luminal loop. Am. J. Hum. Genet. 68 (6), 1373–1385. http://dx.doi.org/10.1086/320606.
Möbius, W., Herzog, V., Sandhoff, K., Schwarzmann, G., 1999. Intracellular distribution of a biotin-labeled ganglioside, GM1, by immunoelectron microscopy after endocytosis in fibroblasts. J. Histochem. Cytochem. 47 (8), 1005–1014.
Norman, A.W., Demel, R.A., de Kruyff, B., van Deenen, L.L., 1972. Studies on the biological properties of polyene antibiotics. Evidence for the direct interaction of filipin with cholesterol. J. Biol. Chem. 247 (6), 1918–1929.
Ordonez, M.P., 2012. Defective mitophagy in human Niemann-Pick Type C1 neurons is due to abnormal autophagy activation. Autophagy 8 (7), 1157–1158. http://dx.doi.org/10.4161/auto.20668.
Ordonez, M.P., Steele, J.W., 2016. Modeling Niemann Pick type C1 using human embryonic and induced pluripotent stem cells. Brain Res. http://dx.doi.org/10.1016/j.brainres.2016.03.007.
Ory, D.S., 2000. Niemann-Pick type C: a disorder of cellular cholesterol trafficking. Biochim. Biophys. Acta 1529 (1–3), 331–339.
Park, W.D., O'Brien, J.F., Lundquist, P.A., Kraft, D.L., Vockley, C.W., Karnes, P.S., Patterson, M.C., Snow, K., 2003. Identification of 58 novel mutations in Niemann-Pick disease type C: correlation with biochemical phenotype and importance of PTC1-like domains in NPC1. Hum. Mutat. 22 (4), 313–325.
Patterson, M.C., Hendriksz, C.J., Walterfang, M., Sedel, F., Vanier, M.T., Wijburg, F., 2012. Recommendations for the diagnosis and management of Niemann-Pick disease type C: an update. Mol. Genet. Metab. 106 (3), 330–344. http://dx.doi.org/10.1016/j.ymgme.2012.03.012.
Pentchev, P.G., Comly, M.E., Kruth, H.S., Patel, S., Proestel, M., Weintroub, H., 1986. The cholesterol storage disorder of the mutant BALB/c mouse. A primary genetic lesion closely linked to defective esterification of exogenously derived cholesterol and its relationship to human type C Niemann-Pick disease. J. Biol. Chem. 261 (6), 2772–2777.
Pentchev, P.G., Brady, R.O., Blanchette-Mackie, E.J., Vanier, M.T., Carstea, E.D., Parker, C.C., Goldin, E., Roff, C.F., 1994. The Niemann-Pick C lesion and its relationship to the intracellular distribution and utilization of LDL cholesterol. Biochim. Biophys. Acta 1225 (3), 235–243.
Peter, F., Trilck, M., Rolfs, A., Frech, M.J., 2016. Dataset in support of the generation of Niemann-Pick disease Type C1 patient specific iPS cell lines carrying the novel NPC1 mutation c.1180T > C or the prevalent c.3182T > C mutation – analysis of pluripotency and neuronal differentiationhallmarks. Data in Brief.
Pfaffl, M.W., 2001. A new mathematical model for relative quantification in real-time RT-PCR. Nucleic Acids Res. 29 (9), 45. http://dx.doi.org/10.1093/nar/29.9.e45.
Saito, M., Chakraborty, G., Shah, R., Mao, R.F., Kumar, A., Yang, D.S., Dobrenis, K., 2012. Elevation of GM2 ganglioside during ethanol-induced apoptotic neurodegeneration in the developing mouse brain. J. Neurochem. 121 (4), 649–661.
Salvioli, R., Scarpa, S., Ciaffoni, F., Tatti, M., Ramoni, C., Vanier, M.T., Vaccaro, A.M., 2004. Glucosylceramidase mass and subcellular localization are modulated by cholesterol in Niemann-Pick disease type C. J. Biol. Chem. 279 (17), 17674–17680. http://dx.doi.org/10.1074/jbc.M313517200.
Schneider, C.A., Rasband, W.S., Eliceiri, K.W., 2012. NIH Image to ImageJ: 25 years of image analysis. Nat. Methods 9 (7), 671–675.
Stenson, P.D., Ball, E.V., Mort, M., Phillips, A.D., Shiel, J.A., Thomas, N.S.T., Abeysinghe, S., Krawczak, M., Cooper, D.N., 2003. Human Gene Mutation Database (HGMD): 2003 update. Hum. Mutat. 21 (6), 577–581. http://dx.doi.org/10.1002/humu.10212.
Sun, X., Marks, D.L., Park, W.D., Wheatley, C.L., Puri, V., O'Brien, J.F., Kraft, D.L., Lundquist, P.A., Patterson, M.C., Pagano, R.E., Snow, K., 2001. Niemann-Pick C variant detection by altered sphingolipid trafficking and correlation with mutations within a specific domain of NPC1. Am. J. Hum. Genet. 68 (6), 1361–1372.
Suzuki, Y., Jacob, J.C., Suzuki, K., Kutty, K.M., 1971. Gm2-gangliosidosis with total hexosaminidase deficiency. Neurology 21 (4), 313–328.
Taniguchi, M., Shinoda, Y., Ninomiya, H., Vanier, M.T., Ohno, K., 2001. Sites and temporal changes of gangliosides GM1/GM2 storage in the Niemann-Pick disease type C mouse brain. Brain Dev. 23 (6), 414–421.
Terry, R.D., Weiss, M., 1963. Studies in Tay-Sachs disease. II. Ultrastructure of the cerebrum. J. Neuropathol. Exp. Neurol. 22, 18–55.
Trilck, M., Hübner, R., Seibler, P., Klein, C., Rolfs, A., Frech, M.J., 2013. Niemann-Pick type C1 patient-specific induced pluripotent stem cells display disease-specific hallmarks. Orphanet J. Rare. Dis. 8 (1), 144.
Trilck, M., Hübner, R., Frech, M.J., 2016. Generation and neuronal differentiation of patient-specific induced pluripotent stem cells derived from niemann-pick type C1 fibroblasts. Methods Mol. Biol. 1353, 233–259. http://dx.doi.org/10.1007/7651_2014_166.
Trott, O., Olson, A.J., 2010. AutoDock Vina: improving the speed and accuracy of docking with a new scoring function, efficient optimization, and multithreading. J. Comput. Chem. 31 (2), 455–461. http://dx.doi.org/10.1002/jcc.21334.
Vanier, M.T., 1999. Lipid changes in Niemann-Pick disease type C brain: personal experience and review of the literature. Neurochem. Res. 24 (4), 481–489.
Vanier, M.T., 2010. Niemann-Pick disease type C. Orphanet J. Rare. Dis 16 (5), 1172–1750 (Linking).
Walkley, S.U., Zervas, M., Wiseman, S., 2000. Gangliosides as modulators of dendritogenesis in normal and storage disease-affected pyramidal neurons. Cereb. Cortex 10 (10), 1028–1037.
Walter, M., Chen, F.W., Tamari, F., Wang, R., Ioannou, Y.A., 2009. Endosomal lipid accumulation in NPC1 leads to inhibition of PKC, hypophosphorylation of vimentin and Rab9 entrapment. Biol. Cell 101 (3), 141–152.
Yu, D., Swaroop, M., Wang, M., Baxa, U., Yang, R., Yan, Y., Coksaygan, T., DeTolla, L., Marugan, J.J., Austin, C.P., McKew, J.C., Gong, D.-W., Zheng, W., 2014. Niemann-pick disease type C: induced pluripotent stem cell-derived neuronal cells for modeling neural disease and evaluating drug efficacy. J. Biomol. Screening 19 (8), 1164–1173. http://dx.doi.org/10.1177/1087057114537378.
Zervas, M., Dobrenis, K., Walkley, S.U., 2001. Neurons in Niemann-Pick disease type C accumulate gangliosides as well as unesterified cholesterol and undergo dendritic and axonal alterations. J. Neuropathol. Exp. Neurol. 60 (1), 49–64.

Data in Brief 12 (2017) 123–131

Contents lists available at ScienceDirect

Data in Brief

journal homepage: www.elsevier.com/locate/dib

Data Article

Dataset in support of the generation of Niemann-Pick disease Type C1 patient-specific iPS cell lines carrying the novel NPC1 mutation c.1180T > C or the prevalent c.3182T > C mutation – Analysis of pluripotency and neuronal differentiation

Franziska Peter [1], Michaela Trilck [1], Michael Rabenstein, Arndt Rolfs, Moritz J. Frech *

Albrecht-Kossel-Institute for Neuroregeneration (AKos), University Medicine Rostock, Gehlsheimer Straße 20, 18147 Rostock, Germany

ARTICLE INFO

Article history:
Received 22 February 2017
Received in revised form
10 March 2017
Accepted 28 March 2017
Available online 2 April 2017

Keywords:
Induced pluripotent stem cells
Niemann-Pick Type C1
Neuronal differentiation

ABSTRACT

Data presented in this article demonstrate the generation and characterization of two novel Niemann-Pick disease Type C1 (NPC1) patient-specific induced pluripotent stem cell (iPSC) lines, related to the research article Trilck et al. (Diversity of Glycosphingolipid GM2 and Cholesterol Accumulation in NPC1 Patient-Specific iPSC-Derived Neurons; Brain Res.; 2017; 1657:52-61. doi: 10.1016/j.brainres.2016.11.031). For reprogramming fibroblasts, carrying the novel homozygous mutation c.1180T > C and the prevalent homozygous mutation c.3182T > C, were used. Reprogramming into patient-specific iPSCs was induced by retroviral transduction of the transcription factors Sox2, Klf4, Oct4 and c-Myc, and confirmed according to their pluripotency. The iPSCs were subsequently differentiated into neural progenitor cells, which were terminally differentiated into functional neurons and glial cells. The generation of these cell lines provides further

DOI of original article: http://dx.doi.org/10.1016/j.brainres.2016.11.031
* Corresponding author. Fax: +49 381 494 4699.
E-mail addresses: franziska.peter2@uni-rostock.de (F. Peter), michaela.trilck@neuro.uni-luebeck.de (M. Trilck), michael.rabenstein2@uni-rostock.de (M. Rabenstein), arndt.rolfs@med.uni-rostock.de (A. Rolfs), moritz.frech@med.uni-rostock.de (M.J. Frech).
[1] These authors contributed equally.

http://dx.doi.org/10.1016/j.dib.2017.03.042

valuable tools to investigate pathogenic mechanism of NPC1 in human neuronal cells carrying different NPC1 mutations.

Specifications Table

Subject area	Cell biology
More specific subject area	Patient specific induced pluripotent stem cells and neuronal derivatives
Type of data	Phase contrast and fluorescence images, graphs of current and voltage traces of patch clamp recordings
How data was acquired	Fluorescence microscopy was performed with Keyence Biozero 8000 and a Carl Zeiss LSM780 microscope. Whole cell Patch clamp experiments in the current and voltage clamp mode were performed with a HEKA EPC-10-double amplifier with the according PatchMaster software
Data format	analyzed
Experimental factors	Human fibroblasts were transduced to induced pluripotent stem cells by retroviral transfection of Sox2, Klf4, Oct4 and c-Myc
Experimental features	Reprogramming of fibroblasts by retroviral system. Determination of karyotype by Giemsa Trypsin banding. Detection of marker for pluripotency by alkaline phosphatase (AP) staining and immunocytochemistry in induced pluripotent stem cells, embryoid bodies and neural progenitor cells. Specific marker for neurons and glial cells were detected by immunocytochemistry. Recording of functional ion channels by patch clamp technique.
Data source location	Albrecht-Kossel-Institute for Neuroregeneration (AKos), University Medicine Rostock, Rostock, Germany
Data accessibility	Data is provided with this article

Value of the data

- Data in support of the generation of patient-specific iPSCs carrying novel NPC1 mutation.
- Data demonstrating the pluripotency of generated iPSCs and derived neural progenitors.
- Data showing differentiation of neural progenitors into neurons and glial cells.
- Data describing the establishment of human cell model applicable in NPC1 disease modeling and drug discovery.

1. Data

These data show the generation of NPC1 patient-specific induced pluripotent stem cells (iPSCs) using a standardized protocol [1]. Data presented in this article are related to the research article Trilck et al. [2]. Fibroblasts of NPC1 patients, carrying the homozygous *NPC*1 mutation c.1180T > C or c.3182T > C, were used for reprograming. The c.1180T > C is a novel unpublished mutation while mutation c.3182T > C is the most prevalent mutation of the *NPC*1 gene found in patients [3]. Data of the new cell lines were compared with a control cell line for examination of differences in reprogramming and pluripotency which might occur due to *NPC*1 mutation. Data demonstrate the pluripotency of the generated iPSCs by immunocytochemical detection of a panel of specific pluripotency

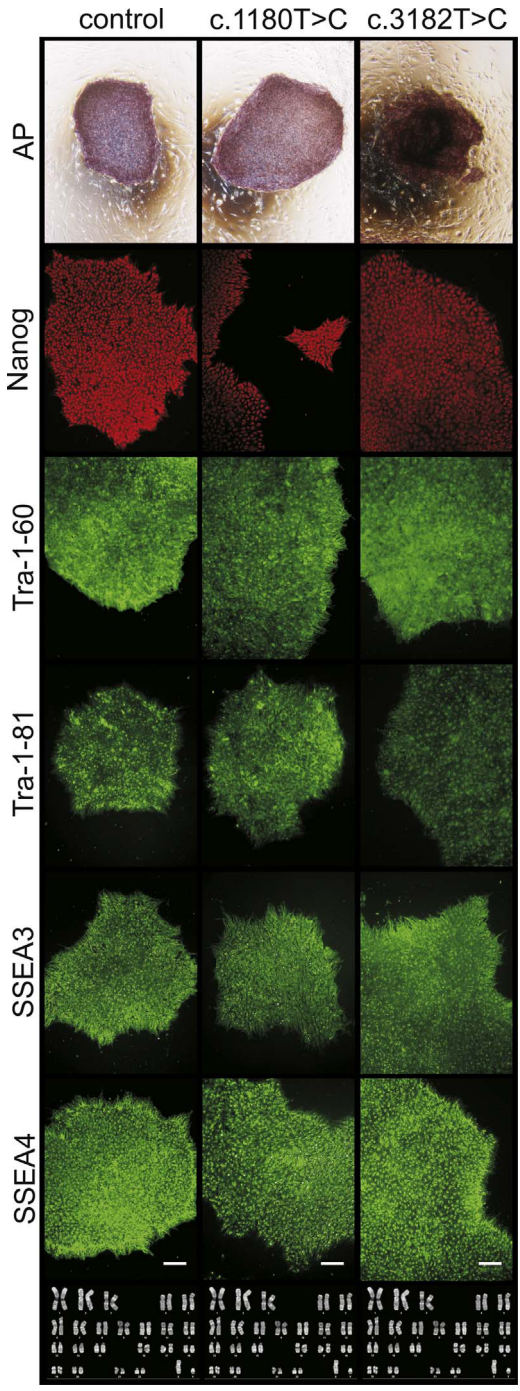

Fig. 1. Examination of pluripotency of iPSCs and karyotype. Alkaline phosphatase (AP) staining (upper row). Photographs of immunocytochemistry, taken with a Keyence Biozero 800 microscope, show iPSC colonies being positive for pluripotency specific marker Nanog (red), Tra-1–60, Tra-1–81, SSEA3 and SSEA4 (all green). Scale bars in lower row are representative for all photographs and indicate 100 μm. Phase contrast picture of karyotype by Giemsa trypsin banding (last row) indicate no abnormalities due to reprogramming. No scale is given for karyotypes.

marker (Fig. 1). Pluripotency was further shown by induction of embryoid bodies and the immunocytochemical detection of nestin, muscle actin and α-feto protein (αFP), specific markers for the three germ layers (Fig. 2). Data present the differentiation of iPSCs into neural progenitor cells (Fig. 3). Terminal neuronal differentiation in neurons and in glial cells is shown by immunocytochemical detection of the neuron specific marker βIII-tubulin (βIII-tub) and synaptophysin (Fig. 5) and the glial cell specific marker GFAP (Fig. 4). Data obtained by patch clamp recordings show differentiation of neural progenitor cells into functional neurons (Fig. 5).

2. Material and methods

2.1. Cell culture

Human dermal fibroblast cell lines from male donors were obtained from Coriell Institute for Medical Research, Camden, USA (NPC1 homozygous mutated: c.3882T > C [p.I1061T], GM18453) and Centogene AG, Rostock, Germany (control and NPC1 homozygous mutated c.1180T > C [p.Y395H]), respectively. Cells were cultivated in fibroblast medium containing DMEM high glucose, 10% FBS and 1% penicillin/streptomycin. Mitotically inactivated mouse embryonic fibroblasts (Amsbio, United Kingdom) were used as the feeder cell layer for iPSCs and were cultivated in fibroblast medium. HEK293FT cells (Invitrogen, Germany) were also cultivated in fibroblast medium but without antibiotics. Human iPSCs were cultured on a feeder cell layer in iPSC medium containing DMEM/F12, 20% knockout serum replacement, 1% penicillin/streptomycin, 1% GlutaMAX, 1% MEM non-essential amino acids, 0.2% 2-mercaptoethanol, and 10 to 15 ng/ml FGF2 (Amsbio, United Kingdom) or on Matrigel (Corning, Netherlands) cultured in mTESR1 medium (Stemcell Technologies, France). Medium was

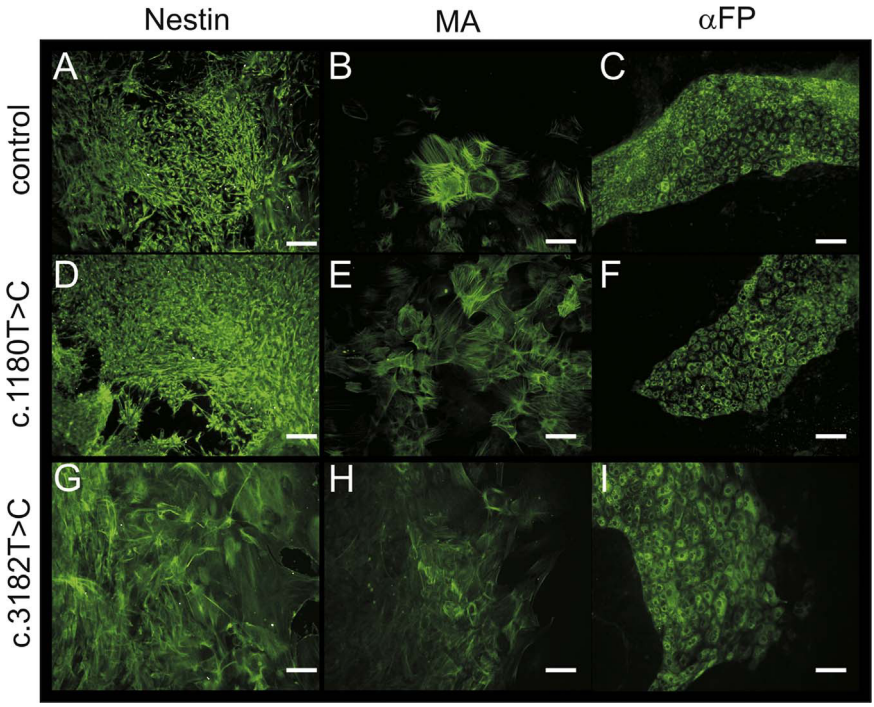

Fig. 2. Tissue specific marker in iPSC-derived embryoid bodies. Immunofluorescence photographs of tissue specific markers Nestin (ectoderm), muscle actin (MA, mesoderm) and α-fetoprotein (αFP, endoderm). Scales show 100 μm.

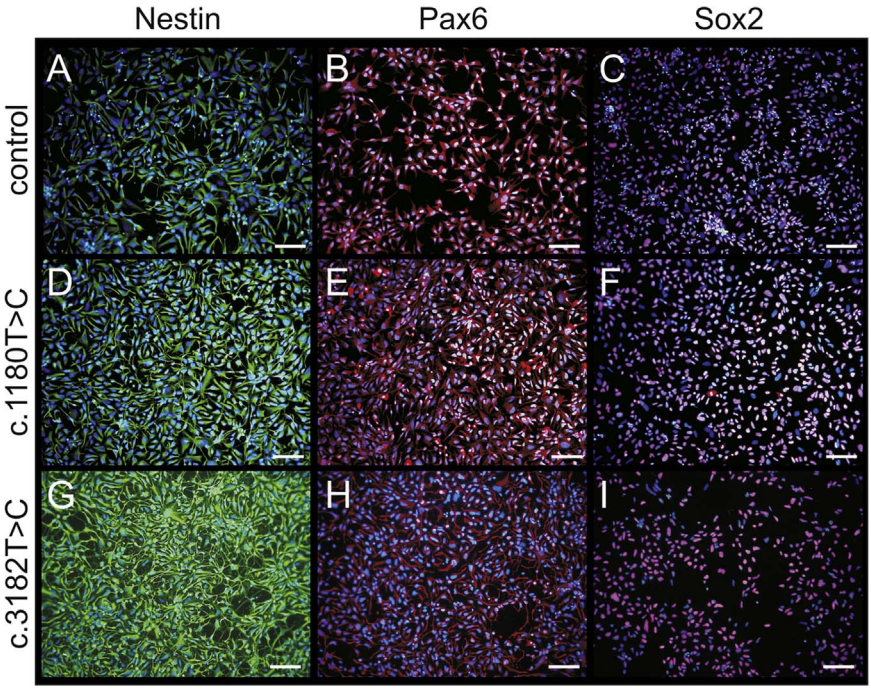

Fig. 3. Examination of pluripotency of iPSCs derived neural progenitor cells. Neural progenitor cells were assessed by immunocytochemical analyses of the neural progenitor markers nestin (A,D,G, green), Pax6 (B,E,H, red) and Sox2 (C,F,I, red). Nuclei were counter stained with DAPI (blue). Scale show 100 μm. All pictures represent an overlay of fluorescence of immunocytochemical staining and DAPI staining.

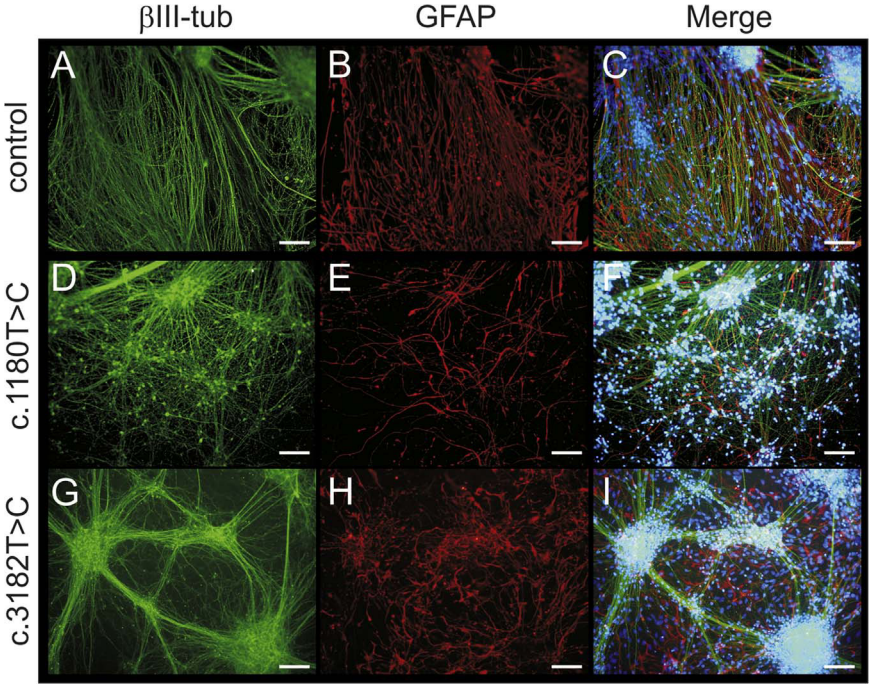

Fig. 4. Examination of neuronal and glial marker in terminally differentiated cells. Neural progenitor cells were terminally differentiated into neurons positive for βIII-tub (A,D,G, green) and into GFAP-positive glial cells (B,E,H, red). Cells were differentiated for 6 weeks. An overlay is shown in the right panel (C,F,I). Nuclei were counter stained with DAPI (C,F,I, blue). Scale show 100 μm for all pictures.

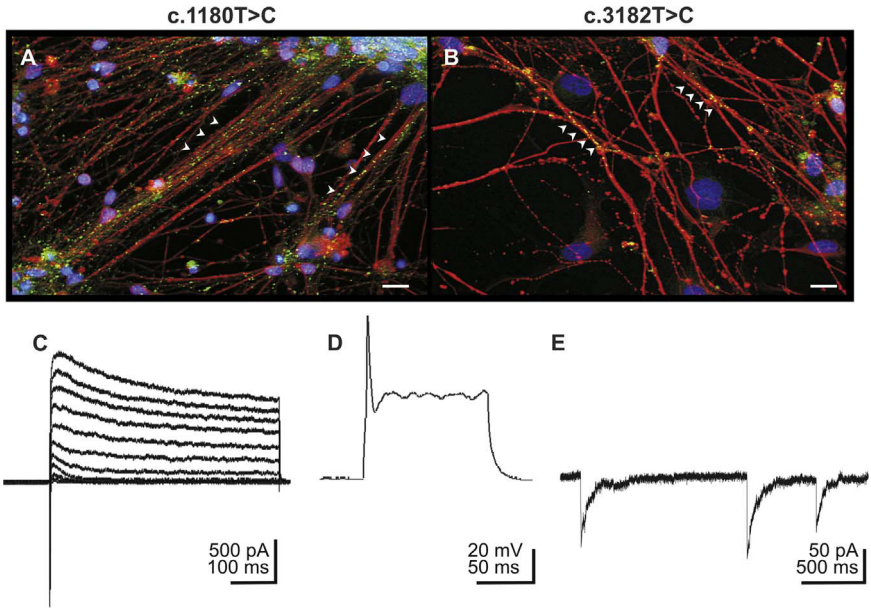

Fig. 5. Examination of neural progenitor cells derived neurons. Neural progenitor cells were differentiated into neurons positive for βIII-tub (red in A and B) and the pre-synaptic marker synaptophysin (green in A and B, arrowheads, scale 20 μm). Nuclei were stained with DAPI (blue in A and B). Patch clamp recordings (examples are taken from cells carrying the c.1180T > C mutation) of neurons revealed functional voltage gated ion channels, demonstrated by inward-directed sodium currents and outward-directed potassium currents (C), as well as elicited action potentials (D). Spontaneous postsynaptic currents proved the maturation of a functional synaptic network (E).

changed daily and cells were passaged weekly. All cells were cultivated at 37 °C in a saturated humidity atmosphere containing 5% CO_2.

2.2. Reprogramming of fibroblasts into iPSCs

Human iPSCs were generated as described earlier [1]. In brief, retroviruses were produced in HEK293FT cells using a retroviral vector encoding for GFP and one of the transcription factors (Sox2, Klf4, Oct4, or c-Myc) as well as VSV-G and Gag-Pol by XtremeGene 9 (Roche, Germany). Virus titering was performed through FACS analysis of the percentage of GFP-positive HEK293FT cells. The human fibroblasts were transduced with Sox2, Oct4, Klf4 (70–80% infection efficiency), and c-Myc (40–50% infection efficiency) in the presence of 5 μg/ml protamine sulfate (in fibroblast medium). After 48 h, cells were reseeded onto a gelatin-coated 6 cm-dish. The following day, medium was replaced with iPSC medium supplemented with 0.5 mM valproic acid to further increase the efficiency of reprogramming. Medium was changed daily and valproic acid was omitted after seven days. Initial iPSC colonies were picked and further cultivated on 45,000 feeder cells/cm^2 until a stable cell line was expanded.

2.3. Karyotyping

Karyotyping was performed by Giemsa Trypsin banding. Colonies were incubated with colcemid solution (10 μg/ml in HBSS) overnight for metaphase arrest. IPSCs were harvested by trypsin treatment (0.25%), wherein the reaction was stopped with Amniomax solution (Invitrogen, Germany), centrifuged at 300*g* for 10 min and the pellet was resuspended in 4 ml KCl solution (5.62%). Cells were incubated for 5 min at 37 °C and centrifuged at 300*g* for 10 min. After resuspension cells were fixed in 5 ml glacial acetic acid and methanol (1:3) and subsequently centrifuged for 7 min at 350*g*. This step

was repeated once. Next, supernatant was removed and cells were resuspended. Cell suspension was dropped onto cold slides and dried at 100 °C for 1 h. Giemsa solution (5%) was added and incubated for 5 min. Slides were washed in distilled water two times, dried at room temperature and sealed with cover slips.

2.4. Alkaline phosphatase staining

Alkaline phosphatase (AP) staining used to prove pluripotency of generated iPSCs. Colonies of iPSCs, cultivated on feeder cells, were fixed with ice-cold methanol (100%) for 10 min and incubated at room temperature for 15 min with the staining solution, containing 75% distilled water, 10% sodium chloride solution (1 M), 10% Tris solution (1 M, pH 9.8), 5% magnesium chloride solution (1 M), and NBT/BCIP solution (1:50, Roche, Germany). Microphotographs were taken using a Nikon Eclipse TS100 microscope system (Nikon, Germany).

2.5. Immunocytochemistry for pluripotency marker

Cells were fixed at room temperature for 15 minutes in 4% paraformaldehyde, washed with PBS and stored in 0.02% NaN_3 at 4 °C. Immunocytochemistry was performed for Nanog (1:100, rabbit IgG), Tra-1–60 (1:100, mouse IgM), Tra-1–81 (1:100, mouse IgM), SSEA3 (1:100, rat IgM), SSEA4 (1:100, mouse IgG, all Stemgent, USA). Blocking and permeabilization was carried out using 0.3% Triton X-100 and 5% normal goat serum (Dako, Denmark; in PBS) for 30 min at room temperature. Cells were incubated with primary antibodies for 2 h at room temperature in 1% normal goat serum, followed by three washing steps with PBS. Alexa Fluor 568 (1:500, goat anti-rabbit IgG, Invitrogen, Germany) and Alexa Fluor 488 (1:500, goat anti-mouse IgG or goat anti-mouse IgM or goat anti-rat IgM, Invitrogen, Germany) were used as secondary antibodies, incubated 1 h at room temperature in PBS. Cells were washed three times with PBS and mounted with Mowiol-DABCO mounting medium. Pictures were taken with a Biozero 8000 microscope system (Keyence, Germany).

2.6. Generation of embryoid bodies

Embroid body (EB) formation was used for proving pluripotency of iPSCs by using marker for the three germ layers. Whole iPSC colonies were mechanically lifted off the feeder cell layer and transferred into the cavity of a low attachment 6-well plate in 5 ml of differentiation medium (knockout DMEM, 20% FBS, 1% MEM non-essential amino acids, 2 mM GlutaMAX, and 0.1 mM beta-mercaptoethanol). EBs were formed after five to seven days and reseeded onto gelatin-coated glass cover slips. After 10 days of random differentiation, spread cells were fixed with 4% PFA for 15 min and immunocytochemically stained for muscle actin (MA, 1:50, mouse IgG, Dako, Denmark), alpha fetoprotein (aFP, 1:500, mouse monoclonal IgG, Sigma-Aldrich, Germany) and nestin (1:100, mouse IgG, R&D, Germany). Alexa Fluor 488 (1:500, goat anti-mouse IgG (Invitrogen, Germany) was used as secondary antibody, incubated 1 h at room temperature in PBS. Cells were washed three times with PBS and mounted with Mowiol-DABCO mounting medium. Pictures were taken with a Biozero 8000 microscope system (Keyence, Germany). Teratoma formation assay in immune deprived mice was not performed any more, following the 3Rs principle, to replace, refine or reduce, the use of animals, mandated by the German Protection of Animal Act. In regards of the teratoma formation assay in stem cell research the applicability of the *in vitro* embryoid body formation assay is discussed by Sheridan and colleagues [4].

2.7. Neural and neuronal differentiation

Neural differentiation of iPSCs was induced by density-dependent growing of the iPSCs on Matrigel (Corning, Netherlands). After neural rosettes had been formed spontaneously, cells were washed with DMEM/F12, singled using Accutase® and then magnetically sorted using magnetic beads against the surface marker PSA-NCAM (Miltenyi Biotec, Germany) which is a marker of the neural lineage. The generated neural progenitor cells were used for 25 passages and seeded at an expansion

density of 100,000 cells/cm^2 on poly-L-ornithine (15 μg/ml; Sigma, Seelze, Germany)/laminin (10 μg/ml; Trevigen, USA)-coated dishes in proliferation medium containing 60% DMEM, 40% DMEM/F-12, 1X B27, 0.5% penicillin/streptomycin, 20 ng/ml FGF2 (Amsbio, United Kingdom), 20 ng/ml EGF (Peprotech, Germany). Pluripotency of neural progenitor cells was proven by stainings for Sox2 (1:200, rabbit IgG, Abcam, United Kingdom), nestin (1:100, mouse IgG, R&D, Germany), Pax6 (1:200, rabbit IgG, Abcam, United Kingdom). Alexa Fluor 568 (1:500, or goat anti-rabbit IgG, Invitrogen, Germany) and Alexa Fluor 488 (1:500, goat anti-mouse IgG, Invitrogen, Germany) were used as secondary antibodies, incubated 1 h at room temperature with 1% normal goat serum in PBS. Cells were washed three times with PBS and mounted with Mowiol-DABCO mounting medium. Pictures were taken with a Biozero 8000 microscope system (Keyence, Germany).

For terminal neuronal differentiation cells were plated at a density of 45,000 cells/cm^2 in differentiation medium, containing 60% DMEM, 40% DMEM/F-12, 1X B27, 0.5% penicillin/streptomycin, which was changed every 4 days over a period of 6 weeks. Cells were stained for the neuronal marker beta III-tubulin (1:100, mouse IgG Tu-20, Santa Cruz biotechnology, Germany or rabbit IgG, Abcam, United Kingdom), GFAP (1:500, rabbit IgG, Dako, Denmark) and synaptophysin (1:100, mouse IgG, Sigma, Germany). Blocking and permeabilization was carried out using 0.3% Triton X-100 and 5% normal goat serum (Dako, Denmark; in PBS) for 30 min at room temperature. Cells were incubated with primary antibodies for 2 hours at room temperature in 1% normal goat serum, followed by three washing steps with PBS. Alexa Fluor 568 (1:500, goat anti-mouse IgG or goat anti-rabbit IgG, Invitrogen, Germany) and Alexa Fluor 488 (1:500, goat anti-mouse IgG, Invitrogen, Germany) were used as secondary antibodies, incubated 1 h at room temperature with 1% normal goat serum in PBS. After washing with PBS, cells were stained with DAPI (5 min, 250 ng/ml), washed three times and mounted with Mowiol-DABCO mounting medium. Pictures were taken with a Biozero 8000 microscope system (Keyence, Hamburg, Germany).

2.8. Patch clamp recordings

Patch clamp recordings were performed using an EPC-10 amplifier (Heka, Germany). Patch pipettes were pulled from borosilicate glass tubing (Harvard Apparatus, USA). The internal solution contained (mM): KCl 130, NaCl 10, HEPES 10, EGTA 11, $MgCl_2x6H_2O$ 1, $CaCl_2xH_2O$ 2, Mg-ATP 2. pH was adjusted to 7.2. When filled, electrodes had a resistance of 6–8 MΩ. Cell cultures were continuously superfused with an extracellular solution consisting of (mM): NaCl 125, KCl 2.5, $CaCl_2xH_2O$ 2, $MgCl_2x6H_2O$ 1, $NaHCO_3$ 26, $NaH_2PO_4xH_2O$ 1.25, glucosexH_2O 25. Solution was continuously bubbled with carbogen to maintain a pH of 7.4. Recordings were made in the whole cell configuration with holding potentials (V_H) of −60 or −80 mV. Current voltage responses were evoked by applying 100 ms voltage steps from −60 mV to +50 mV in 10 mV increments. Current clamp mode was used to apply current steps to induce action potentials or to measure spontaneous action potentials. Postsynaptic currents were measured in the voltage clamp mode at a V_H of −60 mV. Mini Analysis 6 (Synaptosoft, USA) was used to analyze recordings of post-synaptic currents.

Acknowledgements

We thank Centogene AG, Rostock, Germany, for providing human fibroblasts and Sebastian Rost for his excellent technical support.

Transparency document. Supporting information

Transparency data associated with this article can be found in the online version at http://dx.doi.org/10.1016/j.dib.2017.03.042.

References

[1] M. Trilck, R. Hübner, M.J. Frech, Generation and neuronal differentiation of patient-specific induced pluripotent stem cells derived from Niemann-Pick Type C1 fibroblasts, Methods Mol. Biol. 1353 (2016) 233–259.
[2] M. Trilck, F. Peter, C. Zheng, M. Frank, K. Dobrenis, H. Mascher, A. Rolfs, M.J. Frech, Diversity of glycosphingolipid GM2 and cholesterol accumulation in NPC1 patient-specific iPSC-derived neurons // diversity of glycosphingolipid GM2 and cholesterol accumulation in NPC1 patient-specific iPSC-derived neurons, Brain Res. 1657 (2017) 52–61.
[3] G. Millat, C. Marcais, M.A. Rafi, T. Yamamoto, J.A. Morris, P.G. Pentchev, K. Ohno, D.A. Wenger, M.T. Vanier, Niemann-Pick C1 disease: the I1061T substitution is a frequent mutant allele in patients of Western European descent and correlates with a classic juvenile phenotype, Am. J. Hum. Genet. 65 (1999) 1321–1329 (PM:10521297).
[4] S.D. Sheridan, V. Surampudi, R.R. Rao, Analysis of embryoid bodies derived from human induced pluripotent stem cells as a means to assess pluripotency, Stem Cells Int. 2012 (2012) 738910 (PM:22550517).

Peter et al. Orphanet Journal of Rare Diseases (2017) 12:145
DOI 10.1186/s13023-017-0697-y

Orphanet Journal of Rare Diseases

RESEARCH Open Access

Activation of PKC triggers rescue of NPC1 patient specific iPSC derived glial cells from gliosis

Franziska Peter, Sebastian Rost, Arndt Rolfs and Moritz J. Frech*

Abstract

Background: Niemann-Pick disease Type C1 (NPC1) is a rare progressive neurodegenerative disorder caused by mutations in the *NPC1* gene. The pathological mechanisms, underlying NPC1 are not yet completely understood. Especially the contribution of glial cells and gliosis to the progression of NPC1, are controversially discussed. As an analysis of affected cells is unfeasible in NPC1-patients, we recently developed an in vitro model system, based on cells derived from NPC1-patient specific iPSCs. Here, we asked if this model system recapitulates gliosis, observed in non-human model systems and NPC1 patient post mortem biopsies. We determined the amount of reactive astrocytes and the regulation of the intermediate filaments GFAP and vimentin, all indicating gliosis. Furthermore, we were interested in the assembly and phosphorylation of these intermediate filaments and finally the impact of the activation of protein kinase C (PKC), which is described to ameliorate the pathogenic phenotype of NPC1-deficient fibroblasts, including hypo-phosphorylation of vimentin and cholesterol accumulation.

Methods: We analysed glial cells derived from NPC1 patient specific induced pluripotent stem cells, carrying different NPC1 mutations. The amount of reactive astrocytes was determined by means of immuncytochemical stainings and FACS-analysis. Semi-quantitative western blot was used to determine the amount of phosphorylated GFAP and vimentin. Cholesterol accumulation was analysed by Filipin staining and quantified by Amplex Red Assay. U18666A was used to induce NPC1 phenotype in unaffected cells of the control cell line. Phorbol 12-myristate 13-acetate (PMA) was used to activate PKC.

Results: Immunocytochemical detection of GFAP, vimentin and Ki67 revealed that *NPC1* mutant glial cells undergo gliosis. We found hypo-phosphorylation of the intermediate filaments GFAP and vimentin and alterations in the assembly of these intermediate filaments in *NPC1* mutant cells. The application of U18666A induced not only NPC1 phenotypical accumulation of cholesterol, but characteristics of gliosis in glial cells derived from unaffected control cells. The application of phorbol 12-myristate 13-acetate, an activator of protein kinase C resulted in a significantly reduced number of reactive astrocytes and further characteristics of gliosis in NPC1-deficient cells. Furthermore, it triggered a restoration of cholesterol amounts to level of control cells.

(Continued on next page)

* Correspondence: moritz.frech@med.uni-rostock.de
Albrecht-Kossel-Institute for Neuroregeneration (AKos), University Medicine Rostock, Gehlsheimer Straße 20, 18147 Rostock, Germany

(Continued from previous page)

Conclusion: Our data demonstrate that glial cells derived from NPC1-patient specific iPSCs undergo gliosis. The application of U18666A induced comparable characteristics in un-affected control cells, suggesting that gliosis is triggered by hampered function of NPC1 protein. The activation of protein kinase C induced an amelioration of gliosis, as well as a reduction of cholesterol amount. These results provide further support for the line of evidence that gliosis might not be only a secondary reaction to the loss of neurons, but might be a direct consequence of a reduced PKC activity due to the phenotypical cholesterol accumulation observed in NPC1. In addition, our data support the involvement of PKCs in NPC1 disease pathogenesis and suggest that PKCs may be targeted in future efforts to develop therapeutics for NPC1 disease.

Keywords: NPC1, IPSCs, PKC, Vimentin, GFAP

Background

Niemann-Pick type C1 is a rare lysosomal storage disorder with an incidence of 1.12:100.000 live births [1]. The phenotype of this lipidosis exhibit various symptoms ranging from hepatosplenomegaly, motor dysfunctions, cerebellar ataxia and seizures to dementia, whereby the age of onset varies from early infantile to adult onset forms. The phenotype is based on mutations in either NPC1 (90%) or NPC2 (10%) gene [2]. Due to the defect of the cholesterol transporting NPC1 or NPC2 proteins, located in the lysosomal membrane and lumen, respectively, cholesterol and other lipids like sphingolipids GM2 and GM3 gangliosides accumulate [3]. Recent studies support an interaction of NPC1 and NPC2 mediating the cholesterol efflux from lysosomes, but the exact mechanism is still unexplained [4]. Diagnosis can be performed by biochemical tests like Filipin staining of patient fibroblasts and cholesterol esterification tests, as well as the detection of highly disease specific biomarker, but for final validation a genetic testing is essential [5, 6]. Currently, there is only one, by the European Medicines Agency (EMA) approved, therapy for NPC1 disease, using Miglustat, a reversible inhibitor of glucosylceramide synthase. Miglustat was approved to treat Gaucher disease Type 1, but also improves neurological symptoms in NPC1-patients, whereby the hypothesized mode of action is substrate reduction effect [7, 8]. Further potential therapy approaches are discussed containing the use of cyclodextrins, histone deacetylase inhibitors and chaperons [9, 10]. In regards of the neurological symptoms, like cerebellar ataxia, based on a progressive loss of cerebellar Purkinje cells, the pathological mechanism is not yet understood. Alike, the contribution of gliosis, described in NPC1 patients and different animal models is controversially discussed [11]. Gliosis is not only a ubiquitous event in the central nervous system after any kind of tissue damage [12], but is discussed to be an integral player in neurodegenerative diseases like Alzheimer disease [13], wherein reactive astrocytes can be beneficial as well detrimental for neuroprotection and tissue regeneration [14]. Interestingly, Alzheimer disease and NPC1 share some common features including abnormal cholesterol metabolism, and involvement of amyloid-β and tau pathology [15]. However, gliosis can be elucidated by an increased number of GFAP positive reactive astrocytes [16, 17]. Besides GFAP, an upregulation of other intermediate filaments (IFs) like vimentin and nestin can be observed, as well as an increased number of proliferative cells, demonstrated by Ki67 expression or BrDU incooperation experiments [18, 19]. In regards of NPC1 an increased number of reactive astrocytes and abnormal morphological changes are described in a commonly used NPC1 mouse model [20–22]. NPC1 deficient mice revealed an upregulation of glia cells after 4 weeks of age and astrocytes showed an atypical morphology by less elaborated processes and swollen cell bodies [23]. Gliosis was also shown in human post mortem brain biopsy [24–26]. Although, gliosis is a certainly proved pathological feature of NPC1 the role of glial cells in the progression of the disease is controversially discussed.

Recently we developed a human cell model system, based on induced pluripotent stem cells [27, 28], which was used in this study to elucidate if iPSC derived glial cells resemble gliosis, as a pathogenic hallmark of NPC1. This NPC1 cell model displays typical NPC1 hallmarks, like cholesterol and GM2 accumulations [27, 28], which is in accordance to other studies using comparable approaches [29–31]. However, a description of gliosis in such an in vitro model system is still missing.

Here we investigated gliosis and phosphorylation status of the intermediate filaments GFAP and vimentin in NPC1 patient-specific iPSC-derived glial cells. Intermediate filaments are a non-enzymatic, rod-shaped cytoskeleton component with a length of 8 to 15 nm diameter [32]. IFs are divided into 6 classes whereby class III contains structural proteins like nestin, vimentin and glial fibrillary acidic protein (GFAP). Functions of intermediate filaments are also very variable like cytoarchitecture, cell mobility, mechanical support but also vesicular trafficking and signal modulation [33]. The assembly of intermediate filaments is based on association of monomers whereby this is an assembly cycle consisting of polymerization via dephosphorylation of soluble monomers and depolimerization by

phosphorylation of filaments. IFs are phosphorylated by many different kinases like protein kinase C (PKC) or protein kinase A [34–36]. In NPC1 fibroblasts a disturbed vimentin assembly cycle with altered vimentin phosphorylation status and aggregation of vimentin was described [37]. Furthermore, they proved that sphingosine accumulation inhibits protein kinase C, subsequently vimentin was not phosphorylated, the pool of soluble vimentin was decreased and vesicular trafficking was blocked. An increased cholesterol storage in the endosomal/lysosomal system was hypothesized. Consequently activation of PKC, especially PKCε, could increase soluble vimentin and rescued cholesterol esterification effect in NPC1 fibroblasts [37, 38]. Here we demonstrated that NPC1 patient specific iPSC derived glial cells undergo spontaneously gliosis, reflecting a pathological characteristic of NPC1. In addition, we found a disturbed assembly cycle of GFAP and vimentin. Moreover, we were able to rescue the IF phenotype via the activation of PKC by phorbol 12-myristate 13-acetate, also leading to a decreased amount of reactive glial cells, an increased fraction of phosphorylated GFAP and vimentin, and decreased cholesterol accumulation in NPC1 mutant cells.

Methods

Cell culture

Human dermal fibroblast cell lines were obtained from Coriell Institute for Medical Research, Camden, USA (NPC1 compound heterozygous mutated: c.1836 A > C [p.E612D], c.1628 delC [p.P543Rfs*20]; GM18436 and NPC1 homozygous mutated: c.3882 T > C [p.I1061T]; GM18453) and Centogene AG, Rostock, Germany (control and NPC1 homozygous mutated: c.1180 T > C [p.Y395H]), respectively. Cells were cultivated in fibroblast medium containing DMEM high glucose, 10% FBS and 1% penicillin/streptomycin. All cells were cultivated at 37 °C in a saturated humidity atmosphere containing 5% CO_2.

Differentiation of progenitor cells

The generated neural progenitor cells, differentiated from patient-specific iPS cells [27], were used for 20 passages and seeded at an expansion density of 100,000 cells/cm^2 on poly-L-ornithine-coated (15 μg/ml; Sigma, Germany)/laminin (10 μg/ml; Trevigen, USA) dishes in proliferation medium containing DMEM, 30% DMEM/F-12, 1X B27, 0.5% penicillin/streptomycin, 20 ng/ml FGF2 (Amsbio, United Kingdom), 20 ng/ml EGF (Peprotech, Germany). For terminal differentiation cells were plated with a density of 45,000 cells/cm^2 in differentiation medium (DMEM, 30% DMEM/F-12, 1X B27, 0.5% penicillin/streptomycin), which was changed every 4 days over a period of 40 days. For experiments comprising an application of PMA or U18666A, cells were differentiated for 40 days and PMA (10 nM, Cayman Chemicals, USA) or U18666A (1 μg/ml Sigma, Germany) were applied for 24 h or 48 h.

Immunocytochemistry

Cells were fixed at room temperature for 15 min in 4% paraformaldehyde (PFA), washed with PBS and stored in 0.02% NaN_3 at 4 °C. Immunocytochemistry was performed for GFAP (1:500, rabbit IgG, Dako, Germany), Vimentin (1:100, mouse IgG, V9, Invitrogen, Germany), Blocking and permeabilization was carried out using 0.3% Triton X-100 and 5% normal goat serum (Dako, Germany) in PBS for 30 min at room temperature. Cells were incubated with primary antibodies for 1 h at room temperature in 1% normal goat serum, followed by three washing steps with PBS. Alexa Fluor 568 (1:500, goat anti-mouse IgG or goat anti-rabbit IgG, Invitrogen, Germany), Alexa Fluor 488 (1:500, goat anti-mouse IgG or goat anti-rabbit IgG, Invitrogen, Germany) were used as secondary antibodies, incubated 1 h at room temperature with 1% normal goat serum in PBS. After washing with PBS cells were stained with DAPI (5 min, 250 ng/ml), washed three times and mounted with Mowiol-DABCO mounting medium. Pictures were taken with a Biozero8000 microscope system (Keyence, Germany) and LSM780 laser scanning microscope (Zeiss, Germany).

Colocalization image analysis

Colocalization analysis was performed in three independent experiments with digital images taken of randomly chosen fields ($N = 3$, $n = 12$). Mander's coefficient [39] was used to determine colocalization of GFAP and Vimentin, and of GFAP and Nestin. Mander's coefficient represents the proportion of overlapping pixels in two channels and it ranges from 0 for no colocalization to 1 for absolute colocalization. The Mander's coefficient is not dependent on signal intensities of both channels so it can be used even if the intensities differ [39]. Costes automatic threshold quantifies amount of colocalization automatically based on spatial statistics. Therefore, correlation in different regions of the two-dimensional histogram of a two-color image is used to automatically estimate the threshold by identifying the pixel values with a positive Pearson's correlation coefficient [40]. NIH Image J software [41] plugin JaCoP [42] was used for analysis and determination of colocalization.

Filipin staining

For Filipin staining cells were fixed at room temperature for 15 min in 4% PFA, washed with PBS, and stored in 0.02% NaN_3 at 4 °C. Fixated cells were incubated with 0.1 mg/ml Filipin for 45 min. After three washing steps with PBS cells were mounted with Mowiol-DABCO mounting medium. Filipin fluorescence intensities were quantitative determined by taking 10 random pictures of three replicates using a Keyence Biozero 8000 microscope (Keyence, Germany). Analysis of the fluorescence intensities was performed using ImageJ [41] by automatic

determination of the threshold and subsequent measurement of the intensities taking area above threshold into account for normalization. Finally, results were normalized to wildtype intensities [43, 44].

Western blot

Whole cell lysates were obtained by incubation in RIPA-buffer for 15 min on ice. After centrifugation for 20 min at 15,000 xg at 4 °C supernatant was transferred.

Protein concentrations in samples were measured using the bicinchoninic acid assay (Pierce BCA Protein Assay Kit, Thermo Scientific, USA). Samples were boiled for 15 min at 95 °C in 5× Laemmli buffer and separated by SDS-PAGE with precast gels (4–15%, Bio-Rad Laboratories GmbH, Germany). Proteins were transferred to nitrocellulose membrane with a semi-dry blotting system Tans-Blot Turbo (Bio-Rad Laboratories GmbH, Germany). After blotting, membrane was washed with TBS and blocked with TBST, containing 0.1% Tween-20 and 5% milk powder (pH 7.6) or 5% BSA (Roth, Germany), for 1 h at room temperature. Followed by incubation with primary antibodies, Vimentin (1:10,000, rabbit IgG, GeneTex, USA), pSer38-Vimentin (1:1000, GeneTex, USA), GFAP (1:1000, mouse IgG, Cell Signalling Technology, USA) and pSer38-GFAP (1:1000, rabbit IgG, GeneTex, USA) at 4 °C over night and GAPDH (1:10,000, mouse IgG, Abcam, United Kingdom) and β-Actin (1:10,000, mouse IgG, Sigma, Germany) 1 h at room temperature. Western blots were rinsed 3 times with TBST between the usages of several antibodies and incubated with fluorescent dye labelled secondary antibodies, IRDye 680 LT (1:20,000, goat anti-rabbit IgG), IRDye 800 (1:10,000, goat anti-mouse IgG, all LI-COR, Germany), AlexaFluor 680 (1:10,000, goat anti-rat IgG), Invitrogen, Germany). Precision Plus Protein Dual Xtra Standards (Bio-Rad Laboratories GmbH, Germany) was used as a molecular weight marker. Visualization and quantification was performed with Odyssey Infrared Imaging System (LI-COR, Germany). Expression of glyceraldehyde 3-phosphate dehydrogenase (GAPDH) was used for normalization.

FACS

Cells were harvested by using Accutase (Stemcell Technologies, Germany) for 5 min. Reaction was stopped using differentiation media. After centrifugation for 5 min at 3000 xg cells were fixed in 1% PFA in PBS for 15 min. Fixed cells were stored in FACS washing buffer at 4 °C. For analysis cells were incubated with primary antibodies, GFAP (1:500, rabbit IgG, DAKO, Germany or 1:100, Rat IgG, Thermo Scientific, USA), Vimentin (1:100, mouse IgG, Invitrogen, Germany), Ki67 (1:100, rabbit IgG, Santa Cruz Biotechnology, Germany) in Saponin buffer (0.5% Saponin, 0,5% BSA, 0.02% NaN3) for 2 h gently shaking. After washing cells were incubated with secondary antibodies, Alexa Fluor 488 (1:1000, goat anti-rabbit IgG), Alexa Flour 647 (1:1000, goat anti-mouse IgG) or Alexa Fluor 568 (1:1000, goat anti-rat IgG; all Molecular Probes, Germany) for 1 h gently shaking. FACSCalibur and CellQuest Pro (BD, Germany) were used for cell analysis.

Amplex red assay

Amplex Red cholesterol assay (Molecular Probes, Germany) was used to quantify the amount of cholesterol as described recently [44–46]. Therefore, differentiated cells were washed with HBSS and harvested with Accutase (Stemcell Technologies, Germany). Enzymatic reaction was stopped with medium and cells were centrifuged at 3000 xg for 5 min. Cell pellets were resuspended in 0.1% SDS solution (in PBS) and lysis of the cells was performed by 5 freeze and thaw cycles using liquid nitrogen and tap water. Protein concentrations in lysates were measured using the bicinchoninic acid assay (Thermo Scientific, USA).

Statistical analysis

Analysis of the data was carried out with GraphPad Prism 6 (GraphPad Software Inc., USA). Data are given as mean ± SEM. Unless otherwise stated, unpaired t-test was used to test for significance, with * = $p < 0.05$, ** = $p < 0.01$, *** = $p < 0.001$.

Results

Gliosis is accompanied by the emergence of reactive astrocytes and can be determined not only by an increased number of GFAP positive ($GFAP^+$) cells but also by the upregulation of other IFs like vimentin and nestin, as well as a rise of proliferating Ki67 positive cells. Here, we used these criteria to approve gliosis in iPSC derived glial cells. Differentiation of the progenitor cells resulted in a mixed population of glia cells and of neurons, wherein the cultures contained around 35% neurons (data not shown), independent of the genotype of the cells, but an increased glial population in the mutated cell lines. Experiments were performed with cells differentiated for 6 weeks as we found other hallmarks of NPC1 like accumulation of cholesterol or GM2 after this time of differentiation [27, 28].

Analysis of gliosis in NPC1 patient specific iPSC derived glial cells

At first we were interested in the amount of glia cells in the here used human patient-specific iPSC derived cell model. Therefore, glial fibrillary acidic protein (GFAP) and vimentin were stained (Fig. 1a-d), revealing an increased amount of GFAP positive cells ($GFAP^+$), as well as vimentin positive ($vimentin^+$) cells, in cell lines bearing a *NPC1* mutation. Higher coefficients of colocalization

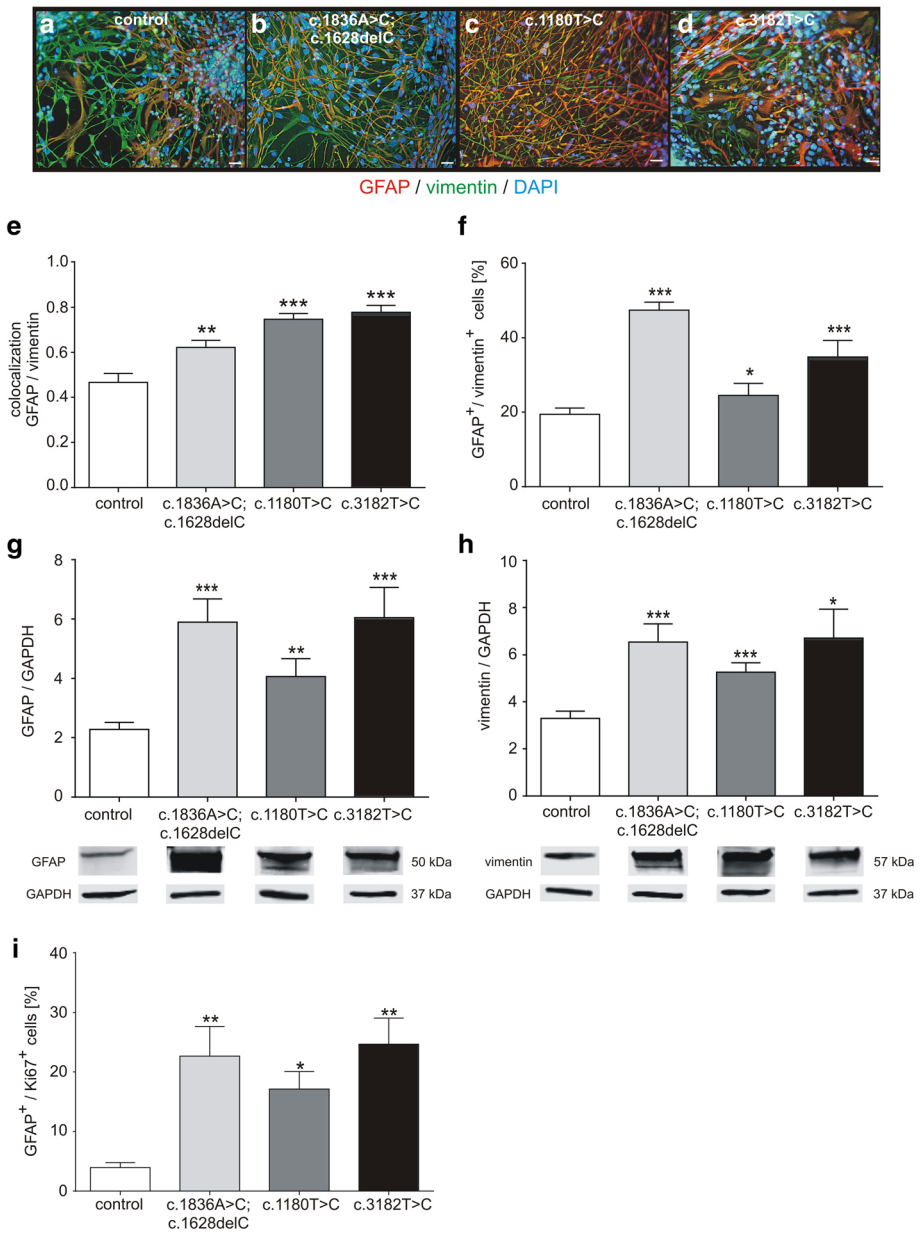

Fig. 1 Analysis of gliosis marker. **a**-**d** *NPC1* mutant cell lines contained a higher amount of GFAP$^+$ and vimentin$^+$ cells (red, **a**-**d**). DAPI staining (blue) indicates nuclei. Scale 100 μm. (**e**). Colocalization analysis of GFAP and vimentin revealed a significantly increased amount of double positive cells in all *NPC1* mutant cell lines. **f** FACS analysis of GFAP$^+$/vimentin$^+$ cells confirmed an increased amount of glia cells in *NPC1* mutant cell lines (N = 5–7, n = 14–23). **g** In addition, semi-quantitative protein measurement by western blot demonstrated a higher amount of GFAP (N = 7–11, n = 26–43) and **h** an increased amount of vimentin in NPC1 mutant cells (N = 5–7, n = 14–23). **i** FACS analysis of cells positive for GFAP and Ki67, elucidated an increased amount of double positive cells indicating gliosis *NPC1* mutant cell lines (**g**; N = 3–4, n = 7–9)

analysis confirmed this observation in *NPC1* mutant cells (Fig. 1e). In addition, flow cytometry analyses were done to quantify the proportion of GFAP$^+$/vimentin$^+$ cells (Fig. 1f), revealing a significantly increased amount of glial cells in all *NPC1* mutant cell lines in comparison to the control cell line after 6 weeks of differentiation. No differences between the amount of GFAP$^+$ control cells after 2 and 6 weeks of differentiation were found (data not shown), as well as no differences were found between control cells and mutated cells after 2 weeks of differentiation (data not shown), indicating an onset of gliosis in the mutated cells later than 2 weeks of differentiation. However, to further affirm gliosis we determined the protein level of GFAP (Fig. 1g) and vimentin (Fig. 1h)

by semi-quantitative western blot analyses, demonstrating significantly increased amounts of GFAP and vimentin. As further criteria of gliosis we proved the appearance of proliferative cells by means of a parallel staining of GFAP and Ki67 and determined the number of double positive cells by FACS analysis. This experiment revealed a significantly increased number of $GFAP^+/Ki67^+$ cells in all *NPC1* mutant cell lines in comparison to control cell line (Fig. 1i).

Taken together, these results demonstrate gliosis in NPC1 patient specific iPSC derived glial cells, proved by an increased number of proliferative glial cells and an increased number of $GFAP^+$ and $vimentin^+$ cells. As we have demonstrated an upregulation of vimentin in our cell model system, we speculated about an altered assembly of vimentin, as well as of GFAP, both belonging to the class of intermediate filaments type III, in the iPSC derived glial cells used here. Therefore, we analysed the assembly of GFAP and vimentin, as well as the phosphorylation status of these filaments.

Assembly and phosphorylation of IFs in iPSC derived glial cells

Recently, it was demonstrated that the assembly of vimentin is altered on fibroblasts of NPC1 patients [37], wherein the *NPC1* mutant fibroblasts showed a disturbed arrangement of vimentin. The here used iPSC derived glial cells demonstrated comparable pattern of IF structure. Figure 2 represents immunocytochemical stainings of vimentin in control and NPC1 mutant cell lines (Fig. 2a-d). In comparison to the control cells (Fig. 2a), the NPC1 mutant cell lines revealed longer and thicker criss-crossed bundles of vimentin (Fig. 2b-d). We observed comparable changes for GFAP (Fig. 2e-h). The altered appearance is in accordance to observations in fibroblasts of NPC1 patients and indicates an altered assembly of these IFs. Next, we were interested in the phosphorylation of vimentin and GFAP as the assembly/disassembly of these IFs is regulated by phosphorylation of the IF monomers.

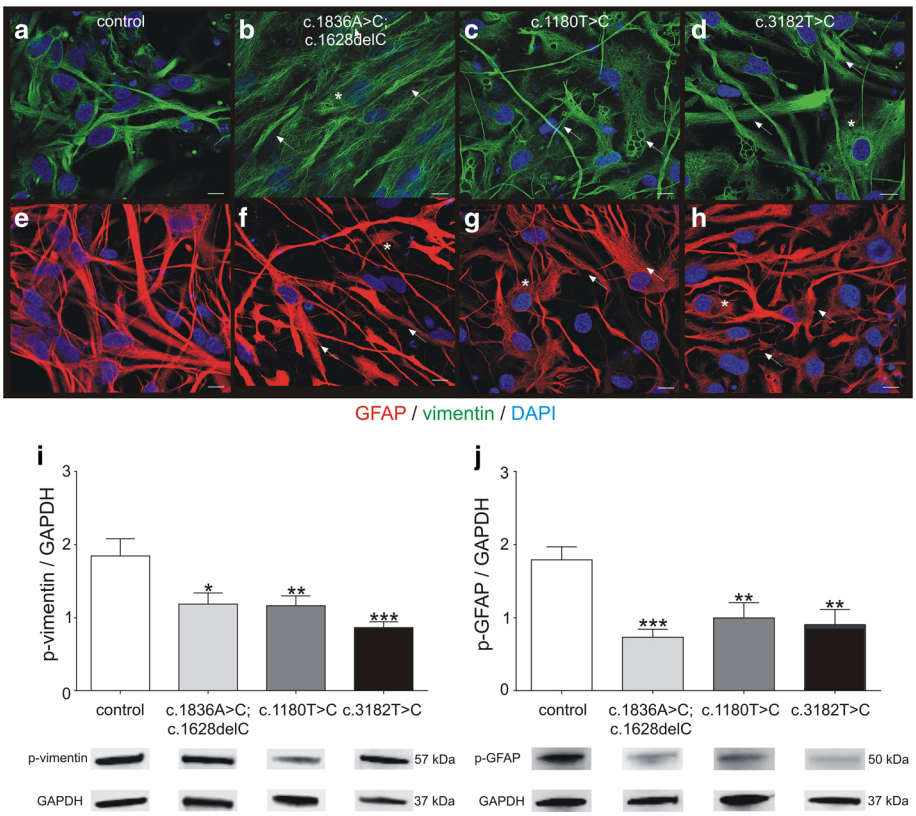

Fig. 2 Assembly and phosphorylation of vimentin and GFAP. **a**-**d** Immunocytochemical analysis of vimentin (green) indicates altered vimentin arrangement in cells bearing a *NPC1* mutation. These cells display longer and thicker vimentin bundles (arrows), arranged in a criss-crossed manner (asterik), in comparison to control cells. **e**-**h** Similar observations were made in cells stained for GFAP red). Nuclei are stained by DAPI (blue). Scale 10 μm. **i**, **j** Amount of phosphorylated vimentin (p-vimentin) and phosphorylated GFAP (p-GFAP) was quantified by semi-quantitative western blot. All *NPC1* mutant cell lines displayed a significantly reduced amount of p-vimentin and p-GFAP indicating a hypo-phosphorylation of the IFs. (p-vimentin: $N = 6–8$, $n = 26–40$; p-GFAP: $N = 5–7$, $n = 18–31$). Examples of according western blot bands are shown below the bar graphs

We used antibodies detecting the phosphorylation side serin 38 and determined the amount of phosphorylated vimentin and GFAP (p-vimentin, p-GFAP) by western blot (Fig. 2i, j). Control cells displayed the highest amount of p-vimentin and all mutant cell lines had a significantly decreased pool of p-vimentin (Fig. 2i). Comparable results were obtained for the amount of p-GFAP showing a significantly decreased amount of p-GFAP.

Induction of gliosis by U18666A

U18666A is a widely used blocker of intracellular cholesterol transport, used to study the effect of induced cholesterol accumulations on cellular homeostasis [47]. Here, we used U18666A to induce cholesterol accumulations in cells of the control cell line, as we asked if this will induce gliosis. We applied U18666A (1 μg/ml) for 24 h to control cells which were differentiated for 6 weeks and analysed the above described parameters indicating gliosis. First, the application of U18666A induced clearly cholesterol accumulations, shown by Filipin staining (Fig. 3b), in contrast to untreated control cells (Fig. 3a). The determination of relative fluorescence units (Fig. 3c), as well as the quantification of cholesterol by the Amplex Red assay (Fig. 3d), demonstrated an increased amount of cholesterol in the U18666A treated cells. Moreover, we found a significantly increased amount of GFAP$^+$/vimentin$^+$ cells (Fig. 3e) and GFAP$^+$/Ki67$^+$ cells (Fig. 3f), demonstrating an U18666A dependent induction of reactive astrocytes. Accordingly to the observed hypo-phosphorylation in NPC1 deficient cells, we observed a significantly reduced amount of p-vimentin (Fig. 3g) and GFAP (Fig. 3 h) in U18666A treated cells. These results demonstrate that U1866A induces gliosis in control cells and suggests, that the accumulation of cholesterol reflects the trigger. If the accumulation of cholesterol directly induces gliosis or if gliosis is induced by the hypo-phosphorylation of intermediate filaments stays elusive.

Rescue from gliosis and NPC1 phenotypical cholesterol accumulation

As we have demonstrated an altered assembly of GFAP and vimentin, as well as an altered amount of p-GFAP and p-vimentin in cells carrying a NPC1 mutation and in unaffected control cells treated with U18666A, we asked next if the activation of PKC leads to a rescue of the observed gliosis as well as of the NPC1 phenotypical accumulation of cholesterol. Therefore, we treated the cells with phorbol 12-myristate 13-acetate. PMA is an activator of the protein kinase C which phosphorylates GFAP and vimentin and increases the amount of the

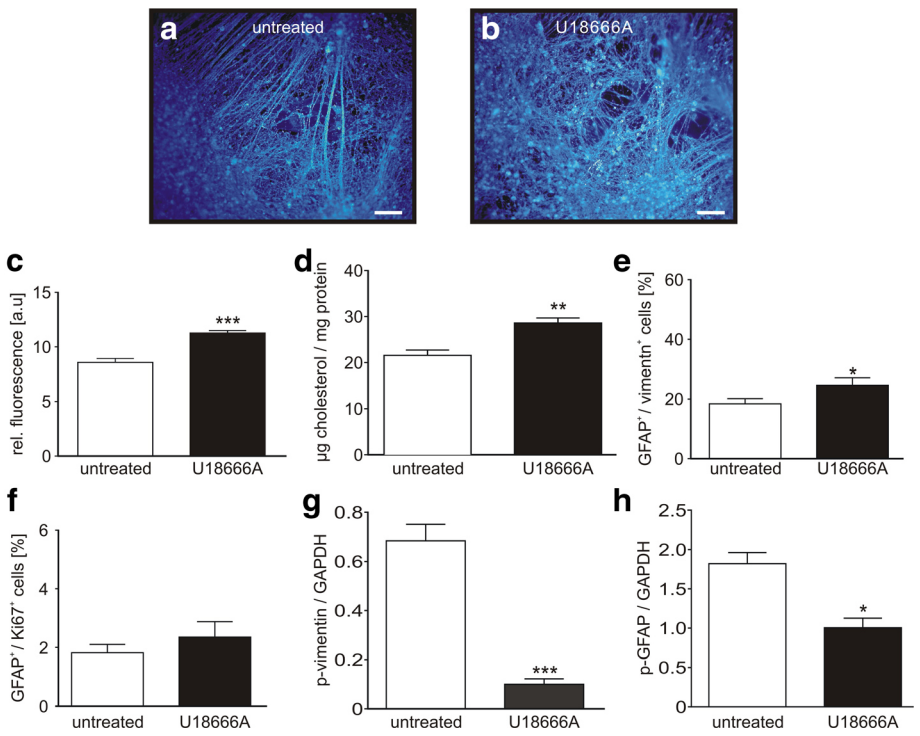

Fig. 3 Induction of gliosis by U18666A. **a** Unaffected control cells were treated with (**b**) U18666A to induce cholesterol accumulations shown by Filipin staining (blue). Scale 100 μm. **c** Calculation of relative fluorescence confirmed higher cholesterol amount in U18666A treated cells ($N = 4$, $n = 6–8$). **d** Increased cholesterol amount in U18666A treated cells was also detected by means of the Amplex red assay ($N = 4$, $n = 7–8$). **e** FACS analysis of GFAP$^+$/vimentin$^+$ cells and **f** GFAP$^+$/Ki67$^+$ cells revealed an increased amount of reactive astrocytes ($N = 4$, $n = 7–12$). **g** Treatment with U18666A resulted in a reduced amount of p-vimentin and (**h**) p-GFAP ($N = 4$, $n = 8–12$)

soluble monomers. We treated the cells with 10 nM PMA for 48 h and measured the amount of GFAP$^+$/vimentin$^+$ cells and the amount of GFAP$^+$/Ki67$^+$ cells by flow cytometry (Fig. 4). The treatment of NPC1 mutant cell lines resulted in a significantly reduced number of GFAP$^+$/vimentin$^+$ cells (Fig. 4a), as well as a significantly reduced amount of GFAP$^+$/Ki67$^+$ cells (Fig. 4b), indicating a rescue of the glial cells from gliosis. To evidence the influence of PMA on the assembly cycle of intermediate filaments and the distribution of the soluble fraction, we used western blot to determine the fraction of p-vimentin (Fig. 5a) and p-GFAP (Fig. 5b). Comparable to the effect of PMA on the amount of GFAP$^+$, vimentin$^+$ and Ki67$^+$ cells, the quantity of p-vimentin and p-GFAP increased after PMA treatment in all *NPC1* mutant cell lines, demonstrating a rescue of the disturbed intermediate filament assembly cycle.

Finally, we asked if the activation of PKC and the subsequently restoration of p-vimentin and p-GFAP had an impact on the NPC1 phenotypical cholesterol accumulation, which we described recently for these *NPC1* mutant cell lines [27, 28]. The effect of PMA on the cholesterol accumulation was assessed by Filipin staining, the quantitation of the staining by fluorescence intensities, and the total cholesterol amount by using the Amplex Red assay.

We observed the typical accumulation of cholesterol in the *NPC1* mutant cell lines in Filipin stainings in comparison to the control (Fig. 6a-d). Treatment of the cells with PMA (Fig. 6e-h) resulted in a decrease of the Filipin staining, at least in the cells carrying the mutations c.1180 T > C and c.3182 T > C, indicating less accumulation of cholesterol. This was confirmed by the analysis of the Filipin fluorescence signal (Fig. 6i), as well as by the Amplex Red assay (Fig. 6j). All *NPC1* mutant cell lines displayed a significantly reduced amount of cholesterol. Moreover, these amounts were not distinguishable from the cholesterol amount of the control cell line. Taken together, the activation of PKC by PMA triggered a rescue of iPSC derived glial cells from gliosis, induced an increase of phosphorylated IFs and attenuated the NPC1 phenotypical accumulation of cholesterol.

Discussion

Analysis of gliosis in NPC1 patient specific iPSC derived glial cells

Gliosis, the emergence of reactive astrocytes and microglia, is a universal event in the central nervous system after any kind of tissue damage and displays a physiological, normally, neuroprotective, reaction. But, in case of long lasting, chronical activation, glial cells starts to

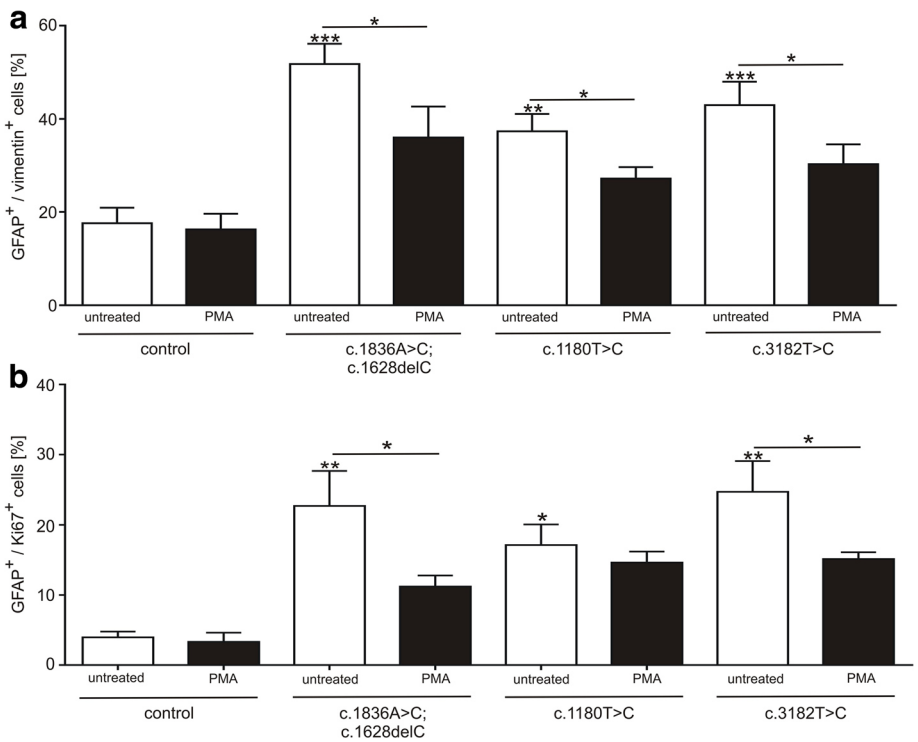

Fig. 4 Effect of PMA on gliosis. **a** Cells were treated with 10 nM PMA and number of GFAP$^+$/vimentin$^+$ cells and (**b**) GFAP$^+$/Ki67$^+$ cells was quantified. FACS analysis revealed a significant reduction of GFAP$^+$/vimentin$^+$ cells in all *NPC1* mutant cell lines after PMA treatment (N = 4–5, n = 11–28). Number of GFAP$^+$/Ki67$^+$ cells (**b**) was reduced in all *NPC1* mutant cell lines after treatment with PMA (N = 4–5, n = 7–16). Asterisks above bars indicate significance to untreated control and asterisks above lines indicate significances between treated and untreated cells

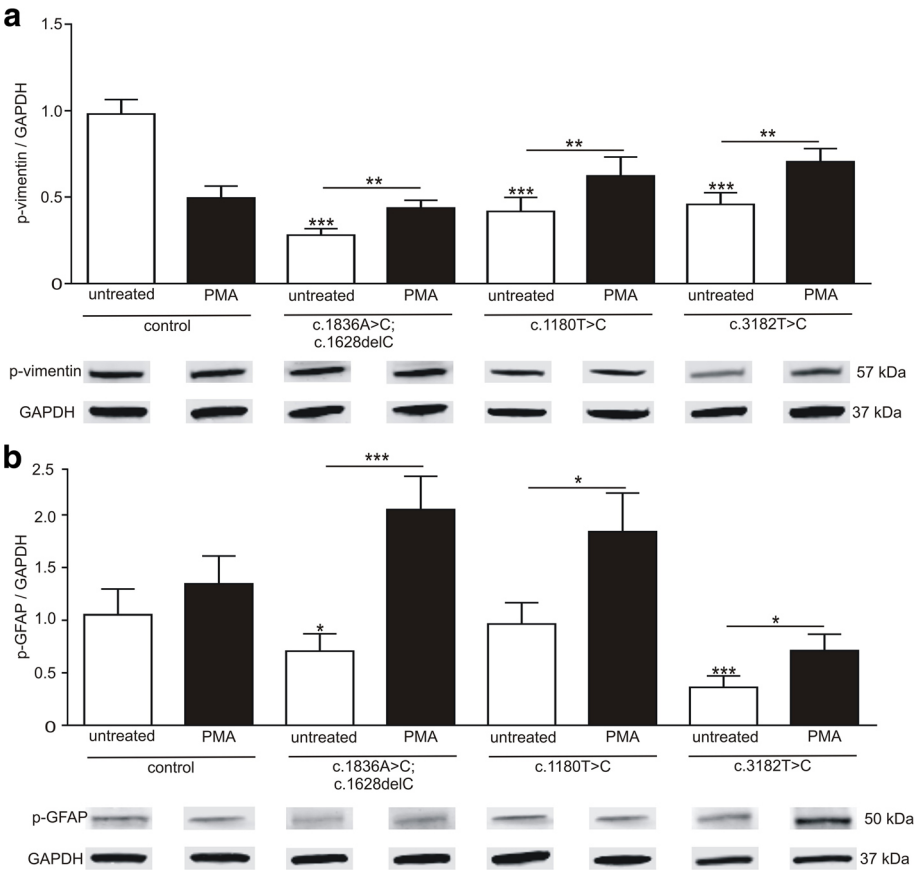

Fig. 5 Effect of PMA on p-vimentin and p-GFAP amounts. **a** Cells were treated with 10 nM PMA and fractions of p-vimentin and **b** p-GFAP were analysed by semi-quantitative western blot. Treatment with PMA resulted in all *NPC1* mutant cell lines in significantly elevated fractions of p-vimentin ($N = 4–5$, $n = 18–30$) and p-GFAP ($N = 4–5$, $n = 11–30$). Asterisks above bars indicate significance to untreated control and asterisks above lines indicate significances between treated and untreated cells

release mediators of cytotoxicity leading to a higher vulnerability of surrounding neurons or neuronal death [48]. Consequently, it stands to reason that dysregulation of normal astrocyte function contributes to the progression neurological disorders.

However, a major hallmark of gliosis is an increased amount of glia cells, especially reactive astrocytes, which upregulate GFAP and vimentin and re-express nestin [49]. Consequently, gliosis can be elucidated by an increased number of GFAP positive cells [16] and an upregulation of the IFs vimentin and nestin, as well as an increased number of proliferative cells, demonstrated by Ki67 expression or BrDU incooperation. In regards of NPC1, gliosis, as well as marker for neuroinflammation, were shown in human post mortem brain biopsy material in several regions of the brain and in murine models of NPC1 [24–26]. An increased number of reactive astrocytes and abnormal morphological changes are described in the broadly used BALB/c_Nctr-Npc1m1N/−J NPC1-deficient mouse strain [20, 21, 50]. NPC1-deficient mice revealed an upregulation of glia cells after 4 weeks of age and astrocytes showed an atypical morphology by less elaborated processes and swollen cell bodies [23]. In accordance to findings in murine models, we observed higher amounts of $GFAP^+$/$vimentin^+$ cells, as well as an increased protein amount of both IFs in our human disease model system. Cells double positive for GFAP and $Ki67^+$ reflect proliferative reactive astrocytes in NPC1 mutational cell lines, displaying a further characteristic of gliosis. Thus, we conclude that glial cells derived from NPC1 patient-specific iPS cells undergo gliosis, representing a further hallmark observed during the progression of NPC1. We emphasize that gliosis was not induced, but displays an intrinsic feature of NPC1 deficient cells of this model system. Until now, studies analyzing gliosis in human in vitro cell model systems are missing and to our knowledge this is the first study demonstrating gliosis in a human iPSC based cell model.

Beyond the question if iPSC derived glial cells undergo gliosis, we were interested in the assembly of the GFAP and vimentin as it was recently described

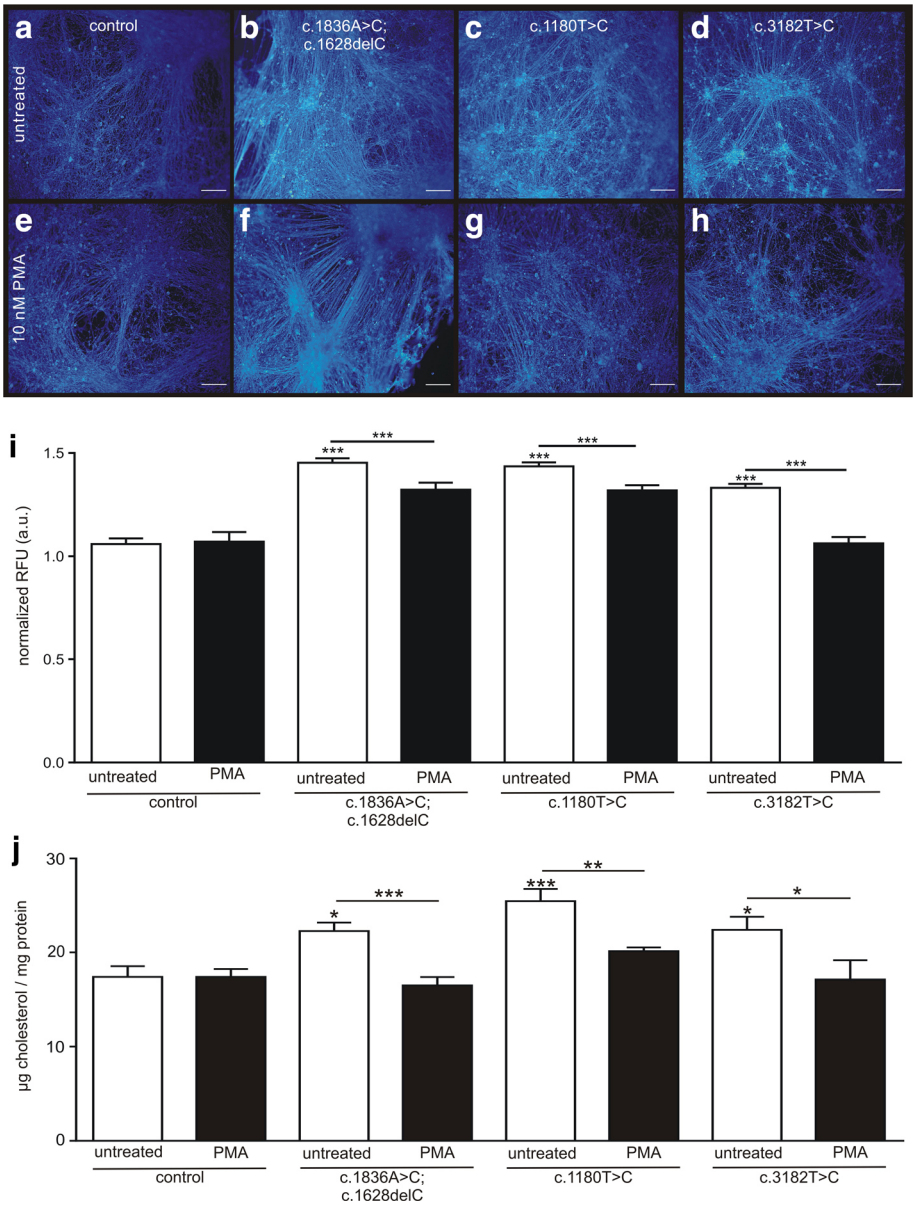

Fig. 6 Effect of PMA on cholesterol amounts. **a**-**h** Filipin staining (blue) was used to assess cholesterol content and demonstrated typical accumulations in all *NPC1* mutant cell lines. Cholesterol accumulations were ameliorated after the treatment with PMA, resulting in a Filipin staining pattern comparable to the control cells. Scale 100 µm (**i**). Accordingly the analysis of the fluorescence intensities revealed a decreased amount of cholesterol ($N = 4$, $n = 40–50$). **j** Similar results are shown for the quantification of the cholesterol amount using the Amplex red assay. The amount decreased significantly to the cholesterol amount of control cells ($N = 4–5$, $n = 6–18$). Asterisks above bars indicate significance to untreated control and asterisks above lines indicate significances between treated and untreated cells

that NPC1-patient derived fibroblasts display hypo-phosphorylation of vimentin [37]. While vimentin is down-regulated during brain development it is upregulated in astrocytes undergoing gliosis [16]. Nevertheless, vimentin is discussed to be also upregulated as a damage-response mechanism in neurons in neurodegenerative disease like Huntington or Alzheimer disease, whereby vimentin is involved in neurite extension and synaptic recovery [51]. This aspect merits further studies of the function of vimentin in neurodegenerative diseases, to elucidate the contribution of IFs to the progression or attenuation of disease emergence.

Assembly and phosphorylation of IFs in iPSC derived glial cells

In regards of the assembly of the IFs GFAP and vimentin, we observed changes in the appearance in NPC1 mutant cell lines. In immunocytochemical stainings GFAP and

vimentin appeared in more densely packed aggregates, organized in a criss-cross manner within the cytosol. This appearance is in accordance with stainings of vimentin in fibroblasts of NPC1 patients [37] and indicates a disturbed assembly/disassembly cycle for vimentin and GFAP. Consistently, we found significantly decreased amounts of the phosphorylated, soluble, forms of GFAP and vimentin in *NPC1* mutant cell lines, in accordance to studies performed with fibroblasts of NPC1 patients [37, 38]. These studies demonstrated not only a disturbance of vimentin assembly, but vimentin was found to interact with Rab9, during lipid movement from late endosomes, and Rab7a, involved in vesicular membrane trafficking [52]. This interaction is altered in NPC1 disease due to lipid and cholesterol accumulation in late endosomes resulting in an inhibition of PKC, hypo-phosphorylation of vimentin and endosomal dysfunction. Hypo-phosphorylation of vimentin leads to aggregation and enclosure of Rab9, finally resulting in transport deficiencies and blocked lipid egress [37, 38]. Most recently, vimentin aggregates were shown to inhibit trafficking of mitochondria in giant axonal neuropathy [53] strengthening the hypothesis that reduced phosphorylation of intermediate filaments leads to a trafficking defect in neurodegenerative disease. These alterations in IF type III are assumed to inhibit lysosomal exocytosis [37, 38] which is a known mechanism for NPC1 mutational cells to release stored cholesterol. For instance, cholesterol lysosomal exocytosis could be enhanced by HPB-cyclodextrin [54] and δ-tocopherol [55]. A possible mode of action of these substances could be the induction of a calcium-influx which in turn activates PKC, subsequently leading to a phosphorylation of IFs, initiating the lysosomal exocytosis leading to a depletion of cholesterol in *NPC1* mutant cells.

Rescue from gliosis and NPC1 phenotypical cholesterol accumulation

As an inhibition of PKC, by lysosomal lipid accumulation, was demonstrated in fibroblasts of NPC1 patients [37, 38] and PKC activation restores subcellular cholesterol transport in NPC1-deficient fibroblasts [38], we asked if an activation of PKC ameliorates the features of gliosis, hypophosphorylation of IFs, and finally the accumulation of cholesterol observed in iPSC derived glial cells. Thus, we treated the cell cultures with the PKC activator PMA and determined marker for gliosis, amount of phosphorylated IFs, and cholesterol. In regards of gliosis, PMA treated cell cultures demonstrated a reduced number of GFAP $^{+}$/vimentin^{+} cells, as well as reduced number of GFAP $^{+}$/Ki67^{+} cells, revealing an amelioration of gliosis.

In accordance to the study of Walter and coworker [37], the treatment with PMA increased the phosphorylated amount of vimentin. In addition to this study, we analysed glial cells and consequently GFAP and vimentin and found a similar impact of PMA on GFAP. This was to be expected as GFAP and vimentin belong both to the family of intermediate filaments type III. The cascade leading to a reduced amount of phosphorylated GFAP stays elusive, but we speculate that the suggested interrelationship of PKC activation, vimentin and Rab9 [37] can be adapted to GFAP. Following this model, the lysosomal accumulation of cholesterol would be the starting point of this vicious circle.

In support of this hypothesis we used U18666A to induce an accumulation of cholesterol in control cells. The treatment with U18666A resulted in an accumulation of cholesterol as expected, but moreover we observed gliosis in the control cells, demonstrated by a significantly increased number of GFAP^{+}/vimentin^{+} cells, accompanied by a reduced amount of phosphorylated GFAP and vimentin. Recent studies described U1866A induced cholesterol accumulations in rat astrocytes influencing the metabolic pathway of these cells [56, 57], but effects in regards of gliosis were not topic of these studies.

Moreover, we observed a strong impact of the PMA treatment on the cholesterol amount in NPC1 mutant cells. As a hallmark of NPC1, the here used NPC1 mutant cell lines [27, 28], as well as other iPSC derived NPC1 neuronal cells [29–31] showed significant cholesterol accumulations. PMA induced a reduction of cholesterol accumulations, demonstrated by Filipin stainings and by Amplex Red Assay, where latter one elucidated a normalization of the cholesterol amount, comparable to the cholesterol amount of control cells. In accordance to our results, a redistribution of cholesterol upon the activation of PKC was recently demonstrated in NPC1-deficnet fibroblasts [38].

Bringing together our results and the results obtained from NPC1-deficient fibroblasts [37, 38], we conclude that the accumulation of cholesterol initiates a perturbation of PKC signaling, leading to altered assembly of IFs. We speculate, that this cascade contributes to the initiation of gliosis, observed in NPC1 mutant cell lines as well as in U18666A treated control cells. Consequently, gliosis appears to be primary effect of the cholesterol accumulation within glial cells and not a secondary effect mediated by the loss of neurons in NPC1. Actually, the contribution of gliosis to the progression and/or phenotypical occurrence of NPC1 is controversially discussed. One certain feature of NPC1 is an activation of astrocytes, observed both in mouse models and NPC1 patients [58]. But, the contribution of astrocytes to the neurodegenerative processes is controversially discussed. Knock-down experiments of *NPC1*, restricted to astrocytes or neurons in the CNS of mice hint at astrogliosis as a secondary process with a low impact on the disease progression [59–62]. On the other hand, severe symptoms of murine NPC1-models were significantly ameliorated upon the astrocyte-specific

knock-in of *NPC1* [63, 64]. Still, an almost complete recovery was only achieved by double knock-in of *NPC1* into astrocytes and neurons [65], indicating a cooperative mechanism underlying the recovery. If an impaired signaling in astrocytes, based on a corrupted PKC signaling and thus corrupted PKC dependent processes, ends up in a deleterious vicious circle leading to cell loss is speculative and stays enigmatic, but merits further studies regarding the contribution of glial cells and gliosis to the pathogenic mechanism underlying NPC1, wherein patient specific iPSC models provide promising tools in regards of disease modelling.

Conclusion

Here we demonstrated gliosis in a cell model system based on NPC1 patient specific iPS cells. We found that gliosis is an intrinsic feature of this model system, reflecting one of the pathological distinguishing marks of NPC1. For sure, this feature provides the opportunity to study the impact of gliosis as well as the interplay between glial cells and neurons on the pathogenic mechanisms of NPC1 in a human model system. Besides the applicability of these model system in disease modelling of NPC1, we described the alterations of intermediate filaments in regards of structural features and regulation by PKC. More importantly, we confirmed an impact of PKC signaling on the pathogenesis of NPC1, presenting the possibility to develop new intervention strategies to ameliorate the progression of NPC1.

Abbreviations

DMEM: Dulbecco's Modified Eagle's Media; GAPDH: Glyceraldehyde 3-phosphate dehydrogenase; GFAP: Glial fibrillary acidic protein; $GFAP^+$: GFAP positive cells; IFs: Intermediate filaments; NPC1: Niemann-Pick disease Type C1; PBS: Phosphate Buffered Saline; PFA: Paraformaldehyde; p-GFAP: Phosphorylated GFAP; PKC: Protein kinase C; PMA: Phorbol 12-myristate 13-acetate; p-vimentin: Phosphorylated vimentin; $vimentin^+$: Vimentin positive cells

Acknowledgements

We thank Janine Petter for her excellent technical support.

Funding

Not applicable

Availability of data and materials

The datasets supporting the conclusion of this article are included within the article.

Authors' contributions

FP: conception and design, collection and/or assembly of data, data analysis and interpretation, manuscript writing. SR: conception and design, collection and/or assembly of data, data analysis and interpretation. AR: conception and design, manuscript writing, final approval of manuscript. MJF: conception and design, collection and/or assembly of data, data analysis and interpretation, manuscript writing, final approval of manuscript. All authors read and approved the final manuscript.

Ethics approval and consent to participate

Not applicable

Consent for publication

Not applicable

Competing interests

The authors declare that they have no competing interests.

Publisher's Note

Received: 12 July 2017 Accepted: 20 August 2017
Published online: 25 August 2017

References

1. Wassif CA, Cross JL, Iben J, Sanchez-Pulido L, Cougnoux A, Platt FM, et al. High incidence of unrecognized visceral/neurological late-onset Niemann-pick disease, type C1, predicted by analysis of massively parallel sequencing data sets. Genet Med. 2016;18:41–8. doi:10.1038/gim.2015.25.
2. Vanier MT. Niemann-pick disease type C. Orphanet J Rare Dis. 2010;5:16. doi:10.1186/1750-1172-5-16.
3. Zervas M, Dobrenis K, Walkley SU. Neurons in Niemann-pick disease type C accumulate gangliosides as well as unesterified cholesterol and undergo dendritic and axonal alterations. J Neuropathol Exp Neurol. 2001;60:49–64.
4. Infante RE, Wang ML, Radhakrishnan A, Kwon HJ, Brown MS, Goldstein JL. NPC2 facilitates bidirectional transfer of cholesterol between NPC1 and lipid bilayers, a step in cholesterol egress from lysosomes. Proc Natl Acad Sci U S A. 2008;105:15287–92. doi:10.1073/pnas.0807328105.
5. Giese A-K, Mascher H, Grittner U, Eichler S, Kramp G, Lukas J, et al. A novel, highly sensitive and specific biomarker for Niemann-pick type C1 disease. Orphanet J Rare Dis. 2015;10:2006. doi:10.1186/s13023-015-0274-1.
6. Vanier MT, Gissen P, Bauer P, Coll MJ, Burlina A, Hendriksz CJ, et al. Diagnostic tests for Niemann-pick disease type C (NP-C): a critical review. Mol Genet Metab. 2016;118:244–54. doi:10.1016/j.ymgme.2016.06.004.
7. Cuisset J-M, Sukno S, Trauffler A, Latour P, Dobbelaere D, Michaud L, Vallee L. Impact of miglustat on evolution of atypical presentation of late-infantile-onset Niemann-pick disease type C with early cognitive impairment, behavioral dysfunction, epilepsy, ophthalmoplegia, and cerebellar involvement: a case report. J Med Case Rep. 2016;10:241. doi:10.1186/s13256-016-1038-9.
8. Heron B, Valayannopoulos V, Baruteau J, Chabrol B, Ogier H, Latour P, et al. Miglustat therapy in the French cohort of paediatric patients with Niemann-pick disease type C. Orphanet J Rare Dis. 2012;7:36. doi:10.1186/1750-1172-7-36.
9. Peake KB, Vance JE. Normalization of cholesterol homeostasis by 2-hydroxypropyl-beta-cyclodextrin in neurons and glia from Niemann-pick C1 (NPC1)-deficient mice. J Biol Chem. 2012;287:9290–8.
10. Pipalia NH, Cosner CC, Huang A, Chatterjee A, Bourbon P, Farley N, et al. Histone deacetylase inhibitor treatment dramatically reduces cholesterol accumulation in Niemann-pick type C1 mutant human fibroblasts. Proc Natl Acad Sci U S A. 2011;108:5620–5. doi:10.1073/pnas.1014890108.
11. Erickson RP. Current controversies in Niemann-pick C1 disease: steroids or gangliosides; neurons or neurons and glia. J Appl Genet. 2013;54:215–24. doi:10.1007/s13353-012-0130-0.
12. Sofroniew MV. Molecular dissection of reactive astrogliosis and glial scar formation. Trends Neurosci. 2009;32:638–47. doi:10.1016/j.tins.2009.08.002.
13. Osborn LM, Kamphuis W, Wadman WJ, Hol EM. Astrogliosis: an integral player in the pathogenesis of Alzheimer's disease. Prog Neurobiol. 2016;144:121–41. doi:10.1016/j.pneurobio.2016.01.001.
14. Buffo A, Rolando C, Ceruti S. Astrocytes in the damaged brain: molecular and cellular insights into their reactive response and healing potential. Biochem Pharmacol. 2010;79:77–89. doi:10.1016/j.bcp.2009.09.014.
15. Malnar M, Hecimovic S, Mattsson N, Zetterberg H. Bidirectional links between Alzheimer's disease and Niemann-Pick type C disease. Neurobiol Dis. 2014;72:37–47.
16. Norton WT, Aquino DA, Hozumi I, Chiu FC, Brosnan CF. Quantitative aspects of reactive gliosis: a review. Neurochem Res. 1992;17:877–85.
17. Eng LF, Ghirnikar RS, Lee YL. Glial fibrillary acidic protein: GFAP-thirty-one years (1969–2000). Neurochem Res. 2000;25:1439–51.
18. Hol EM, Pekny M. Glial fibrillary acidic protein (GFAP) and the astrocyte intermediate filament system in diseases of the central nervous system. Curr Opin Cell Biol. 2015;32:121–30. doi:10.1016/j.ceb.2015.02.004.
19. Kamphuis W, Kooijman L, Orre M, Stassen O, Pekny M, Hol EM. GFAP and vimentin deficiency alters gene expression in astrocytes and microglia in wild-type mice and changes the transcriptional response of reactive glia in

mouse model for Alzheimer's disease. Glia. 2015;63:1036–56. doi:10.1002/glia.22800.
20. German DC, Quintero EM, Liang CL, Ng B, Punia S, Xie C, Dietschy JM. Selective neurodegeneration, without neurofibrillary tangles, in a mouse model of Niemann-pick C disease. JComp Neurol. 2001;433:415–25.
21. German DC, Liang CL, Song T, Yazdani U, Xie C, Dietschy JM. Neurodegeneration in the Niemann-pick C mouse: glial involvement. Neuroscience. 2002;109:437–50.
22. Suzuki M, Sugimoto Y, Ohsaki Y, Ueno M, Kato S, Kitamura Y, et al. Endosomal accumulation of toll-like receptor 4 causes constitutive secretion of cytokines and activation of signal transducers and activators of transcription in Niemann-pick disease type C (NPC) fibroblasts: a potential basis for glial cell activation in the NPC brain. J Neurosci. 2007;27:1879–91. doi:10.1523/JNEUROSCI.5282-06.2007.
23. Baudry M, Yao Y, Simmons D, Liu J, Bi X. Postnatal development of inflammation in a murine model of Niemann-pick type C disease: immunohistochemical observations of microglia and astroglia. Exp Neurol. 2003;184:887–903.
24. Chiba Y, Komori H, Takei S, Hasegawa-Ishii S, Kawamura N, Adachi K, et al. Niemann-pick disease type C1 predominantly involving the frontotemporal region, with cortical and brainstem Lewy bodies: an autopsy case. Neuropathology. 2014;34:49–57. doi:10.1111/neup.12047.
25. Cologna SM, Cluzeau CVM, Yanjanin NM, Blank PS, Dail MK, Siebel S, et al. Human and mouse neuroinflammation markers in Niemann-pick disease, type C1. J Inherit Metab Dis. 2014;37:83–92. doi:10.1007/s10545-013-9610-6.
26. Yamashita S. A case of a girl with poor school achievement, ataxia and neurological deterioration. Neuropathology. 2012;32:105–9. doi:10.1111/j.1440-1789.2011.01230.x.
27. Trilck M, Hübner R, Seibler P, Klein C, Rolfs A, Frech MJ. Niemann-pick type C1 patient-specific induced pluripotent stem cells display disease specific hallmarks. Orphanet J Rare Dis. 2013;8:144. doi:10.1186/1750-1172-8-144.
28. Trilck M, Peter F, Zheng C, Frank M, Dobrenis K, Mascher H, et al. Diversity of Glycosphingolipid GM2 and cholesterol accumulation in NPC1 patient-specific iPSC-derived neurons//diversity of glycosphingolipid GM2 and cholesterol accumulation in NPC1 patient-specific iPSC-derived neurons. Brain Res. 2017;1657:52–61. doi:10.1016/j.brainres.2016.11.031.
29. Efthymiou AG, Steiner J, Pavan WJ, Wincovitch S, Larson DM, Porter FD, et al. Rescue of an in Vitro Neuron Phenotype Identified in Niemann-pick disease, type C1 induced Pluripotent stem cell-derived neurons by modulating the WNT pathway and calcium signaling. Stem Cells Transl Med. 2015;4:230–8. doi:10.5966/sctm.2014-0127.
30. Maetzel D, Sarkar S, Wang H, Abi-Mosleh L, Xu P, Cheng AW, et al. Genetic and chemical correction of cholesterol accumulation and impaired Autophagy in hepatic and neural cells derived from Niemann-pick type C patient-specific iPS cells. Stem Cell Reports. 2014;2:866–80.
31. Yu T, Lieberman AP, Haldar K. Npc1 acting in neurons and Glia is essential for the formation and maintenance of CNS myelin. PLoS Genet. 2013;9:e1003462. doi:10.1371/journal.pgen.1003462.
32. Margiotta A, Bucci C. Role of Intermediate Filaments in Vesicular Traffic. Cells 2016. doi:10.3390/cells5020020.
33. Coulombe PA, Wong P. Cytoplasmic intermediate filaments revealed as dynamic and multipurpose scaffolds. Nat Cell Biol. 2004;6:699–706. doi:10.1038/ncb0804-699.
34. Eriksson JE, He T, Trejo-Skalli AV, Harmala-Brasken A-S, Hellman J, Chou Y-H, Goldman RD. Specific in vivo phosphorylation sites determine the assembly dynamics of vimentin intermediate filaments. J Cell Sci. 2004;117:919–32. doi:10.1242/jcs.00906.
35. Ivaska J, Vuoriluoto K, Huovinen T, Izawa I, Inagaki M, Parker PJ. PKCepsilon-mediated phosphorylation of vimentin controls integrin recycling and motility. EMBO J. 2005;24:3834–45. doi:10.1038/sj.emboj.7600847.
36. Snider NT, Omary MB. Post-translational modifications of intermediate filament proteins: mechanisms and functions. Nat Rev Mol Cell Biol. 2014;15:163–77. doi:10.1038/nrm3753.
37. Walter M, Chen FW, Tamari F, Wang R, Ioannou YA. Endosomal lipid accumulation in NPC1 leads to inhibition of PKC, hypophosphorylation of vimentin and Rab9 entrapment. BiolCell. 2009;101:141–52.
38. Tamari F, Chen FW, Li C, Chaudhari J, Ioannou YA. PKC activation in Niemann pick C1 cells restores subcellular cholesterol transport. PLoS One. 2013;8:e74169.
39. Manders EMM, Verbeek FJ, Aten JA. Measurement of co-localization of objects in dual-colour confocal images. J Microsc. 1993;169:375–82. doi:10.1111/j.1365-2818.1993.tb03313.x.
40. Costes SV, Daelemans D, Cho EH, Dobbin Z, Pavlakis G, Lockett S. Automatic and quantitative measurement of protein-protein colocalization in live cells. Biophys J. 2004;86:3993–4003. doi:10.1529/biophysj.103.038422.
41. Schneider CA, Rasband WS, Eliceiri KW. NIH image to ImageJ: 25 years of image analysis. Nat Methods. 2012;9:671–5.
42. Bolte S, Cordelieres FP. A guided tour into subcellular colocalization analysis in light microscopy. JMicrosc. 2006;224:213–32.
43. Hawes CM, Wiemer H, Krueger SR, Karten B. Pre-synaptic defects of NPC1-deficient hippocampal neurons are not directly related to plasma membrane cholesterol. J Neurochem. 2010;114:311–22.
44. Nunes MJ, Moutinho M, Gama MJ, Rodrigues CMP, Rodrigues E. Histone deacetylase inhibition decreases cholesterol levels in neuronal cells by modulating key genes in cholesterol synthesis, uptake and efflux. PLoS One. 2013;8:e53394. doi:10.1371/journal.pone.0053394.
45. Li J, Deffieu MS, Lee PL, Saha P, Pfeffer SR. Glycosylation inhibition reduces cholesterol accumulation in NPC1 protein-deficient cells. Proc Natl Acad Sci U S A. 2015;112:14876–81. doi:10.1073/pnas.1520490112.
46. Tängemo C, Weber D, Theiss S, Mengel E, Runz H. Niemann-pick type C disease: characterizing lipid levels in patients with variant lysosomal cholesterol storage. J Lipid Res. 2011;52:813–25. doi:10.1194/jlr.P013524.
47. Kuzu OF, Toprak M, Noory MA, Robertson GP. Effect of lysosomotropic molecules on cellular homeostasis. Pharmacol Res. 2017;117:177–84. doi:10.1016/j.phrs.2016.12.021.
48. Marchetti B, L'episcopo F, Morale MC, Tirolo C, Testa N, Caniglia S, et al. Uncovering novel actors in astrocyte-neuron crosstalk in Parkinson's disease: the Wnt/beta-catenin signaling cascade as the common final pathway for neuroprotection and self-repair. Eur J Neurosci. 2013;37:1550–63.
49. Pekny M, Nilsson M. Astrocyte activation and reactive gliosis. Glia. 2005;50:427–34. doi:10.1002/glia.20207.
50. Suzuki H, Sakiyama T, Harada N, Abe M, Tadokoro M. Pathologic changes of glial cells in murine model of Niemann-pick disease type C: immunohistochemical, lectin-histochemical and ultrastructural observations. Pediatr Int. 2003;45:1–4.
51. Levin EC, Acharya NK, Sedeyn JC, Venkataraman V, D'Andrea MR, Wang HY, Nagele RG. Neuronal expression of vimentin in the Alzheimer's disease brain may be part of a generalized dendritic damage-response mechanism. Brain Res. 2009;1298:194–207.
52. Cogli L, Progida C, Bramato R, Bucci C. Vimentin phosphorylation and assembly are regulated by the small GTPase Rab7a. Biochim Biophys Acta. 1833;2013:1283–93. 10.1016/j.bbamcr.2013.02.024.
53. Lowery J, Jain N, Kuczmarski ER, Mahammad S, Goldman A, Gelfand VI, et al. Abnormal intermediate filament organization alters mitochondrial motility in giant axonal neuropathy fibroblasts. Mol Biol Cell. 2016;27:608–16. doi:10.1091/mbc.E15-09-0627.
54. Chen FW, Li C, Ioannou YA. Cyclodextrin induces calcium-dependent lysosomal exocytosis. PLoS One. 2010;5:e15054.
55. Xu M, Liu K, Swaroop M, Porter FD, Sidhu R, Firnkes S, et al. Delta-Tocopherol reduces lipid accumulation in Niemann-pick type C1 and Wolman cholesterol storage disorders. J Biol Chem. 2012;287:39349–60.
56. Santos DC, da Silva GC, de Andrade CV, Daitx VV, da Costa MV, Rohden F, Coelho JC. Effect of u18666a on beta-glucosidase, sphingomyelinase, and beta-galactosidase activities in astrocytes of young rats. J Membr Biol. 2015;248:215–22. doi:10.1007/s00232-014-9761-x.
57. Copetti-Santos D, Moraes V, Weiler DF, de Mello AS, FdS M, Marinho JP, et al. U18666A treatment results in cholesterol accumulation, reduced Na(+), K(+)-ATPase activity, and increased oxidative stress in rat cortical Astrocytes. Lipids. 2015;50:937–44. doi:10.1007/s11745-015-4062-4.
58. Karten B, Peake KB, Vance JE. Mechanisms and consequences of impaired lipid trafficking in Niemann-pick type C1-deficient mammalian cells. Biochim Biophys Acta. 2009;1791:659–70. doi:10.1016/j.bbalip.2009.01.025.
59. Ko DC, Milenkovic L, Beier SM, Manuel H, Buchanan J, Scott MP. Cell-autonomous death of cerebellar purkinje neurons with autophagy in Niemann-pick type C disease. PLoS Genet. 2005;1:81–95. doi:10.1371/journal.pgen.0010007.
60. Yu T, Shakkottai VG, Chung C, Lieberman AP. Temporal and cell-specific deletion establishes that neuronal Npc1 deficiency is sufficient to mediate neurodegeneration. Hum Mol Genet. 2011;20:4440–51. doi:10.1093/hmg/ddr372.

61. Elrick MJ, Pacheco CD, Yu T, Dadgar N, Shakkottai VG, Ware C, et al. Conditional Niemann-pick C mice demonstrate cell autonomous Purkinje cell neurodegeneration. Hum Mol Genet. 2010;19:837–47. doi:10.1093/hmg/ddp552.
62. Lopez ME, Scott MP. Genetic dissection of a cell-autonomous neurodegenerative disorder: lessons learned from mouse models of Niemann-pick disease type C. Dis Model Mech. 2013;6:1089–100.
63. Zhang M, Strnatka D, Donohue C, Hallows JL, Vincent I, Erickson RP. Astrocyte-only Npc1 reduces neuronal cholesterol and triples life span of Npc1−/− mice. J Neurosci Res. 2008;86:2848–56. doi:10.1002/jnr.21730.
64. Kapur R, Donohue C, Jelinek D, Erickson RP. Amelioration of enteric neuropathology in a mouse model of Niemann-pick C by Npc1 expression in enteric glia. J Neurosci Res. 2009;87:2994–3001. doi:10.1002/jnr.22126.
65. Borbon I, Totenhagen J, Fiorenza MT, Canterini S, Ke W, Trouard T, Erickson RP. Niemann-pick C1 mice, a model of "juvenile Alzheimer's disease", with normal gene expression in neurons and fibrillary astrocytes show long term survival and delayed neurodegeneration. J Alzheimers Dis. 2012;30:875–87. doi:10.3233/JAD-2012-120199.

Molecular and Cellular Neuroscience 83 (2017) 27–36

Contents lists available at ScienceDirect

Molecular and Cellular Neuroscience

journal homepage: www.elsevier.com/locate/ymcne

Decreased calcium flux in Niemann-Pick type C1 patient-specific iPSC-derived neurons due to higher amount of calcium-impermeable AMPA receptors

Michael Rabenstein [1], Franziska Peter [1], Sarah Joost, Michaela Trilck, Arndt Rolfs, Moritz J. Frech *

Albrecht-Kossel-Institute for Neuroregeneration (AKos), University Medicine Rostock, Gehlsheimer Straße 20, D-18147 Rostock, Germany

ARTICLE INFO

Article history:
Received 13 March 2017
Revised 8 June 2017
Accepted 25 June 2017
Available online 27 June 2017

Keywords:
NPC1
GluA2
AMPA
Calcium
Patch clamp
Fura2
iPSC derived neurons

ABSTRACT

Niemann-Pick disease type C1 (NPC1) is a rare progressive neurodegenerative disorder caused by mutations in the *NPC1* gene, resulting mainly in the accumulation of cholesterol and the ganglioside GM2. Recently, we described accumulations of these lipids in neuronal differentiated cells derived from NPC1 patient-specific induced pluripotent stem cells (iPSCs). As these lipids are essential for proper cell membrane composition, we were interested in the expression and function of voltage-gated ion channels and excitatory AMPA receptors (AMPARs) in neurons derived from three patient-specific iPSC lines. By means of patch clamp recordings and microfluorimetric measurements of calcium (Ca^{2+}), we examined the expression of voltage-gated ion channels and AMPARs. Cells of the three used cell lines carrying the c.1836A>C/c.1628delC, the c.1180T>C or the c.3182T>C mutation demonstrated a significantly reduced AMPA-induced Ca^{2+}-influx, suggesting an altered expression profile of these receptors. RT-qPCR revealed a significant upregulation of mRNA for the AMPA receptor subunits GluA1 and GluA2 and western blot analysis showed increased protein level of GluA2. Thus, we conclude that the observed reduced Ca^{2+}-influx is based on an increase of GluA2 containing Ca^{2+}-impermeable AMPARs. An attenuated function of GluRs in neurons potentially contributes to the progressive neurodegeneration observed in NPC1 and might represent an objective in regard of the development of new therapeutic approaches in NPC1.

1. Introduction

Niemann-Pick disease type C1 (NPC1) is a rare progressive neurodegenerative disease caused by mutations in the *NPC1* gene encoding a transmembrane glycoprotein (Carstea et al., 1997; Davies and Ioannou, 2000; Morris et al., 1999). Mutations lead to an impaired lipid transport, resulting in an accumulation of cholesterol and gangliosides, like GM2 or GM3 (Sokol et al., 1988). Besides clinical manifestations like hepatosplenomegaly, seizures, dementia, and a progressive neurological degradation (Vanier, 2013), a hallmark of NPC1 is a striking loss of cerebellar Purkinje cells leading to cerebellar ataxia (Higashi et al., 1993; Sarna et al., 2001). The pathogenic mechanisms ultimately leading to degeneration and loss of neurons in the central nervous system are not exactly understood.

Since the development of patient-specific induced pluripotent stem cell (iPSC) lines, these model systems have been used to model neurodegenerative diseases to gain a better understanding of the pathogenic mechanisms, and to develop new therapeutic approaches (Sayed et al., 2016; Singh et al., 2015). Since the first description of a NPC1 patient-specific iPS cell line by our group (Trilck et al., 2013), a number of publications presented comparable model systems for elucidating different aspects of NPC1 (Bergamin et al., 2013; Lee et al., 2014; Maetzel et al., 2014; Yu et al., 2014; Efthymiou et al., 2015; Kuo et al., 2015). However, until now a functional characterization of neural derivatives of NPC1 patient-specific iPSCs carrying different mutations is still missing.

Recently, we described the cell lines used in this study in regard to accumulation of cholesterol and GM2, revealing an accumulation of these macro molecules in cells carrying a *NPC1* mutation (Trilck et al., 2017; Trilck et al., 2013). As cholesterol is crucial for proper formation of cell membranes and the localization of e.g. ion channels, we were interested in the expression and function of voltage-gated (VGICs) and ligand-gated ion channels (LGICs). We focused on excitatory AMPA receptors (AMPARs), expressed by neurons, as these receptors are crucial for fast synaptic transmission. A proper trafficking towards and localization of AMPARs in synapses is crucial to establish and maintain synaptic transmission. Therefore, a complex transport machinery is needed to localize the receptors at synapses to establish basal synaptic function and activity dependent regulation of synaptic strength (Chater and Goda, 2014; Gratacos-Batlle et al., 2014; Jurado, 2014). Disturbances of function

* Corresponding author at: Albrecht-Kossel-Institute for Neuroregeneration, University Medicine Rostock, Gehlsheimer Straße 20, D-18147 Rostock, Germany.
E-mail addresses: michael.rabenstein2@uni-rostock.de (M. Rabenstein), franziska.peter2@uni-rostock.de (F. Peter), sarah.joost@med.uni-rostock.de (S. Joost), michaela.trilck@neuro.uni-luebeck.de (M. Trilck), arndt.rolfs@med.uni-rostock.de (A. Rolfs), moritz.frech@med.uni-rostock.de (M.J. Frech).
[1] These authors contributed equally.

http://dx.doi.org/10.1016/j.mcn.2017.06.007
1044-7431/

and/or expression of AMPARs are often linked to neurodegenerative diseases. In regard of NPC1 altered glutamatergic synaptic transmission was observed in a mouse model of NPC1 (D'Arcangelo et al., 2011), which, in turn, depends on a proper distribution of cholesterol (Frank et al., 2008). Thus, we especially examined differences in the function and expression of AMPARs in neurons derived from NPC1 patient-specific iPSCs.

2. Material and methods

2.1. Cell culture

Human iPSCs and neural progenitor cells were generated as described earlier (Peter et al., 2017; Trilck et al., 2017). In brief, neural differentiation of iPSCs was induced by density-dependent growing of the iPSCs on Matrigel (Corning, Netherlands), resulting in the formation of neural rosettes. Neural rosettes were harvested and PSA-NCAM positive neural progenitor cells were sorted using magnetic beads. Isolated neural progenitor cells (NPCs) were seeded on poly-L-ornithine (15 μg/ml; Sigma, Germany)/laminin (10 μg/ml; Trevigen, USA)-coated dishes in proliferation medium containing 60% DMEM, 40% DMEM/F-12, 1× B27, 0.5% penicillin/streptomycin, 20 ng/ml FGF2 (Amsbio, United Kingdom), 20 ng/ml EGF (Peprotech, Germany). For the functional analysis of neural progenitor cell derived neurons, progenitor cells were seeded poly-L-ornithine/laminin coated class cover slips in density of 45,000 cells/cm^2. Neuronal differentiation was induced by withdrawal of growth factors FGF2 and EGF. Cells were cultured in medium, containing 60% DMEM, 40% DMEM/F-12, 1× B27, 0.5% penicillin/streptomycin, which was changed every 4 days. After 6–7 weeks of differentiation cells were used for patch clamp recordings and microfluorimetric Ca^{2+}-measurements.

2.2. Patch clamp recordings

Patch clamp recordings were performed using an EPC10-amplifier (HEKA, Germany). Patch pipettes were pulled from borosilicate glass tubing (Harvard Apparatus, USA) with a DMZ-Universal-Puller (Zeitz-Instruments, Germany). Electrodes had resistances between 5 and 7 MΩ, when filled with intracellular solution consisting of (given in mM): 140 KCl, 10 HEPES, 11 EGTA, 1 $CaCl_2$, 1 $MgCl_2$, pH 7.2. The cells were superfused with an extracellular solution consisting of (given in mM): 151 NaCl, 1.25 NaH_2PO_4, 10 HEPES, 2.5 KCl, 2 $CaCl_2$, 1 $MgCl_2$, 10 glucose, pH 7.4. For voltage clamp recordings in the whole cell configuration, holding potential was set to −60 mV. Current responses were evoked by applying voltage steps (100 ms, −60 to +50 mV, 10 mV increments). Data were filtered at 3 kHz, digitized and stored on-line using Pulse or PatchMaster software (Heka, Germany). Sodium and potassium current densities were calculated by normalising the currents with the cell capacitance. Spontaneous action potentials (APs) were recorded in current clamp mode at membrane potentials of −60 mV. Additionally, APs were induced by current injections from a membrane potential of −60 mV. For substance application, a focal application tool (Octaflow, ALA Scientific Instruments, USA) was used. Neurons were selected by visual inspection.

2.3. Microfluorimetric Ca^{2+}-measurements

For microfluorimetric Ca^{2+}-measurements, cells were loaded with Ca^{2+}-indicator Fura2-AM (5 μM, Molecular Probes, Germany) for 30 min. Afterwards, cells were washed twice with extracellular solution and incubated for another 30 min to allow de-esterification of Fura2-AM. During measurements, cells were superfused with external solution as indicated above. Fluorescence images were taken at a frequency of 1 Hz using the software Tillvision (v4.0, TILL Photonics GmbH, Germany) mounted on a Axioskop2-FSmot microscope (Carl Zeiss AG, Germany) coupled to Polychrome V (Till Photonics GmbH, Germany) and a SensiCam camera (PCO AG, Germany). Excitation wavelengths of 340 and 380 nm were used, emission was measured at a wavelength of 510 nm. For analysis of the Ca^{2+} responses, the ratio of the fluorescence intensities at 340 and 380 nm was calculated after background correction. For comparison of Ca^{2+} signals, the area under the curve (AUC) was calculated and analysed with GraphPad Prism6 (GraphPad Software Inc., USA). Neurons were selected by visual inspection.

2.4. Reverse transcription quantitative real-time PCR

Reverse transcription quantitative real-time PCR (RT-qPCR) was performed using a LightCycler Nano (Roche, Germany) in combination with the LightCycler Nano software (v1.1.0, Roche, Germany). Cell harvest and synthesis of cDNA was carried out by using FastLane cDNA Kit (Qiagen, Germany) following the manufacturer's instructions. PCR was performed using the FastStart Essential DNA Green Master (Roche, Germany) according to the manufacturer's instructions. PCR products were verified by melting point analysis. Relative mRNA expression was calculated by use of the ΔΔCt and Pfaffl method (Pfaffl, 2001). For normalisation of the mRNA amount, the housekeeping gene glucose-6-phosphate-dehydrogenase (G6PD) was used. All samples were run in duplicates. Cycling parameters were as follows: denaturation at 95 °C for 10 min, 40 cycles of 20 s at 95 °C for denaturation, 20 s at 55 °C for annealing, and 23 s at 72 °C for extension. Forward/reverse primer sequences and product size:

GluA1: GGTCTGCCCTGAGAAATCCAG/CTCGCCCTTGTCGTACCAC/101.
GluA2: GGTCTGCCCTGAGAAATCCAG/CTCGCCCTTGTCGTACCAC/139.
GluA3: CGAGAGGGGTGTATGCCATC/GAAGCTAGGCGTAACAAAGGAT/104.
GluA4: ATTGGTGTCAGCGTGGTCTTA/CCAGGGAAAACCAGAGGCT/145.

2.5. Membrane extraction and biotinylation assay

Cell membranes were extracted according to Ferrante et al. (2016). In brief, cells were harvested using a cell scraper and washed twice with DPBS. After centrifugation (3000 ×g, 5 min, 4 °C) cells were resuspended in 300 μl Membrane Extraction Buffer (5 mM Tris-HCl, 1 mM EGTA, 1 mM DTT, 0.32 mM sucrose, complete mini protease inhibitor (Roche, Germany)) and sonicated. The supernatant after centrifugation at 500 ×g for 5 min at 4 °C was again centrifuged at 22,000 ×g for 30 min at 4 °C. The obtained pellet was resuspended in Membrane Extraction Buffer without sucrose and sonicated. Samples were subsequently used for western blot using GluA2 antibody.

For extraction of membrane proteins the biotinylation protocol after Tarradas et al. (2013) was used. In brief, cells were washed twice with 1.0 ml ice-cold $DPBS^{+/+}$ (with Ca^{2+} and Mg^{2+}). Afterwards cells were incubated on ice 2.5 mg/ml Biotin (EZ-Link, Sulfo-NHS-SS-Biotin, Thermo Fisher Scientific, Germany) for 30 min with agitation. Cells were washed for 5 min with 1.0 ml cold buffer containing 100 nM glycin in DPBS and subsequently with 1.0 ml cold buffer containing 20 nM glycin in DPBS. This step was repeated three times. Cells were harvested with 400 μl Lysis Buffer 1 containing, 50 mM Tris-HCl, 150 mM NaCl, 1 mM EDTA, 1% Triton, 1× complete mini protease inhibitor in DPBS. Next, cells were transferred into fresh reaction tubes and lysed under rotation for 1 h at 4 °C. Agarose beads (Streptavidin Agarose Resin, Thermo Fisher Scientific, Germany) were prepared by washing 60 μl beads per sample twice with DPBS, twice with Lysis Buffer 2, containing 50 mM Tris-HCl, 150 mM NaCl, 1 mM EDTA, 1% Triton in DPBS, and were resuspended in Lysis Buffer 1. Lysed cells were centrifuged for 15 min at 16,000 ×g at 4 °C and supernatant was transferred into a fresh reaction tube and referred as input sample. After determination of total protein content of the samples 100 μg protein per sample was used for the pull down with agarose beads. Beads were incubated rotating over night at 4 °C. Afterwards beads were centrifuged for 1 min at 16,000 ×g at 4 °C and washed once with 1.0 ml Lysis Buffer 1, twice with Lysis Buffer 2, twice with SWS buffer containing 350 nM NaCl, 5 mM EDTA and 0.1% Triton in DPBS and once with Lysis Buffer 3 containing 50 mM Tris-HCl, 150 mM NaCl, 1 mM EDTA in DBPS. Beads were suspended in 40 μl 5× Laemmli Buffer and heated at 70 °C for

10 min. Samples were subsequently used for western blot using GluA2 antibody. For quantification of membrane GluA2 after pull-down input samples were used referring to contain total GluA2 amount.

2.6. Western blot

Western blot analysis was performed as described earlier (Giese et al., 2010) with minor modifications. Neuronal differentiated cells were lysed in ice cold RIPA buffer. Protein concentrations of total cell lysates were measured using the bicinchoninic acid assay (Pierce BCA, Thermo Scientific, USA). Samples were boiled for 5 min at 95 °C in 5× Laemmli-buffer and separated by SDS-PAGE with precast gels (4–15%, Bio-Rad Laboratories GmbH, Germany). Proteins, contained in total cell lysate or membrane fraction, were transferred to nitrocellulose membranes with a trans-blot turbo transfer system (all Bio-Rad Laboratories GmbH, Germany). Membranes were washed with TBS, blocked with TBS containing 0.1% Tween20 (TBST) and 5% skim milk powder (pH 7.5) for 1 h at room temperature, and incubated with primary antibodies GluA1 (H-301), GluA2 (N-19), GluA4 (C-20, all Santa Cruz Biotechnologies, USA), GluA3 (LSBio, USA), GAPDH (Abcam, UK) and, β-actin (Sigma-Aldrich, Germany) at least 1 h in TBST containing 3% skim milk powder. Between the usages of several antibodies, blots were rinsed 3 times with TBST and incubated with fluorescent dye-conjugated secondary antibodies (IRDye 680 LT goat anti-rabbit IgG, 1:20,000; IRDye 800 goat anti-mouse IgG, 1:10,000; all LI-COR Biosciences GmbH, Germany). As a molecular weight marker, the Precision Plus Protein Dual Xtra Standards (Bio-Rad Laboratories GmbH, Germany) was used. Visualization and quantification were performed with the Odyssey Infrared Imaging System (LI-COR Biosciences GmbH, Germany). Expression of β-actin or GAPDH was used for normalisation.

2.7. Statistical analysis

Data were analysed with GraphPad Prism6 (GraphPad Software Inc., USA). Unpaired two-tailed *t*-test, Mann-Whitney-Test and Fisher's exact test with a confidence interval of 0.95 were used, when applicable. If not otherwise stated, data are given as mean ± SEM, with * = $p < 0.05$, ** = $p < 0.01$ and *** = $p < 0.001$. Significance level was set to $p < 0.05$. All experiments contain at least three independent biological replicates. Data from the electrophysiological and microfluorimetric experiments are summarized in Table 1.

3. Results

Recently, we described the generation of a patient-specific iPSC-based cell model for NPC1, containing functional neurons (Peter et al., 2017; Trilck et al., 2017). We established those cell lines to elucidate differences in their cellular phenotypes and gain insight into the underlying pathogenic mechanism of NPC1. In this study, we were interested in consequences of the accumulation of cholesterol and other lipids, like GM2 (Trilck et al., 2017), in regard to the expression of functional voltage-gated and ligand-gated ion channels in iPSC-derived neurons, carrying mutations in the *NPC1* gene. We used a control cell line of a healthy individual and three cell lines carrying the compound heterozygous mutation c.1836A>C/c.1628delC, the homozygous mutation c.1180T>C or the prevalent homozygous mutation c.3182T>C.

3.1. Functional analysis of voltage-gated ion channels in iPSC-derived neurons

First, we were interested in the expression of different types of VGICs, namely sodium- (Na_V), potassium- (K_V) and Ca^{2+}-channels (Ca_V) on iPSC-derived neurons. Therefore, we used the patch clamp technique and recorded currents mediated by Na_V, K_V and Ca_V in the whole cell configuration.

Neurons were selected visually and were recognized by their round to oval shaped cell bodies with clearly visible processes (Fig. 1A inset). Regarding the expression of Na_V, K_V and Ca_V, cells of all cell lines expressed functional VGICs as demonstrated by fast inactivating inward currents and persistent outward currents (Fig. 1A). They were furthermore capable to initiate spontaneous action potentials (Fig. 1C, AP_{spon}) or showed induced APs (data not shown) after depolarizing current injections. We observed spontaneous post synaptic currents (PSCs), confirming not only the expression of LGICs, but also the maturation of functional synapses between the cells. Using a holding potential of −60 mV, in combination with a symmetrical Cl^- concentration, we observed PSCs as inward currents, displaying different decay kinetics (Fig. 1D), most likely due to the expression of different LGICs, like glutamate receptors (GluRs) or GABA receptors (GABARs). A more detailed analysis of these currents was not done as the number of cells presenting PSCs and the frequency of PSCs was not sufficient for a sound statistically analysis. Cells of all cell lines demonstrated comparable cell capacities (Fig. 1E) and resting potentials (V_{rest}), ranging between −40 mV and −32 mV. The resting potential of cells bearing the mutation c.1180T>C or c.3182T>C was significantly less negative in comparison to control cell line (Fig. 1F). The low number of PSCs and the low range of V_{rest} suggest an incomplete maturation of the cells, which might increase with longer times of differentiation. A time dependent maturation of iPSC derived neurons is commonly observed (Halliwell, 2017; Kuijlaars et al., 2016; Lam et al., 2017), with varying times of differentiation lasting up to 12 weeks (Kuijlaars et al., 2016; Lam et al., 2017). In our study we used cells which were differentiated for 6 to 7 weeks, as we described clear hallmarks of NPC1 at this point in time (Trilck et al., 2017; Trilck et al., 2013). The majority of cells

Table 1
Electrophysiological parameters were recorded by means of patch clamp recordings in the whole cell configuration using voltage or current clamp mode. Changes of $Ca^{2+}_{[i]}$ were measured by means of Fura2. The area under the curve (AUC) of AMPA-induced responses was measured and is given in arbitrary units (a.u.). Values for C_M and V_{rest} are given as mean ± SEM.

	Control	c.1836A>C/c.1628 delC	c.1180T>C	c.3182T>C
C_M (pF)	14.2 ± 0.8 (n = 73)	12.6 ± 0.6 (n = 102)	13.4 ± 0.7 (n = 93)	13.1 ± 0.8 (n = 48)
V_M (mV)	−40.3 ± 1.2 (n = 65)	−38.3 ± 1.1 (n = 64)	−34.4 ± 1.4 (n = 45)	−32.5 ± 1.2 (n = 44)
% cells with Na_V	97	100	100	93
% cells with K_V	100	87	100	48
% cells with Ca_V	67	50	51	88
% cells with AP_{ind}	100	98	93	97
% with AP_{spon}	14	14	8	15
% cells with PSCs	43	25	63	52
Frequency PSCs (Hz)	0.04 ± 0.01 (n = 17)	0.18 ± 0.08 (n = 22)	0.07 ± 0.01 (n = 28)	0.14 ± 0.11 (n = 14)
% cells reacting to AMPA patch clamp	76	90	66	72
CD AMPA-response (pA/pF)	2.7 ± 0.4 (n = 15)	2.6 ± 0.3 (n = 10)	1.7 ± 0.2 (n = 13)	1.9 ± 0.2 (n = 12)
% cells reacting to AMPA Ca^{2+}-imaging	92	84	91	84
AUC AMPA-response (a.u.)	2357 ± 169 (n = 315)	1756 ± 205 (n = 155)	1306 ± 135 (n = 188)	796 ± 62 (n = 278)

C_M = cell capacity, V_{rest} = resting potential; Na_V = voltage-gated Na^+-channels; K_V = voltage-gated K^+-channels, Ca_V = voltage-gated Ca^{2+}-channels, AP_{ind} = induced action potentials, AP_{spon} = spontaneous action potentials. CD = current density.

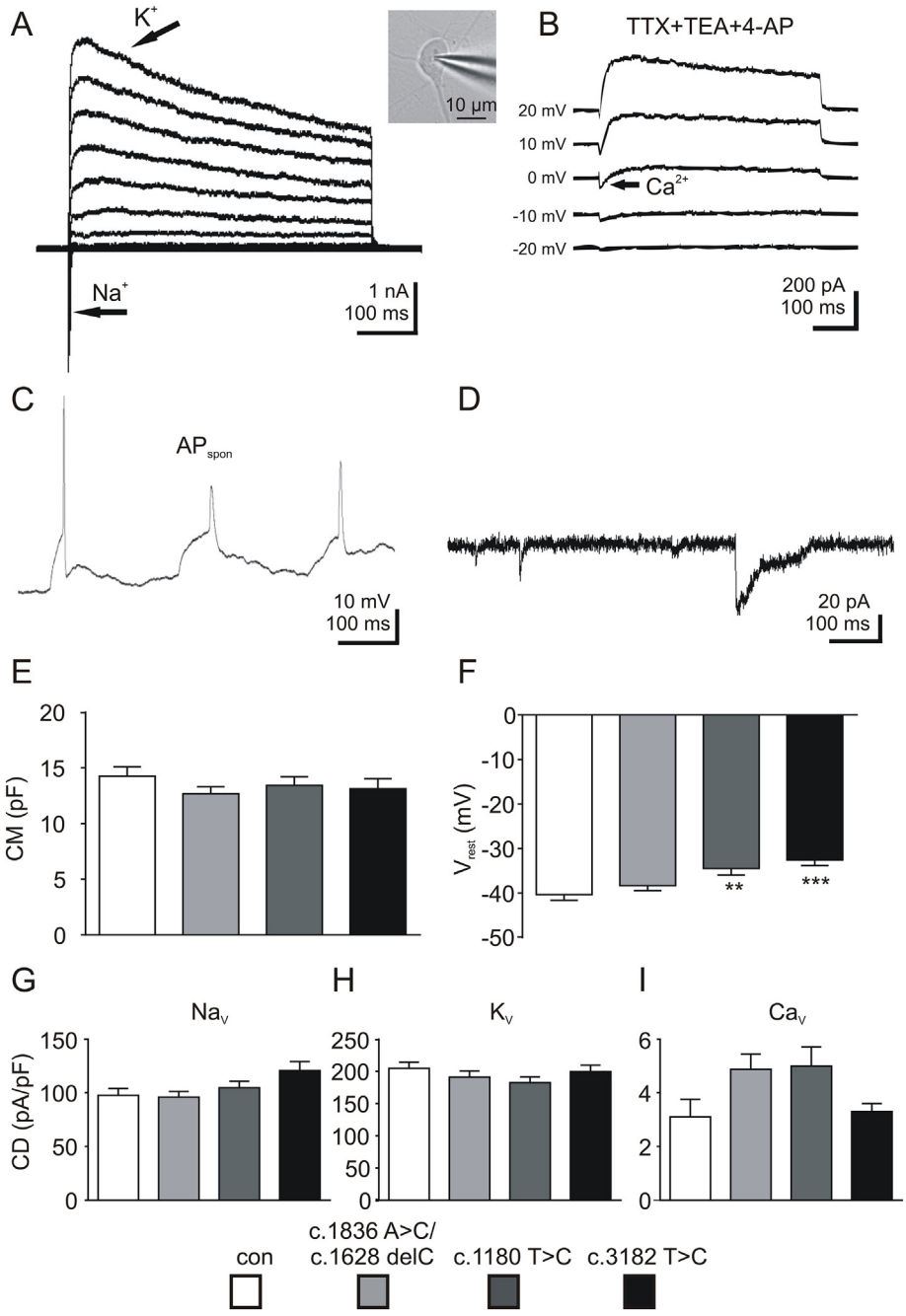

Fig. 1. Patch clamp recordings of VGICs in iPSC-derived neurons. (A) iPSC-derived neurons were selected by their round to oval shape (insert between panel A and B) and displayed inward-directed sodium currents (Na^+) and outward-directed potassium currents (K^+). (B) In a subset of experiments TTX, TEA and 4-AP were applied to isolate Ca_V mediated currents (Ca^{2+}). (C) Neurons were capable to generate spontaneous action potentials (AP_{spon}). (D) Recordings of postsynaptic currents proved the maturation of functional chemical synapses. (E) Neurons of all four cell lines had comparable cell capacities. (F) Resting potential of cells carrying a homozygous mutation was slightly, but significantly less negative in comparison to control cells. (G–I) Peak current densities of Na^+-, K^+-, and Ca^{2+}-currents did not differ between the genotypes. Data are given as mean ± SEM. Data are summarized in Table 1. TTX = tetrodotoxin; TEA = tetraethylammonium chloride; 4-AP = 4-aminopyridine.

demonstrated Na_V and K_V. In regard of Ca_V, we used in a subset of experiments the Na_V antagonist tetrodotoxin and the K_V antagonists 4-aminopyridine and tetraethylammonium chloride to isolate Ca_V mediated currents. The observed putative Ca^{2+}-currents displayed only small amplitudes (Fig. 1B), preventing a detailed description or further classification of Ca^{2+}-currents. Regarding the number of cells displaying Ca_V-, K_V- or Na_V-currents, we found no differences between the cell lines carrying a mutation and in comparison with the control cell line, with exception of a significantly lower number of cells expressing K_V bearing the c.31823T>C mutation. However, no differences were found in the Na_V-, K_V- and Ca_V-current densities (Fig. 1G–I) or the percentage of cells with AP_{spon} or AP_{ind}. Data of the patch clamp experiments are summarized in Table 1.

3.2. Functional analysis of AMPA receptors in iPSC-derived neurons

To reveal functional differences of AMPARs in iPSC-derived neurons we applied AMPA to induce AMPARs mediated currents, measured by means of patch clamp recordings (Fig. 2AC; E) and microfluorimetric measurements of $Ca^{2+}{}_{[i]}$ (Fig. 2B, D, F). Cells reacted to the application of AMPA with an inward current (Fig. 2A). The number of cells reacting to AMPA was not different between the cell lines bearing a mutation

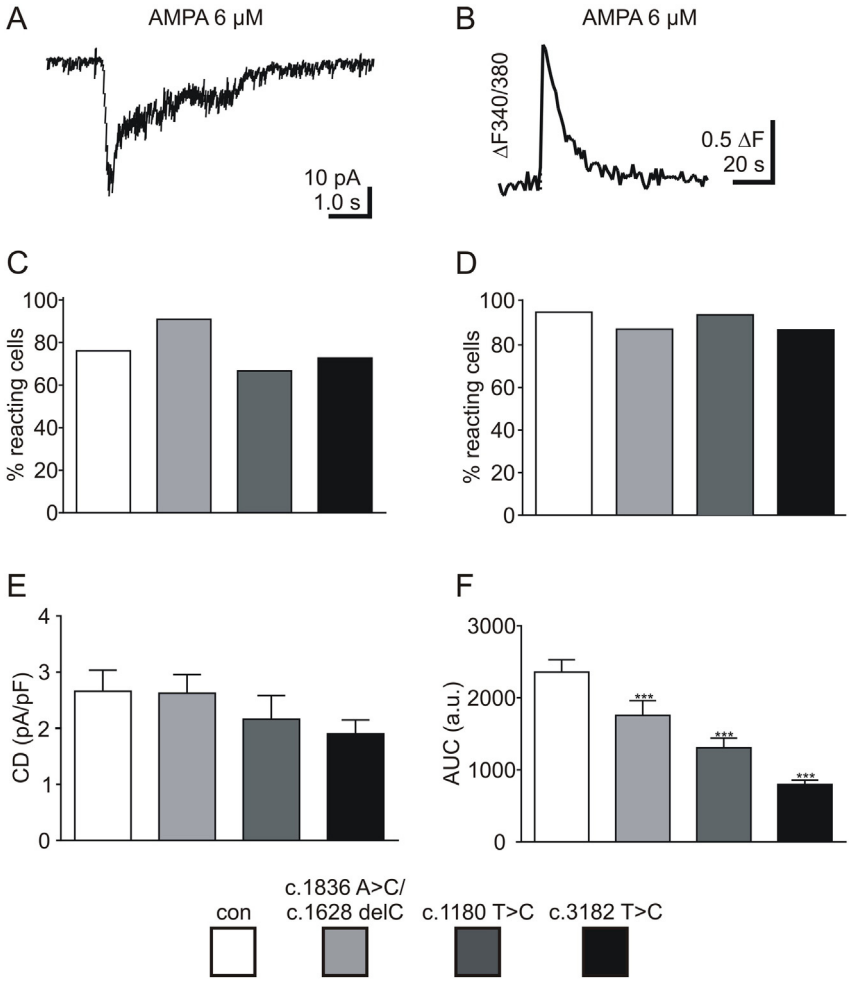

Fig. 2. AMPA-induced changes of $Ca^{2+}_{[i]}$. (A) Application of AMPA resulted in transient inward-directed currents in patch clamp recordings. (C) The vast majority of neurons reacted to the application of AMPA. (E) Peak current density of AMPA-induced currents was lower in cells carrying a *NPC1* mutation. (B) Fura2 was used for microfluorimetric Ca^{2+}-determination, to assess AMPA-induced increase of $Ca^{2+}_{[i]}$. (D) The majority of cells demonstrated an AMPA-induced increase of $Ca^{2+}_{[i]}$ and no differences of the number of reacting cells were found. (F) Determination of the AUC of AMPA-induced Ca^{2+} responses elucidated significantly lower increases of $Ca^{2+}_{[i]}$ in all cell lines carrying a mutation in comparison to control cells. Data are given as mean ± SEM. Data are summarized in Table 1.

and the control cells (Fig. 2C). Regarding the peak-current amplitude, we observed a reduction of the current density for cells bearing the mutation c.1180T>C or c.3182T>C (Fig. 2E). Besides patch clamp recordings, we used measurements of the intracellular Ca^{2+} concentration ($Ca^{2+}_{[i]}$) by means of the Ca^{2+} indicator Fura2-AM and studied AMPA-induced changes of $Ca^{2+}_{[i]}$. The application of AMPA resulted in an increase of $Ca^{2+}_{[i]}$ (Fig. 2B), which could be antagonized by CNQX (6-cyano-7-nitroquinoxaline-2,3-dione), a selective AMPARs antagonist (data not shown). The number of cells reacting to AMPA was comparable between all four cell lines (Fig. 2D). But in contrast to the patch clamp measurements, we found a significantly decreased rise of $Ca^{2+}_{[i]}$ in response to AMPA in all cell lines bearing a mutation in comparison to the control cells (Fig. 2F). In accordance with the patch clamp recordings, the strongest reduction was observed in cells carrying the c.3182T>C mutation, displaying five times lower Ca^{2+}-influx than the control cells. Results of patch clamp and Ca^{2+}-imaging experiments are collected in Table 1. To elucidate the reason for the decreased rises of $Ca^{2+}_{[i]}$ induced by AMPA, we analysed the expression of the AMPAR subunits GluA1–A4 by RT-qPCR and western blot.

3.3. RT-qPCR and western blot analysis of GluA1–4 subunits

To elucidate the underlying mechanism of the hampered Ca^{2+}-influx, we assessed the expression of the four AMPAR subunits by RT-qPCR. The analysis revealed heterogeneous changes of the expression of GluA1–4 in cell lines carrying a mutation (Fig. 3A–D). The cell line with the mutation c.1836A>C/c.1628delC did not show any alterations of the transcription level of any subunit. In contrast, the cell lines with homozygous mutations demonstrated a significantly higher level of GluA1 and GluA2 mRNA and an increased level of GluA3 or GluA4 mRNA. These findings are in accordance to the findings of the Ca^{2+}-imaging experiments, in which cells with the c.1836A>C/c.1628delC mutation were less effected than cells with a homozygous mutation. The Ca^{2+}-permeability of AMPARs can be steered by the insertion of the GluA2 subunit, as receptors containing this subunit are not permeable for Ca^{2+} anymore (Traynelis et al., 2010). As the cells with the c.1180T>C and the c.3182T>C mutation demonstrated an upregulation of the mRNA for GluA2, we wondered if the lower AMPA-induced raise of $Ca^{2+}_{[i]}$ is due to a higher GluA2 protein expression. Thus, we performed western blot analysis of the AMPAR subunits GluA1–4 (Fig. 4). Analysing whole cell lysates, we found a clearly increased GluA2 protein level in all three cell lines carrying a *NPC1* mutation, although these alterations were statistically not different in comparison to the control cell line (Fig. 4B). Furthermore, we were interested in the subcellular localization of the GluA2 protein and thus we used first isolated membrane fractions of the cells and secondly a biotinylation assay to extract biotinylated GluA2 protein from the membrane. The analysis of the amount of GluA2 protein in the membrane fraction (Fig. 4D, $GluA2_{membrane}$) revealed a statistically significant increase of the protein amount. In accordance to the amount of GluA2 in the membrane

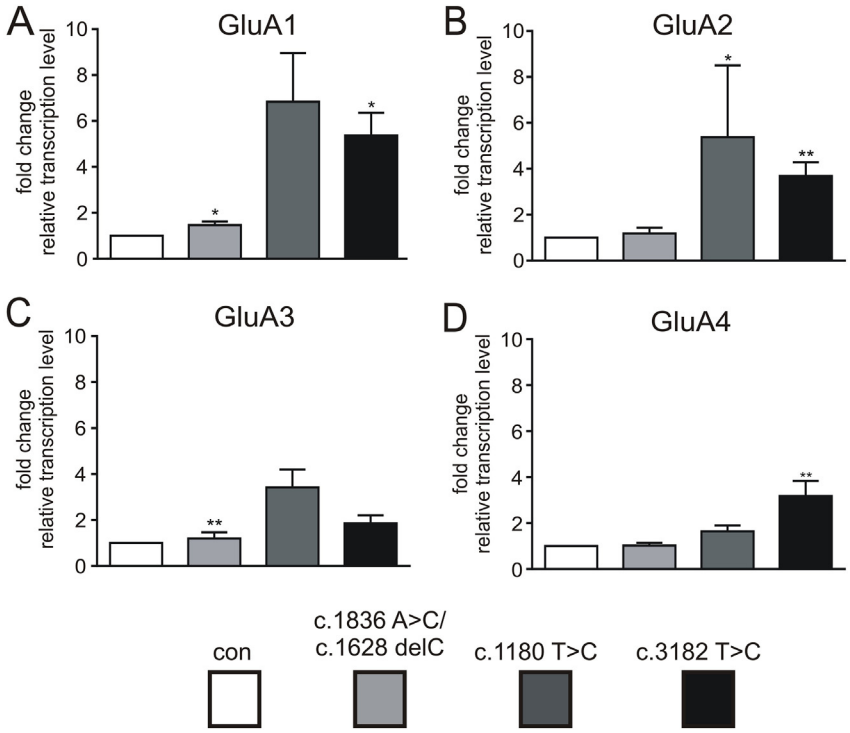

Fig. 3. RT-qPCR analysis of AMPARs subunits GluA1–4. RT-qPCR (A–D) revealed significantly increased transcription level of GluA1 (A) and GluA2 (C) in the cell lines bearing the mutation c.1180T>C or c.3182T>C, but not in the cell line bearing the mutation c.1836A>C/c.1628delC. Data are given as mean ± SEM. N = 3–4.

fraction, we found an increased amount of GluA2 in the samples of the immunoprecipitation of biotinylated GluA2 protein (Fig. 4F). Taking these findings together, we conclude that the reduced AMPA-induced Ca^{2+}-influx is based on a higher level of GluA2 containing and thus Ca^{2+} impermeable AMPARs in cells carrying a *NPC1* mutation.

4. Discussion

Several studies using genetically modified mouse model systems suggest a cell autonomous mechanism underlying the loss of neurons observed in NPC1 (Elrick et al., 2010; Ko et al., 2005; Lopez and Scott, 2013; Yu et al., 2011). Most of these studies are focused on cerebellar Purkinje cells, as the degeneration of these cells is the most obvious one in the CNS. However, cerebellar Purkinje cells are highly specialized cells with unique properties based on unique expression profiles of proteins, which even differ between the single lobes of the cerebellum (Chung et al., 2016; Cologna et al., 2012; Liao et al., 2010). Thus, one can speculate about a varying impact of the *NPC1* mutation on different cell populations. Moreover, these studies are based on the mostly used BALB/c NPC1 mouse model (Pentchev et al., 1980) comprising a complete knock-down of the NPC1 protein and do not reflect the situation in patients suffering from various mutations with different effects on the expression and function of the NPC1 protein (Fancello et al., 2009; Macías-Vidal et al., 2011; Millat et al., 2001; Ribeiro et al., 2001; Sun et al., 2001; Tang et al., 2010). In this study, we have chosen an approach which is not focused on a certain subtype of highly specialized neurons from a murine NPC1 model, but on neurons derived from NPC1 patient-specific iPSCs. Recently, we described these cell lines in regard to the accumulation of cholesterol and GM2 (Trilck et al., 2017; Trilck et al., 2013). As cholesterol is crucial for proper formation of cell membranes and the localization of e.g. ion channels, we wondered if these cell lines vary in regard of expression and function of ion channels. Thus, we used patch clamp recordings and microfluorimetric Ca^{2+}-measurements to study differences in VGICs and AMPARs, a subtype of the glutamate receptor family.

4.1. Voltage-gated and ligand-gated ion channels of iPSC-derived neurons

Regarding iPSC-derived neurons, we demonstrated the expression of voltage-gated Na^+-, K^+-, and Ca^{2+}- channels by an electrophysiological approach. Cells of all cell lines displayed currents mediated by these VGICs and were capable to generate spontaneous and induced action potentials. These results demonstrate a physiological maturation of the cells unharmed from hampered function of the NPC1 protein. However, we found differences of the resting potential between control cells and cells carrying a *NPC1* mutation, showing a significantly less negative resting potential. This contrasts with findings in primary neuronal cultures of the BALB/c NPC1 mouse model, demonstrating no differences in the resting potential or other electrophysiological parameters (Deisz et al., 2005).

The resting potential is determined by the activity of potassium channels and a hampered function of these channels might lead to functional changes in cells carrying a *NPC1* mutation. This is supported by data from gene expression profiling of fibroblasts carrying the c.3182T>C mutation, which showed an altered expression level for different voltage-gated potassium channels (Reddy et al., 2006). Regarding the resting potential of neurons, a less negative V_{rest} was described in iPSC-derived neurons generated from fibroblasts of patients suffering from Gaucher Disease Type 2, another fatal lysosomal storage disorder. A hallmark of this disease is the accumulation of glycolysosphingosine and glycosylceramide (Sun et al., 2015), the latter one is described to accumulate also in NPC1 (Zervas et al., 2001). However, no other data from human NPC1-deficient cells is available. But still, one has to keep in mind that even small changes of V_{rest} can have a fatal impact on CNS function, e.g. by initiating epilepsy. A further consequence of a less negative V_{rest} might be a higher susceptibility of the cells for excitotoxicity, as V_{rest} is shifted towards the activation threshold for Na_V and Ca_V channels. Indeed, an increased excitability based on a loss of function of K_V is described for a mouse model of Alzheimer's disease and is discussed to be a potential initiator of a deleterious vicious circle ending up in excitotoxicity (Duan et al., 2014; Flierl et al., 2014; Frazzini et al., 2016). In regard of NPC1, comparable studies with murine models are missing until now. But it seems to be worth to elucidate a possible

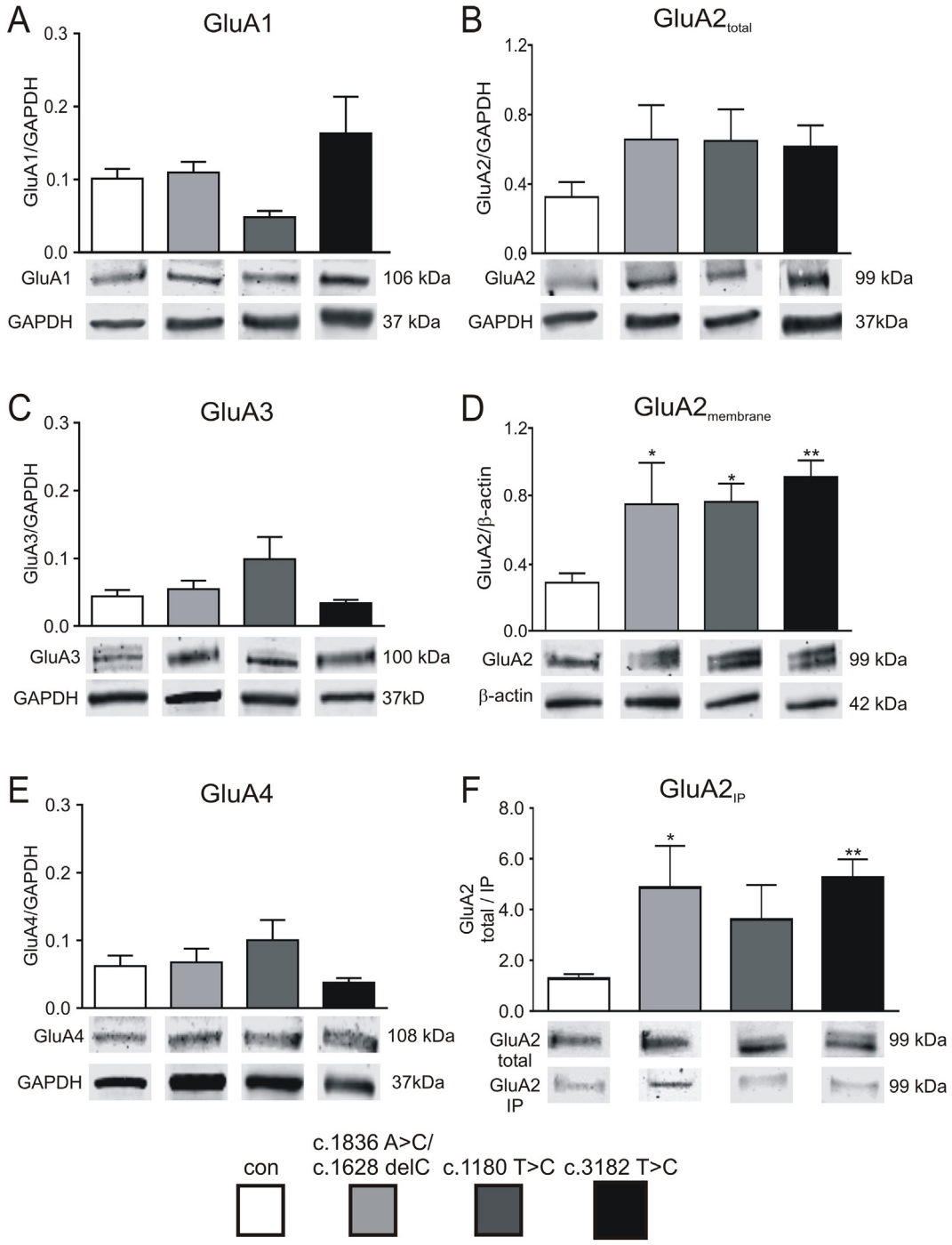

Fig. 4. Western blot analysis of AMPARs subunits GluA1–4. Determination of the protein level of GluA1–4 (A,B,C,E) by western blot analysis revealed an increased amount of GluA2 in total cell lysates (B, $GluA2_{total}$). No significant changes were found for the other AMPARs subunits. Content of GluA2 in isolated membrane fractions was increased in all mutant cell lines (D, $GluA2_{membrane}$). An increased membrane located amount of GluA2 was confirmed by immunoprecipitation of biotinylated GluA2 protein (F, $GluA2_{IP}$). Data are given as mean ± SEM. N = 3–4.

contribution of altered function of voltage gated ion channels to the progression of NPC1.

4.2. AMPA receptors in iPSC-derived neurons

Cholesterol is essential for a proper synaptic transmission, as receptor clustering depends on cholesterol (Zonta and Minichiello, 2013), as well as fusion and release of synaptic vesicles (Churchward and Coorssen, 2009; Dason et al., 2014). Regarding LGICs, especially GluRs, the contribution to the pathogenic mechanism of NPC1 is still not completely clear. An altered excitatory synaptic transmission, determined by recordings of PSCs, was observed in cultured hippocampal neurons and in hippocampal slices obtained from the BALB/c NPC1 mouse model (Esteban et al., 2010; Wasser et al., 2007; Xu et al., 2011; Xu et al., 2010; Zhou et al., 2011). NPC1-deficient animals displayed altered inhibitory and excitatory transmission based on changes of the presynaptic vesicle release (Xu et al., 2010). Using this mouse model, we recently described GABA-mediated IPSCs of hippocampal pyramidal cells, without finding a difference between wild type and NPC1-deficient mice (Frech et al., 2015). However, the analysis of post synaptic currents is an instructive approach as alterations of frequency, amplitudes and decay kinetics of PSCs are directly linked to the

functionality of ligand-gated ion channels. Here, we found that cells of all cell lines are able to establish functional chemical synapses, proven by the recording of spontaneous PSCs. Although the number of recorded PSCs was not sufficient for a meaningful analysis, we proved that the cells receive inhibitory and excitatory input, demonstrated by the different amplitudes and decay kinetics of the PSCs. Fast decay kinetics most likely reflect PSCs mediated by GluRs and slow kinetics reflect PSCs mediated by GABARs or GlyRs (Frech et al., 2001). However, as the PSC frequency was too low to determine any functional differences, we applied AMPA to evoke current responses mediated by excitatory AMPARs. We did not find any differences in the number of cells reacting to this agonist, neither by analysing the cells by means of patch clamp recordings, nor by analysing AMPA-induced increase of the intracellular Ca^{2+} concentration. In regard of peak current densities of AMPA-induced currents, we observed a slight decrease in the cells carrying a homozygous mutation, although these differences were statistically not different from the control cells. But, the microfluorimetric determination of intracellular Ca^{2+} concentrations revealed a significant reduction of the AMPA-induced Ca^{2+}-influx in all cell lines with a *NPC1* mutation in comparison to the control cell line. A possible explanation is a downregulation of AMPARs in these cells. Thus, we performed RT-qPCR for the AMPAR subunits GluA1–A4 and revealed not a downregulation but an increase of GluA1 and GluA2 mRNA in cell lines with the c.1180T>C and c.3182T>C mutation. An upregulation of the transcription level of GluA2 might lead to a decreased Ca^{2+}-influx through GluA2 containing AMPARs, as receptors containing the GluA2 subunit are not permeable for Ca^{2+} anymore (Traynelis et al., 2010). Consequently, we analysed the protein level of GluA1–A4 and found an increased GluA2 protein level in all cell lines carrying a *NPC1* mutation. These differences were found in whole cell lysates, isolated membrane fractions, as well as in the immunoprecipitation of biotinylated GluA2 subunits. Thus, we conclude that membranes of cells carrying a *NPC1* mutation possess a higher amount of AMPARs containing the GluA2 subunit, consequently leading to Ca^{2+} impermeable AMPARs. One can speculate about different mechanisms leading to an increased amount of GluA2 subunits:

I) The increased mRNA for GluA2 may indicate a feedback mechanism and a subsequently upregulation of GluA2 protein to anticipate an abnormal toxic Ca^{2+} overload of the cells. But, we observed an increased GluA2 protein amount in the cells carrying the compound heterozygous mutation without demonstrating an increased mRNA level.

II) Cholesterol is crucial for the maintenance of lipid rafts, highly specialized membrane microdomains involved in the organization of synaptic structures (Head et al., 2014). A depletion of cholesterol in the membrane, impacts the organization of lipid rafts and contained ion channels (Hering et al., 2003; Hou et al., 2008). Moreover, accumulating evidence support an important role of lipid rafts in neurodegenerative diseases (Kim and Vellis, 2009; Sebastiao et al., 2013). A hallmark of cells lacking functional NPC1 protein is a lysosomal accumulation of cholesterol which in turn is not available for cell membranes and may lead to changes in lipid rafts. The crucial role of cholesterol has already been demonstrated, e.g. in the CNS of aging rodents. It was shown that reduced availability of cholesterol impacts the internalization of GluA2, subsequently perturbing long term depression (Martin et al., 2014). According to these findings, the elevated protein level of GluA2 may result from an altered cholesterol availability in lipid rafts. On the other hand, this hypothesis does not explain the increased mRNA expression in cells with homozygous NPC1 mutations.

III) AMPARs are crucial for the fast excitatory glutamatergic neurotransmission and are involved in cognition and learning, displaying the underlying mechanism of long term potentiation and depression (Malenka and Bear, 2004). Accordingly, trafficking towards and composition of these receptors within excitatory synapses is highly regulated and a well-balanced subunit composition of GluRs is needed (Hastie and Henley, 2009; Henley and Wilkinson, 2016). AMPARs are tetrameric channels and the vast majority contains the edited, Ca^{2+}-impermeable, GluA2 subunit. The here observed increased amount of GluA2 protein in the membrane, of cells carrying a *NPC1* mutation, may be based on a disturbance of trafficking towards synapses, hampered lateral diffusion, or reduced exchange of this receptor subunit. Uncoupling GluA2 from synaptic scaffolds depends on the phosphorylation of the subunit mediated by phosphokinase c (PKC) and C kinase 1 (PICK1) (Hastie and Henley, 2009; Henley and Wilkinson, 2016). A disturbance of this process impacts the exchange of GluRs taking place e.g. in long term potentiation. Intriguingly, an attenuation of PKC activity is described in fibroblasts of NPC1 patients (Tamari et al., 2013; Walter et al., 2009), contributing to hypophosphorylation of cytoskeletal proteins. With respect to the here used cells, we described a decreased amount of the phosphorylated intermediate filaments vimentin and GFAP and the rescue of this hypophosphorylation by activation of PKC (Peter et al., 2016), comparable to the data obtained from patient's fibroblasts (Tamari et al., 2013). Based on our findings we suggest an impairment of the machinery regulating the composition of AMPARs, leading to an imbalance of especially the Ca^{2+} impermeable GluA2 subunit.

5. Conclusion

In this study, we described impaired Ca^{2+}-signaling in NPC1-deficient neurons based on a decreased Ca^{2+}-influx through GluA2 containing AMPARs. We speculate, that the increased amount of the GluA2 subunit is the consequence of a corrupted PKC activity, described in NPC1-deficient cells. In turn, an altered Ca^{2+}-signaling through AMPARs itself may impact PKC-activity, reflecting a deleterious vicious circle. Although a direct proof of the impact of PKC on the GluA2 subunit is missing until now, our results recommend further investigations in regard to the impact of an altered Ca^{2+}-homeostasis. As the regulation of esp. AMPA receptors is crucial for the maintenance of synaptic transmission, a dysfunction may not only contribute to the disease progression, but displays a possible intervention strategy to ameliorate the disease linked clinical picture.

Acknowledgement

We thank Sebastian Rost for his excellent technical support.

References

Bergamin, N., Dardis, A., Beltrami, A., Cesselli, D., Rigo, S., Zampieri, S., Domenis, R., Bembi, B., Beltrami, C.A., 2013. A human neuronal model of Niemann Pick C disease developed from stem cells isolated from patient's skin. Orphanet J. Rare Dis. 8:34. http://dx.doi.org/10.1186/1750-1172-8-34.

Carstea, E.D., Morris, J.A., Coleman, K.G., Loftus, S.K., Zhang, D., Cummings, C., Gu, J., Rosenfeld, M.A., Pavan, W.J., Krizman, D.B., Nagle, J., Polymeropoulos, M.H., Sturley, S.L., Ioannou, Y.A., Higgins, M.E., Comly, M., Cooney, A., Brown, A., Kaneski, C.R., Blanchette-Mackie, E.J., Dwyer, N.K., Neufeld, E.B., Chang, T.Y., Liscum, L., Strauss, J.F.I., Ohno, K., Zeigler, M., Carmi, R., Sokol, J., Markie, D., O'Neill, R.R., van Diggelen, O.P., Elleder, M., Patterson, M.C., Brady, R.O., Vanier, M.T., Pentchev, P.G., Tagle, D.A., 1997. Niemann-Pick C1 disease gene: homology to mediators of cholesterol homeostasis. Science 277 (5323), 228–231.

Chater, T.E., Goda, Y., 2014. The role of AMPA receptors in postsynaptic mechanisms of synaptic plasticity. Front. Cell. Neurosci. 8:401. http://dx.doi.org/10.3389/fncel.2014.00401.

Chung, C., Elrick, M.J., Dell'Orco, J.M., Qin, Z.S., Kalyana-Sundaram, S., Chinnaiyan, Am, Shakkottai, V.G., Lieberman, A.P., 2016. Heat shock protein beta-1 modifies anterior to posterior Purkinje cell vulnerability in a mouse model of Niemann-Pick type C disease. PLoS Genet. 12 (5):e1006042. http://dx.doi.org/10.1371/journal.pgen.1006042.

Churchward, M.A., Coorssen, J.R., 2009. Cholesterol, regulated exocytosis and the physiological fusion machine. Biochem. J. 423 (1), 1–14.

Cologna, S.M., Jiang, X.-S., Backlund, P.S., Cluzeau, C.V.M., Dail, M.K., Yanjanin, N.M., Siebel, S., Toth, C.L., Jun, H.-s., Wassif, C.A., Yergey, A.L., Porter, F.D., Bush, A.I., 2012.

Quantitative proteomic analysis of Niemann-Pick disease, type C1 cerebellum identifies protein biomarkers and provides pathological insight. PLoS ONE 7 (10): e47845. http://dx.doi.org/10.1371/journal.pone.0047845.
D'Arcangelo, G., Grossi, D., Chiara, G. de, Stefano, M.C. de, Cortese, G., Citro, G., Rufini, S., Tancredi, V., Merlo, D., Frank, C., 2011. Glutamatergic neurotransmission in a mouse model of Niemann-Pick type C disease. Brain Res. 1396, 11–19.
Dason, J.S., Smith, A.J., Marin, L., Charlton, M.P., 2014. Cholesterol and F-actin are required for clustering of recycling synaptic vesicle proteins in the presynaptic plasma membrane. J. Physiol. 592 (Pt 4), 621–633.
Davies, J.P., Ioannou, Y.A., 2000. Topological analysis of Niemann-Pick C1 protein reveals that the membrane orientation of the putative sterol-sensing domain is identical to those of 3-hydroxy-3-methylglutaryl-CoA reductase and sterol regulatory element binding protein cleavage-activating protein. J. Biol. Chem. 275 (32), 24367–24374.
Deisz, R.A., Meske, V., Treiber-Held, S., Albert, F., Ohm, T.G., 2005. Pathological cholesterol metabolism fails to modify electrophysiological properties of afflicted neurones in Niemann-Pick disease type C. Neuroscience 130 (4):867–873. http://dx.doi.org/10.1016/j.neuroscience.2004.09.065.
Duan, L., Bhattacharyya, B.J., Belmadani, A., Pan, L., Miller, R.J., Kessler, J.A., 2014. Stem cell derived basal forebrain cholinergic neurons from Alzheimer's disease patients are more susceptible to cell death. Mol. Neurodegener. 9 (3) (1750-1326 (Linking)).
Efthymiou, A.G., Steiner, J., Pavan, W.J., Wincovitch, S., Larson, D.M., Porter, F.D., Rao, M.S., Malik, N., 2015. Rescue of an in vitro neuron phenotype identified in Niemann-Pick disease, type C1 induced pluripotent stem cell-derived neurons by modulating the WNT pathway and calcium signaling. Stem Cells Transl. Med. 4 (3):230–238. http://dx.doi.org/10.5966/sctm.2014-0127.
Elrick, M.J., Pacheco, C.D., Yu, T., Dadgar, N., Shakkottai, V.G., Ware, C., Paulson, H.L., Lieberman, A.P., 2010. Conditional Niemann-Pick C mice demonstrate cell autonomous Purkinje cell neurodegeneration. Hum. Mol. Genet. 19 (5):837–847. http://dx.doi.org/10.1093/hmg/ddp552.
Esteban, M.A., Wang, T., Qin, B., Yang, J., Qin, D., Cai, J., Li, W., Weng, Z., Chen, J., Ni, S., Chen, K., Li, Y., Liu, X., Xu, J., Zhang, S., Li, F., He, W., Labuda, K., Song, Y., Peterbauer, A., Wolbank, S., Redl, H., Zhong, M., Cai, D., Zeng, L., Pei, D., 2010. Vitamin C enhances the generation of mouse and human induced pluripotent stem cells. Cell Stem Cell 6 (1), 71–79.
Fancello, T., Dardis, A., Rosano, C., Tarugi, P., Tappino, B., Zampieri, S., Pinotti, E., Corsolini, F., Fecarotta, S., D'Amico, A., Di Rocco, M., Uziel, G., Calandra, S., Bembi, B., Filocamo, M., 2009. Molecular analysis of NPC1 and NPC2 gene in 34 Niemann–Pick C Italian patients: identification and structural modeling of novel mutations. Neurogenetics 10 (3):229–239. http://dx.doi.org/10.1007/s10048-009-0175-3.
Ferrante, A., Nuccio, C. de, Pepponi, R., Visentin, S., Martire, A., Bernardo, A., Minghetti, L., Popoli, P., 2016. Stimulation of adenosine A2A receptors reduces intracellular cholesterol accumulation and rescues mitochondrial abnormalities in human neural cell models of Niemann-Pick C1. Neuropharmacology 103:155–162. http://dx.doi.org/10.1016/j.neuropharm.2015.11.022.
Flierl, A., Oliveira, L.M., Falomir-Lockhart, L.J., Mak, S.K., Hesley, J., Soldner, F., Arndt-Jovin, D.J., Jaenisch, R., Langston, J.W., Jovin, T.M., Schule, B., 2014. Higher vulnerability and stress sensitivity of neuronal precursor cells carrying an alpha-synuclein gene triplication. PLoS ONE 9 (11):e112413. http://dx.doi.org/10.1371/journal.pone.0112413.
Frank, C., Rufini, S., Tancredi, V., Forcina, R., Grossi, D., D'Arcangelo, G., 2008. Cholesterol depletion inhibits synaptic transmission and synaptic plasticity in rat hippocampus. Exp. Neurol. 212 (2):407–414. http://dx.doi.org/10.1016/j.expneurol.2008.04.019.
Frazzini, V., Guarnieri, S., Bomba, M., Navarra, R., Morabito, C., Mariggiò, M.A., Sensi, S.L., 2016. Altered Kv2.1 functioning promotes increased excitability in hippocampal neurons of an Alzheimer's disease mouse model. Cell Death Dis. 7 (2):e2100. http://dx.doi.org/10.1038/cddis.2016.18.
Frech, M.J., Perez-Leon, J., Wassle, H., Backus, K.H., 2001. Characterization of the spontaneous synaptic activity of amacrine cells in the mouse retina. J. Neurophysiol. 86 (4), 1632–1643.
Frech, M.J., Rabenstein, M., Bovensiepen, K., Rost, S., Rolfs, A., 2015. Cyclodextrin alters GABAergic input to CA1 pyramidal cells in wild-type but not in NPC1-deficient mice. BioResearch Open Access 4 (1):358–362. http://dx.doi.org/10.1089/biores.2015.0023.
Giese, A.K., Frahm, J., Hübner, R., Luo, J., Wree, A., Frech, M.J., Rolfs, A., Ortinau, S., 2010. Erythropoietin and the effect of oxygen during proliferation and differentiation of human neural progenitor cells. BMC Cell Biol. 11 (1), 94.
Gratacos-Batlle, E., Yefimenko, N., Cascos-Garcia, H., Soto, D., 2014. AMPAR interacting protein CPT1C enhances surface expression of GluA1-containing receptors. Front. Cell. Neurosci. 8:469. http://dx.doi.org/10.3389/fncel.2014.00469.
Halliwell, R.F., 2017. Electrophysiological properties of neurons derived from human stem cells and iNeurons in vitro. Neurochem. Int. 106:37–47. http://dx.doi.org/10.1016/j.neuint.2016.10.003.
Hastie, P., Henley, J.M., 2009. AMPA receptor cell biology/trafficking. In: Squire, L.R. (Ed.), Encyclopedia of Neuroscience. Academic Elsevier, London, pp. 295–302.
Head, B.P., Patel, H.H., Insel, P.A., 2014. Interaction of membrane/lipid rafts with the cytoskeleton: impact on signaling and function: membrane/lipid rafts, mediators of cytoskeletal arrangement and cell signaling. Biochimica et biophysica acta 1838 (2): 532–545. http://dx.doi.org/10.1016/j.bbamem.2013.07.018.
Henley, J.M., Wilkinson, K.A., 2016. Synaptic AMPA receptor composition in development, plasticity and disease. Nat. Rev. Neurosci. 17 (6):337–350. http://dx.doi.org/10.1038/nrn.2016.37.
Hering, H., Lin, C.C., Sheng, M., 2003. Lipid rafts in the maintenance of synapses, dendritic spines, and surface AMPA receptor stability. J. Neurosci. 23 (8), 3262–3271.
Higashi, Y., Murayama, S., Pentchev, P.G., Suzuki, K., 1993. Cerebellar degeneration in the Niemann-Pick type C mouse. Acta Neuropathol. 85 (2), 175–184.
Hou, Q., Huang, Y., Amato, S., Snyder, S.H., Huganir, R.L., Man, H.-Y., 2008. Regulation of AMPA receptor localization in lipid rafts. Mol. Cell. Neurosci. 38 (2):213–223. http://dx.doi.org/10.1016/j.mcn.2008.02.010.
Jurado, S., 2014. The dendritic SNARE fusion machinery involved in AMPARs insertion during long-term potentiation. Front. Cell. Neurosci. 8:407. http://dx.doi.org/10.3389/fncel.2014.00407.
Kim, S.U., Vellis, J. de, 2009. Stem cell-based cell therapy in neurological diseases: a review. J. Neurosci. Res. 87 (10), 2183–2200.
Ko, D.C., Milenkovic, L., Beier, S.M., Manuel, H., Buchanan, J., Scott, M.P., 2005. Cell-autonomous death of cerebellar purkinje neurons with autophagy in Niemann-Pick type C disease. PLoS Genet. 1 (1):81–95. http://dx.doi.org/10.1371/journal.pgen.0010007.
Kuijlaars, J., Oyelami, T., Diels, A., Rohrbacher, J., Versweyveld, S., Meneghello, G., Tuefferd, M., Verstraelen, P., Detrez, J.R., Verschuuren, M., Vos, W.H. de, Meert, T., Peeters, P.J., Cik, M., Nuydens, R., Brône, B., Verheyen, A., 2016. Sustained synchronized neuronal network activity in a human astrocyte co-culture system. Sci Rep 6: 36529. http://dx.doi.org/10.1038/srep36529.
Kuo, S.Y., Castoreno, A.B., Aldrich, L.N., Lassen, K.G., Goel, G., Dancik, V., Kuballa, P., Latorre, I., Conway, K.L., Sarkar, S., Maetzel, D., Jaenisch, R., Clemons, P.A., Schreiber, S.L., Shamji, A.F., Xavier, R.J., 2015. Small-molecule enhancers of autophagy modulate cellular disease phenotypes suggested by human genetics. Proc. Natl. Acad. Sci. U. S. A. 112 (31):7. http://dx.doi.org/10.1073/pnas.1512289112.
Lam, R.S., Töpfer, F.M., Wood, P.G., Busskamp, V., Bamberg, E., 2017. Functional maturation of human stem cell-derived neurons in long-term cultures. PLoS ONE 12 (1): e0169506. http://dx.doi.org/10.1371/journal.pone.0169506.
Lee, H., Lee, J.K., Park, M.H., Hong, Y.R., Marti, H.H., Kim, H., Okada, Y., Otsu, M., Seo, E.-J., Park, J.-H., Bae, J.-H., Okino, N., He, X., Schuchman, E.H., Bae, J.-S., Jin, H.K., 2014. Pathological roles of the VEGF/SphK pathway in Niemann-Pick type C neurons. Nat. Commun. 5:5514. http://dx.doi.org/10.1038/ncomms6514.
Liao, G., Wen, Z., Irizarry, K., Huang, Y., Mitsouras, K., Darmani, M., Leon, T., Shi, L., Bi, X., 2010. Abnormal gene expression in cerebellum of Npc1 −/− mice during postnatal development. Brain Res. 1325:128–140. http://dx.doi.org/10.1016/j.brainres.2010.02.019.
Lopez, M.E., Scott, M.P., 2013. Genetic dissection of a cell-autonomous neurodegenerative disorder: lessons learned from mouse models of Niemann-Pick disease type C. Dis. Model. Mech. 6 (5), 1089–1100.
Macías-Vidal, J., Rodríguez-Pascau, L., Sánchez-Ollé, G., Lluch, M., Vilageliu, L., Grinberg, D., Coll, M.J., 2011. Molecular analysis of 30 Niemann-Pick type C patients from Spain. Clin. Genet. 80 (1):39–49. http://dx.doi.org/10.1111/j.1399-0004.2010.01504.x.
Maetzel, D., Sarkar, S., Wang, H., Abi-Mosleh, L., Xu, P., Cheng, A.W., Gao, Q., Mitalipova, M., Jaenisch, R., 2014. Genetic and chemical correction of cholesterol accumulation and impaired autophagy in hepatic and neural cells derived from Niemann-Pick type C patient-specific iPS cells. Stem Cell Rep. 2 (6), 866–880.
Malenka, R.C., Bear, M.F., 2004. LTP and LTD: an embarrassment of riches. Neuron 44 (1): 5–21. http://dx.doi.org/10.1016/j.neuron.2004.09.012.
Martin, M.G., Ahmed, T., Korovaichuk, A., Venero, C., Menchon, S.A., Salas, I., Munck, S., Herreras, O., Balschun, D., Dotti, C.G., 2014. Constitutive hippocampal cholesterol loss underlies poor cognition in old rodents. EMBO Mol. Med. 6 (7):902–917. http://dx.doi.org/10.15252/emmm.201303711.
Millat, G., Marçais, C., Tomasetto, C., Chikh, K., Fensom, A.H., Harzer, K., Wenger, D.A., Ohno, K., Vanier, M.T., 2001. Niemann-Pick C1 disease: correlations between NPC1 mutations, levels of NPC1 protein, and phenotypes emphasize the functional significance of the putative sterol-sensing domain and of the cysteine-rich luminal loop. Am. J. Hum. Genet. 68 (6):1373–1385. http://dx.doi.org/10.1086/320606.
Morris, J.A., Zhang, D., Coleman, K.G., Nagle, J., Pentchev, P.G., Carstea, E.D., 1999. The genomic organization and polymorphism analysis of the human Niemann-Pick C1 gene. Biochem. Biophys. Res. Commun. 261 (2), 493–498.
Pentchev, P.G., Gal, A.E., Booth, A.D., Omodeo-Sale, F., Fouks, J., Neumeyer, B.A., Quirk, J.M., Dawson, G., Brady, R.O., 1980. A lysosomal storage disorder in mice characterized by a dual deficiency of sphingomyelinase and glucocerebrosidase. Biochim. Biophys. Acta 619 (3), 669–679.
Peter, F., Rabenstein, M., Rolfs, A., Frech, M.J., 2016. Gliosis in Niemann-Pick type C1 patient-specific iPSC derived glia cells. Abstract 10th FENS Forum 2016.
Peter, F., Trilck, M., Rabenstein, M., Rolfs, A., Frech, M.J., 2017. Dataset in support of the generation of Niemann-Pick disease Type C1 patient-specific iPS cell lines carrying the novel NPC1 mutation c.1180T>C or the prevalent c.3182T>C mutation – analysis of pluripotency and neuronal differentiation. Data Brief http://dx.doi.org/10.1016/j.dib.2017.03.042.
Pfaffl, M.W., 2001. A new mathematical model for relative quantification in real-time RT-PCR. Nucleic Acids Res. 29 (9):45. http://dx.doi.org/10.1093/nar/29.9.e45.
Reddy, J.V., Ganley, I.G., Pfeffer, S.R., 2006. Clues to neuro-degeneration in Niemann-Pick type C disease from global gene expression profiling. PLoS ONE 1:e19. http://dx.doi.org/10.1371/journal.pone.0000019.
Ribeiro, I., Marcao, A., Amaral, O., Sa, M.M.C., Vanier, M.T., Millat, G., 2001. Niemann-Pick type C disease: NPC1 mutations associated with severe and mild cellular cholesterol trafficking alterations. Hum. Genet. 109 (1), 24–32.
Sarna, J., Miranda, S.R., Schuchman, E.H., Hawkes, R., 2001. Patterned cerebellar Purkinje cell death in a transgenic mouse model of Niemann Pick type A/B disease. Eur. J. Neurosci. 13 (10), 1873–1880.
Sayed, N., Liu, C., Wu, J.C., 2016. Translation of human-induced pluripotent stem cells: from clinical trial in a dish to precision medicine. J. Am. Coll. Cardiol. 67 (18): 2161–2176. http://dx.doi.org/10.1016/j.jacc.2016.01.083.
Sebastiao, A.M., Colino-Oliveira, M., Assaife-Lopes, N., Dias, R.B., Ribeiro, J.A., 2013. Lipid rafts, synaptic transmission and plasticity: impact in age-related neurodegenerative diseases. Neuropharmacology 64, 97–107 (0028-3908 (Linking)).
Singh, V.K., Kalsan, M., Kumar, N., Saini, A., Chandra, R., 2015. Induced pluripotent stem cells: applications in regenerative medicine, disease modeling, and drug discovery. Front. Cell Dev. Biol. 3. http://dx.doi.org/10.3389/fcell.2015.00002.

Sokol, J., Blanchette-Mackie, J., Kruth, H.S., Dwyer, N.K., Amende, L.M., Butler, J.D., Robinson, E., Patel, S., Brady, R.O., Comly, M.E., 1988. Type C Niemann-Pick disease. Lysosomal accumulation and defective intracellular mobilization of low density lipoprotein cholesterol. J. Biol. Chem. 263 (7), 3411–3417.

Sun, X., Marks, D.L., Park, W.D., Wheatley, C.L., Puri, V., O'Brien, J.F., Kraft, D.L., Lundquist, P.A., Patterson, M.C., Pagano, R.E., Snow, K., 2001. Niemann-Pick C variant detection by altered sphingolipid trafficking and correlation with mutations within a specific domain of NPC1. Am. J. Hum. Genet. 68 (6), 1361–1372.

Sun, Y., Florer, J., Mayhew, C.N., Jia, Z., Zhao, Z., Xu, K., Ran, H., Liou, B., Zhang, W., Setchell, K.D.R., Gu, J., Grabowski, G.A., 2015. Properties of neurons derived from induced pluripotent stem cells of Gaucher disease type 2 patient fibroblasts: potential role in neuropathology. PLoS ONE 10 (3):e0118771. http://dx.doi.org/10.1371/journal.pone.0118771.

Tamari, F., Chen, F.W., Li, C., Chaudhari, J., Ioannou, Y.A., 2013. PKC activation in Niemann pick C1 cells restores subcellular cholesterol transport. PLoS ONE 8 (8), e74169.

Tang, Y., Li, H., Liu, J.P., 2010. Niemann-Pick Disease Type C: from molecule to clinic. Clin. Exp. Pharmacol. Physiol. 37 (1):132–140. http://dx.doi.org/10.1111/j.1440-1681.2009.05235.x.

Tarradas, A., Selga, E., Riuro, H., Scornik, F., Brugada, R., Verges, M., 2013. Cell surface protein biotinylation and analysis. Bio-protocol 3 (16). http://dx.doi.org/10.21769/BioProtoc.857.

Traynelis, S.F., Wollmuth, L.P., McBain, C.J., Menniti, F.S., Vance, K.M., Ogden, K.K., Hansen, K.B., Yuan, H., Myers, S.J., Dingledine, R., 2010. Glutamate receptor ion channels: structure, regulation, and function. Pharmacol. Rev. 62 (3):405–496. http://dx.doi.org/10.1124/pr.109.002451.

Trilck, M., Hübner, R., Seibler, P., Klein, C., Rolfs, A., Frech, M.J., 2013. Niemann-Pick type C1 patient-specific induced pluripotent stem cells display disease specific hallmarks. Orphanet J. Rare Dis. 8:144. http://dx.doi.org/10.1186/1750-1172-8-144.

Trilck, M., Peter, F., Zheng, C., Frank, M., Dobrenis, K., Mascher, H., Rolfs, A., Frech, M.J., 2017. Diversity of glycosphingolipid GM2 and cholesterol accumulation in NPC1 patient-specific iPSC-derived neurons. Brain Res. 1657:52–61. http://dx.doi.org/10.1016/j.brainres.2016.11.031.

Vanier, M.T., 2013. Niemann-Pick diseases. Handb. Clin. Neurol. 113, 1717–1721 (0072-9752 (Linking)).

Walter, M., Chen, F.W., Tamari, F., Wang, R., Ioannou, Y.A., 2009. Endosomal lipid accumulation in NPC1 leads to inhibition of PKC, hypophosphorylation of vimentin and Rab9 entrapment. Biol. Cell. 101 (3), 141–152.

Wasser, C.R., Ertunc, M., Liu, X., Kavalali, E.T., 2007. Cholesterol-dependent balance between evoked and spontaneous synaptic vesicle recycling. J. Physiol. 579 (Pt 2), 413–429.

Xu, S., Zhou, S., Xia, D., Xia, J., Chen, G., Duan, S., Luo, J., 2010. Defects of synaptic vesicle turnover at excitatory and inhibitory synapses in Niemann-Pick C1-deficient neurons. Neuroscience 167 (3):608–620. http://dx.doi.org/10.1016/j.neuroscience.2010.02.033.

Xu, S., Chen, X., Wei, X., Liu, G., Wang, Q., 2011. Presynaptic impairment in Niemann-Pick C1-deficient neurons: not dependent on presence of glial cells. Neurosci. Lett. 496 (1):54–59. http://dx.doi.org/10.1016/j.neulet.2011.03.097.

Yu, T., Shakkottai, V.G., Chung, C., Lieberman, A.P., 2011. Temporal and cell-specific deletion establishes that neuronal Npc1 deficiency is sufficient to mediate neurodegeneration. Hum. Mol. Genet. 20 (22):4440–4451. http://dx.doi.org/10.1093/hmg/ddr372.

Yu, D., Swaroop, M., Wang, M., Baxa, U., Yang, R., Yan, Y., Coksaygan, T., DeTolla, L., Marugan, J.J., Austin, C.P., McKew, J.C., Gong, D.-W., Zheng, W., 2014. Niemann-Pick disease type C: induced pluripotent stem cell-derived neuronal cells for modeling neural disease and evaluating drug efficacy. J. Biomol. Screen. 19 (8):1164–1173. http://dx.doi.org/10.1177/1087057114537378.

Zervas, M., Dobrenis, K., Walkley, S.U., 2001. Neurons in Niemann-Pick disease type C accumulate gangliosides as well as unesterified cholesterol and undergo dendritic and axonal alterations. J. Neuropathol. Exp. Neurol. 60 (1), 49–64.

Zhou, S.Y., Xu, S.J., Yan, Y.G., Yu, H.M., Ling, S.C., Luo, J.H., 2011. Decreased purinergic inhibition of synaptic activity in a mouse model of Niemann-Pick disease type C. Hippocampus 21 (2), 212–219.

Zonta, B., Minichiello, L., 2013. Synaptic membrane rafts: traffic lights for local neurotrophin signaling? Front Synaptic. Neurosci. 5, 9 (1663-3563 (Linking)).

SCIENTIFIC REPORTS

OPEN

Impact of Reduced Cerebellar EAAT Expression on Purkinje Cell Firing Pattern of NPC1-deficient Mice

Received: 23 October 2017
Accepted: 12 February 2018
Published online: 20 February 2018

Michael Rabenstein, Franziska Peter, Arndt Rolfs & Moritz J. Frech

Niemann-Pick disease Type C1 (NPC1) is a rare hereditary neurodegenerative disease. NPC1-patients suffer, amongst others, from ataxia, based on a loss of cerebellar Purkinje cells (PCs). Impaired expression/function of excitatory amino acid transporters (EAATs) are suspected of contributing to PC-degeneration in hereditary spinocerebellar ataxias (SCAs). Thus, we studied EAAT-expression and its impact to PC-activity in NPC1$^{-/-}$mice. Western blot revealed reduced EAAT1, EAAT2, EAAT4, and βIII-spectrin levels in NPC1$^{-/-}$mice. EAATs play a crucial role in synaptic transmission, thus we were interested in the impact of the reduced EAAT-expression on the function of PCs. Patch-clamp recordings of PCs showed no differences in the firing patterns of NPC1$^{+/+}$and NPC1$^{-/-}$mice using a low internal chloride concentration. Because EAAT4 also comprises a chloride permeable ion pore, we perturbed the chloride homeostasis using a high internal chloride concentration. We observed differences in the firing patterns of NPC1$^{+/+}$and NPC1$^{-/-}$mice, suggesting an impact of the altered EAAT4-expression. Additionally, the EAAT-antagonist DL-TBOA acts differently in NPC1$^{+/+}$and NPC1$^{-/-}$mice. Our data support the line of evidence that an altered EAAT-expression/function is involved in neurodegeneration of PCs observed in SCAs. Thus, we suggest that similar pathogenic mechanisms contribute the loss of PCs in NPC1.

Niemann Pick Type C1 (NPC1) is a recessive hereditary lysosomal storage disease with an incidence of 1:100,000 newborns[1]. The mutations in the NPC1 gene which cause the disease reduce the function of the lysosomal/late endolysosomal cholesterol transporter NPC1. This leads to intracellular accumulation of cholesterol as well as other lipids such as gangliosides and sphingosines[1]. Patients present neurological symptoms such as cerebellar ataxia, caused by degeneration and loss of Purkinje cells (PCs)[1]. Purkinje cells play a major role in movement coordination and are the sole output of the cerebellar cortex. Loss of these cells or a disturbance in their activity lead to ataxia, a pathological hallmark, not only of NPC1[1], but hereditary spinocerebellar ataxias (SCAs)[2]. In the pathogenesis of SCAs βIII spectrin, a cytoskeletal protein, is discussed to be a key player in a common pathogenic pathway[3]. βIII spectrin plays a crucial role in the maintenance of dendritic structures of PCs and the trafficking and localization of ion channels and EAATs, acting as glutamate transporters[3], which in turn are involved in the modulation of the intrinsic activity of cerebellar PCs[4]. In regards of NPC1 a reduced expression of EAAT3 in the hippocampus is described for NPC1$^{-/-}$ mice[5], and EAAT1 in Bergmann glia of NPC1^{nmf164} mice[6], but no data are available for PCs of the cerebellum of NPC1 deficient mice. Thus, we examined the expression of EAAT1, EAAT2, and EAAT4 in the cerebella of NPC1$^{-/-}$ mice and studied the impact on Purkinje cell function.

Results

Cerebellar expression of glutamate transporters is reduced in NPC1$^{-/-}$. A hampered function and/or loss of cerebellar glutamate transporters play a crucial role in the pathology of e.g. spinocerebellar ataxias[3,7], suggesting a contribution to the ataxia observed in NPC1. Therefore, we analyzed the cerebellar expression levels of the Purkinje cell (PC) specific excitatory amino acid transporter 4 (EAAT4), the on glia cell located EAAT1 and EAAT2, as well as cytoskeletal protein βIII spectrin, acting as an anchor for EAAT4[8]. Semi-quantitative western blot was used to analyze whole cerebella from p55 NPC1$^{+/+}$ and NPC1$^{-/-}$ mice.

In accordance with recent studies[9,10], in NPC1$^{-/-}$ mice we found a graduated loss of calbindin positive PCs from the anterior lobes to the posterior lobes, wherein lobe X appears to be unaffected (Fig. 1A), which is in

Albrecht-Kossel-Institute for Neuroregeneration (AKos), University Medicine Rostock, Gehlsheimer Straße 20, D-18147, Rostock, Germany. Correspondence and requests for materials should be addressed to M.J.F. (email: moritz.frech@med.uni-rostock.de)

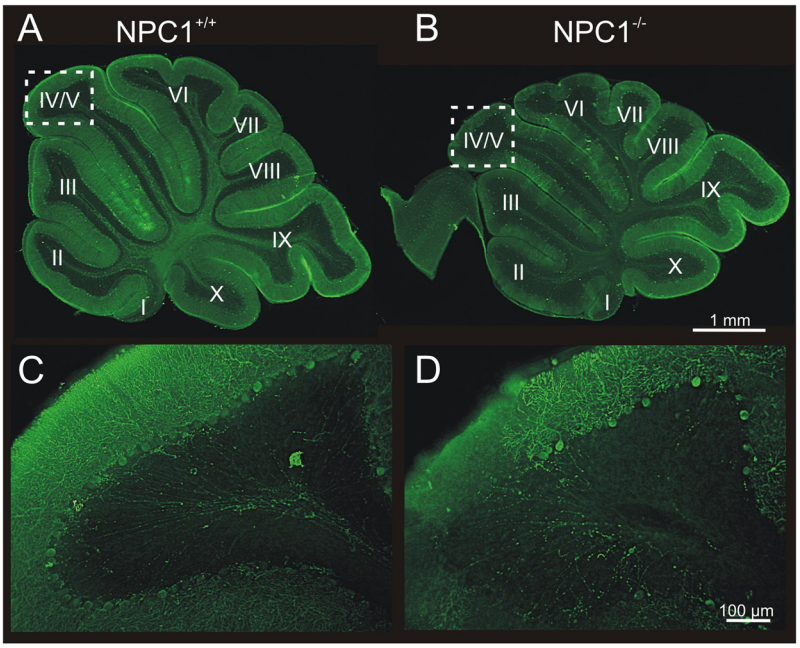

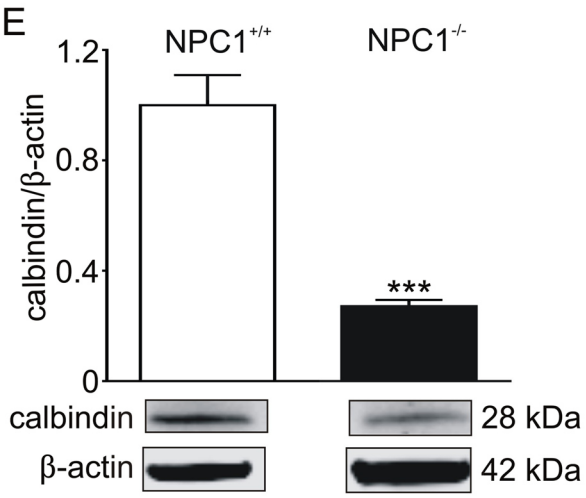

Figure 1. Purkinje cell degeneration in p55 NPC1$^{-/-}$ mice NPC1$^{+/+}$ mice. (**A**) show an even distribution of calbindin positive PCs in contrast to NPC1$^{-/-}$ mice (**B**). A higher magnification of lobe IV/V of NPC1$^{+/+}$ (**C**) and NPC1$^{-/-}$ mice (**D**) demonstrates the loss of Purkinje cell somata in NPC1$^{-/-}$ mice. (**E**) Western blot analysis confirmed a reduced number of PCs by a significantly decreased protein level of calbindin (NPC1$^{+/+}$: N = 8, n = 25; NPC1$^{-/-}$: N = 8, n = 23). Western blot bands display corresponding examples of the same gel. ***$p < 0.001$, data shown as mean ± sem. Student´s unpaired t-test was used to determine significance.

accordance with previous studies[11,12]. In pictures with a higher magnification of lobe IV/V (Fig. 1C,D, areas indicated by dotted rectangle in A and B) one can observe a reduced number of Purkinje cells in NPC1$^{-/-}$ mice. Determination of protein level revealed a significantly reduced amount of calbindin (Fig. 1E). Regarding the expression of the EAATs, we observed a significantly reduced amount of EAAT4 and the EAAT4 stabilizing cytoskeletal protein βIII spectrin (Fig. 2A,B). The protein level of the glial EAAT1 and EAAT2 was also significantly reduced (Fig. 2C,D). EAATs, acting as glutamate transporters, are not only crucial for the modulation of synaptic transmission, e.g. by the uptake of glutamate from the synaptic cleft, but can influence the activity of the cells due to their dual action, comprising the function of a transporter as well the function of an Cl^- permeable ion channel such as EAAT4[13]. As we observed significantly reduced expression of EAATs in NPC1$^{-/-}$ mice, we were interested in the impact on the function of Purkinje cells.

Purkinje cell activity pattern depends on internal chloride concentration. To check the functional impact of EAAT downregulation, we recorded the action potential firing pattern of PCs of mice between p45 and p55. Firing pattern of optical identified PCs in lobe III-V (Fig. 3A) were recorded by means of whole-cell patch clamp recordings using the current-clamp mode. Recordings revealed different activity patterns, and we

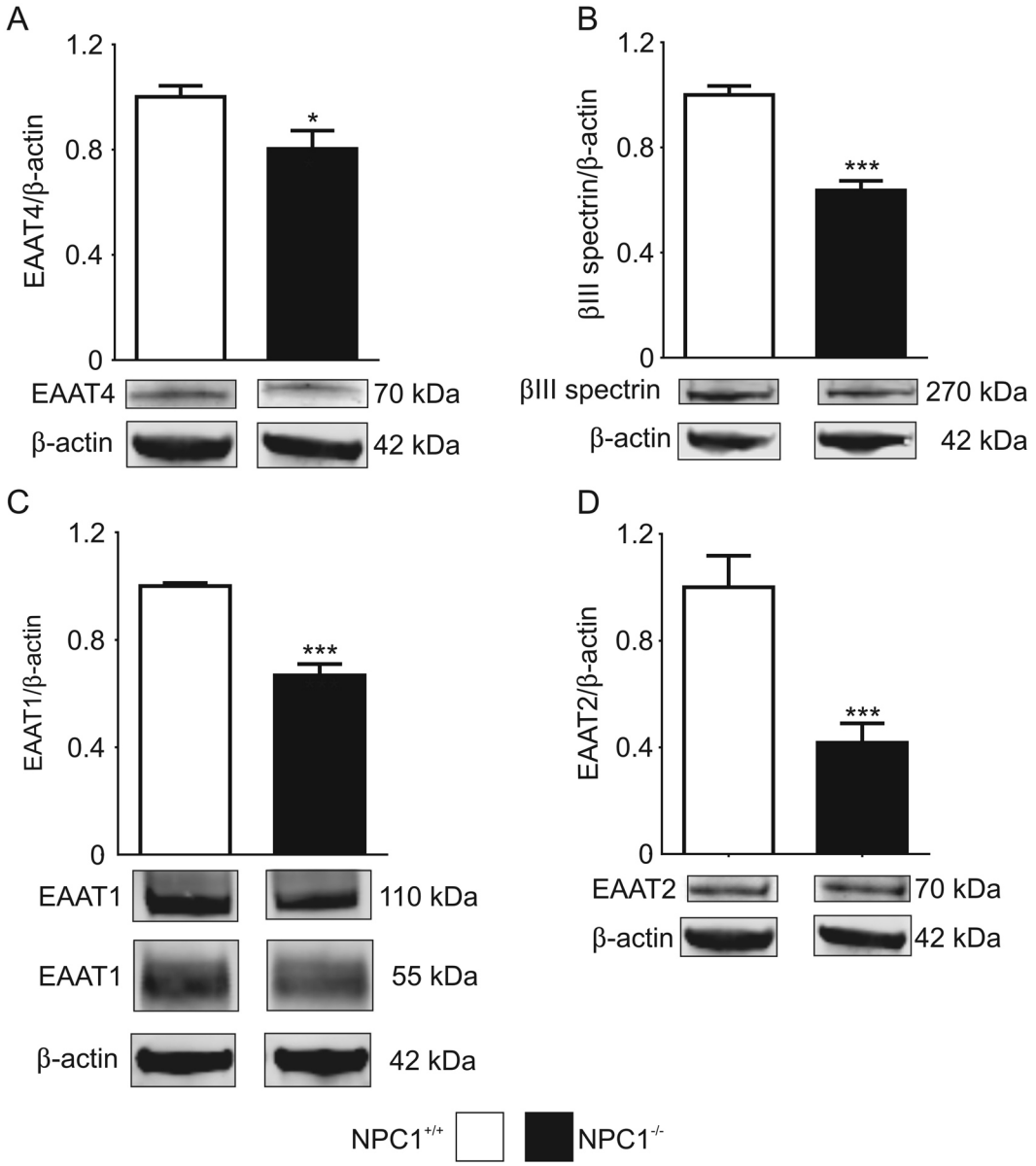

Figure 2. EAAT expression in cerebella of NPC1$^{+/+}$ and NPC1$^{-/-}$ mice. (**A**) Expression of PC specific EAAT4 (NPC1$^{+/+}$: N = 8, n = 25; NPC1$^{-/-}$: N = 8, n = 23) as well as (**B**) the EAAT4 stabilizing protein βIII spectrin (NPC1$^{+/+}$: N = 8, n = 25; NPC1$^{-/-}$: N = 8, n = 24) were significantly reduced in NPC1$^{-/-}$ mice. (**C**) Expression of on glia cell located EAAT1 (NPC1$^{+/+}$: N = 5, n = 10; NPC1$^{-/-}$: N = 5, n = 8) and (**D**) EAAT2 (NPC1$^{+/+}$: N = 8, n = 16; NPC1$^{-/-}$: N = 8, n = 13) was also significantly reduced in NPC1$^{-/-}$ mice. Bar graph of EAAT1 shows the sum of EAAT1 110 kDA and 55 kDa band. Western blot bands display corresponding examples of the same gel. *$p < 0.05$, ***$p < 0.001$, data shown as mean ± sem. Student´s unpaired t-test was used to determine significance.

defined three groups of PCs: tonic firing, burst firing, and inactive cells (Fig. 3B). Using a low internal chloride concentration ($Cl^-_{[i]}$) 80% of the PCs (NPC1$^{+/+}$: 24/29, NPC1$^{-/-}$: 24/30) generated action potentials in bursts, independent of the genotype (Fig. 3C). Only a few cells showed a tonic pattern (NPC1$^{+/+}$: 1/29, NPC1$^{-/-}$: 1/30) or were inactive (NPC1$^{+/+}$: 4/29, NPC1$^{-/-}$: 5/30). Because we found a significantly reduced expression of EAAT4, and due to the intrinsic Cl^- conductibility of the transporter, we decided to perturb the Cl^- homeostasis using a high $Cl^-_{[i]}$. This revealed a shift from burst firing pattern to tonic firing pattern (Fig. 3D). Moreover, the activity pattern distribution was different between NPC1$^{+/+}$ and NPC1$^{-/-}$ mice, wherein significantly more tonic firing cells were observed in NPC1$^{-/-}$ mice (NPC1$^{+/+}$: 14/52, NPC1$^{-/-}$: 25/43), whereas less cells were generating bursts (NPC1$^{+/+}$: 27/52, NPC1$^{-/-}$: 14/43) or were inactive (NPC1$^{+/+}$: 13/52, NPC1$^{-/-}$: 4/43). The analysis of the tonic firing pattern revealed significantly reduced AP frequencies in PCs of NPC1$^{-/-}$ mice (Fig. 3E) and a lower CV of mean interspike intervals (Fig. 3F). The latter suggests that PCs of NPC1$^{-/-}$ mice generate action potentials more regularly than the PCs of NPC1$^{+/+}$ mice.

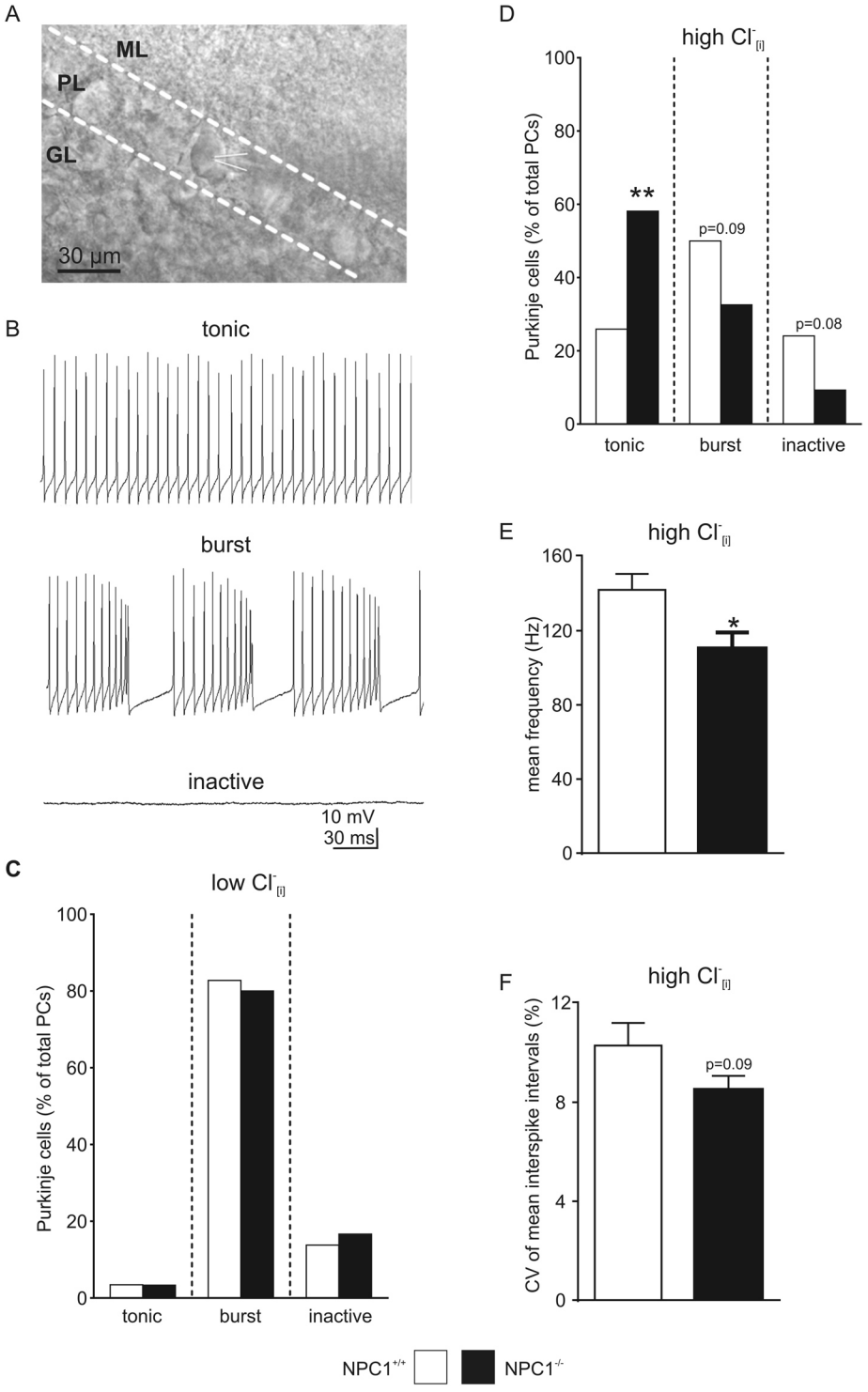

Figure 3. Chloride-dependent alterations of Purkinje cell activity pattern. (**A**) Optical identified PCs in lobes III-V were used for whole-cell patch clamp recordings. Recording electrode attached to PC is depicted by white lines. (**B**) Using the current clamp mode, three different activity patterns of PCs were found: tonic firing, burst firing and inactive. (**C**) No differences in pattern distribution between NPC1$^{+/+}$ and NPC1$^{-/-}$ mice were observed using a low $Cl^-_{[i]}$ (NPC1$^{+/+}$: N = 11, n = 29; NPC1$^{-/-}$: N = 8, n = 30). (**D**) Significantly more tonic firing PCs were found in NPC1$^{-/-}$ mice using a high $Cl^-_{[i]}$, whereas more PCs in NPC1$^{+/+}$ mice showed burst activity or were inactive (NPC1$^{+/+}$: N = 19, n = 52; NPC1$^{-/-}$: N = 15, n = 43). (**E**) The tonic firing PCs of NPC1$^{-/-}$ mice showed a significantly reduced action potential frequency and (**F**) a higher spike regularity using a high $Cl^-_{[i]}$ (NPC1$^{+/+}$: N = 12, n = 14; NPC1$^{-/-}$: N = 11, n = 25). *$p < 0.05$, **$p < 0.01$, data shown as mean ± sem. ML = molecular layer, PL = Purkinje layer, GL = granular layer. Barnard's 2 × 2 test was used to determine significance for data shown in C and D. Student´s unpaired t-test was used to determine significance for data shown in E and F.

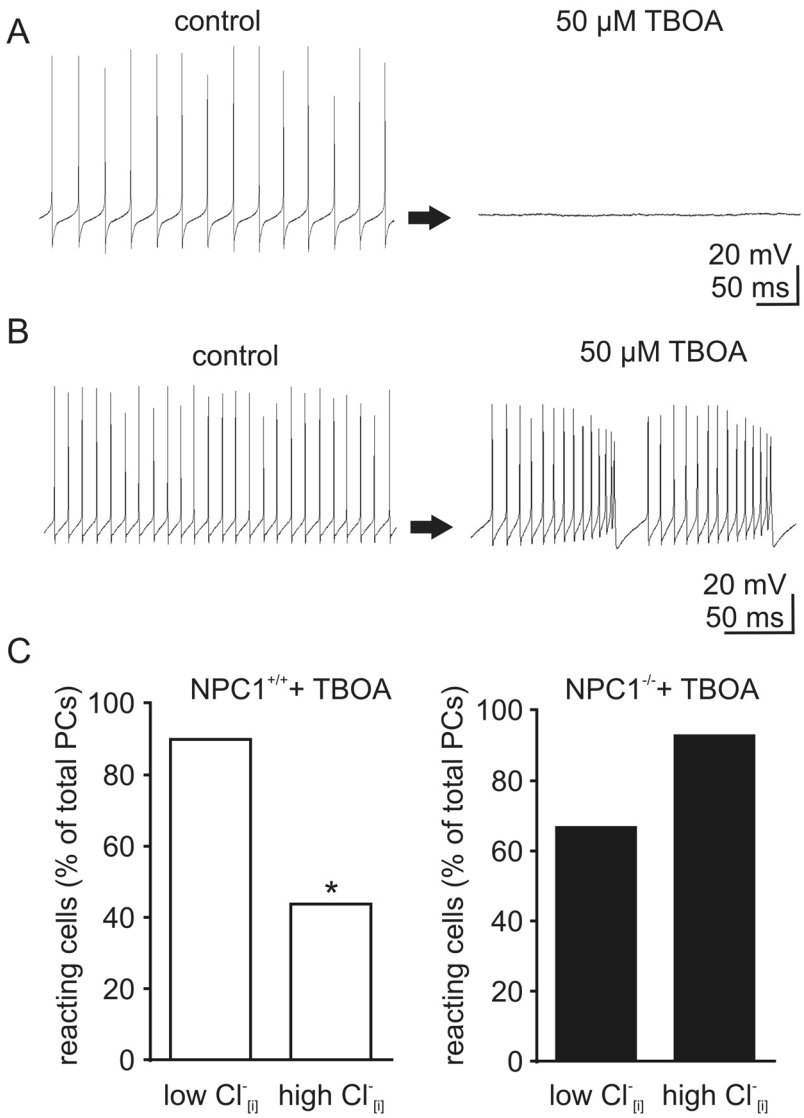

Figure 4. Chloride-dependent effect of TBOA on Purkinje cell activity pattern. (**A**) Example traces of TBOA induced change of activity pattern from tonic firing to inactive and (**B**) tonic to burst firing. (**C**) Applying TBOA, a significantly reduced number of PCs in NPC1$^{+/+}$ mice changed their activity pattern using different $Cl^-_{[i]}$ (Low $Cl^-_{[i]}$: N = 3, n = 10; high $Cl^-_{[i]}$: N = 7, n = 16). No such effect was observed in NPC1$^{-/-}$ mice (Low $Cl^-_{[i]}$: N = 5, n = 12; high $Cl^-_{[i]}$: N = 5, n = 14). *$p < 0.05$. Barnard's 2 × 2 test was used to determine significance for data shown in C.

To further address the impact of reduced EAAT4 expression on the activity pattern, we applied 50 µM of the EAAT inhibitor DL-TBOA (TBOA). We observed various effects of TBOA on the activity pattern, e.g. a shift from tonic firing to inactive (Fig. 4A) or an alteration of frequency, length of bursts, or interburst intervals (Fig. 4B). Independent of the kind of alteration, we determined the percentage of cells affected by TBOA using once again a low and a high $Cl^-_{[i]}$ to perturb the Cl^- homeostasis. In 90% (9/10) of the NPC1$^{+/+}$ PCs, TBOA induced changes in the activity pattern with a low $Cl^-_{[i]}$, while the number of cells reacting was significantly lower (44%, 7/16), with a high $Cl^-_{[i]}$ (Fig. 4C). In contrast, only 67% (8/12) of the NPC1$^{-/-}$ Purkinje cells were affected by TBOA using a low $Cl^-_{[i]}$, but when using a high $Cl^-_{[i]}$ 93% (13/14) of the PCs reacted to TBOA, although the difference was not significant (Fig. 4D). In sum, we noticed a reduced cerebellar expression of glial glutamate transporters EAAT1, EAAT2, the PC specific EAAT4, and βIII spectrin in NPC1$^{-/-}$ mice. Furthermore, we found Cl^- dependent alterations in the activity pattern distribution of Purkinje cells as well as in the number of Purkinje cells showing a TBOA-induced activity pattern switch. These data suggest that the modulation of the activity of cerebellar PCs by EAATs is altered in NPC1$^{-/-}$ mice.

Discussion

Purkinje cells are the sole output of the cerebellar cortex. Loss of these cells or a disturbance in their activity lead to ataxia, a pathological hallmark of NPC1[1] or hereditary spinocerebellar ataxias (SCAs)[2]. In the pathogenesis of

SCAs βIII spectrin, a cytoskeletal linker protein, is discussed to be a key player in a common pathogenic pathway[3]. βIII spectrin plays a crucial role in the maintenance of dendritic structures of PCs and the trafficking and localization of ion channels and EAATs[3], which in turn are involved in the modulation of the intrinsic activity of cerebellar PCs[4]. Thus, we were interested in alterations of the expression of βIII spectrin and EAATs in the cerebellum of NPC1$^{-/-}$ mice and the impact on the intrinsic activity of cerebellar PCs.

The here observed lower expression of βIII spectrin is in line with findings in different SCAs and supports the idea of a common pathogenic pathway for cerebellar ataxias[3], wherein alterations of the cytoskeleton lead to dislocation of e.g. ion channels or transporters like EAATs. In regards of NPC1 other cytoskeletal alterations like hypophosphorylation of vimentin[14–16] or GFAP[16] are described, as well as changed expression of e.g. excitatory AMPA receptors[17]. Regarding EAATs, βIII spectrin stabilizes EAAT4 in the membrane of PCs and a loss of βIII spectrin affects EAAT4 expression as described for SCA5[7]. A lower EAAT4 expression is also described for the *staggerer* mice, a model system for SCA1[18,19]. Thus, one can speculate that the here observed decreased protein amount of EAAT1, EAAT2 and EAAT4 is based on the decreased amount of βIII spectrin. Another reason for the decreased EAAT amount might be due to a reduced number of granulare cells, observed in NPC1, and thus a reduced number of synapses established between parallel fibers and PCs[20,21]. However, the underlying mechanism of the reduced βIII spectrin amounts stay elusive and needs further examination. For further studies it might also be of interest to focus on EAATs located in glial cells as e.g. in SCA5, PC degeneration is proposed to be induced by a loss of EAAT1, located on Bergmann glia cells[7]. Interestingly, Bergmann glia reduce their EAAT1 expression during disease progression, without expressing the mutated βIII spectrin themselves. It was proposed that this is caused by an altered communication between PCs and Bergmann glia cells[7]. This point is especially interesting for NPC1 as the role of glial cells in NPC1 is contradictory. A neuron specific deletion of the NPC1 gene induced neurodegeneration in mice, but not a glia cell specific deletion[11]. In contrast, a knock in of the normal gene in glia cells was sufficient to extended the survival of NPC1$^{-/-}$ mice[22]. Here, we demonstrated a reduced amount of EAAT1 and EAAT2, located in the cerebellum mainly on glial cells, and EAAT4, mainly located on PCs, suggesting a contribution of both cell types to the pathogenic mechanism. However, the impact of a *NPC1* mutation seems to be region specific, as a EAAT3 downregulation but an unaltered EAAT1 and EAAT2 expression was found in the hippocampus of NPC1$^{-/-}$ mice[5], in contrast to the here observed changes of EAAT1 and EAAT2.

To determine the functional impact of reduced EAAT and βIII spectrin expression, we checked the action potential generation of PCs, which is affected in several ways in different ataxias. Changes in the firing pattern distribution, e.g. in SCA2 and SCA3[23,24], altered action potential frequency, e.g. in SCA2, SCA3, and SCA5[7,23,24], or a higher action potential irregularity, as described in SCA2 and episodic ataxia type 2[23,24] show the pathophysiological heterogeneity of hereditary ataxias. Unlike these studies, describing different activity pattern of PCs in wild type and mutant mice, we observed no such differences between NPC1$^{+/+}$ and NPC1$^{-/-}$ mice using a low $Cl^-_{[i]}$, reflecting the physiological situation. This is in accordance with a previous study, using a mouse model with a specific deletion of NPC1 in PCs, were also no alterations in PC activity was found[25]. But, as EAAT4, which is predominantly expressed in the cerebellum by PCs, acts not only as a glutamate transporter but also comprises a Cl^- permeable ion pore[13], we used a high $Cl^-_{[i]}$ to perturb the Cl^- homeostasis of PCs. And indeed a high $Cl^-_{[i]}$, reversing the effect of Cl^- mediated currents from inhibitory to excitatory, did result in a change of firing pattern, indicating an altered chloride conductibility of the PCs. Furthermore, the different effect of EAAT inhibition, on the activity pattern between the genotypes suggests, that EAATs can contribute to the observed alterations in different ways. Firstly, considering the Cl^- conductibility of EAAT4, even a moderate loss of 20% of the protein in NPC1$^{-/-}$ mice, contributes to an alteration of the overall Cl^- conductibility in PCs. Secondly, not only the loss of EAAT4, but also of EAAT1 and EAAT2 could affect the synaptic transmission, due to a decreased glutamate uptake and a subsequently increased glutamate level in the synaptic cleft. In turn, the activity of e.g. GABAergic interneurons, could be affected leading to an altered GABAergic synaptic transmission to PCs[26], resulting in altered tuning of PCs activity. In this line, an inhibition of EAATs by TBOA could lead to an additional accumulation of glutamate and therefore differently impact the activity of PCs, as we observed in NPC1$^{+/+}$ and NPC$^{-/-}$ mice.

In sum, our results demonstrate a reduced level of glial and neuronal EAATs, as well as the anchoring protein βIII spectrin. We conclude that these alterations contributes to Cl^- dependent alterations of the activity pattern of PCs in NPC1$^{-/-}$ mice. Our data are in line of evidence with an altered function and/or expression of EAATs playing a role in the neurodegenerative mechanisms leading to a loss of PCs observed in spinocerebellar ataxias. Thus, we suggest that similar pathogenic mechanisms contribute the progressive loss of Purkinje cells in NPC1.

Methods

Animal housing. Heterozygote mice of the BALB/c_Nctr-Npc1m1N/-J strain[27] (Jackson Laboratories, USA), housed in accordance with German animal welfare law, were bred to obtain homozygous NPC1-deficient (NPC1$^{-/-}$) and unaffected, wild type (NPC1$^{+/+}$) animals. The animals had access to food and water ad libidum. A 12 h light/dark cycle was maintained and room temperature was set to 22 °C. Tail tip samples were used to determine the genotype of the animals by polymerase chain reaction.

Preparation of cerebellar slices. Preparation of parasagittal cerebellar vermis slices was adapted from Bischofberger *et al.*[28]. Mice were decapitated and brains were removed rapidly and incubated in an ice-cold buffer containing (mM): NaCl 125, KCl 2.5, $CaCl_2xH_2O$ 2, $MgCl_2x6H_2O$ 1, $NaHCO_3$ 26, $NaH_2PO_4xH_2O$ 1.25, glucosexH_2O 25, pH 7.4. After separation of the cerebellum and removal of the cerebellar hemispheres, 250 µm thick slices were cut with a vibratome (Leica VT 1200 S) in the buffer and incubated for 30 minutes at 37 °C. All steps were performed with a buffer supplied with carbogen (95% O_2, 5% CO_2).

Patch clamp recordings. Patch clamp recordings of optically identified Purkinje cells were performed using an EPC-10 amplifier controlled by PatchMaster software (Heka, Germany). Patch pipettes were pulled from borosilicate glass tubing (GC150F-10, Harvard Apparatus, USA) using a DMZ-Universal-Electrode-Puller (Zeitz, Germany). The intracellular solution with a low Cl^- concentration IC_{low} contained (mM): K-D-Gluconate 130, KCl 10, HEPES 10, EGTA 11, $MgCl_2x6H_2O$ 1, $CaCl_2x2H_2O$ 1. The intracellular solution with a high Cl^- concentration (IC_{high}) contained (mM): KCl 140, HEPES 10, EGTA 11, $MgCl_2x6H_2O$ 1, $CaCl_2x2H_2O$ 1. The pH was adjusted to 7.2 with KOH in both solutions. The electrodes had a resistance of 5–7 MΩ when filled with IC_{low} and 3–5 MΩ with IC_{high}. Recordings of PC activity were made in the whole cell configuration in the current clamp mode with a holding current of 0pA at 34 °C. To validate the impact of EAAT function on the PC activity, EAATs were inhibited in a subset of experiments using DL-TBOA (Tocris Bioscience, United Kingdom). Data were filtered at 3 kHz and digitized with 10 kHz using PatchMaster software (Heka, Germany). Mini Analysis 6.0.7 (SynaptoSoft, USA) was used to detect action potentials and determine the activity pattern of the PCs. Frequency and coefficient of variation (CV) of mean interspike intervals were analyzed in R 3.1.2 (The R Foundation for Statistical Computing, Austria) with RStudio 0.98.1091 (RStudio, Inc., USA).

Western blot. For western blot analysis, whole cerebella were frozen in liquid nitrogen and stored at −80 °C. For protein extraction, cerebella were placed in a tissue grinder and 1 ml RIPA-lysis buffer (in mM: TRIS 20, NaCl 137, sodium deoxycholate 12, EDTA 2, 0.1% SDS, 1% Triton® X-100, 10% glycerol supplemented with cOmplete™, Mini, EDTA-free Protease Inhibitor Cocktail (Roche Diagnostics GmbH, Germany) was added. After grinding the cerebella, the samples were incubated on ice for 30 min. The samples were centrifuged at 15,000 g for 30 min at 4 °C and the pellet was discarded. Protein concentration was determined using the Pierce™ BCA Protein Assay Kit (Thermo Fisher Scientific, USA) according to the manual. Samples were boiled for 10 minutes at 95 °C in 5 × Laemmli-buffer (125 mM TRIS, 20% glycerol, 2% SDS, 5% β-mercaptoethanol, 10% bromphenol blue) and centrifuged at 17,530 g for 1 min at 4 °C. Proteins were separated using the Criterion™ Vertical Electrophoresis Cell with Criterion™ TGX Stain-Free™ Precast Gels (4–15%) (Bio-Rad Laboratories, Germany). The electrophoresis buffer contained 25 mM TRIS, 200 mM glycine, and 0.1% SDS. For Western blot the Trans-Blot® Turbo™ Transfer System with Trans-Bolt® Turbo™ Transfer Pack (Midi Format, 0.2 µm Nitrocellulose) (Bio-Rad Laboratories, Germany) was used. Membranes were washed in TRIS-buffered saline (TBS), containing 20 mM TRIS and 137 mM NaCl, pH 7.5) for 5 min and then blocked with 5% skim milk powder in TBS supplemented with 0.1% Tween® 20 (TBST) for 1 h. Then membranes were incubated with a primary antibody solution (3% skim milk powder in TBST) for 1 h, washed 3 × with TBST, and incubated with DyLight™ secondary antibody for 1 h. Finally, membranes were washed 3 × with TBST and 1 × with TBS and dried. The Odyssey Infrared Imaging System (LI-COR Biosciences GmbH, Germany) was used to visualize and quantify the protein signals. Antibodies used for western blot: EAAT1 (1:5000), EAAT4 (1:1000 both Proteintech Group, USA), EAAT2 (1:1000) Calbindin d28k (1:500, both Santa Cruz Biotechnology, USA), βIII spectrin (1:2000, Thermo Fisher Scientific, USA), β-actin (1:10,000, Sigma-Aldrich, Germany), GAPDH (1:10,000, Abcam, UK), Anti-Rabbit IgG (H&L), DyLight™ 680 (1:10,000), Anti-Mouse IgG (H&L), DyLight™ 800 (1:10,000, both Rockland Immunochemicals Inc., USA). Expression of β -actin was used for normalization, and Precision Plus Protein Dual Xtra Standards (Bio-Rad Laboratories GmbH, Germany) were used as a molecular weight marker.

Immunocytochemistry. Cerebellar brain slices with a thickness of 150 µm were prepared accordingly to the protocol used for patch clamp experiments. Staining was performed based on the protocol provided by Abcam[29]. Slices were fixed with 4% paraformaldehyde (PFA) in phosphate buffered saline (PBS) overnight at 4 °C. Fixed slices were washed 3 × for 10 min with TBS-Triton (50 mM TRIS, 150 mM NaCl, pH 7.5 supplemented with 1% Triton® X-100). Afterwards slices were blocked with 4% normal goat serum (NGS) in TBS-Triton for 1 h under agitation at room temperature. Primary antibodies in 1% NGS TBS-Triton were incubated overnight under agitation at 4 °C. The next day slices were washed 3 × and a secondary antibody in 1% NGS TBS-Triton was added for 1 h at room temperature. After washing, DAPI in PBS was added, incubated for 10 min at room temperature. Afterwards the slices were washed 3 × and mounted in Mowiol-DABCO (10% Mowiol® 4–88, 2.5% DABCO (1,4-diazabicyclo[2.2.2]octane), 25% glycerol, 0.1 M Tris-HCl (pH 8.5). Slices were visualized using a BZ-8000K microscope (KEYENCE, Germany). Pictures of the higher magnification (Fig. 1C,D), consist of z-stacks of 18 single pictures and were merged using the Full Focus function of the Analyser Software (KEYENCE, Germany).

Statistical analysis. All data were obtained from at least three animals of both genotypes. The number of animals is given as "N", the number of individual experiments is given as "n". Analysis of the data was carried out with GraphPad Prism 6 (GraphPad Software Inc., USA). and R 3.1.2 (The R Foundation for Statistical Computing, Austria). Data are given as mean ± sem. Unless otherwise stated, unpaired Student´s t-test was used to test for significance of two sets of data differing in one variable (GraphPad Prism 6, GraphPad Software Inc., USA). Barnard's 2 × 2 test[30] was used to compare the two variables of data of the experimental settings comparing activity pattern differences in $NPC1^{+/+}$ and $NPC1^{-/-}$ mice. P-values < 0.05 were considered statistically significant, with $^*p < 0.05$, $^{**}p < 0.01$, and $^{***}p < 0.001$.

Ethics approval and consent to participate. Housing and breeding of animals, and experimental procedures were done in accordance with the German Animal Welfare Law (Deutsches Tierschutzgesetz). Approval was given by Landesamt für Landwirtschaft, Lebensmittelsicherheit und Fischerei Mecklenburg-Vorpommern (LALLF-MV), Rostock, Germany.

Availability of data and material. The datasets used and/or analyzed in this study are available from the corresponding author on reasonable request.

References

1. Vanier, M. T. Niemann-Pick disease type C. *Orphanet journal of rare diseases* **5**, 16 (2010).
2. Bird, T. D. in *GeneReviews®*, edited by M. P. Adam, *et al.* (Seattle (WA), 1993).
3. Perkins, E., Suminaite, D. & Jackson, M. Cerebellar ataxias. B-III spectrin's interactions suggest common pathogenic pathways. *The Journal of physiology* **594**, 4661–4676 (2016).
4. Engbers, J. D. T., Fernandez, F. R. & Turner, R. W. Bistability in Purkinje neurons. Ups and downs in cerebellar research. *Neural networks: the official journal of the International Neural Network Society* **47**, 18–31 (2013).
5. Byun, K. *et al.* Alteration of the glutamate and GABA transporters in the hippocampus of the Niemann-Pick disease, type C mouse using proteomic analysis. *Proteomics* **6**, 1230–1236 (2006).
6. Caporali, P. *et al.* Developmental delay in motor skill acquisition in Niemann-Pick C1 mice reveals abnormal cerebellar morphogenesis. *Acta neuropathologica communications* **4**, 94 (2016).
7. Perkins, E. M. *et al.* Loss of beta-III spectrin leads to Purkinje cell dysfunction recapitulating the behavior and neuropathology of spinocerebellar ataxia type 5 in humans. *The Journal of neuroscience: the official journal of the Society for Neuroscience* **30**, 4857–4867 (2010).
8. Machnicka, B. *et al.* Spectrins. A structural platform for stabilization and activation of membrane channels, receptors and transporters. *Biochimica et biophysica acta* **1838**, 620–634 (2014).
9. Tanaka, J., Nakamura, H. & Miyawaki, S. Cerebellar involvement in murine sphingomyelinosis. A new model of Niemann-Pick disease. *Journal of neuropathology and experimental neurology* **47**, 291–300 (1988).
10. Sarna, J. R. *et al.* Patterned Purkinje cell degeneration in mouse models of Niemann-Pick type C disease. *The Journal of comparative neurology* **456**, 279–291 (2003).
11. Yu, T., Shakkottai, V. G., Chung, C. & Lieberman, A. P. Temporal and cell-specific deletion establishes that neuronal Npc1 deficiency is sufficient to mediate neurodegeneration. *Human molecular genetics* **20**, 4440–4451 (2011).
12. Lopez, M. E., Klein, A. D. & Scott, M. P. Complement is dispensable for neurodegeneration in Niemann-Pick disease type C. *Journal of neuroinflammation* **9**, 216 (2012).
13. Fairman, W. A., Vandenberg, R. J., Arriza, J. L., Kavanaugh, M. P. & Amara, S. G. An excitatory amino-acid transporter with properties of a ligand-gated chloride channel. *Nature* **375**, 599–603 (1995).
14. Walter, M., Chen, F. W., Tamari, F., Wang, R. & Ioannou, Y. A. Endosomal lipid accumulation in NPC1 leads to inhibition of PKC, hypophosphorylation of vimentin and Rab9 entrapment. *Biology of the cell* **101**, 141–152 (2009).
15. Tamari, F., Chen, F. W., Li, C., Chaudhari, J. & Ioannou, Y. A. PKC activation in Niemann pick C1 cells restores subcellular cholesterol transport. *PloS one* **8**, e74169 (2013).
16. Peter, F. Rabenstein, M. Rolfs, A. & Frech, M. J. Gliosis in Niemann-Pick type C1 patient- specific iPSC derived glia cells. Abstract 10th FENS Forum 2016. Gliosis in Niemann-Pick type C1 patient- specific iPSC derived glia cells. Abstract 10th FENS Forum 2016. *10th FENS Forum* **2016** (2016).
17. Rabenstein, M. *et al.* Decreased calcium flux in Niemann-Pick type C1 patient-specific iPSC-derived neurons due to higher amount of calcium-impermeable AMPA receptors. *Molecular and cellular neurosciences* **83**, 27–36 (2017).
18. Lin, X., Antalffy, B., Kang, D., Orr, H. T. & Zoghbi, H. Y. Polyglutamine expansion down-regulates specific neuronal genes before pathologic changes in SCA1. *Nature neuroscience* **3**, 157–163 (2000).
19. Serra, H. G. *et al.* Gene profiling links SCA1 pathophysiology to glutamate signaling in Purkinje cells of transgenic mice. *Human molecular genetics* **13**, 2535–2543 (2004).
20. Marshall, C. A. *et al.* In Niemann-Pick C1 mouse models, glial-only expression of the normal gene extends survival much further than do changes in genetic background or treatment with hydroxypropyl-beta-cyclodextrin. *Gene* (2017).
21. Nusca, S. *et al.* A marked paucity of granule cells in the developing cerebellum of the Npc1$(^{-/-})$ mouse is corrected by a single injection of hydroxypropyl-beta-cyclodextrin. *Neurobiology of Disease* **70**, 117–126 (2014).
22. Buard, I. & Pfrieger, F. W. Relevance of neuronal and glial NPC1 for synaptic input to cerebellar Purkinje cells. *Molecular and cellular neurosciences* **61**, 65–71 (2014).
23. Kasumu, A. W., Liang, X., Egorova, P., Vorontsova, D. & Bezprozvanny, I. Chronic suppression of inositol 1,4,5-triphosphate receptor-mediated calcium signaling in cerebellar purkinje cells alleviates pathological phenotype in spinocerebellar ataxia 2 mice. *The Journal of neuroscience: the official journal of the Society for Neuroscience* **32**, 12786–12796 (2012).
24. Shakkottai, V. G. *et al.* Early changes in cerebellar physiology accompany motor dysfunction in the polyglutamine disease spinocerebellar ataxia type 3. *The Journal of neuroscience: the official journal of the Society for Neuroscience* **31**, 13002–13014 (2011).
25. Elrick, M. J. *et al.* Conditional Niemann-Pick C mice demonstrate cell autonomous Purkinje cell neurodegeneration. *Human molecular genetics* **19**, 837–847 (2010).
26. Huang, H. & Bordey, A. Glial glutamate transporters limit spillover activation of presynaptic NMDA receptors and influence synaptic inhibition of Purkinje neurons. *The Journal of neuroscience: the official journal of the Society for Neuroscience* **24**, 5659–5669 (2004).
27. Loftus, S. K. Murine Model of Niemann-Pick C Disease. Mutation in a Cholesterol Homeostasis Gene. *Science* **277**, 232–235 (1997).
28. Bischofberger, J., Engel, D., Li, L., Geiger, J. R. P. & Jonas, P. Patch-clamp recording from mossy fiber terminals in hippocampal slices. *Nature protocols* **1**, 2075–2081 (2006).
29. Abcam. IHC for brain slice sections video protocol, http://www.abcam.com/protocols/ihc-for-brain-slice-sections-video-protocol, last accessed 02/06/2018.
30. Calhoun, P. R-package "Exact", https://cran.r-project.org/web/packages/Exact/index.html, last accessed 02/06/2018 (2016).

Acknowledgements

We thank Sebastian Rost for his excellent technical support.

Author Contributions

M. Rabenstein: experimental design, data collection and analysis, writing manuscript; A. Rolfs, F. Peter and M.J. Frech: experimental design, writing and approving manuscript. All authors read and approved the final manuscript."

Additional Information

Competing Interests: The authors declare no competing interests.

Publisher's note: Springer Nature remains neutral with regard to jurisdictional claims in published maps and institutional affiliations.

Danksagung

Dieser Habilitationsschrift liegen die Ergebnisse der Forschungsprojekte zu Grunde die am Albrecht Kossel Institut für Neuroregeneration, Universitätsmedizin Rostock, in den Jahren 2011 bis 2018 durchgeführt wurden.

Dem damaligen Direktor Herrn Professor Dr. med. Arndt Rolfs danke ich herzlich für seine stetige Unterstützung der Forschungsvorhaben und somit der Möglichkeit für die Erstellung der Habilitation.

Prof. Dr. Dr. Andreas Hermann danke ich für die Erstellung des Votums und des Gutachtens.

Mein tiefster Dank gilt allen Kollegen am AKos die durch ihre Arbeit meine Habilitation unterstützt haben. Insbesondere Sebastian Rost und meinen ehemaligen Doktorandinnen Dr. Michaela Trilck-Winkler und Dr. Franziska Peter, die durch ihre unermüdliche Arbeit die Grundlagen für die Forschung an den induzierten pluripotenten Stammzellen gelegt haben, gilt meine tiefe Dankbarkeit.

Meinem Promovenden Michael Rabenstein danke ich für seine Unterstützung in der Haltung und Zucht der NPC1-Mäuse. Sein Engagement hat es erst ermöglicht die spannenden Untersuchungen an den Mäusen durchzuführen. Besonders danke ich ihm aber für seine offene Art der Kommunikation, für die vielen konstruktiven Diskussionen und seiner stetigen Hilfsbereitschaft den Kollegen und mir gegenüber.

Mein Dank gilt ebenfalls den Promovenden Christin Völkner, Alexandra Jürs und Maik Liedtke für die hervorragende Arbeit, die sie im Rahmen ihrer Promotionsprojekte leisten und welche die Fortführung der Arbeiten über die Habilitation hinaus darstellen.

Nicht zuletzt danke ich meiner Frau Dr. Stefanie Frech für ihre Unterstützung und den Rückhalt während des Verfassens der Habilitation und darüber hinaus.

.